Surface Characterisation of Atmospheric Pressure Plasma-Modified and -Coated Polymers

Thesis

Surface Characterisation of Atmospheric Pressure Plasma-Modified and –Coated Polymers

Ph.D Thesis

by

Lesley-Ann O'Hare, BSc (Hons)

Dow Corning Ltd

&

Open University

2005

ABSTRACT

Atmospheric pressure plasma liquid deposition- APPLD, combines atmospheric pressure plasma with injection of atomised liquid from the delivery nozzle directly into the plasma. As such, the liquid within each droplet is protected from the plasma, and is carried intact to the surface, where it spreads and polymerises to form a conformal, high-value functional coating, which retains the properties of the original precursor molecule.

The relationship between the chemistry of surfaces modified or deposited using this technique and the plasma deposition parameters has been investigated using a complementary suite of surface analytical techniques: contact angle analysis, X-ray photoelectron spectroscopy and atomic force microscopy.

It has been shown that atmospheric pressure plasma (APP) can lead to the same level of oxidation as corona discharge. The APP has been shown to be less damaging to the substrate, and leads to a reduction in the formation of low molecular weight oxidised materials, despite the use of higher energy densities.

A new methodology for curve-fitting of the XPS Si 2p and C 1s core levels of siloxane materials has been developed using siloxane standards. This method has been expanded to be used on siloxane coatings thinner than the depth of analysis of XPS. This enabled the chemistry of the coatings to be determined without the influence of the substrate.

The chemistry of siloxane coatings deposited on poly(ethylene terephthalate) film have been related to the plasma parameters utilised during deposition. Up to 95% polymeric

siloxane [$(CH_3)_3SiO_{1/2}$ and $(CH_3)_2SiO_{2/2}$] have been retained for deposition of poly(dimethylsiloxane) precursor. The use of a poly(hydrogenmethylsiloxane) precursor led to a more oxidised coating, with up to 25% siloxane in $(CH_3)SiO_{3/2}$ environment. The trends in deposition rate for PDMS and PHMS were also found to be different.

Siloxane coatings durable to immersion in boiling water for 30 minutes have been achieved by plasma treatment of the substrate prior to deposition, and by plasma treatment of the coating following deposition. It is believed that improved grafting and enhanced crosslinking, respectively are the mechanisms behind this performance improvement.

ACKNOWLDEGEMENTS

As in any thesis, sincerest thanks are due to all the people who helped make it possible...

To all the staff at Dow Corning Plasma Solutions, in particular Seamus Ryan and Dr. Liam O'Neill, for help with sample preparation and training on the Mark I. Thanks are also due to Andy Goodwin, for support throughout the project, and for the opportunity to carry out the PhD. I also extend my appreciation to Dr Stuart Leadley, for introducing me to XPS more years ago than I care to remember. To Walter Castagna for his help in understanding the maths, I am also very grateful.

To Dr Bhukan Parbhoo, for getting the project started, and to Dr Richard Treadgold (Dow Corning Ltd), for administrating.

To Dr Alan Hynes (Dow Corning Plasma Solutions) and Dr Morgan Alexander (University of Nottingham) I am extremely grateful for their constructive feedback, encouragement, and for providing their expertise.

To Stephen, for his patience over the hardest part – the writing up!

To all my friends – super furry and not, but especially Wayne, Rhid, and Sam – for keeping me sane. Ish.

To all my family, but in particular to my mum, Eileen. I couldn't have gotten this far without you.

CHAPTER 1

INTRODUCTION

1.1 ATMOSPHERIC PRESSURE PLASMA LIQUID DEPOSITION (APPLD)

Plasma-enhanced coating processes are recognised as a route to well-adhered, conformal coatings. Currently, the majority of research has been carried out using vapour precursors, with deposition under vacuum. This thesis presents research where deposition onto polymer films occurred at atmospheric pressure in reel-to-reel conditions, using liquid siloxane precursors.

Atmospheric pressure plasma liquid deposition- APPLD, combines atmospheric pressure plasma with injection of atomised liquid from the delivery nozzle directly into the plasma. As such, the liquid within each droplet is protected from the plasma, and is carried intact to the surface, where it spreads and polymerises to form a conformal, high-value functional coating, which retains the properties of the original precursor molecule.

In addition, the plasma generated is a uniform discharge, and under typical operating conditions contains no filamentary discharges observed in corona discharge. The absence of filamentary discharge results in a more uniform treatment effect, and is less damaging to the substrate. Other atmospheric pressure plasma systems incorporate air into their process, and as such, are limited to oxidative chemistry.

1.2 SILOXANE PRECURSORS

The effect of the chemical structure of the liquid siloxane precursor used to prepare the coated films was of great interest. Two precursors were investigated: a poly(dimethylsiloxane) and a poly(hydrogenmethylsiloxane). It is expected that the

reactivity of these precursors will vary due to the presence of the labile Si-H group in the second precursor.

1.3 AIMS OF PROJECT

This work was primarily undertaken to investigate how the surface chemistry of siloxane deposits were affected by deposition parameters such as precursor flowrate and plasma power. In addition to this, a comparison of the effect of corona discharge treatment and atmospheric pressure glow discharge on the surface of polypropylene film was also made.

A complementary suite of surface analysis techniques: X-ray photoelectron spectroscopy (XPS), atomic force microscopy (AFM) and water contact angle measurements were utilised to provide information about changes in the surface chemistry and morphology occurring as a result of treatment.

1.4 OUTLINE OF THESIS

The thesis is presented in nine chapters, a brief overview of which follows.

Chapter 2 is a review of the literature relevant to this research. An overview of silicon chemistry is presented. In addition, the basic principles behind plasma processing, particularly comparing corona discharge to atmospheric pressure plasma treatment are discussed. A detailed review of the literature relating to atmospheric pressure plasma treatment of polyolefins is presented in *Chapter 4*. The effect of plasma treatment of siloxane is also considered. Finally, the siloxane materials which have been deposited using both low pressure and atmospheric pressure plasma are presented.

In *Chapter 3*, the methods and materials used to prepare samples and to analyse the surface chemistry and morphology are described. The basic principles behind the surface analysis techniques utilised are provided. In-depth descriptions of the corona discharge treater, and the atmospheric pressure glow discharge and liquid deposition apparatus in particular, are presented.

Chapter 4 discusses in detail the surface physico-chemical properties of a polypropylene substrate modified using corona discharge treatment or atmospheric pressure glow discharge. Contact angle measurements, X-ray photoelectron spectroscopy and atomic force microscopy were used to monitor changes in the surface energy, surface chemistry, and morphology, respectively.

Chapter 5 describes the development of a methodology for XPS curve-fitting of the Si 2p core level of siloxane materials. Obtaining reliable binding energies for the various chemical states of silicon allows greater confidence in identifying the chemistry of siloxane deposits discussed in *Chapter 6*. The effect of the plasma parameters (e.g. power and precursor flowrate) on the chemistry of the deposits are discussed in detail here. The effect of changing the polymer precursor structure from poly(dimethylsiloxane) to poly(hydrogenmethylsiloxane) will also be examined in this chapter.

In *Chapter 7*, means of optimising the coating performance, such as plasma treatment of the substrate to enhance grafting, or plasma treatment of the coating are discussed. The relationship between treatment conditions and coating hydrothermal durability is investigated.

A discussion of the result obtained, and comparisons to previous work in the literature is presented in *Chapter 8*, followed by final conclusions drawn from the work in *Chapter* 9.

CHAPTER 2

LITERATURE REVIEW

2.1 SILOXANES: STRUCTURES AND PROPERTIES

Silicone is the generic name of a unique class of polymers comprising an inorganic backbone made of alternating silicon and oxygen atoms. The Si-O bond, known as a siloxane bond, confers to the polymer the name *polysiloxane*. The most commonly known silicone is based on poly(dimethysiloxane), or PDMS, However, there a variety of polysiloxane structures that can be synthesised, from simple linear, to complex three-dimensional structures, of general formula:

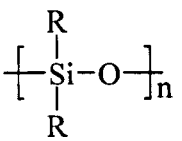

Where R = H, alkyl group or oxygen

These structural variations lead to the appearance of polysiloxanes in various forms, ranging from non-viscous fluids to rubbers to tough resinous materials.

The flexibility of their form results in their use in numerous products[1,2] which combine organic and inorganic character and possess unique physical, chemical and mechanical properties that are unmatched by any other polymeric materials. Their success in a multitude of technologies is due to a range of properties that include low surface energy, hydrophobicity, chemical resistance, electrical insulation, resistance to weathering, stability to extremes of temperature, resistance to thermal shocks, high elasticity, good tear strengths, capability to seal or bond materials of various natures, biocompatibility, etc.

As the chemical names for polymeric siloxane materials can be quite unwieldy, a simplified notation has traditionally been used in industry. The letters

M [$(CH_3)_3SiO_{1/2}$], D [$(CH_3)_2SiO_{2/2}$], T [$(CH_3)SiO_{3/2}$] and Q [$SiO_{4/2}$] have been used to represent siloxy units by indicating the number of oxygen atoms attached to the silicon.

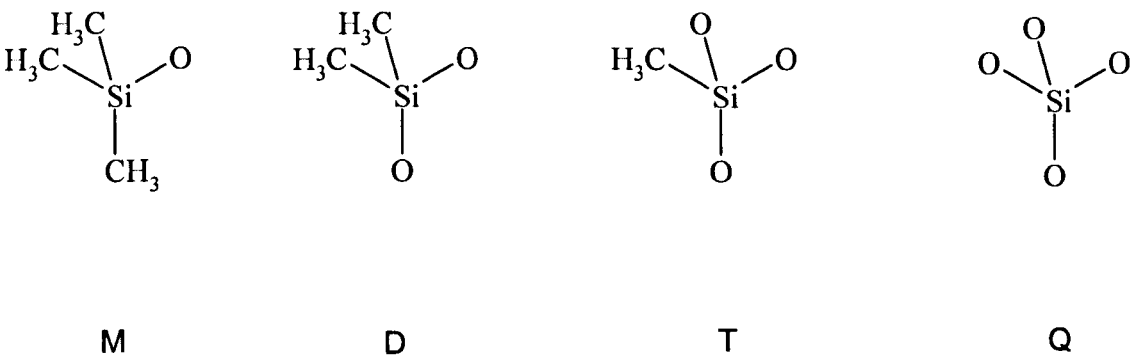

Scheme 1: Representations of the various siloxy units encountered in polysiloxanes

When an organofunctional group replaces a methyl group on a siloxy unit, a superscript is used to describe the unit. The most common groups that are encountered can be symbolised as: alkyl (R), hydrogen (H), phenyl (Ph), hydroxyl, (OH), trifluoropropyl (F) and vinyl (Vi). Thus, the precursors under investigation in this thesis: trimethylsiloxy-endblocked-polydimethylsiloxane (TMS-eb-PDMS) and trimethylsiloxy-endblocked-polyhydrogenmethylsiloxane (TMS-eb-PHMS) can be represented simply by MD_nM and MD^H_nM, respectively.

2.2 ATMOSPHERIC PRESSURE PLASMA TECHNOLOGIES

2.2.1 Definition of plasma

Plasma, often described as the fourth state of matter, is an ionised gas. Although this use of the term *plasma* may be unfamiliar to many, most matter in the known universe occurs in this form. The sun and other stars, the space between galaxies, Aurora Borealis and Australis, lightning, fluorescent light tubes, and neon lighting are all examples of plasma.

Plasmas may be divided into two categories: equilibrium, or 'hot' plasmas, and non-equilibrium, or 'cold' plasmas. The sun and stars are examples of equilibrium plasmas, and are so called because the ions and electrons that constitute it are at the same temperature, which can range between 5000 and 70000K. These plasmas are typically created by exposing the gas molecules to extreme temperatures. Industrial applications of hot plasmas are plasma torches, or apparatus used for the deposition of metals. Low-temperature plasmas are generally created by the application of electric discharge to the feed gas. In this case, the electrons are 100 – 1000 times the temperature of the gas molecules or atoms. However, as the electron mass is so small, minimal effect is had on the overall plasma temperature. This type of plasma is most often created under vacuum conditions, and is more suited to applications involving temperature-sensitive substrates, for example polymer films.

In the case of polymer films, plasmas are often used as a means of modifying the surface properties of the substrate, whilst having minimal effect on the bulk characteristics of the material. Obtaining a thin, uniform, covalently-bonded conformal

coating with specific, and perhaps high-value, properties on a cheap, commodity polymer is very desirable.

There are many applications where thin siloxane coatings are required, for example for release liners or to provide barrier properties. These two applications, although both surfaces contain silicon, have very different chemistries. For release properties to be achieved, the siloxane must be in an 'organic', polymeric state. However, for barrier properties are more likely achieved using siloxane materials in an inorganic, resinous form. Other favourable properties that may be achieved using thin silicon coatings are enhanced hydrophobicity, lubricity, thermal stability, and anti-fouling.

2.2.2 Corona or dielectric barrier discharge

Dielectric barrier discharge (DBD), typically referred to as 'corona' disharge in industrial applications, allow the formation of non-equilibrium plasmas at atmospheric pressure. The discharge is generated by the application of a high voltage to a gas between parallel electrodes, covered by either one or two dielectric plates.

The high voltage causes the gas to break down into many microdischarges or 'filaments'. DBD is carried out in air, resulting in heat, light and active species such as O, O_3, O_2^*, N_2^* and radicals. The proposed mechanisms of surface modification are through the incorporation of polar groups, leading to increased surface energy. Both crosslinking and polymer chain scission reaction mechanisms compete, resulting in the formation of hydroxyl, carbonyl, carboxyl and nitro functional groups. Increased surface roughening is often reported as an additional effect of corona treatment.

2.2.3 Atmospheric pressure plasma

The first report of a glow discharge plasma generated at atmospheric pressure was by Von Engle in the 1930's[3]. Key papers by Kanazawa *et al*[4] and Massines *et al*[5] have discussed the use of helium, or argon with acetone to generate a glow discharge plasma. In this modification technique, an AC voltage is applied to the gas. This accelerates any free electrons present in the gas, which can then ionise the neutral atoms. This in turn releases further electrons, and leads to an 'avalanche' ionisation. When the density of ions and electrons is sufficiently high, so that they begin to act collectively, a plasma is generated.

Generation of plasmas from helium at atmospheric pressure has several advantages over conventional surface modification techniques, such as corona discharge treatment (CDT). The plasma generated is a uniform discharge, and under typical operating conditions contains no filamentary discharges observed in corona discharge. The absence of filamentary discharge results in a more uniform treatment effect, and is less damaging to the substrate. Additionally, APP provides both activation and deposition processes. The use of helium to generate the APP, rather than ambient air used in CDT, allow more versatile chemistries to be deposited. Other atmospheric pressure plasma systems incorporate air into their process, and as such limit to oxidative chemistry.

2.3 PLASMA TREATMENT OF SILOXANE

2.3.1 Hydrophobic recovery of siloxanes following exposure to plasma

Of great interest in the plasma treatment of siloxane is the effect known as hydrophobic recovery. This phenomenon describes the return from a wettable, oxidised siloxane to the more typically observed hydrophobic, polymeric siloxane structure.

There are several key papers in the literature that describe hydrophobic recovery, and several researchers have used a variety of analytical tools (both surface sensitive and bulk) to evaluate the changes, with the aim of proposing a mechanism.

In 1975, a Dow Corning internal report by Lee and Homan[6] suggested that a possible mechanism of hydrophobic recovery was through condensation of silanol species present on the surface of the silicone after electrical discharge. This hypothesis is applicable to treatment of silicone elastomers by helium plasma treatment, as the same species are generated through radical attack. For example, as shown in **Scheme 2**:

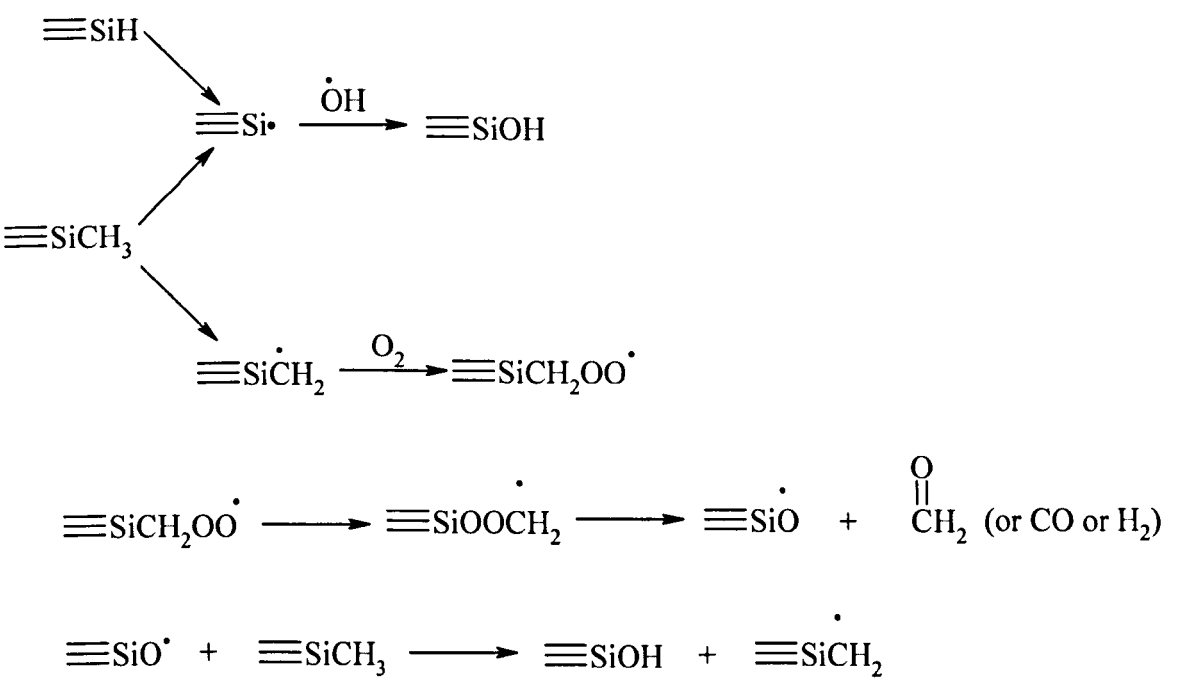

Scheme 2: Formation of silanol species through radical attack of Si-Me or Si-H groups

The paper states that the rate of recovery is based on the reactivity of the –OH functionality. This will be dependent on the other substituents on the Si atom to which the –OH is bonded. A further mechanism for hydrophobic recovery is also suggested:

migration of chain segments from the bulk of the material to the surface. This will be driven by the thermodynamic need for the surface to obtain the lowest energy surface configuration; the high-energy oxidised PDMS would prefer to be covered by a layer of low surface energy PDMS.

Lee and Homan further expanded the hypothesis of the formation of a thin fluid film on the surface of the activated siloxane elastomer in a subsequent internal report[7]. Here, an explanation is given for the formation of cracks in the surface of the siloxane caused by corona discharge treatment. Crosslinking of the surface caused by recombination of radicals create a surface layer that is subject to internal stresses. These stresses may be relieved by cracking, through which PDMS may migrate from the bulk. They believed that this thin fluid film prevented the formation of further Si-OH in fresh cracks, resulting in a hydrophobic surface, maintenance of which was the aim of their study. Such cracking of the surface is mentioned in many publications on the subject, and is illustrated in Figure 2-1, where AFM micrographs clearly show the formation of cracks in the smooth surface of a cured siloxane elastomer that had been plasma treated to excess.

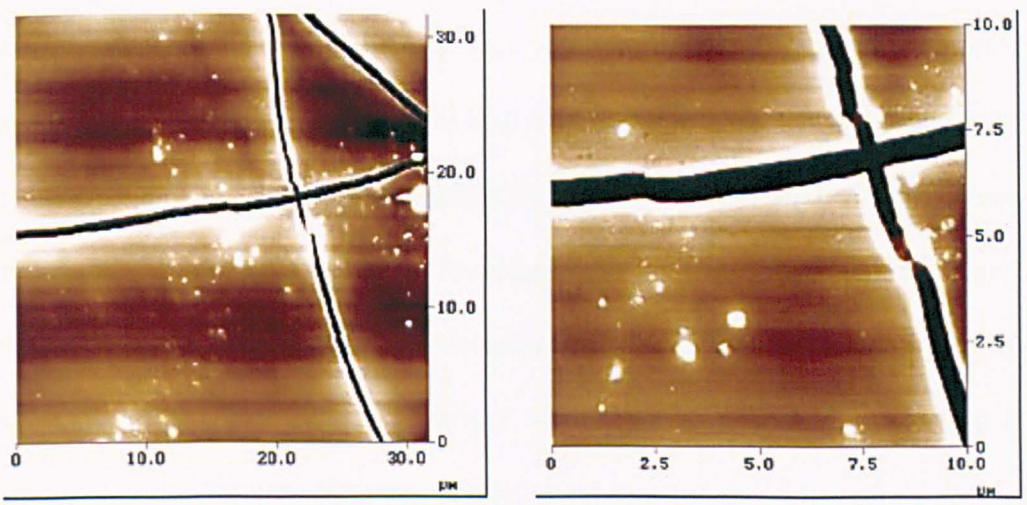

Figure 2-1: TappingMode ® AFM images of the surface of cured silicone after excessive (30s, 7.16W) plasma treatment whilst sample was under tension. Maximum height (white areas = 50 nm)

A good overview of all the possible mechanisms of hydrophobic recovery is provided by Owen *et al*, initially in a DC internal report[8], and later elsewhere[9]

- Reorientation of surface hydrophilic groups away from surface
- Migration of treated chains from surface to bulk
- Migration of untreated polymer chains from the bulk to the surface
- Loss of volatile, oxygen-rich or other polar species to the atmosphere
- Surface silanol condensation
- Changes in surface roughness
- External contamination of the polymer surface

Subsequent research[10-12] has narrowed this list of possible mechanisms down to two major ones: the migration of PDMS from the bulk of the sample to the surface, and the reorientation, or overturn, of active species at the surface. Both these mechanisms are driven by the desire of the system to reach an equilibrium state by minimising the surface free energy.

The migration mechanism is proven to occur by comparing the elemental composition of the surface using both grazing-angle and normal-angle XPS. Grazing angle XPS is more surface sensitive than normal angle XPS, with the former analysing the outermost 1-2nm of the surface, and the latter investigating ~8nm into the sample. Kim *et al* report that the outermost surface is less oxidised than the slightly deeper thin film that normal angle XPS investigates. However, since extracted samples recovered at the same rate as non-extracted samples, it is believed that pre-existing mobile species are

not the dominant diffusing species, but that the treatment process itself may generate mobile species through chain scission of the polymer during activation.

The overturn mechanism is thought to be unlikely in this scenario, since the formation of the highly crosslinked oxidised network will be less able to reorient. Instead, reference is made to work by Morra *et al*[13] who interpreted a lower advancing contact angle of water and a higher receding contact angle of water as being due to decreased orientational freedom. They believed this was a result of ageing causing a more rigid backbone caused by crosslinking by silanol condensation.

It has also been observed that the dominant mechanism of hydrophobic recovery may also be dependent on the specimen type, and also on the extent of treatment. For example, in their work on siloxane elastomers exposed to electrical discharge, Owen *et al*[14] showed different dominant mechanisms of recovery for extracted elastomers, versus those which had not been extracted, and also between samples that had been treated at low intensity, versus those treated at high intensity. Their findings may be summarised as follow:

- For extracted samples
    - At low power discharges, oxidation of the methyl groups attached to silicon occurs. Slower recovery is observed, which is assigned to reorientation as opposed to migration
    - At higher power discharges, accelerated recovery is observed, suggesting hydrophobic recovery is due to migration of in-situ formed low molecular weight species
- For non-extracted samples

- The key mechanism at low discharge is migration of pre-existing LMW PDMS from the bulk to the surface
- At higher discharges, again, hydrophobic recovery is dominated by the in-situ formation of LMW species

2.4 PLASMA POLYMERISATION

2.4.1 Plasma polymerisation of siloxanes at low pressure

The majority of plasma polymerisation of siloxanes has been carried out at low pressure, using gaseous or vapour precursors. The precursors most frequently discussed in the literature are hexamethyldisiloxane (HMDSO), tetraethoxysilane (TEOS), tetramethoxysilane (TMOS), tetramethyldisiloxane (TMDSO), and SiH_4, reflecting the need to use small molecules, easily converted to a gas or vapour[15-18]. The work has tended to focus on deposition to achieve barrier properties.

2.4.2 Plasma polymerisation of siloxanes at atmospheric pressure

Dielectric barrier discharges have been used to deposit siloxane coatings at atmospheric pressure[19-21]. These papers have also used small molecule siloxanes as the precursors: TMS, TEOS, SiH_4, HMDSO and hexamethyldisilazane (HMDSN). Recent developments using atmospheric pressure glow discharge have enabled low molecular weight cyclic siloxane polymers, octamethylcyclotetrasiloxane (OMCTS) and tetramethylcyclotetrasiloxane (TMCTS) to be deposited to achieve siloxane coatings with tunable chemistries[22]. TEOS, HMDOS and SiH_4 have also been used as precursors for deposition using atmospheric pressure glow discharge[23,24]

2.5 REFERENCES

[1]Noll, W., *Chemistry and technology of silicones'* Academic Press, New York, 1968

[2] Ranney, M.W., *Silicones Vols 1+2*, Noyes Data, Park Ridge, NJ, 1977

[3] VonEngle, A.; Seeliger, R.; Steenbeck, M., 'On the glow discharge at high pressure', *Z. Phys.* **85**, 144-160

[4] Kanazawa, S.; Kogoma, M.; Moriwaki, T.; Okazaki, S., 'Stable glow discharge plasma at atmospheric pressure', *J. Phys. Appl. Phys.*, **21**, 838 - 840

[5] Massines, F.; Rabehi, A.; Decops, P.; Ben Gadri, R.; Segu, P.; Mayoux., C., 'Experimental and theoretical study of a glow discharge at atmospheric pressure controlled by dielectric barrier discharge', *J. Appl. Phys.*, **83**(6), 1998, 2950 - 2957

[6] Lee, C.-L.; Homan, G.R., 'Protective coatings for high voltage insulators, Part I. Role of DC 1107 in DC 96-083 silicone adhesive', *Dow Corning Internal Report # 1975-I0030-4425*

[7]Lee, C.-L.; Homan, G.R., 'Protective coatings for high voltage insulators, Part II. Thin fluid film hypothesis.' *Dow Corning Internal Report # 1975-I0030-4430*

[8]Smith, P.J.; Owen, M.J.; Holm, P.H.; Fritz, J.L.; Li, C.-T., 'Analysis of plasma and corona modified poly(dimethylsiloxane) surfaces', *Dow Corning Internal Report # 1991-I0000-36687*

[9] Kim, J.; Chaudhury, M.K.; Owen, M.J., 'Hydrophobicity loss and recovery of silicone HV Insulation', *IEEE Transactions on Dielectrics and Electrical Insulation*, **6**(5), 1999

[10] Kim, J.; Chaudhury, M.K.; Owen, M.J., 'Hydrophobicity Loss and Recovery of Silicone High Voltage Insulators', *Dow Corning Internal Report # 1999-I0000-47488*

[11] Hillborg, H.; Gedde, U.W., 'Hydrophobicity recovery of polydimethylsiloxane after exposure to corona discharges', *Polymer*, **39**(10), 1998

[12] Hillborg, H.; Gedde, U.W., 'Hydrophobicity changes in silicone rubbers', *IEEE Transactions on Dielectrics and Electrical Insulation*, **6**(5), 1999

[13] Morra, M.; Occhiello, E.; Marola, R.; Garbassi, F.; Humphrey, P.; Johnson, D., 'On the ageing of oxygen plasma-treated polydimethylsiloxane surfaces', *J. Coll. Int. Sci.*, **137**(1), 1990

[14] Owen, M.J.; Chaudhury, M.K.; Kim, J., 'Study on Hydrophobic Recovery Mechanisms of Polydimethylsiloxane Elastomers Exposed to Different Intensity Partial Electrical Discharges', *Dow Corning Internal Report # 2000-I0000-48824*

[15] Gaur, S.; Vergason, G., 'Plasma polymerisation: Theory and Practice', *Society of Vacuum Coaters: 43rd Annual Technical Conference Proceedings*, 2000, 267 - 271

[16]Favia, P.; Creatore, M.; Palumbo, F.; Colaprico, V.; d'Agostino, R. 'Process control for plasma processing of polymers', *Surface and Coatings Technology*, **142-148**, 2001, 1-6

[17] Itani, T.; Fukuyama, S., 'Low temperature synthesis of plasma TEOS SiO_2', *Mat. Res. Soc. Symp. Proc.*, **446**, 1997, 255 - 259

[18] Weikart, C.M.; Miyama, M.; Yasuda, H.K., 'Surface modification of conventional polymers by depositing plasma polymers of trimethylsilane and of trimethylsiloxane/O_2', *Journal of Colloid and Interface Science*, **211**, 1999, 28 – 38

[19] Thyen, R.; Weber, A.; Klages, C.-P., 'Plasma-enhanced chemical-vapour-deposition of thin films by corona discharge at atmospheric pressure', *Surface and Coatings Technology*, **97**, 1997, 426 - 434

[20] Gherardi, N.; Martin, S.; Massines, F., 'A new approach to SiO_2 deposit using a N_2-SiH_4-N_2O glow dielectric barrier-controlled discharge at atmospheric pressure' *J. Phys. D: Appl. Phys.*, **33**, 2000, L104 – L108

[21] Schmidt-Szalowski, K.; Rzanek-Boroch, Z.; Sentech, J.; Rymuza, Z.; Kusznierewicz, Z.; Misiak, M., 'Thin films deposition form hexamethyldisiloxane and hexamethyldisilazane under delectric-barrier discharge conditions', *Plasmas and Polymers*, **5**(3/4), 2000, 173 - 190

[22] Ward, L.J.; Schofield, W.C.E, Badyal, J.P.S.; Goodwin, A.J.; Merlin, P.J., 'Atmsospheric pressure glow discharge deposition of polysiloxane and SiO_x films', *Langmuir*, **19**, 2003, 2110 - 2114

[23] Sawada, Y.; Ogawa, S.; Kogoma, M., 'Synthesis of plasma-polymerised tetraethoxysilxane and hexamethyldisiloxane films prepared by atmospheric pressure glow discharge', *J. Phys. D: Appl. Phys.*, **28**, 1995, 1661 - 1669

[24] Massines, F.; Gherardi, N.; Sommer, F., 'Silane-based coatings on polypropylene, deposited by atmospheric pressure glow discharge plasmas', *Plasmas and Polymers*, **5**(3/4), 2000, 151 - 171

CHAPTER 3

METHODS AND MATERIALS

3.1 INTRODUCTION

In this chapter, the corona discharge and atmospheric pressure plasma apparatus used to generate modified surfaces are introduced. This section deals specifically with the apparatus; the means by which coronas and plasmas are formed were discussed in *Chapter 2*. In addition, the basic principles of each of the techniques used to characterise the modified surfaces, following both corona discharge and atmospheric pressure plasma treatment, and following deposition of siloxane coatings, are discussed. X-ray photoelectron spectroscopy (XPS), atomic force microscopy (AFM) and contact angle measurements are a complementary range of surface sensitive analytical techniques essential to understanding the effect of surface modification on the substrate. The three techniques provide the researcher with information about the surface chemistry, topography and surface energy. Experimental details about the equipment are also presented in this section.

Finally, the molecular structures and sources of the substrates and precursors utilised in this work are presented. Polypropylene and poly(ethylene terephthalate) films and poly(dimethylsiloxane) and poly(hydrogenmethylsiloxane) were the materials used.

3.2 CORONA DISCHARGE TREATMENT

Corona discharge treatment (CDT) was carried out on a GX10 Corona generator, manufactured by Sherman Treaters (Oxon, Thame, United Kingdom). The GX10 is a bench-top dielectric barrier discharge instrument, with an air gap of ~ 3 mm between the electrode and the sample. The electrode width was 0.4 m. The corona generator power

supply operates at a maximum power of 1.0 kW, with a frequency of 20 kHz ± 5%. The speed of treatment could be varied between 5 and 25 $mmin^{-1}$.

3.3 DCPS ATMOSPHERIC PRESSURE GLOW DISCHARGE SYSTEM

Dow Corning Plasma Solutions (DCPS) Mark I apparatus was used to prepare deposits on flexible substrates, operating in reel-to-reel conditions[1,2]. The plasma source utilizes parallel plate technology to generate a glow discharge plasma. The DCPS Mark I apparatus used in this study comprises a single cell with two plasma zones, each 100 mm wide. The first plasma zone is purely for activation; the second also allows deposition. The electrodes are aluminium fixed to a glass plate set in a polyethylene housing. Flowing water is used to both cool the electrodes, and also provides a more homogeneous plasma. The apparatus is enclosed in a unit that acts both as a Faraday cage, and additionally allows extraction during operation.

3.3.1 Power Supply

A Huttinger (Freiburg, Germany) TIG 10 radio-frequency generator with a maximum power output of 10 kW, and frequency of 20-100 kHz was used as the power supply. Typical operating conditions are at a voltage of 5-10 kV at a frequency of 30-50 kHz.

3.3.2 Gas Control

The gas is controlled using Celerity (Kinetics) 7300 mass flow controllers with Profibus protocol, enabling flow control independent of pressure and temperature. Helium flowrate can be varied between 0 and 30 slm, and oxygen can be varied between 0 and 1.5 slm.

3.3.3 Precursor Control

The precursor is introduced as an atomised liquid directly into the glow discharge. Atomised liquid is generated via an ultrasonic nebuliser such as the Sono-tek, 8700-120[3]. The nozzle frequency is 120 kHz, with variable flowrates between 0 and 2400 $\mu Lmin^{-1}$. The precursor is delivered to the nozzle via temperature-controlled tubing from a syringe pump with automatic flowrate control.

A photograph of the Dow Corning Plasma Solutions Mark I is shown in Figure 3-1, viewed from the perspective of the reel with a cross-sectional view presented schematically in Scheme 1.

Figure 3-1: Photograph of the DCPS Mark I atmospheric pressure glow discharge apparatus taken from the perspective of the reel

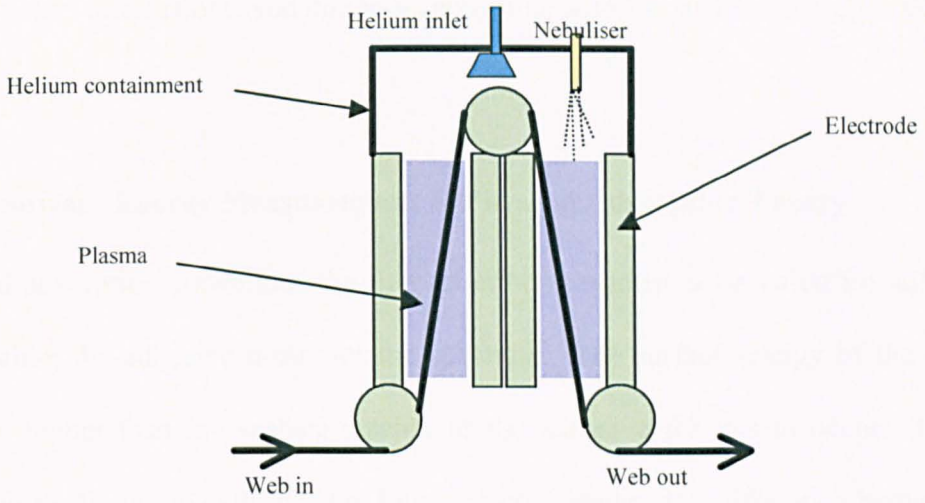

Scheme 1: Cross-sectional schematic of Dow Corning Plasma Solutions Atmospheric Pressure Plasma Liquid Deposition apparatus

3.4 CONTACT ANGLE MEASUREMENTS

3.4.1 Adsorption Theory

Surface modification techniques such as corona discharge and atmospheric pressure plasma treatment are often carried out as a means improve adhesion to plastic films. It is well established that one of the mechanisms of adhesion is adsorption. This proposes that, provided sufficiently intimate contact is achieved at an interface, materials will adhere because of the interatomic and intermolecular forces that are established between the two surfaces[4,5]. To some extent, adsorption will always be involved in an adhesive bond.

Forces that are involved in adsorption theory are often divided into primary and secondary forces, based on the bond energies involved. Primary forces include chemical bonds, such as ionic, covalent and metallic bonds, which are associated with

chemical adsorption (or chemisorption) theory. Physical adsorption (or physisorption) theory is associated with secondary forces. These include dispersion (London) forces, dipole (polar) interactions, and donor-acceptor interactions, such as hydrogen bonds.

3.4.2 Surface Energy Measurements & Physical Adsorption Theory

Physical adsorption constitutes the first criterion that must be satisfied for adhesion to be possible: the adhesive must wet the substrate. The surface energy of the substrate must be higher than the surface tension of the adhesive for this to occur. However, since plastic films typically display low surface energies, the difference between these energies is often not great enough to facilitate wetting. It is for this reason that surface modification techniques are employed: the surface energy of the substrate is raised, and the adhesive can then wet the substrate.

The likelihood of an adhesive wetting the substrate may be evaluated by measurement of the surface energy of the substrate. This is achieved by measurement of the angle formed by a sessile drop of a known liquid on the substrate, known as the ***contact angle***, Figure 3-2. This angle is then converted to surface energy by the use of one of several equations, and provides a measure of the extent of surface modification.

The term ***surface free energy*** is used in relation to the solid surface, whereas the ***surface tension*** is used to refer to liquids. However, these terms are often used interchangeably, since although their units are different (mJm^{-2} versus mNm^{-1}, respectively), their magnitudes are equal, as both are a measure of the force by which molecules cling to each other.

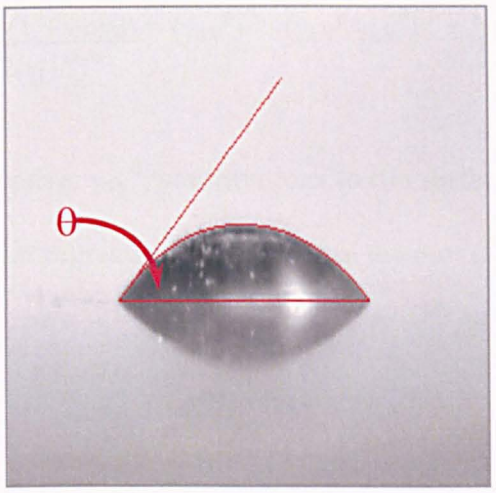

Figure 3-2: A liquid drop at equilibrium on a solid substrate. The contact angle made by the drop is highlighted in red

There are a number of different mathematical approaches used in the calculation of surface energy. None of these are absolute, and so care must be taken to report the contact liquids used, and the mathematical approach taken. In this work, contact angles were converted to surface energy using the geometric mean approach of Owens and Wendt[6], and Kaelble[7].

$$\gamma_{LV}(1 + \cos\theta) = 2(\gamma^{d}_{LV}\gamma^{d}_{SV})^{1/2} + 2(\gamma^{p}_{LV}\gamma^{p}_{SV})^{1/2} \qquad [1]$$

where:

θ = contact angle (degrees)
γ_{LV} = surface tension of the test liquid ($mN.m^{-1}$)
γ_{LV}^{p} = polar contribution to the surface tension of the test liquid ($mN.m^{-1}$)
γ_{LV}^{d} = dispersive contribution to the surface tension of the test liquid ($mN.m^{-1}$)
γ_{SV}^{p} = polar contribution to the surface energy of the solid substrate ($mJ.m^{-2}$)
γ_{SV}^{d} = dispersive contribution to the surface energy of the solid substrate ($mJ.m^{-2}$)

The subscripts S, L, and V correspond to solid, liquid and vapour phases respectively while the combination of letters, e.g., SV, corresponds to the solid / vapour interface.

The Owens-Wendt/Kaelble equation [1] is more generally known as the Owens-Wendt equation, and can be rewritten in the linear form of $y = ax + b$:

$$\frac{\gamma_{LV}(1+\cos\theta)}{2(\gamma_{LV}^{d})^{1/2}} = (\gamma_{SV}^{p})^{1/2} \cdot (\gamma_{LV}^{p}/\gamma_{LV}^{d})^{1/2} + (\gamma_{SV}^{d})^{1/2} \quad [2]$$

The polar, γ_{SV}^{p}, and dispersive, γ_{SV}^{d}, contributions to the surface energy of the substrate are calculated using a linear regression analysis from the plot (Figure 3):

$$\frac{\gamma_{LV}(1+\cos\theta)}{2(\gamma_{LV}^{d})^{1/2}} = f(\gamma_{LV}^{p}/\gamma_{LV}^{d})^{1/2} \quad [3]$$

whereby the slope is equal to $(\gamma_{SV}^{p})^2$ and the intercept on the y-axis is equal to $(\gamma_{SV}^{d})^2$. Since the surface energy of the solid is described by $\gamma_S = \gamma^p + \gamma^p$, γ_S may be simply calculated by:

$$(\text{slope})^2 + (\text{intercept})^2 = \text{surface energy of the substrate} \quad [4]$$

γ_{LV}, γ^{p}_{LV} and γ^{d}_{LV} are known quantities available from several references, Table 3-1. Θ is the measured value.

Liquid (reference)	γ^p (mNm^{-1})	γ^d (mNm^{-1})	γ^{tot} (mNm^{-1})	$\gamma_{LV}/2(\gamma_{LV}^{d})^{1/2}$	$(\gamma_{LV}^{p}/\gamma_{LV}^{d})^{1/2}$
Water ([8])	51.0	21.8	72.8	7.796	1.53
Formamide ([9])	29.5	28.7	58.2	5.432	1.01
Diiodomethane ([8])	2.3	48.5	50.8	3.647	0.22
Ethane-1,2-diol ([9])	17.4	27.3	47.8	4.574	0.80
1-Bromo-naphthalene ([8])	0	44.6	44.6	3.339	0
Benzyl alcohol ([9])	9.8	29.2	39.0	3.609	0.58
Hexadecane ([9])	0	27.1	27.1	2.603	0

Table 3-1: Surface tension and its polar and dispersive contributions of a selection of liquids often used to determine the surface energy of solids

Contact angle measurements were carried out using 1.5 μL drops of HPLG grade water as the probe liquid, with an image captured 20 seconds after the drop was placed on the film. The left- and right-hand angles of at least three drops were measured, and used to provide an average value. Measurements were completed within 20 minutes of film treatment. The instrumentation used were as follow:

Following APGD/APPLD. Contact angles were measured on the modified side of the film using a KSV 2000 video contact angle apparatus. The contact angle between the probe liquid and the substrate was measured using a Young-Laplace curve-fit. approximation.

Following CDT. An Advanced Surface Technology video contact angle VCA 2500 system was used. In this case, the contact angle between the probe liquid and the substrate was measured by placing five cursor points around the image of the drop, and fit using a Young-Laplace

In each case, the apparatus used to measure the contact angles comprised a movable stage, automated volume syringe dispenser and an image capturing system.

3.4.3 Surface Chemistry & Chemical Adsorption Theory

Enhancement of adhesion *via* this mechanism occurs via the formation of covalent, ionic or hydrogen bonds across an interface. The effect of corona discharge or atmospheric pressure plasma on the substrate surface chemistry was evaluated using X-ray photoelectron spectroscopy. This technique is discussed in detail in the following section.

3.5 X-RAY PHOTOELECTRON SPECTROSCOPY

3.5.1 Introduction

Manipulation of the photoelectric effect (Hertz, 1887) in developing a new technique for determining the elemental composition and chemical composition of surfaces began in the 1940's. Two groups played key roles in this development: Steinhard and Serfas (Lehigh University, USA) and Siegbahn (Upsala, Sweden). From 1955 – 1970, Seigbahn's continued research on the topic, leading to his being awarded the Nobel Prize in 1981, led to the observation of the chemical shift effect, and revolutionised what he termed ESCA, or ***Electron Spectroscopy for Chemical Analysis***. This term is used interchangeably with XPS, or ***X-ray Photoelectron Spectroscopy***. Over the last 30 years, commercial instruments have become available, and whilst not commonplace, they are now found in many academic, contract analytical and industrial research facilities.

3.5.2 The Photoelectric Effect

X-ray photoelectron spectroscopy (XPS) involves irradiation of a sample under ultra-high vacuum with soft X-rays, and the energy analysis of photoemitted electrons that are generated close to the sample surface, Figure 3-3.

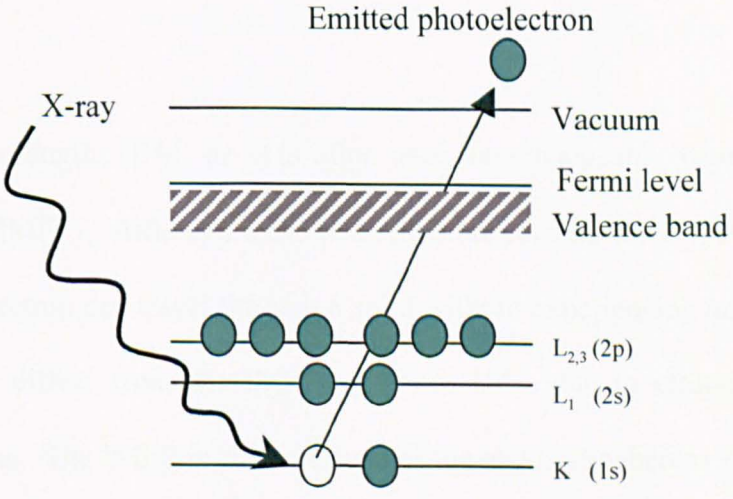

Figure 3-3: Schematic indicating emission of a photoelectron from an atom irradiated with X-ray photon. The energy of the ejected electron identifies the chemical nature and environment of the atom.

The electrons are emitted with a measurable kinetic energy, E_K. However, as the kinetic energy of the photoelectrons is dependent on the photon energy of the X-ray source, it is more convenient to convert this to a binding energy, E_B. The binding energy is used to unambiguously identify the element, and atomic energy level from which the electron has been emitted. The terms are linked by the Einstein relation, shown below:

$$E_B = h\nu - E_K - W$$

where E_B = binding energy, E_K = kinetic energy, $h\upsilon$ is the X-ray photon energy, and W is the spectrometer work function. The computing system of the spectrometer calculates E_B from the other three quantities, which are either known or measurable.

3.5.3 Depth of Analysis

One of the most interesting features of data captured by XPS is its surface sensitivity. The depth of analysis of XPS varies up to a maximum of ~10 nm. It is dependent on the kinetic energy of the electrons being investigated, and is related to the electron attenuation length (λ).

The term 'effective attenuation length' (EAL or λ) is often used interchangeably with the 'inelastic mean free path' (IMFP). Although these two terms are related, the IMFP refers to the distance that an electron can travel through a solid without experiencing an inelastic collision. The EAL differs from the IMPF by about 10%, due to elastic scattering of the signal electrons. The IMFP is characteristic of the material, whereas λ additionally varies due to instrument configuration and film thickness.

The intensity of the emitted electrons is related to the effective attenuation length through the Beer-Lambert equation:

$$I = I_o \exp(-d / \lambda\cos\theta)$$

Where I = intensity of electrons emitted from depths > d

I_o = intensity of electrons from infinitely thick, uniform substrate

d = depth of analysis

λ = effective attenuation length

θ = angle of analysis with respect to sample normal

The EAL used in calculations, where required, was obtained from the NIST database[10]

3.5.4 Spectral Interpretation

Survey spectra and photoelectron peaks

A plot of electron energy against intensity produces what is commonly known as a widescan, or survey spectrum. Each photoelectron peak must be identified using tabulated data such as those in Appendix 7 of Briggs and Seah's book[11]. The intensity of these core level peaks can then be quantified using relative sensitivity factors to obtain the relative concentration of the elements present (with the exception of hydrogen and helium). An example of a survey spectrum generated from a fluoropolymer is presented in Figure 3-4a.

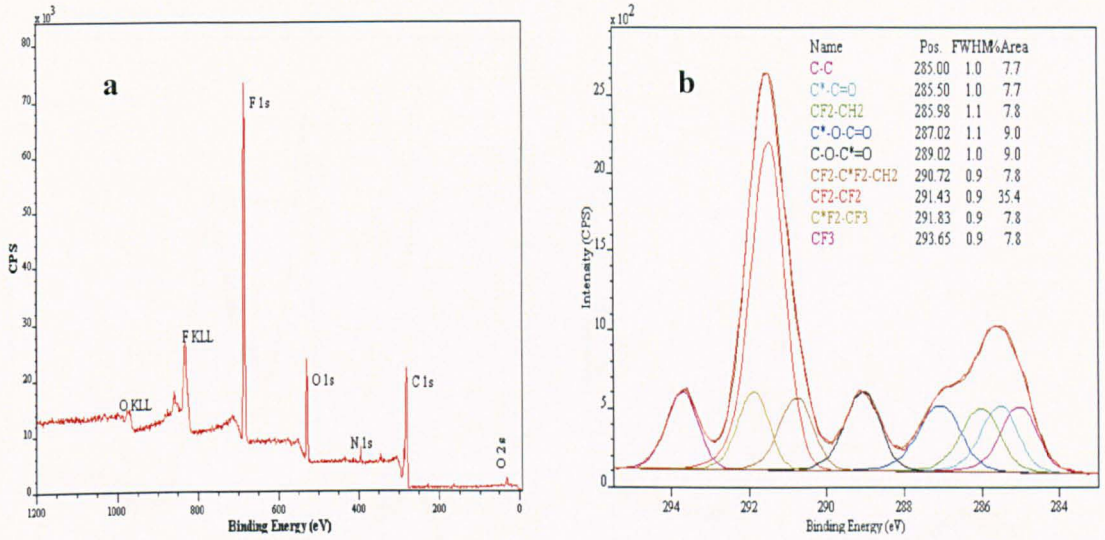

Figure 3-4: Example of a) survey spectrum of a fluoropolymer indicating which elements are present, b) high-resolution spectrum of the C 1s corer level heptadecaflurodecyl acrylate, whose shape can be used to identify which functional groups are present

Auger electron and valence band peaks

In addition to peaks relating to electrons being emitted from core levels (e.g. F 1s, O 1s, N 1s, C 1s), the spectrum has additional peaks caused by the emission of Auger electrons (O KLL, F KLL). These transitions occur when relaxation of the excited atom occurs *via* rearrangement of electrons in the core levels. The core hole is filled by an electron from a higher energy level, with the corresponding ejection of an electron from the higher level.

Additional features are also observed in the low energy region (0 - 30 eV), relating to the valence band, e.g. O 2s, C 2s. This region provides useful information for samples with identical core level spectra. For example, this can be used to differentiate between polyethylene and polypropylene, both of which only contain carbon, and thus have identical C 1score level spectra

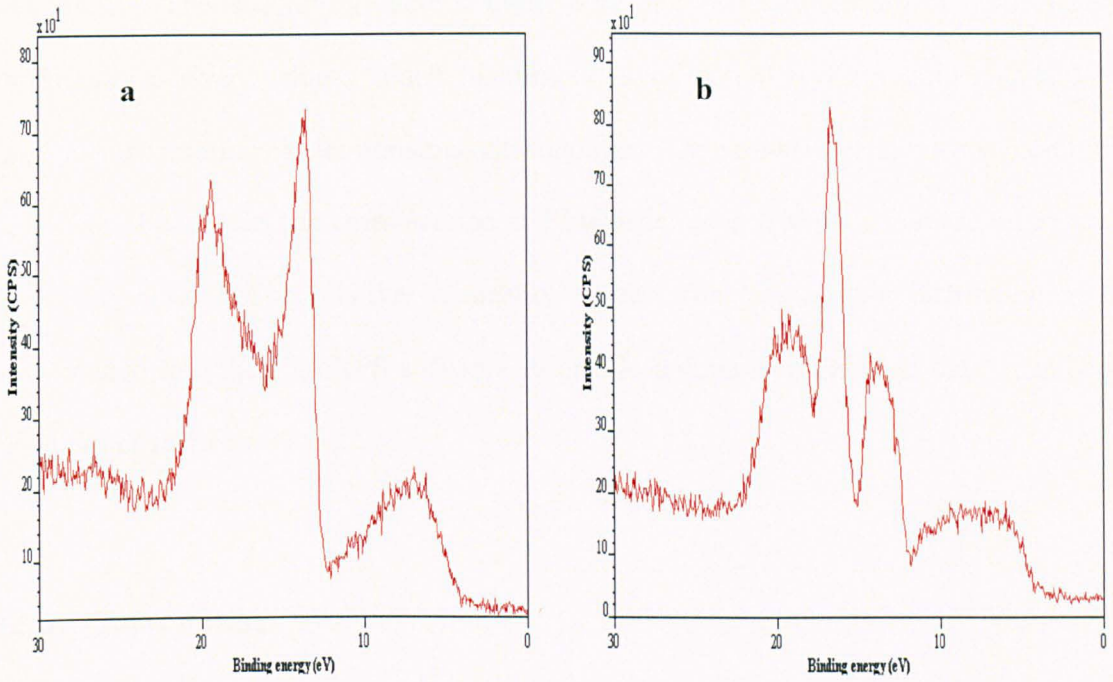

Figure 3-5: Valence band spectra for a) poly(ethylene) and b) polypropylene enabling differentiation that is not possible by examination of the C 1s core level [12]

Chemical state information

More in-depth information can be obtained by carrying out high-resolution XPS. This involves scanning over a narrower energy region, and provides information about the chemical state of the element under investigation. For example, the oxidation state of the element will cause a slight variation in the measured binding energy. This ***binding energy shift*** is also observed when the element under investigation is bonded to a more electronegative element. This is most clearly observed for carbon (C 1s); its bonding to oxygen, nitrogen or fluorine all cause predictable variation in the observed spectrum. An example of the C 1s core level of a fluoroacrylate material is presented in Figure 3-4b. A detailed discussion on the curve-fitting procedure used to assign chemical functionalities will follow.

3.5.5 Data analysis

Quantification of the elemental composition of the films was carried out using both the Kratos Axis Ultra Vision2 software, and later CasaXPS software. A linear background

was used. The sensitivity factors used were the standard Kratos Vision library empirically derived values. Each instrument is calibrated using a gold standard to account for variations in its transmission function. The sensitivity values also combine the effect of photoelectric cross-section and inelastic mean free path, and are referenced to F 1s = 1.00. The relative sensitivity values from the Kratos instrument were downloaded into the CasaXPS software to enable comparison between data quantified using either software.

3.5.6 Curve-fitting

The linewidth, or full width at half maximum (FWHM), ΔE, comprises contributions from

a) the linewidth of the X-ray source
b) the analyser resolution
c) the intrinsic core level FWHM

In addition, these contributions also have associated lineshapes: Lorentzian for the source, Gaussian for the analyser, and Lorentzian with some tailing for the core level, resulting in a hybrid lineshape. In this work, the line-shapes of synthetic components fitted were restrained to be GL(30)T(2.3) in CasaXPS nomenclature, which corresponds to a Gaussian/Lorentzian ratio of 70/30, and an asymmetry index of 0.1776.

An exception to this is the composite line shape used to fit 'as received' polypropylene film. This was used as an alternative to a vibrational progression of four peaks with the lineshape mentioned above. The method for curve-fitting the C 1s core level for polypropylene film following corona discharge treatment or atmospheric pressure glow discharge is described in detail in *Chapter 4*.

Similarly, *Chapter 5* describes in detail the methodology used for curve-fitting the O 1s, C 1s, and more importantly, the Si 2p core levels for siloxane materials. The Si 2p core level comprises a doublet resulting from spin orbit splitting.

3.5.7 Spin Orbit Coupling

Spin orbit splitting is observed in the p, d, or f energy levels of an atom, and results from coupling of the electronic spin and angular momentum. Also known as *j-j* coupling, the term describes the total angular momentum of an isolated electron. As $j = l + s$, it can take values of $^1/_2$, $^3/_2$, $^5/_2$ etc., depending on the angular momentum.

In all cases, a self-consistent manner was used in all the curve-fitting processes, with every attempt to match, for example, the concentration of oxidised functionalities to the concentration of oxygen incorporated by CDT or APGD, or the intensity of C-Si synthetic peaks in the C 1s core level to the concentration of C-Si species determined from the Si 2p core level.

3.5.8 Instrumentation

X-ray Sources

A number of X-ray sources, both achromatic and monochromated, can be chosen for use in XPS, Table 3-2. The source should be chosen such that it can excite electrons from any element in the periodic table (with the exception of helium and hydrogen). Typically, at least two anode materials will be combined in a non-monochromated dual anode on each instrument. In addition, a monochromated source is often incorporated into the instrument. Recent advances have seen the use of monochromated dual-anodes.

Element	Line	Energy (eV)	FWHM (eV)
Y	Mζ	132.3	0.47
Zr	Mζ	151.4	0.77
Mg	$K\alpha_{1,2}$	1253.6	0.7
Al	$K\alpha_{1,2}$	1486.6	0.9
Si	Kα	1739.6	1.0
Zr	Lα	2042.4	1.7
Ag	Lα	2984.4	2.6
Ti	Kα	4510.9	2.0
Cr	Kα	5417.0	2.1

Table 3-2: Possible anode materials for XPS[13]

3.5.9 Calibration and data capture

XPS was carried out on a Kratos Analytical Axis Ultra photoelecton spectrometer. The instrument is equipped with a spherical mirror analyser (165 mm mean radius HSA), an integral automatic charge neutraliser and a magnetic lens. A monochromated aluminium (Al Kα) X-ray source was used to record spectra at normal emission. The magnet linearity, water flow rates, and leakage current were checked on a three monthly basis, or after every bake, which ever was soonest. The magnet linearity check involves varying the kinetic energy, and ensuring that the measured current follows its square root function. The leakage current, determined from the Glassman power supply, is a measure of the conductivity of the water passing through the anode. The alignment of the crystal back-plane was optimised by maximising the counts, whilst minimising the FWHM of an argon sputter-cleaned silver foil. The linearity of the energy scale was also checked regularly in accordance with the instrument manual. Using the Ag foil, the 3d and MNN lines of the sample gave a difference of 547.47, which was within the prescribed limits. A nominal power of 300 W was used for all samples. A pass energy of 160 eV was used to capture wide area scans, whilst 20 eV was used to obtain the high resolution core level spectra. The 'slot' aperture was used during capture (700 x 500 μm). A step interval of 0.1 eV was used for the high-resolution spectra.

3.5.10 Charge Neutralisation

X-ray irradiation of an insulating sample, such as the plastic films used in this work, causes the sample to become positively charged due to the emission of electrons. This causes a shift in the photoelectron peak to a higher binding energy. Additionally, the peak shape can become asymmetric, and negatively affects the resolution of the peak.

The use of an achromatic source can overcome this effect by the emission of low energy electrons from the X-ray source window. However, the use of a monochromatic source, whilst offering benefits, increases this charging problem. Additionally, differential charging can occur, resulting in broader peaks, thus negating the effect of the monochromator.

These effects can be compensated for by the use of a charge neutralisation system. A source of low energy electrons (~ 0.1 eV)[14] is used to flood the sample of interest. As an excess of electrons is typically used, the peak now moves to a lower binding energy, but can be adjusted to the correct value during data processing. This is typically carried out by adjusting the position of the aliphatic C-C component to 285.0 eV.

All of the samples of interest required charge neutralisation. The charge neutralisation value was optimised to be when the signal to noise and FWHM were minimised, using a polypropylene film sample.

3.6 ATOMIC FORCE MICROSCOPY

Binnig, Quate, and Gerber invented the Atomic Force Microscope in 1986 in a collaboration between IBM- Zurich, and Stanford University. Atomic force microscopy (AFM) was derived from a collection of techniques based on scanning probe microscopy (SPM). Scanning probe microscopes have components common to all instruments, shown in Figure 3-6. One additional variation is the ability of the sample to scan, rather than remain stationary during analysis.

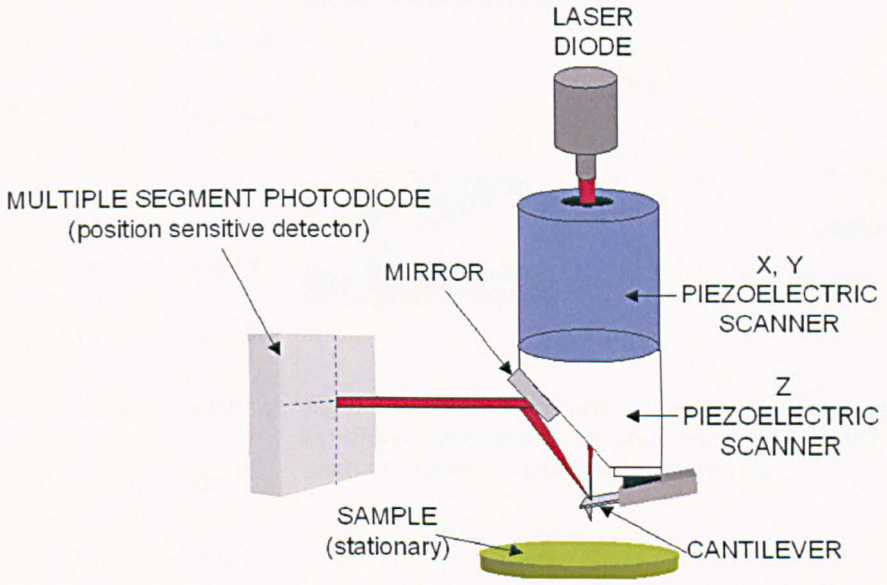

Figure 3-6: Schematic showing the components of the Dimension 3100 atomic force microscope[15]. Image presented courtesy of Drs J. Drelich and ER. Beach, Michigan Technological University

The most commonly used modes of operation in AFM are contact mode, TappingMode™, or using PhaseImaging™. In the first of these, contact mode, the probe is rastered across the surface whilst in contact. This mode provides topographical information, but is heavily influenced by adhesion and frictional properties. This mode is typically unsuitable for soft samples such as polymers as it may damage the surface.

3.6.1 TappingMode™ AFM

In TappingMode™, the cantilever is oscillated at a value close to its resonance frequency using a piezoelectric crystal. The associated amplitude is known as the 'free air' amplitude, and has a specific value. The oscillation amplitude of the cantilever varies with sample topography: as the tip is moved towards, and then into contact with a substrate, this amplitude is reduced (amplitude set-point).

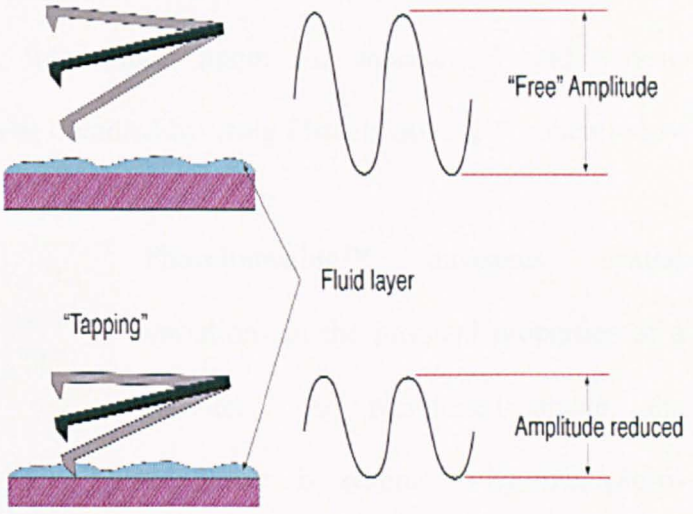

Figure 3-7: Schematic describing TappingMode™ cantilever oscillation in free air and during sample analysis. Image courtesy www.veeco.com

To ensure a reproducible measure of magnitude of the force applied during the tapping regime, the ratio of the amplitude of set-point oscillation on (a zero nm scan size) to the free oscillation was employed. This ratio is abbreviated as R_{SP}. Values of $R_{SP} = 0.8 - 1.0$ are 'light' tapping; $R_{SP} = 0.5 - 0.8$ are 'medium' tapping; $R_{SP} < 0.5$ are 'hard' tapping.

As the tip is then scanned in intermittent contact with the substrate, the amplitude of set-point oscillation will vary with topography. For example, as the tip passes over a region of elevated height, the cantilever oscillation decreases. Conversely, in a depression, the cantilever oscillation can increase, towards that of the cantilever in free air. A feedback

loop adjusts the distance between the tip and the substrate in order to maintain R_{SP} as a constant. These changes are converted to a 3 dimensional image.

In this mode, the force applied to the surface of the substrate is very small, and since no lateral movement occurs, very little or no damage is caused to the surface. This mode is idea for analysis of polymers, and other soft materials. In addition to height information provided using this technique, information about the mechanical and adhesive properties of the sample may also be obtained by using PhaseImageing™ concurrently.

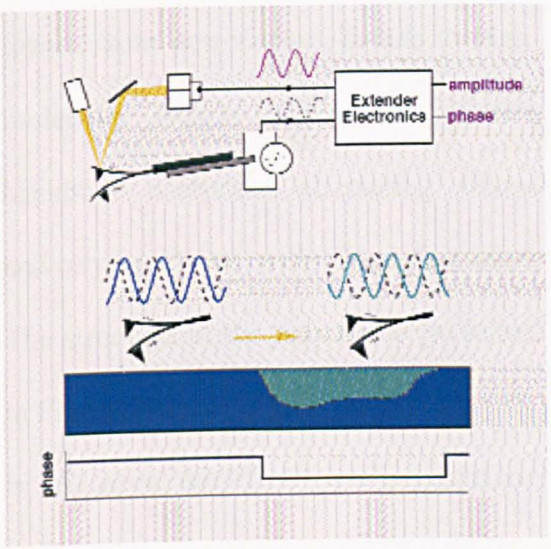

Figure 3-8: Phase imaging measures the phase lag of the cantilever oscillation (solid wave) relative to the piezo drive (dashed wave), and is used to map spatial variations in sample properties, e.g. adhesion and viscoelasticity. Image courtesy www.veeco.com

PhaseImageing™ measures spatial variations in the physical properties of a sample. As mentioned above, the cantilever is resonated by the piezo-electric driver, which results in an oscillation curve. The phase of the cantilever oscillation is monitored relative to the phase of the piezo driver. The measured lag is recorded, and its value provides a measure of variations such as adhesion and viscoelasticity.

In this research, AFM was carried out on a Digital Instruments Dimension 3100 instrument in TappingMode™ using an ultra-sharp silicon tip. Both the height and phase images of scanned areas 1 x 1 μm, 5 x 5 μm, and 25 x 25 μm were captured, using both 'light' and 'medium' tapping. The root-mean-square roughness was also evaluated. Images have been captured with a low tapping force, this represent an R_{SP}

value of 0.7 – 0.8. The R_{SP} values are 0.5 –0.6 where medium force tapping has been utilised in image capture. Automatic plane-fit image manipulation and 'flattening' have been carried out on all images to an order of 1.

3.7 MATERIALS

3.7.1 Poly(dimethylsiloxane)

Poly(dimethylsiloxane), or PDMS, is a transparent material available in many forms, from non-viscous liquids to high-molecular weight gum. Its polymer backbone comprises alternating silicon and oxygen atoms, with CH_3 side groups. The structure of the polymer is presented in Figure 3-9

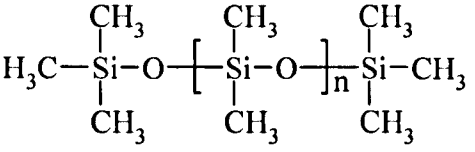

Figure 3-9: Chemical structure of poly(dimethylsiloxane)

In this work, the PDMS was in liquid form, with a viscosity of 10 cSt. The commercial name of the material is DC200 fluid, manufactured and supplied by Dow Corning Corporation.

3.7.2 Poly(hydrogenmethylsiloxane)

Poly(hydrogenmethylsiloxane), or PHMS has a similar structure to PDMS, with the exception that each methyl side group has been replaced with a hydrogen atom, Figure 3-10. This makes the precursor

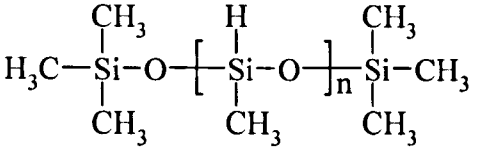

Figure 3-10: Chemical structure of poly(hydrogenmethylsiloxane)

much more reactive as the Si-H bond is more labile than the $Si-CH_3$ bond.

10cSt PHMS, manufactured and supplied by Dow Corning Corporation was the second precursor evaluated in this work.

3.7.3 Poly(propylene) film

Commercially available poly(propylene), or PP, film for food use was used in this investigation. It was 25 μm thickness film, type BS, from AB Supplies. It was not possible to obtain any information about base resin molecular weight, or additives to the film.

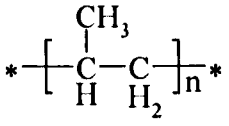

Figure 3-11: Chemical structure of polypropylene

However, no surface contamination, such as silicon or nitrogen, from processing or stabilising additives were identified by XPS.

3.7.4 Poly(ethylene terephthalate) film

25 μm thick, commercially available poly(ethylene terephthalate), or PET, film from Goodfellow, UK. As for BOPP film, no surface contamination, such as silicon or nitrogen, from processing or stabilising additives were identified by XPS

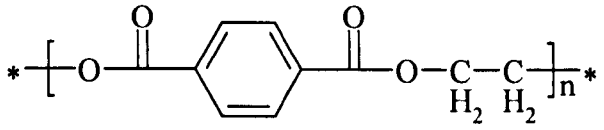

Figure 3-12: Chemical structure of poly(ethylene terephthalate)

3.8 REFERENCES

[1] Herbert A., O'Reilly F., Braddell J., Dobbyn P., PCT Patent WO 01 59809, 16th August 2001.
[2] Unpublished Dow Corning patents
[3] Goodwin A.J., Merlin P.J., Badyal J.P., Ward L., PCT Patent WO 02 28548, 11th April 2002.
[4] Kinloch, A.J., *Adhesion and Adhesives, Science and Technology*, Chapman and Hall, London, 1990
[5] Comyn, J., *Adhesion Science*, RSC Paperbacks, 1997
[6] Owens, D.K.; Wendt, R.C., 'Estimation of the surface free energy of polymers', *J. Appl. Polym. Sci.*, **13**, 1969, 1741
[7] Kaelble, D.H., 'Dispersion-polar surface tension properties of organic solids', *J. Adhesion*, **2**, 1970, 66
[8] Wu, S.; *Polymer Interface and Adhesion*, Table 4.8, Marcel Dekker Inc., New York & Basel
[9] Nobbs, J.H., Colour Chemistry Department, University of Leeds, *Personal Correspondence*
[10] http://www.nist.gov/srd/nist82.htm
[11] Briggs, D., Seah, M.P. *Practical Surface Analysis, 2nd Ed, Vol 1: Auger and X-ray Photoelectron Spectroscopy*, John Wiley & Sons, 1994
[12] Beamson, G., Briggs, D., *The XPS of Polymers Database*, SurfaceSpectra Ltd., 2000
[13] Watts, J.F.; Wolstenholme, J., *An Introduction to Surface Analysis by XPS and AES*, John Wiley and Sons, 2003
[14] Kratos Technology Notes, *The Axis Charge Balance System*, http://www.kratos.com/Agen/neutral.html
[15] E.R. Beach "Fundamental and Applied Studies of Particle-Surface Adhesion Forces Measured by Atomic Force Microscopy, M.S. Thesis, Michigan Technological University, Department of Materials Science and Technology, Houghton, MI 2001

CHAPTER 4

A COMPARISON BETWEEN THE EFFECTS OF CORONA DISCHARGE AND ATMOSPHERIC PRESSURE PLASMA TREATMENTS ON POLYPROPYLENE FILM

4.1 INTRODUCTION

Corona discharge treatment (CDT), is a surface modification technique commonly used to activate plastic films prior to adhesive bonding, printing with inks, lamination to other films, and other coating applications[1], and is the most widely used method for pre-treating polyolefin films[2]. Much work has been published on the effect of CDT on polyolefin films, and the mechanism of surface modification is now well established[3,4,5,6,7,8,9,10,11,12,13]. However, surface chemistry, morphology, and resultant surface energy, vary considerably in the numerous studies carried out. The treatment parameters used in the literature can be extreme, with treatment times ranging from seconds to minutes, and levels of oxygen incorporation being as great as 40%. Previous work is discussed, where the treatment conditions were, in energy density terms, representative of those used in industrial applications. The physico-chemical properties of the surface of untreated and corona discharge treated biaxially oriented polypropylene (BOPP) film were investigated[14] for these well-defined treatment parameters. The current work further expands on this, by comparing the level of activation obtained between biaxially oriented polypropylene film treated with corona discharge treatment (CDT) and atmospheric pressure plasma (APP). CDT was carried out in ambient air, whilst APPs were obtained using helium, a helium / oxygen, or a helium / air. Although some previous research comparing the effect of corona and plasmas have been identified[15,16], the novelty of the current study lies in the use of APP in reel-to-reel conditions. This will provide results pertinent to industrial applications. The CDT is also carried out such that the polymer substrate passes through the treatment region, compared to stationary film treatment.

Comparison of the changes in the surface physico-chemical properties of the BOPP film were investigated using a number of complementary surface analytical techniques:

contact angle measurement, X-ray photoelectron spectroscopy (XPS), and atomic force microscopy (AFM).

4.2 EXPERIMENTAL

4.2.1 Corona Discharge Treatment

The films were exposed to one pass under an electrode of width 0.4 m, in ambient air at 5 $mmin^{-1}$ (0.083 ms^{-1}). The input power was varied. The energy density (kJm^{-2}) delivered to the surface during treatment is calculated from the power (kJs^{-1}) supplied by an electrode of a given width (m) and the linear speed (ms^{-1}) of the film passing under the discharge:

$$\text{Corona Energy Density} = \frac{\text{Power delivered}}{\text{Linear speed} \times \text{electrode width}}$$

The input powers used, along with the conversion to energy density, are described in Table 4-1a.

4.2.2 Atmospheric Pressure Plasma

In this case, the films were transported through a pure helium plasma, a helium/oxygen mix (99%:1%), or a helium/air mix plasma (99%/1%), with path length of 0.5 m, at a rate of 4 $mmin^{-1}$. The addition of an electronegative gas to the helium plasma can extinguish the discharge[17]. The energetic electrons required to maintain the plasma are trapped through the formation of negative ions. To avoid this situation, the additive gas concentration was chosen to be 1%, as this led to enhanced oxidation (observed by a decrease in water contact angle on polypropylene film) with no detrimental effect on the plasma quality assessed visually. The discharge powers were varied using the same input powers as for CDT. The energy densities for APP represents the powers imparted

to the film, and are calculated from the linear speed ($mmin^{-1}$), and the electrode area, and are presented in Table 4-1b.

$$\text{APP Energy Density} = \text{Plasma Power Density x residence time of substrate in plasma}$$

$$\text{Plasma Power Density} = \frac{\text{Power delivered}}{\text{area}}$$

CDT	
Input Power (kW)	Energy density (kJm^{-2})
0.00	0
0.10	3
0.21	6.3
0.29	8.7
0.41	12.3
1.00	30

a

APP	
Input Power (kW)	Energy density (kJm^{-2})
0.00	0
0.10	15
0.20	30
0.30	45
0.40	60
1.00	150

b

Table 4-1: Input powers, and their corresponding energy densities, used in the comparison of the activation effect of corona discharge treatment and atmospheric pressure plasma

4.2.3 Contact Angle Analysis

Contact angle measurement was carried out within 30 minutes of activation by CDT / APP according to the procedure described in more detail in *Chapter 3 : Methods and Materials.* Portions of the treated films were also immersed in HPLC Grade water with no agitation for 10 seconds in order to evaluate the hydrolytic stability of the modified surface layer. Strobel *et al*[18] described no variation in measured contact angles whether samples had been immersed for a few seconds or for 24 hours. For the immersed samples, contact angle measurements were carried out after allowing the samples to dry in ambient air for 4 hours.

There are a number of different mathematical approaches used in the calculation of surface energy. None of these are absolute, and so care must be taken to report the contact liquids used, and the mathematical approach taken. In this work, contact angles

were converted to surface energy using the geometric mean approach of Owens and Wendt[19], and Kaelble[20], as described in more detail in *Chapter 3*.

4.2.4 X-ray Photoelectron Spectroscopy

The activated samples were placed under vacuum in the XPS system within 30 minutes of activation. Analysis of the first sample, according to the method described in *Chapter 3* began within approximately 2 hours of activation. Portions of the films were immersed in HPLC grade water in order to measure the retention of incorporated oxygen. The wet samples were entered into the load lock of the XPS, whereby the vacuum removed the water prior to transfer into the analysis chamber. Similar conditions were used to prepare APP treated samples for analysis by XPS. Unless otherwise described, analyses were carried out at 90° take-off angle (TOA) with respect to the sample surface.

4.2.5 Atomic Force Microscopy

Imaging of the samples using AFM was carried out immediately on the first activated sample, as described in *Chapter 3*. However, imaging of the sample would take approximately 2 hours. The samples that were awaiting analysis were stored in polystyrene petri dishes whose lids were taped on to minimise their exposure to the atmosphere. Analysis of all samples was completed within 24 hours of activation.

4.3 RESULTS AND DISCUSSION

4.3.1 Surface Energy: Influence of treatment method

The surface energy (γ) of the film and its polar and dispersive components were calculated from the contact angles of sessile drops of selected liquids deposited on the BOPP film. The choice of probe liquids is very important for the measurement of contact angles. Ideally, the probe liquid should be inert to the surface; it must neither chemically change during the measurement, nor react with the surface under investigation. In addition, the liquid drop must not dissolve molecules present on the surface that will modify its own surface tension. Previous work has reported that the use of polar probe liquids can dissolve the low molecular weight oxidised materials (LMWOM) formed on the surface of plastic films by corona treatment[8]. This would lead to inconsistencies in the values of contact angles reported, since the surface tension of the probe liquid would be lowered by the incorporation of LMWOM. However, using the pendant drop method to measure the surface tension of liquids, no significant change in the surface tension of water was found after leaving it in contact with the corona treated surface for 30 seconds[21].

In this work, water, ethane-1,2-diol and formamide were used with the method described in 4.2.3. Previous work[21] had shown that this combination of liquids most emphasised the change in the polar nature of the surface following corona treatment, which is the property of interest. The total surface energy was independent of the combination of probe liquids[21].

Figure 4-1 presents the values obtained for γ, γ^p, and γ^d plotted as a function of the corona discharge energy density. Prior to activation, the surface energy of BOPP is composed solely of a dispersive component. This is unsurprising, as BOPP, being a

hydrocarbon polymer, has no polar functional groups. As expected, both the surface energy, and the polar contribution to the surface energy, increased with increasing energy density.

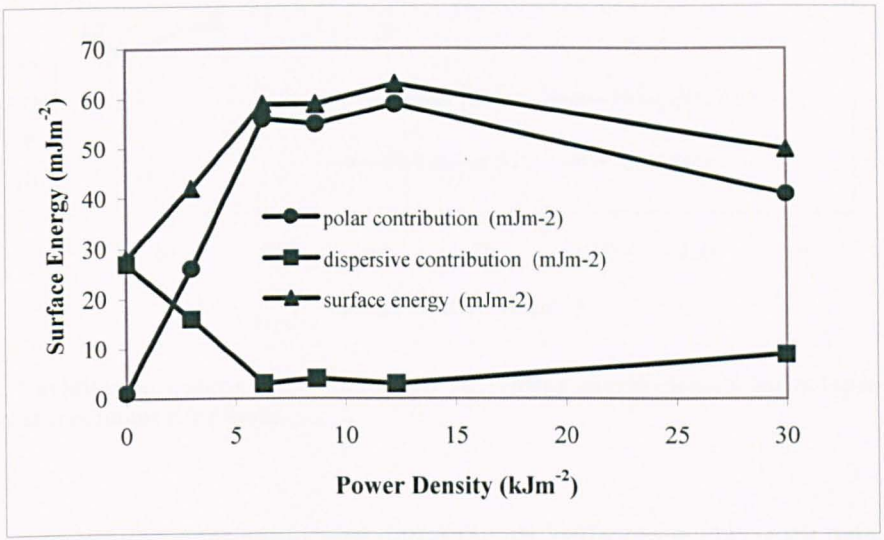

Figure 4-1: Surface energy (γ), and its polar (γ^p) and dispersive (γ^d) contributions for BOPP film corona discharge treated using a range of power densities

The greatest effect on surface energy is noted for power densities between 0 and 6 kJm^{-2}. This represents an increase in γ from 28 to 60 mJm^{-2}, and an increase in γ^p from 0 to ~55 mJm^{-2}. A corresponding decrease in dispersive contribution to surface energy is also noted in this region. Further increases in energy density lead to no significant increase in surface energy. In fact, at the highest energy density of 30 kJm^{-2}, a decrease in surface energy to ~ 50 mJm^{-2} was observed.

The water contact angle may be used to simply represent the change in surface energy of the film. This method allowed for more rapid analysis following corona or plasma treatment as only one probe liquid was used for measurement. As the energy density of the treatment increased, the water contact angle was found to decrease. The variation in water contact angle for BOPP film modified using the four treatment methods is presented in Figure 4-2.

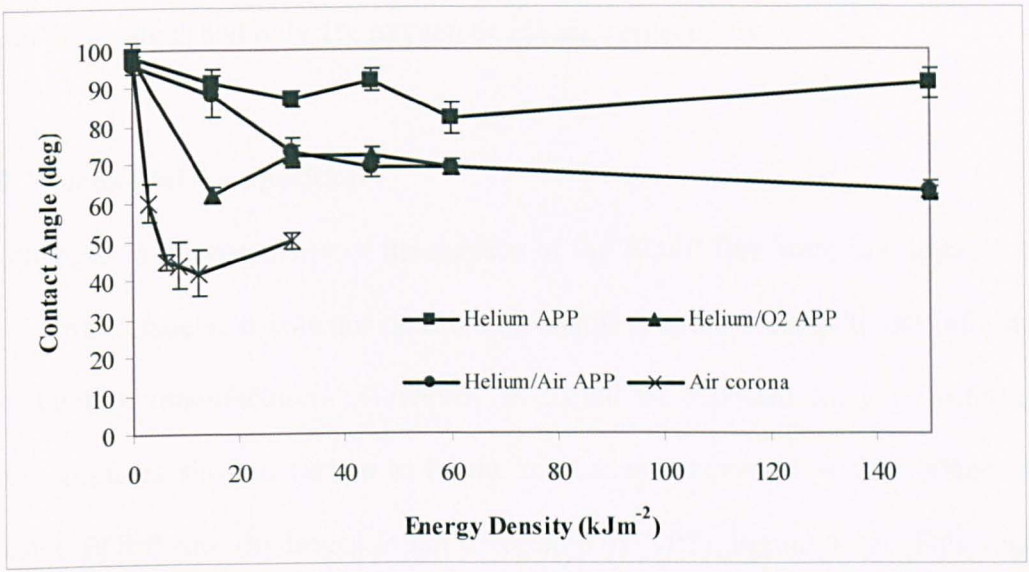

Figure 4-2: Variation in water contact angle with increasing energy density for polypropylene film using different treatment conditions

A decrease in water contact angle was noted for activation by CDT, APP using helium / oxygen mix and helium / air mix, and to a lesser extent, APP using helium. Corona discharge treatment resulted in the greatest change in water contact angle, with a decrease from 98° to 42° over the energy range studied. The results for helium/oxygen and helium/air were very similar; a decrease from 98° to 63° was observed. Treatment in the helium APP showed very little decrease in water contact angle from 98° to 80°. It is hypothesised that helium APP results in the least change in surface energy as APP using an inert gas is more likely to cause crosslinking of the surface, rather than oxidation, due to the lack of oxygen. However, it is generally understood that reaction of free radicals on the surface generated by APP, with oxygen/moisture in the air when the sample is removed from the apparatus results in some oxygen incorporation, thus the slight decrease in water contact angle. The presence of oxygen following helium APP treatment will be confirmed by XPS.

The large decrease in water contact angle observed for corona treatment compared with APP may be due to the oxygen gas present, with corona being carried out in air. The

corona had 21% oxygen in the activating medium, whereas the helium/oxygen and helium/air plasmas had only 1% oxygen or 1% air, respectively.

4.3.2 Elemental Composition

The changes in the chemistry of the surface of the BOPP film were investigated using XPS. Unfortunately, it was not possible to obtain detailed compositional information from the film manufacturer. However, as would be expected for a polyolefin, the survey spectrum showed carbon to be the main element present at the surface of the untreated BOPP film (hydrogen is not detectable by XPS), Figure 4-3a. This suggests that no surface-active additives were present on the film. A very small amount of oxygen (~ 1%) was present in some analyses. This is typical of a hydrocarbon film that has been exposed to the atmosphere over time; Rjeb *et al*[22] investigated the natural ageing of polypropylene film, and showed an increase in oxygen concentration against time.

Following corona or plasma treatment, the most abundant elements present were identified as carbon (C 1s) and oxygen (O 1s), Figure 4-3b. Where the film was treated in an APP generated from helium / air mix, a small quantity of nitrogen (N 1s) was also detected. Both Guimond *et al*[16] and Strobel *et al*[18] reported no nitrogen incorporation into polypropylene following corona treatment. Atomic nitrogen reacts with PP *via* abstraction or scission, and as such results in the formation of nitrogen-containing gaseous species, rather than chemically bound nitrogen groups. Comparison of the RSF-corrected peak areas (as discussed in *Chapter 3: Methods and Materials)* enabled changes in the elemental composition of the film due to treatment to be identified.

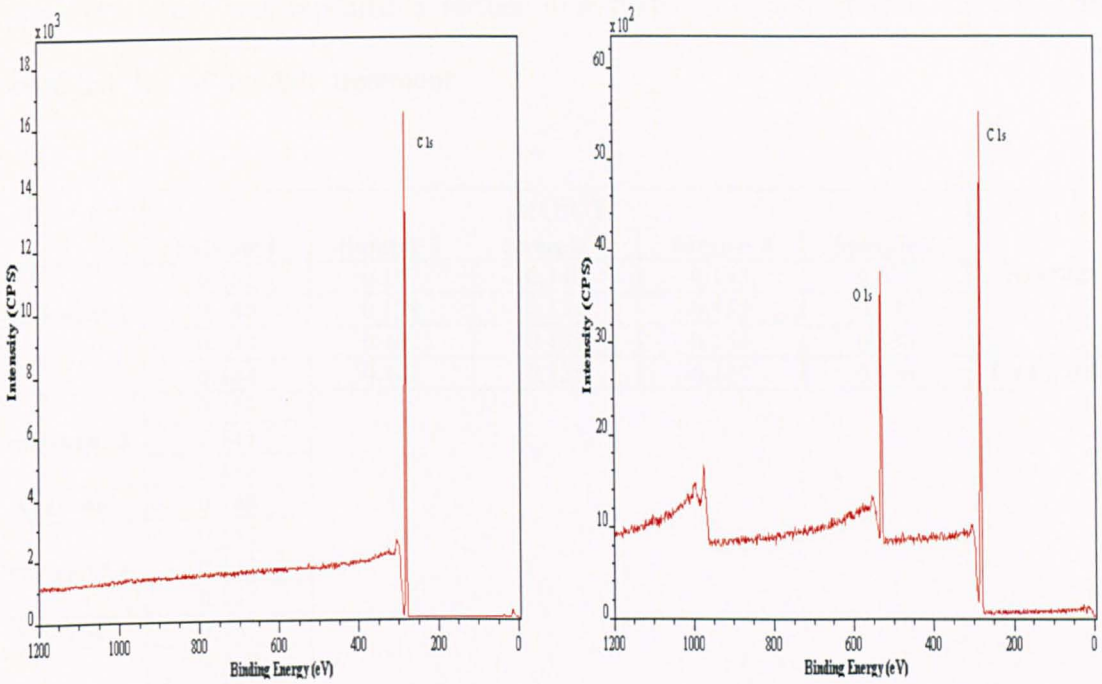

a b

Figure 4-3: Survey spectra for polypropylene film a) 'as received', b) following air corona treatment

The amount of oxygen has present at the surface of the film been presented as Δ(O/C); i.e. the change in oxygen to carbon ratio between the original 'as received' BOPP film, and that of the treated film. Results are presented in this manner to aid comparison between polymers. The effect of oxidative treatment of BOPP film may more easily be compared with similar treatments on oxygen-containing polymer films[10]. The O/C value for the 'as received' film was 0.004.

4.3.3 Run-to-run uniformity and repeatability of Helium/Air APP

In order to evaluate the run-to-run repeatability of the atmospheric pressure plasma treatment, and also the uniformity of treatment across a sample, a short designed experiment was undertaken. A helium/ 1% air plasma was generated, and the BOPP film was treated as described in section 4.2.2, using an input power of 0.4 kW. Five pieces were removed from a 50cm length of treated substrate, and were analysed by XPS. This will provide a measure of the uniformity of the treatment. Additionally, the

same experiment was repeated a further four times to obtain information about the reproducibility of the APP treatment.

	Δ(O/C)					
	Sample 1	**Sample 2**	**Sample 3**	**Sample 4**	**Sample 5**	**Average**
Treatment 1	0.151	0.147	0.140	0.143	0.134	
	0.140	0.139	0.131	0.131	0.130	
	0.140	0.142	0.138	0.138	0.138	
	0.144	**0.142**	**0.136**	**0.137**	**0.134**	**0.14 ± 0.01**
Treatment 2	0.159					
	0.141					
	0.136					
Average	**0.145**					
Treatment 3	0.142					
	0.133					
	0.137					
Average	**0.137**					
Treatment 4	0.138					
	0.130					
	0.121					
Average	**0.130**					
Treatment 5	0.149					
	0.138					
	0.139					
Average	**0.142**	**0.140**				

Table 4-2: Δ(O/C) values, with their averages to 95% confidence for helium/ 1% air APP treated polypropylene film

The average Δ(O/C) value for 5 samples within one run was found to be 0.14 ± 7% with 95% confidence. This represents an oxygen concentration of approximately 12%, and indicates the process uniformity and includes the variance arising from the XPS measurement. Comparison with the averages from run-to-run variation indicates that all runs were within this range. Figure 4-4 presents these values, along with an example using of BOPP treated in helium APP using the same energy density, and shows Δ(O/C) under these conditions, was beyond the range for He/Air treatment.

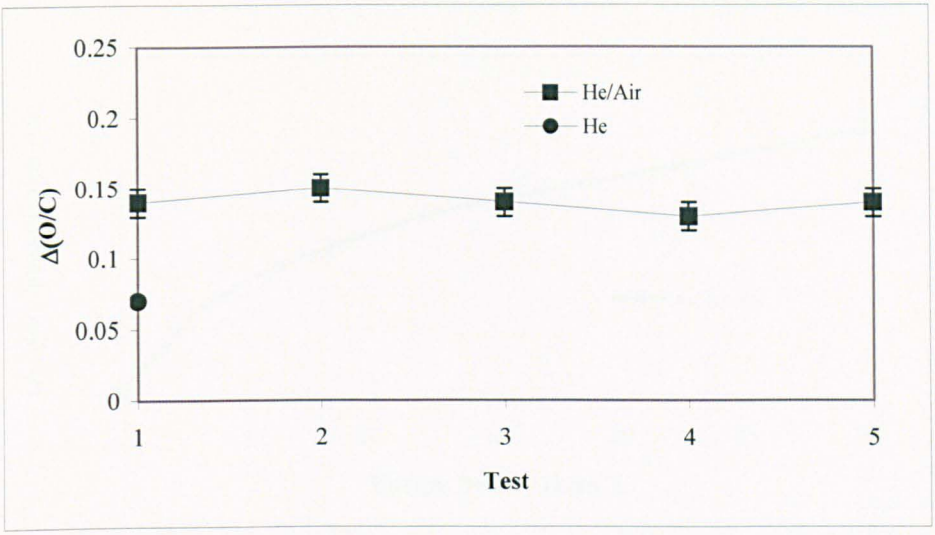

Figure 4-4: Run-to-run variation in Δ(O/C) for helium/1% air plasma treated polypropylene film

4.3.4 Comparison of treatment method on oxygen incorporation

The methods of treatment under investigation, as mentioned previously were corona discharge treatment in air, and atmospheric pressure plasma treatment in helium, helium + 1% oxygen or helium +1 % air. The initial study involved comparison of the amount of oxygen in the surface of the film as measured by XPS following treatment. The oxygen concentration of the sample following immersion in water was also investigated; these results are presented alongside those for the unwashed samples, but are discussed later in the chapter.

a) Corona discharge treated polypropylene film

The concentration of oxygen increased monotonically with increasing energy density of air corona, Figure 4-5.

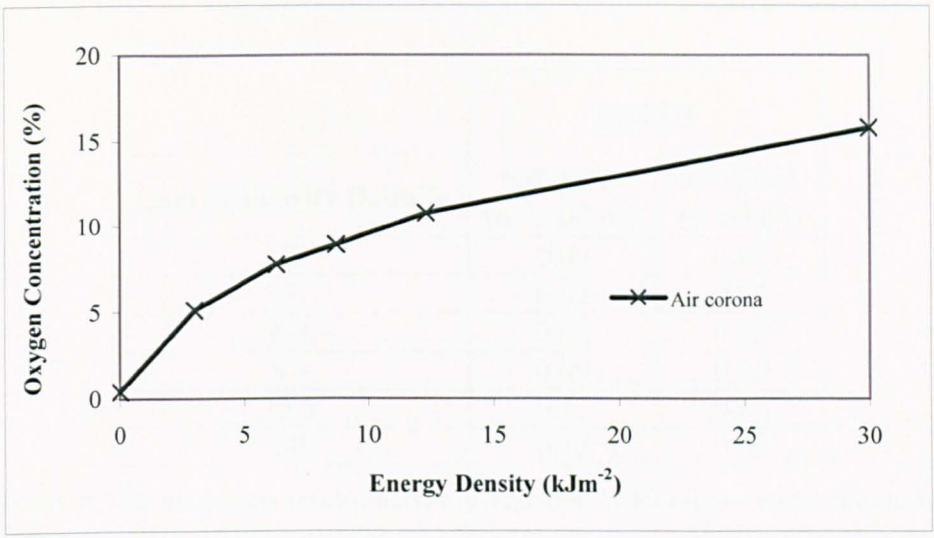

Figure 4-5: Relative concentration of oxygen (%) of air-corona treated polypropylene film, versus corona energy density

An increase from 0.5% to 15% oxygen was observed over the energy density range studied. This represents an increase in Δ(O/C) from 0 to 0.18, Figure 4-6 and Table 4-3.

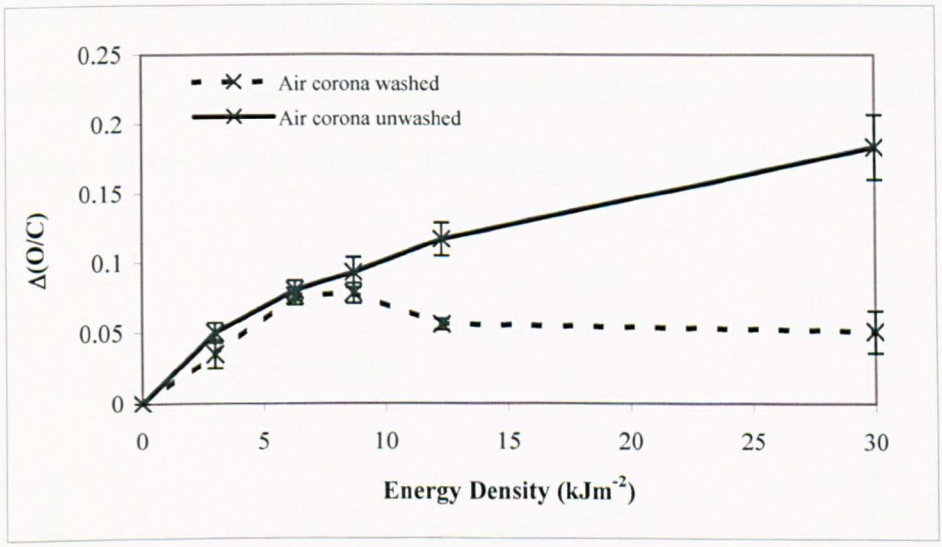

Figure 4-6: Δ(O/C) for air-corona treated polypropylene film versus increasing corona energy density

Energy density (kJm^{-2})	Δ(O/C)	
	90° TOA (unwashed)	90° TOA (washed)
0	0.00	0.00
3	0.05	0.04
6.3	0.08	0.08
8.7	0.09	0.08
12.3	0.12	0.06
30	0.18	0.05

Table 4-3: Δ(O/C) for air-corona treated polypropylene film with one pass under the electrode

b) Helium atmospheric pressure plasma treated polypropylene film

An increase in Δ(O/C) was also observed for BOPP film treated in helium APP, although the difference between the 'as received' film and film treated at the highest power was not as great as that observed after activation by corona discharge, despite the use of higher energy densities, Figure 4-7 and Table 4-4. An increase to a maximum of ~0.08 was observed (equivalent to 8% oxygen) although there was only a slight increase with increasing energy density after the initial treatment at 15 kJm^{-2}.

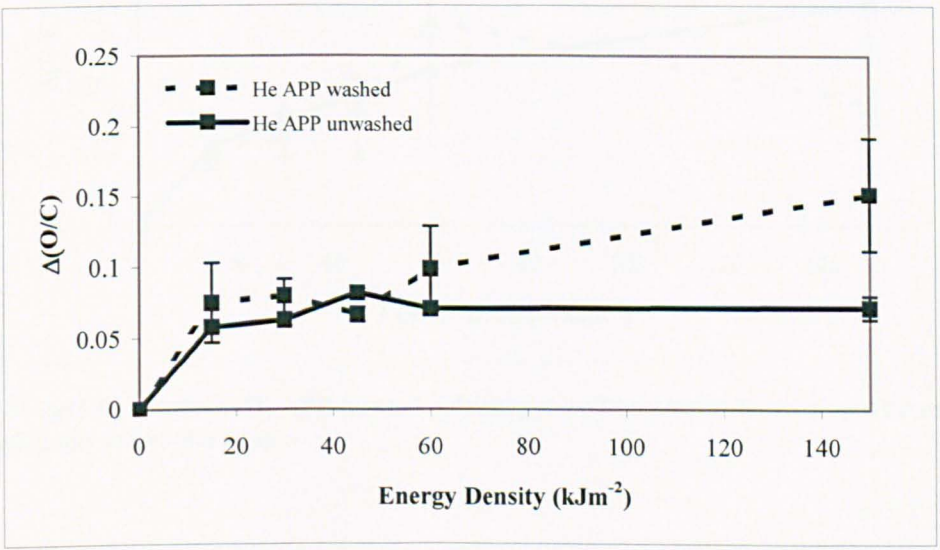

Figure 4-7: Δ(O/C) of helium APP treated polypropylene film, versus increasing APP energy density using one activation zone

Energy density (kJm^{-2})	Δ(O/C)	
	90° TOA (unwashed)	90° TOA (washed)
0	0.00	0.00
15	0.06	0.08
30	0.06	0.08
45	0.08	0.07
60	0.07	0.10
150	0.07	0.15

Table 4-4: Δ(O/C) of helium APP treated polypropylene film with one activation zone

c) Helium/O_2 atmospheric pressure plasma treated polypropylene film

In a manner similar to air corona treatment, a monotonic increase in Δ(O/C) for the BOPP film activated using helium/O_2 was observed, Figure 4-8 and Table 4-5. Over the 150 kJm^{-2} energy density range, an increase of Δ(O/C) from 0 to 0.16 was observed. This corresponds to an increase in oxygen concentration to 14%.

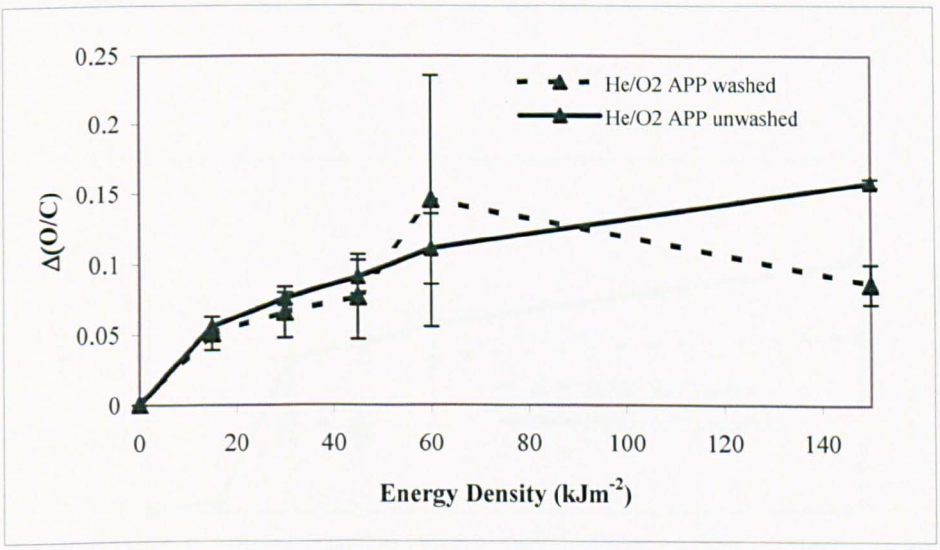

Figure 4-8: Δ(O/C) of helium/O_2 APP treated polypropylene film, versus increasing APP energy density using one activation zone

Energy density (kJm^{-2})	Δ(O/C)	
	90° TOA (unwashed)	90° TOA (washed)
0	0.00	0.00
15	0.06	0.05
30	0.08	0.07
45	0.10	0.08
60	0.12	0.15
150	0.16	0.09

Table 4-5: Δ(O/C) of helium/O_2 APP treated polypropylene film with one activation zone

d) Helium/air atmospheric pressure plasma treated polypropylene film

Increasing oxygen concentration with energy density was also observed for polypropylene film treated in a helium/air APP, Figure 4-9 and Table 4-6. A small increase to 0.01 occurred for treatment at 15 kJm^{-2}, followed by a step increase to 0.1 at 30 kJm^{-2}, after which the Δ(O/C) continued to increase approximately linearly. The maximum oxygen concentration was 15%.

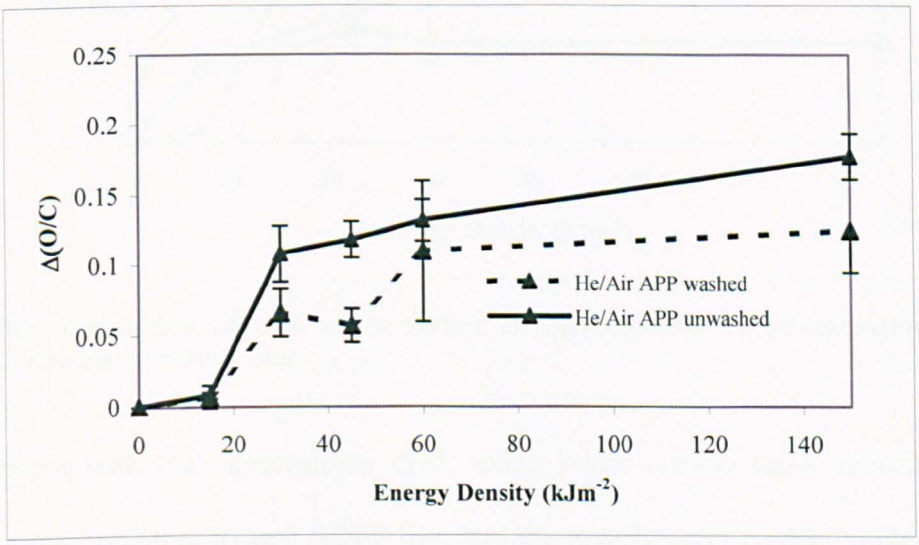

Figure 4-9: Δ(O/C) of helium/air APP activated polypropylene film, versus increasing APP energy density using one activation zone

Energy density (kJm^{-2})	Δ(O/C)	
	90° TOA (unwashed)	90° TOA (washed)
0	0	0
15	0.01	0.01
30	0.11	0.07
45	0.12	0.06
60	0.13	0.11
150	0.18	0.13

Table 4-6: Δ(O/C) of helium/air APP activated polypropylene film with one activation zone

e) Comparative summary of Δ(O/C) of plasma treated polypropylene film

A comparative summary of the results from the four treatment methods is presented in Figure 4-10.

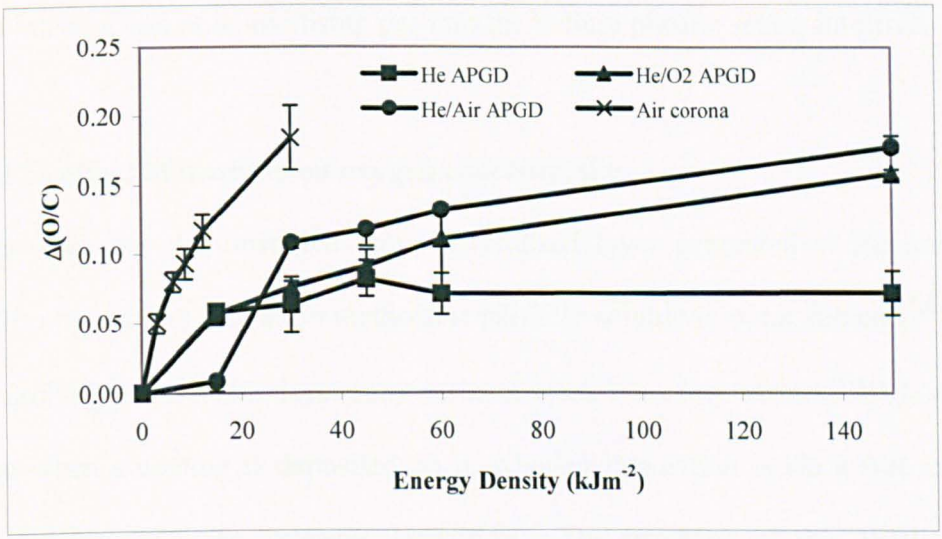

Figure 4-10: Comparison of ΔO/C at the surface of polypropylene film by the various plasma treatments with one activation zone

In agreement with the observations made using water contact angle measurements, where corona discharge treated BOPP film had the lowest water contact angles, i.e. the surface was more hydrophilic, corona discharge treated film had the greatest oxygen content. The Δ(O/C) ratio varied between 0.05 and 0.18 for energy densities between 3 and 30 kJm^{-2}. These are of the order measured by Strobel *et al*[8], where they found

Δ(O/C) to be between 0.03 and 0.08 for the treatment energy density range 3 to 17 kJm^{-2}. Similarly, the range of energy densities (7 – 100 kJm^{-2}) used by Sapieha *et al*[23] resulted in Δ(O/C) between 0.07 and 0.33 for corona discharge treatment of polyethylene.

Helium APP treatment results in the lowest amount of oxygen incorporation, with a maximum Δ(O/C) ratio of 0.08 being achieved. Values of Δ(O/C) from 0.11 were reported by Massines *et al*[15], although direct comparison between treatment conditions were not possible.

This is the first study to compare the effects of helium/air or helium/oxygen atmospheric pressure plasma. However, the increase of Δ(O/C) from 0.08 to ~ 0.17 with the introduction of an oxidising gas into the helium plasma seems intuitive.

4.3.5 The effect of washing on oxygen concentration

Previous work has demonstrated that the oxidised layer generated at the surface of BOPP film by various activation methods is partially soluble in polar solvents[3,8,9,10,18,24]. This hydrolytically unstable layer may act as a weak boundary layer (WBL), affecting adhesion when a coating is deposited on it, whether deposition is *via* a wet, chemical coating process, or a dry, plasma deposition. The presence of this WBL will be detrimental to adhesion. Strobel *et al*[8] showed practical adhesion between corona discharge treated film and polyamide ink was improved by the presence of low molecular weight oxidised material (LMWOM) due its solubility in the ink. However, we[25] have previously demonstrated a link between the amount of water-soluble oxidised material generated on BOPP film by corona treatment, and loss of adhesion between said films and a siloxane coating. By minimising the amount of oxygen present in a

water-soluble form through optimisation of the corona energy, it was found that prolonged adhesive performance could be achieved.

A comparison of Δ(O/C) for corona activated BOPP film following immersion in water is presented in Figure 4-6 and Table 4-3. The Δ(O/C) value is lower for the washed samples at energy densities above 8 kJm^{-2}. The optimum energy density for corona discharge treatment under these conditions lies between 5 and 10 Jm^{-2}, where the optimum is assessed in terms of wash-stable, oxygen-containing surface species. At these energy densities, there is the highest concentration of oxygen present in an insoluble form, with between 80 and 100% being insoluble. Above this optimum treatment level, chain scission and oxidation occurs, leading to the formation of a water-soluble surface layer, where only 28 to 50% of the oxygen is insoluble.

The trend is much less clear for samples activated in helium APP; at the highest discharge energy density of 150 kJm^{-2}, the Δ(O/C)) is significantly higher for the immersed film, Figure 4-7 and Table 4-4. This may be explained by the hypothesis that long-living peroxy and hydroperoxy species on the surface may react with water. Pochan *et al*[26] have proven the existence of hydroperoxy species using gas-phase derivatisation.

Immersion of BOPP film that had been treated in a helium/oxygen APP using high energy density led to a decrease in Δ(O/C), Figure 4-8 and Table 4-5, as seen for the samples treated using corona discharge. However, the retention of oxygen following immersion was better for helium/oxygen treated samples than for corona treated samples. The Δ(O/C) value was higher for the sample treated in APP, at 30 kJm^{-2} Δ(O/C) was 0.07, compared with 0.05 for corona treated BOPP. The surface generated

by helium /oxygen APP is thus determined to be more hydrolytically stable than corona treatment.

A decrease in Δ(O/C) was observed after washing the helium / air activated BOPP, Figure 4-8 and Table 4-6. The oxidised surface created by helium / air APP was less hydrolytically stable than that generated by helium / oxygen APP. At 30 kJm^{-2}, although the Δ(O/C) values were the same (0.66), the initial oxygen concentration at this energy density was higher for the helium / air APP activated sample. This sample was, however, more stable than the corona activated BOPP.

A summary of the Δ(O/C) values after washing for the four activation methods is presented in Figure 4-11.

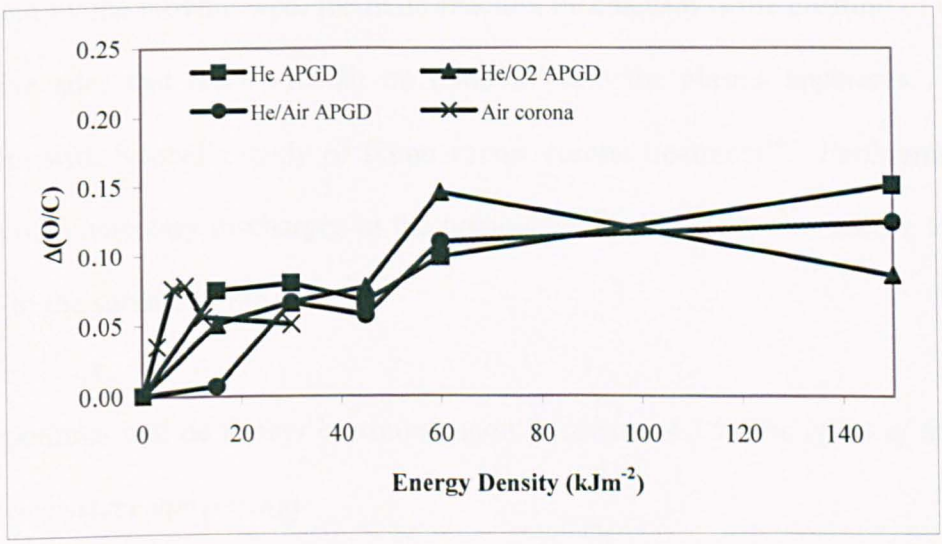

Figure 4-11: Comparison of the level of oxygen retained on the surface following immersion of polypropylene film after activation by various methods

The highest level of oxygen retained following immersion was observed for the sample activated by helium / oxygen APP at 60 kJm^{-2}, and by helium APP at 150 kJm^{-2}. In general, a higher concentration of oxygen is retained at higher power densities by the APP activations, compared with the corona activation at lower power densities. This indicates that the use of atmospheric pressure plasma causes less damage to the surface

of the film through chain scission. An example of a stable oxidised surface generated by plasma treatment of polypropylene was given by Strobel *et al*[18] where the effect of a flame treatment was compared with that created using corona. In this case, although similar levels of oxidation and morphology were obtained using the flame treatment, immersion of the sample in water led to no decrease in oxygen concentration or change in morphology. Immersion of the corona treated sample led to a decrease in the Δ(O/C) ratio, with the amount of water soluble material being generated increasing with increasing treatment energy density as described previously by O'Hare *et al*[14,25]. It is our hypothesis that the absence of atomic oxygen in the helium plasma leads to a reduction in chain scission, whereby the oxidised materials generated are of intermediate molecular weight, and as such are insoluble in water. Whilst a small concentration of molecular oxygen may be present in the plasma by air being drawn into the system by the moving web, the main reaction mechanism is the creation of radicals and active sites that react with air on removal from the plasma apparatus. This is consistent with Strobel's study of flame versus corona treatment[18]. Furthermore, the absence of filamentary discharges in the homogeneous APP may also reduce localised damage to the surface of the film.

This hypothesis will be further expanded upon in section *4.3.9, The effect of treatment method on surface morphology.*

4.3.6 Surface Chemistry: Development of a self-consistent protocol for curve-fitting of the carbon (C 1s) core level

In addition to the oxygen concentration of the modified surfaces, XPS can also provide chemical state information. In this case, examination of the carbon C1s core level allows identification of the functional groups incorporated onto the surface, and enables further comparison between the activation methods through a procedure known as curve-fitting.

Here, a number of synthetic peaks are added to the experimental envelope to produce a good fit. Through the concept of binding energy shift, a number of different chemical environments for carbon can be identified. In addition to providing detailed information about the surface, this data can be related to, for example, potential adhesive performance of the surface.

a) 'As received' Polypropylene Film

The carbon C 1s core level from the 'as received' BOPP film was curve-fitted using a vibrational progression of synthetic peaks as described by Beamson *et al* for hydrocarbon polymers[27], Figure 4-12a. Here, the asymmetry observed on the high binding energy side of the C 1s core level, resulting from excitation of C-H stretching vibrations during photoionisation, is curve-fitted using a series of synthetic peaks with small chemical shifts. A commonly employed internal referencing method: the application of a charge correction value to set the most intense synthetic peak to 285.0 eV[28] was employed to compensate for surface charging, which is discussed more fully in *Chapter 3: Methods and Materials*. The full width at half maximum (FWHM) for the four peaks was constrained to be equal, as were the binding energy separations and the lineshape for the four peaks, and showed good agreement with the literature[27,28]. For

clarity, these four peaks were then replaced by a composite model line-shape generated to represent these four peaks, Figure 4-12b. This model will be applied to experimental data obtained from the corona or atmospheric pressure plasma treated polypropylene. The composite line shape will be used to represent only the hydrocarbon component of the experimental data. Synthetic peaks with a Gaussian-Lorentizian mix of 70:30 will be used to represent the additional components assigned to oxidised carbon functionalities.

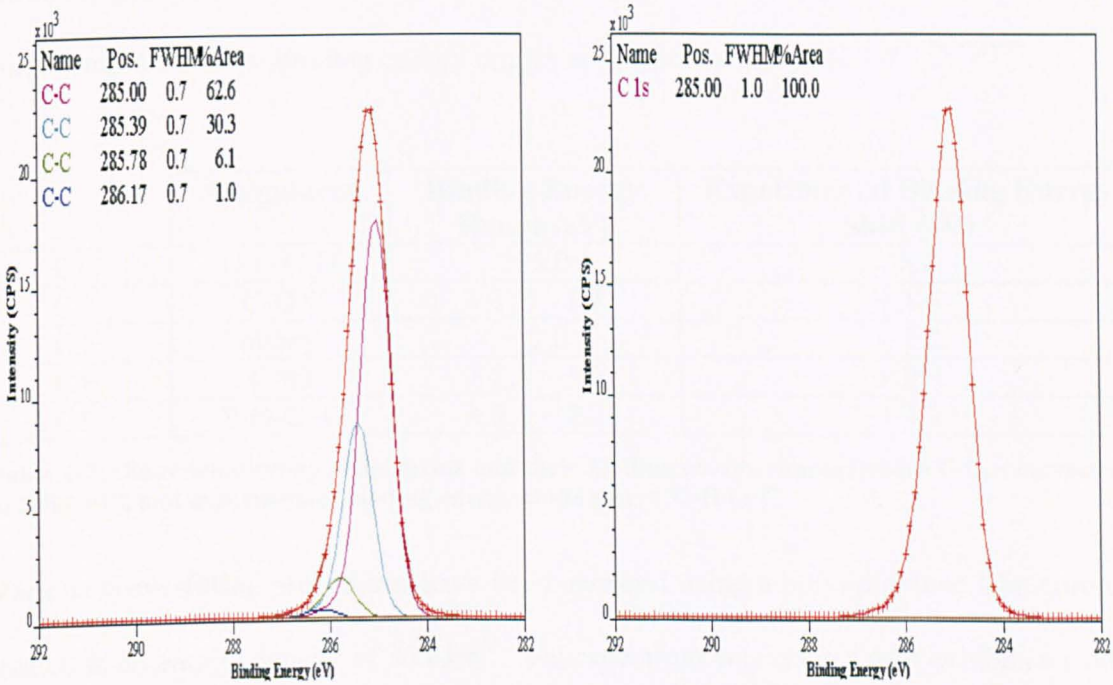

Figure 4-12: Curve-fit for carbon (C 1s) core level for 'as received' polypropylene film a) using vibrational progression of four peaks, b) using model line shape

b) Corona Discharge Treated Polypropylene Film

Several peak combinations were possible when applying synthetic peaks to the C 1s core level of corona discharge or atmospheric pressure plasma treated polypropylene. For this reason, it was essential to develop a self-consistent and repeatable protocol for the curve-fit. The effect of varying the number of synthetic components (representing different functionalities introduced by the treatment), their FWHM, and binding energy

positions were all examined. With the exception of the component for C-C/C-H, the shape of the peaks were constrained to GL(30) with slight asymmetry.

From a study of the literature on curve fitting of the C 1s core level for polyolefins oxidised using corona, dielectric barrier discharge, or plasma treatment, four functional groups were found to be commonly assigned. Following charge referencing of the most abundant, lowest binding energy peak to 285.0 eV (C-C/C-H), functional groups have been assigned: alcohol or ether, (C-OX where X = C or H); epoxy, carbonyl (C=O) and carboxyl groups (X-O-C=O, where X = C or H). The environments and their most commonly referenced binding energy ranges are presented in Table 4-7[3, 29,30,31,32].

	Assignment	Binding Energy Range (eV)	Experimental Binding Energy Shift (eV)
C1	C-C/C-H	285.0	X
C2	C-OX	+ 1.2 – 1.7	+ 1.5
C3	epoxy	+ 2.0	+ 2.2
C4	C=O	+ 2.8 – 3.0	+ 2.9
C5	X-O-C=O	+ 3.8 – 4.2	+ 4.1

Table 4-7: Functional group assignments and their binding energy ranges (where C-C is corrected to 285.0 eV), and experimental binding energy shifts where X=H or C.

Various curve-fitting procedures have been assessed using a polypropylene film corona treated at an energy density of 30 kJm^{-2}. This spectrum was chosen as it exhibits a well-defined feature on the high binding energy side of the C 1s core level enabling a relatively high level of confidence in positioning the C-O_2X (C5) component. When the process was optimised, it was applied consistently to all samples. A measure of the goodness of fit (*G*) for this work will be the χ^2 value divided by the number of degrees of freedom. The number of degrees of freedom results from the number of variables (e.g. synthetic peak positions applied and can be reduced by applying constraints). However, in CasaXPS the χ^2 value reported is purely a measure of the number of data points used to determine the curve fit. The smaller the resulting number is, the better

the fit. However, this measure is only a guide, and more importance will be given to the visual examination of the plot of the residuals and an understanding of the chemistry involved.

c) Constraining FWHM and binding energy position

The first attempt at curve-fitting was using five synthetic peaks, with the FWHM of all components constrained to be equal to that of the C-C/C-H (C1) synthetic peak at 285.0 eV as described by Alexander *et al*[33]. The FWHM of C1 was allowed to vary. The shape of the additional synthetic components was maintained throughout all curve-fits; with a 70:30 Gaussian:Lorentzian mix, with a slight asymmetry. The binding energies were constrained to be equal to the average position from the literature, as presented in Table 4-7. The resulting curve-fit is shown in Figure 4-13.

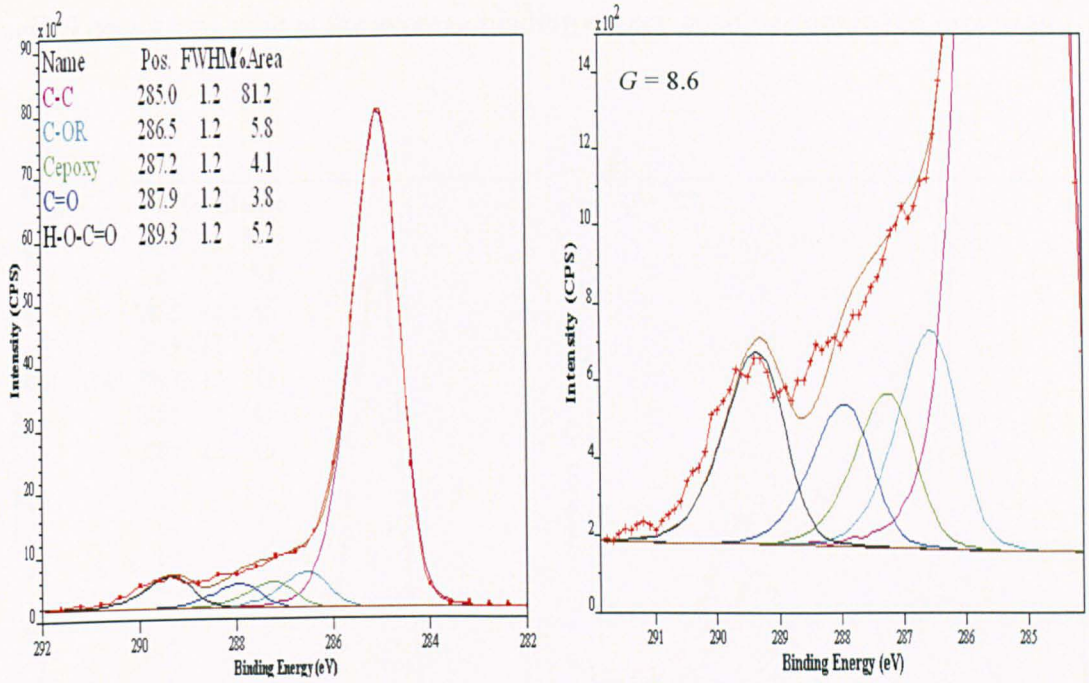

a b

Figure 4-13: Curve-fit 1 for C 1s core level of polypropylene film treated using corona discharge at an energy density of 30 kJm^{-2}. Synthetic components were constrained in shape and FWHM to be equal to that for C-C/C-H synthetic peak.

It can be seen that this curve-fit does not fit the experimental data well. Displaying the data with expanded intensity and binding energy-axes in Figure 4-13b, clearly shows the difference between the synthetic peak envelope produced by the curve-fit and the experimental data. There is a poor fit at binding energies above the CO_2X (C5) synthetic component and also between this peak and that assigned to C=O (C4). *G* was calculated to be 8.6.

d) Constraining FWHM and binding energy position and varying the number of synthetic components

In an attempt to obtain a better fit at high binding energies above the CO_2X synthetic component and also between this peak and that assigned to C=O, two additional synthetic peaks were used (C6, C7), resulting in an improved *G* value of 7.7. The

FWHM were constrained to be equal to that of C1, which was allowed to vary. The five original peaks remained at the average binding energy positions described previously

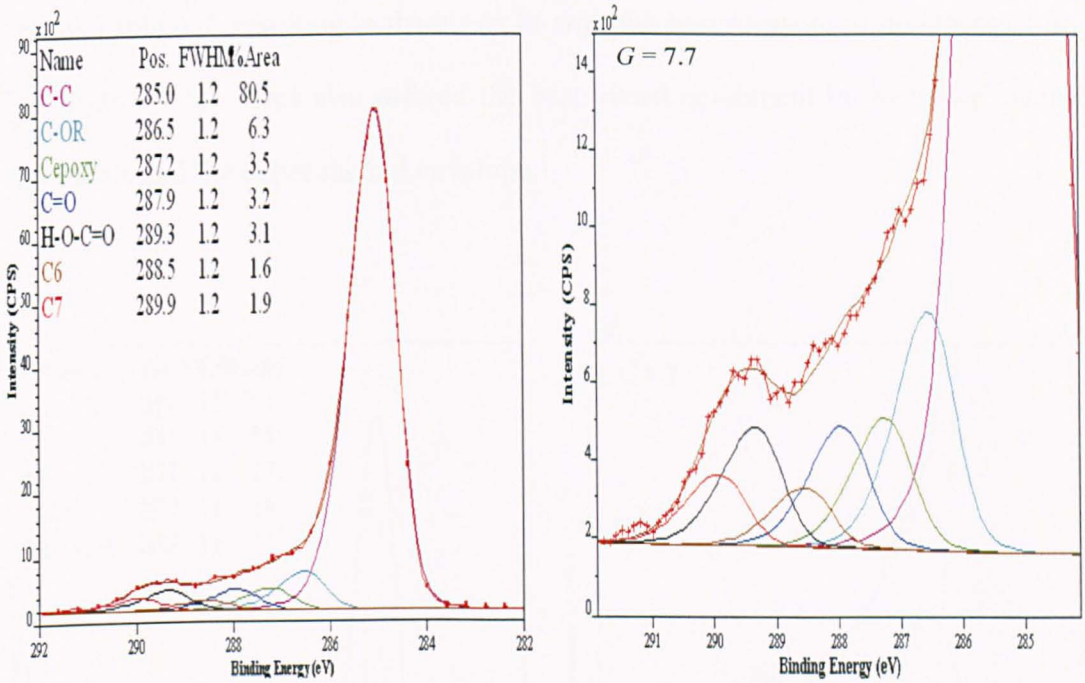

Figure 4-14: Curve-fit 2 for C 1s core level of polypropylene film treated using corona discharge at an energy density of 30 kJm^{-2}. Synthetic components were constrained in position and FWHM to be equal to that for C-C/C-H synthetic peak. Two additional synthetic peaks were required, with binding energy shifts of +3.5 eV, and +4.9 eV.

The component at 289.9 eV (C7) may be assigned to carbonate species. Boyd *et al*[3] have demonstrated, using time-of-flight secondary ion mass spectrometry (ToF-SIMS), the presence of CO_3^- and HCO_3^- in small quantities on the surface of BOPP exposed to atmospheric non-equilibrium plasma. The synthetic peak at 288.5eV (C6) has previously been assigned to $COO^-{}^+Metal$[34], in work dealing with XPS of polymer films on aluminium substrates. However, since no counter cation was observed in the wide area scans, this was not felt to be a valid assignment in this example. No other realistic assignment could be made for this component; as such it was removed from the curve-fitting process.

e) Constraining binding energy position and allowing FWHM to vary

An alternative to the addition of these two peaks is to allow the FWHMs of the five original peaks to vary. Their binding energies were constrained to be the average values given in Table 4-7, resulting in the curve fit with the best measure of goodness of fit, G = 2.8 Figure 4-15. This also offered the best visual agreement between the synthetic components and the experimental envelope.

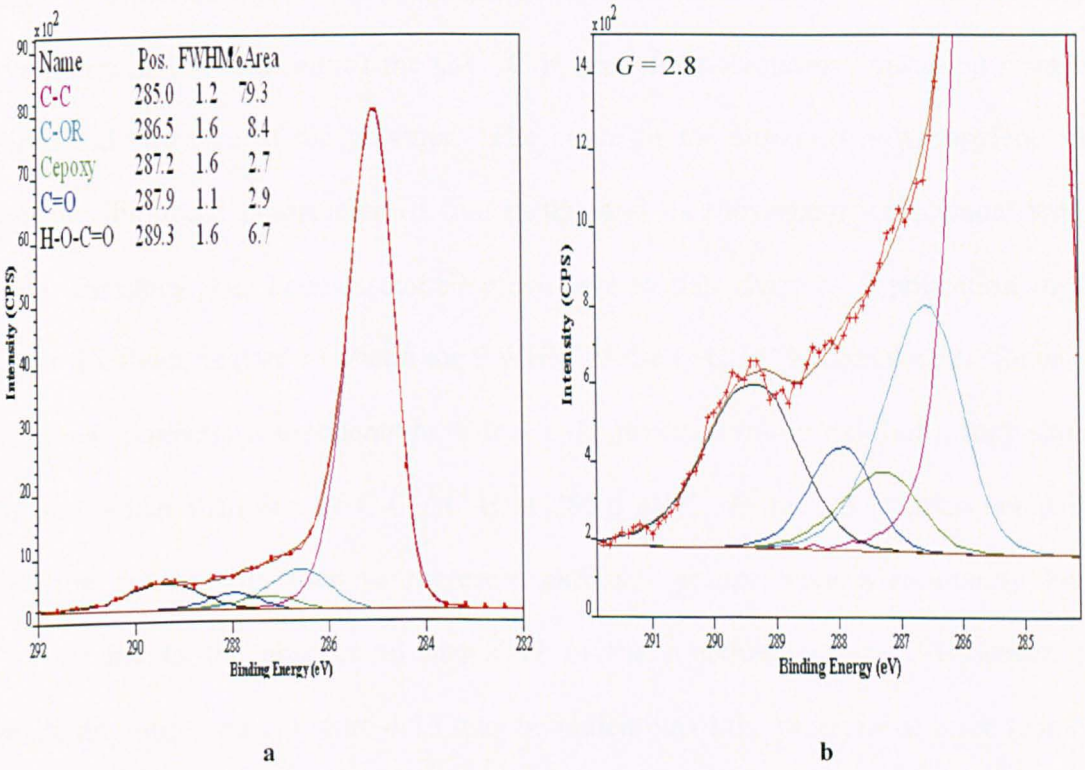

Figure 4-15: Curve-fit 1 for C 1s core level of polypropylene film treated using corona discharge at an energy density of 30 kJm^{-2}. Synthetic components were constrained in position and FWHM allowed to vary to obtain the best fit.

Few studies using a monochromated Al Kα anode could be found in the literature. However, those that were found[9], determined a FWHM for untreated polypropylene film close to 1.2 eV, in agreement with that used in Fig 3. However, in this manuscript by Strobel *et al*, the C 1s core level was not curve-fitted to determine the functionalities introduced by corona treatment. Foerch *et al*[12] reported the linewidth for C-C/C-H of untreated polyethylene to be 1.6 eV using a monochromated Al anode, increasing to

~2.2 eV following oxygen plasma treatment. Gerenser *et al*[7] found the FWHM of C-C/C-H to be 1.8 eV, and that of O-C=O to be 2.2 eV using monochromated Al to analyse corona discharge treated polyethylene. This represents a ratio of $FWHM_{CO_2X}$/ $FWHM_{C\text{-}C/C\text{-}H}$ of 1.22. By comparison, the $FWHM_{CO_2X}$/ $FWHM_{C\text{-}C/C\text{-}H}$ ratio in Figure 4-15 was 1.33.

It is recommended that for the majority of synthetic components their FWHM is no larger than that of C-C / C-H. The use of high-resolution instruments has shown the asymmetry and broadening of the C-C /C-H peak for polyolefins[35] resulting from the vibrational structure of the polymer. The curve fit for untreated polypropylene film using a vibrational progression of four peaks, and its subsequent replacement with a model lineshape has been discussed previously in this chapter. Application of the model lineshape is used to obtain the FWHM of the C-C / C-H component. Since the additional synthetic components have less C-H structure (more oxidised), they should not be broader than that of C-C / C-H at 285.0 eV[36]. In fact, it is often noted that synthetic components used to represent carboxyl groups have a resultantly lower FWHM due to the absence of any C-H in the functional group[35]. However, the broadening observed in Figure 4-15 may be indicative of the presence of more than one functional group in a similar binding energy position. For example, the broadening, and slightly high binding energy position, of the CO_2X peak may indicate the presence of H-O-C=O, C-O-C=O, O=C-O-C=O, and/or CO_3. One possible explanation as to why the synthetic peak associated with epoxy should be so broad is that is contains a variety of environments, although it has not been possible to prove this unambiguously in this work.

f) Constraining FWHM and allowing the synthetic component binding energies to vary

The final variation when curve-fitting was to constrain the FWHM of the four peaks representing oxidised carbon groups to be equal to C1 (where $FWHM_{C1}$ was allowed to vary) but the binding energy positions of C3 and C5 were allowed to vary to obtain the best fit, Figure 4-16. The component representing C-C / C-H was charge referenced to 285.0 eV.

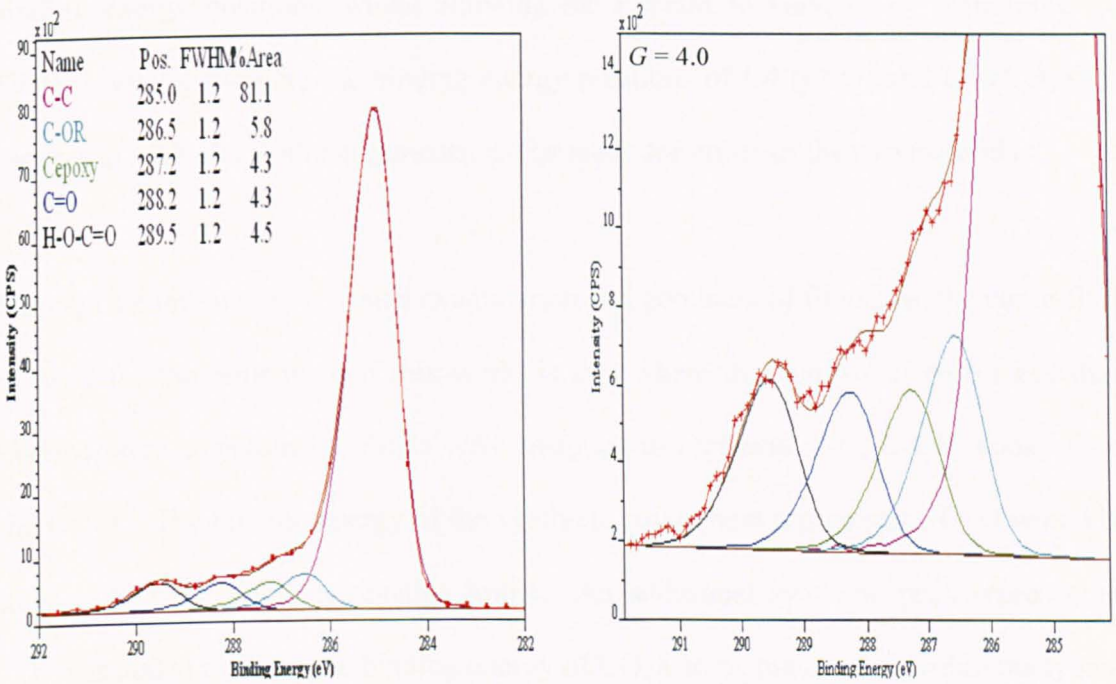

Figure 4-16: Curve-fit 1 for C 1s core level of polypropylene film treated using corona discharge at an energy density of 30 kJm^{-2}. The FWHM of the additional synthetic peaks were constrained to be equal to that for C-C/C-H synthetic peak. The binding energy positions of the synthetic components were allowed to vary.

By allowing the synthetic peak assigned to CO_2X (C5) to move to 289.5 eV, and that assigned to C=O (C3) to move to 288.2 eV, the measure of goodness of fit, $G = 4.0$, and visually the fit is good. A binding energy of 289.5 and 289.6 eV for CO_2X was reported by Briggs[36] and Borcia[37], respectively, for corona discharge treatment in air, whilst Watts *et al* reported a value of 288.2 eV for the carboxylic ester component of poly(methylmethacrylate) deposited onto aluminium and silicon[38]. However, this increase in binding energy for C=O was caused by the interaction between hydroxide

ions of an inorganic surface with an organic polymer. This effect may be noted for corona treated polymer surfaces where increasing concentrations of functional groups may allow similar interactions.

g) Summary of development of C 1s curve-fitting protocol

Two curve-fit methodologies have been found to be most relevant. By restraining binding energy positions, whilst allowing the FWHM to vary, or by restraining the FWHM, whilst allowing the binding energy positions of C4 (C=O) and C5 (CO_2X) to vary up to +0.3 eV. Valid arguments can be made for either of the two methods.

Through a combination of visual examination and goodness of fit values, the curve-fit to be used for the remainder of this work, is that where the number of peaks and their FWHM were constrained. Peaks were assigned to represent C-C, C-OR, epoxy C=O and CO_2X. The binding energy of the synthetic component representing C=O would be allowed to vary within reasonable limits. An additional synthetic peak representing CO_3 was added to allow the binding energy of CO_2X to be maintained within the typical values described in the literature

4.3.7 Surface Chemistry: Influence of treatment method

a) Curve-fitting of the C 1s core level for corona discharge treated BOPP film

The full dataset for corona discharge treated polypropylene film is presented in Figure 4-17. The FWHM was constrained, while the binding energy positions of C3 and C5 were allowed to vary up to +0.2 eV. The C-C / C-H component was referenced to 285.0 eV.

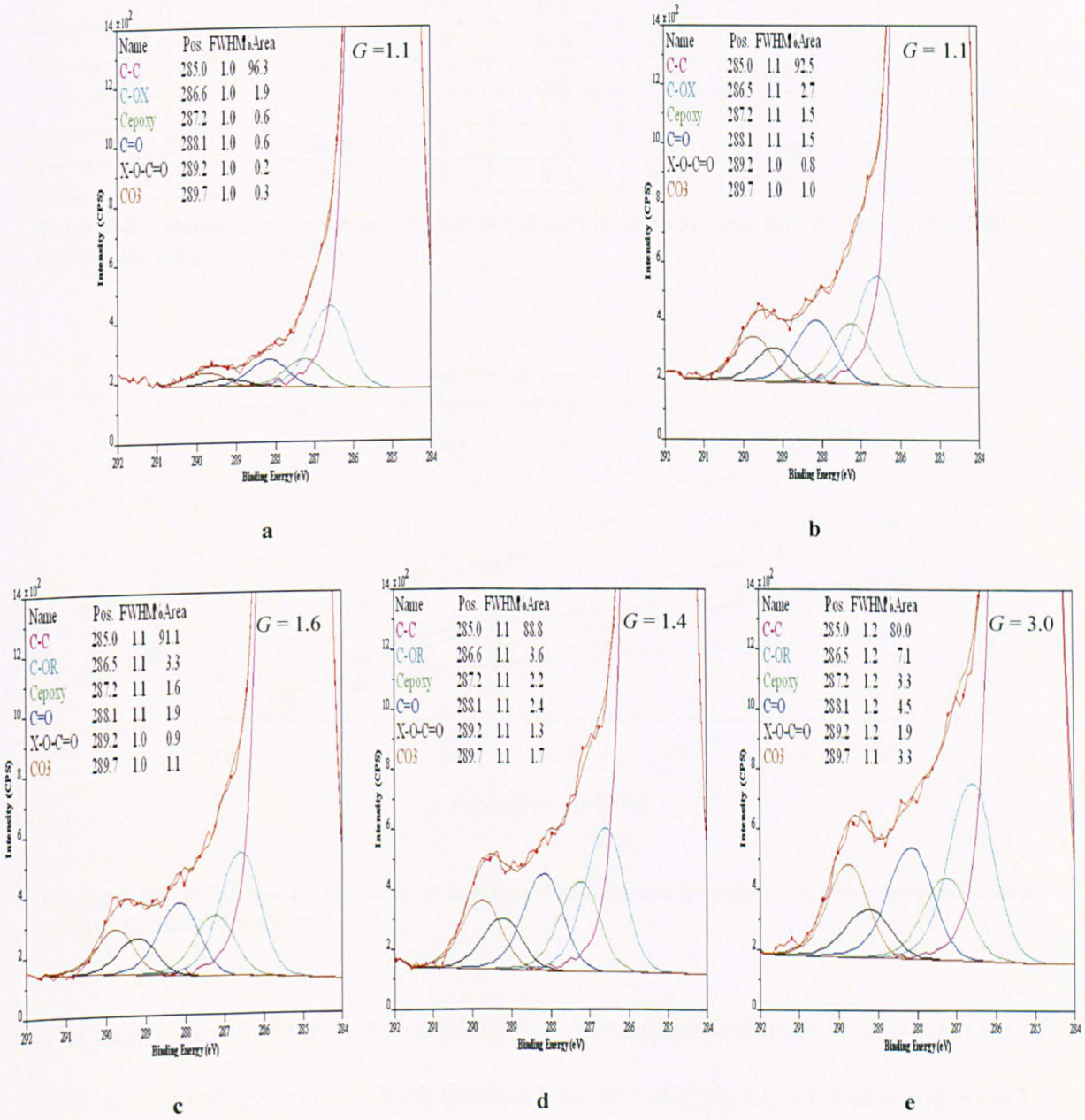

Figure 4-17: XPS curve fit for the carbon (C 1s) core level of polypropylene film activated using air corona with energy density a) 3 kJm^{-2}, b) 6.3 kJm^{-2}, c) 8.7 kJm^{-2}, d) 12.3 kJm^{-2}, e) 30 kJm^{-2}

It is clear that with increasing corona energy density, the intensity of the shoulder on the high binding energy side of the core level increases. By curve-fitting using the previously discussed method, the concentration of each incorporated functional groups can be monitored. The relative concentrations are presented in Table 4-8, and Figure 4-18.

Energy Density (kJm^{-2})	Relative Concentration (%)						*G*
	C-C	C-OX	C_{epoxy}	C=O	X-O-C=O	CO_3	
0.0	100.0	0.0	0.0	0.0	0.0	0.0	
3.0	96.2	1.9	0.6	0.6	0.2	0.3	1.1
6.3	92.5	2.7	1.5	1.5	0.8	1.0	1.1
8.7	91.1	3.3	1.6	1.9	0.9	1.1	1.6
12.3	88.8	3.6	2.2	2.4	1.3	1.7	1.4
30.0	80.0	7.1	3.3	4.5	1.9	3.3	3.0

Table 4-8: Relative concentration of functional groups incorporated into polypropylene film by corona discharge treatment in air

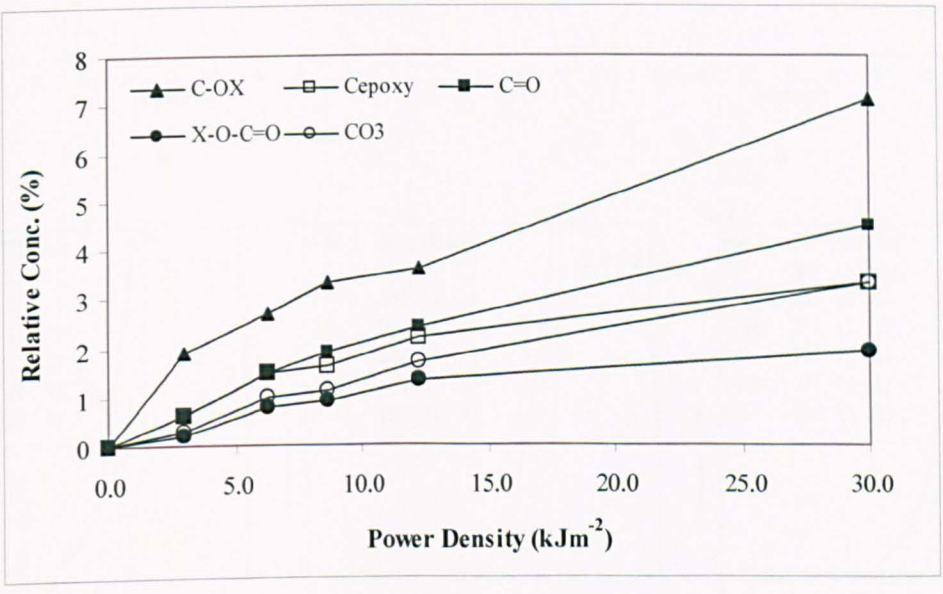

Figure 4-18: Relative concentration of functional groups incorporated into polypropylene film by corona discharge treatment in air

The relative areas of the synthetic peaks representing oxidised functional groups varied with corona energy density. With the exception of a slightly higher concentration of C-OX groups at lower energy densities, each functional group increased with energy density at a similar rate.

b) Curve-fitting for the C 1s core level of helium plasma treated BOPP film

The full dataset for helium APP treated polypropylene film is presented in Figure 4-19. The FWHM was constrained to be equal to that of the synthetic peak for C-C/C-H, while the binding energy positions of C3 and C5 were allowed to vary up to +0.2 eV. Charge referencing was again carried out to set the C-C / C-H component to 285.0 eV.

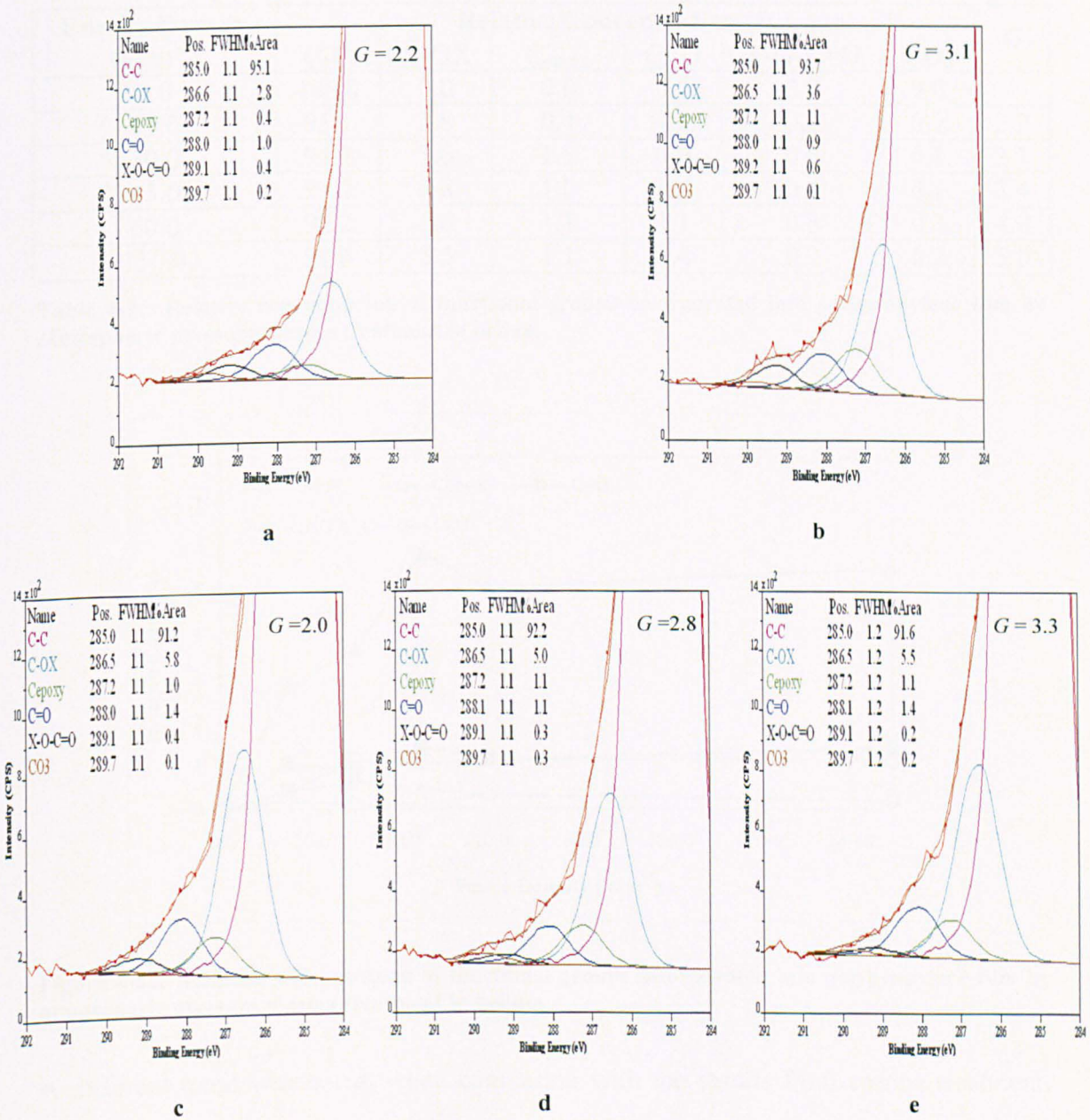

Figure 4-19: XPS curve fit for the carbon (C 1s) core level of polypropylene film activated using helium APP with energy density a) 15 kJm^{-2}, b) 30 kJm^{-2}, c) 45 kJm^{-2}, d) 60 kJm^{-2}, e) 150 kJm^{-2}

The *G* values for the curve fits of helium plasma treated BOPP film were slightly higher than those for the corona treated films, with the exception of at the highest energy density, where the *G* values were similar. However, the visual fit was good in all cases.

The relative concentrations of the functional groups are presented versus power density in Table 4-9 and Figure 4-20.

Energy Density (kJm^{-2})	Relative Concentration (%)						*G*
	C-C	C-OX	C_{epoxy}	C=O	X-O-C=O	CO_3	
0.0	100.0	0.0	0.0	0.0	0.0	0.0	
15.0	95.1	2.8	0.4	1.0	0.4	0.2	2.2
30.0	93.7	3.6	1.1	0.9	0.6	0.1	3.1
45.0	91.2	5.8	1.0	1.4	0.4	0.1	2.4
60.0	92.2	5.0	1.1	1.1	0.3	0.3	4.0
150.0	91.6	5.5	1.1	1.4	0.2	0.2	5.0

Table 4-9: Relative concentration of functional groups incorporated into polypropylene film by atmospheric pressure plasma treatment in helium

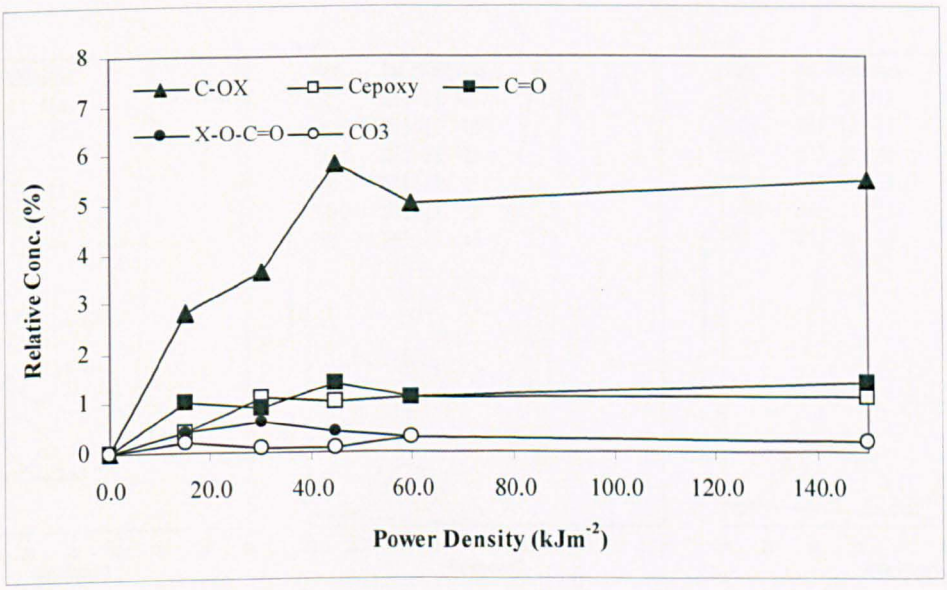

Figure 4-20: Relative concentration of functional groups incorporated into polypropylene film by atmospheric pressure plasma treatment in helium

A different trend was noted, when comparing with the results from corona treatment. For helium APP, with increasing power, the intensity of the peak assigned to C-OX is much greater than any other functional group. The least abundant is CO_2X, which remains relatively constant, independent of energy density.

c) Curve-fitting of the C 1s core level for helium/1% oxygen plasma treated BOPP film

Similarly, small values of G, representative of the goodness of fit, were achieved for the curve-fitting of polypropylene treated in helium/oxygen plasma, Figure 4-21.

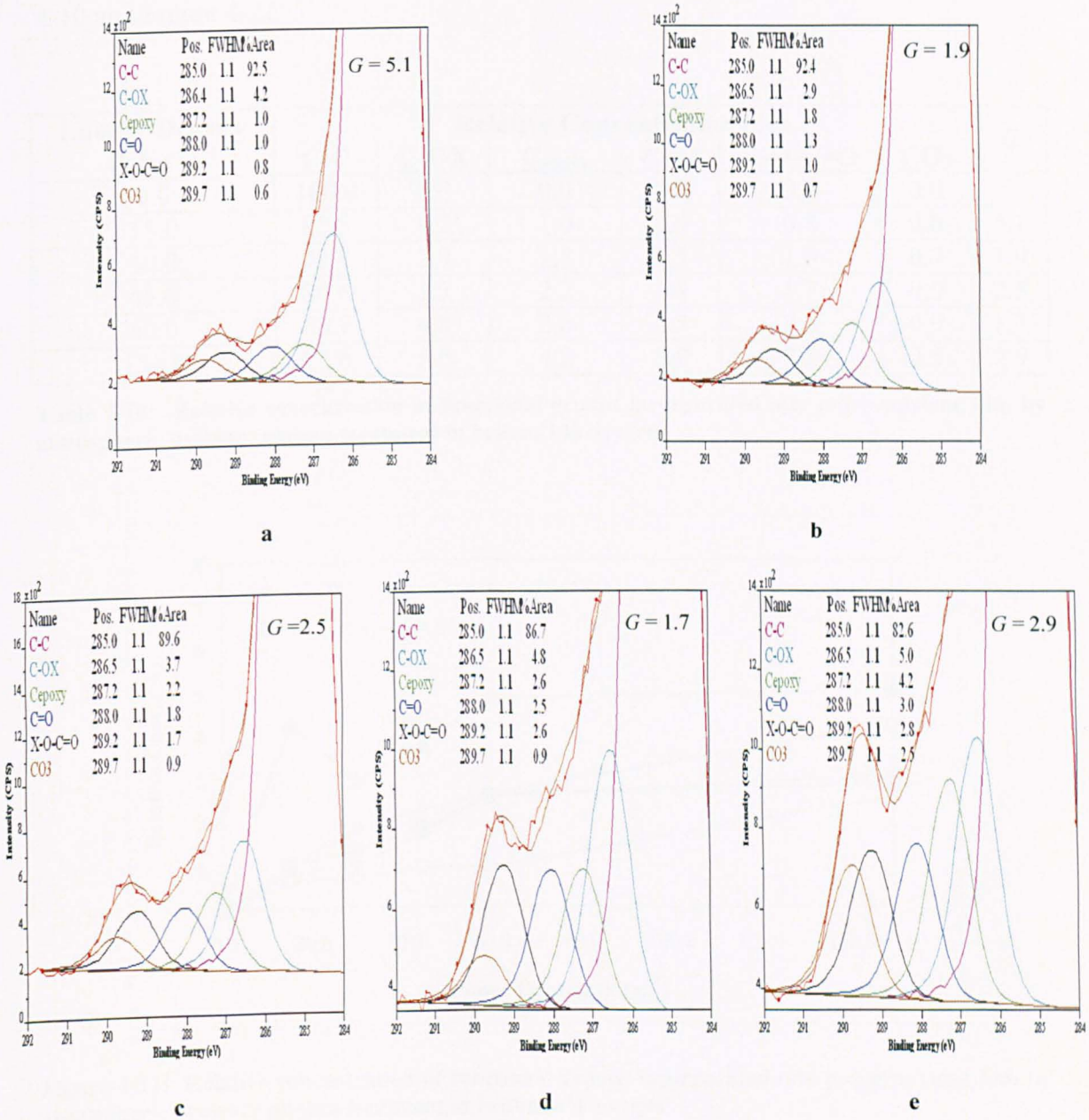

Figure 4-21: XPS curve fit for the carbon (C 1s) core level of polypropylene film activated using helium/1% oxygen APP with energy density a) 15 kJm^{-2}, b) 30 kJm^{-2}, c) 45 kJm^{-2}, d) 60 kJm^{-2}, e) 150 kJm^{-2}

Whereas all *G* values had been of the order of ~ 3 or less, the curve fit of BOPP treated in a helium/oxygen plasma at 15 kJm^{-2} resulted in a *G* value of 5.2. Although

considerably higher, visual examination of the curve fit confirms that the synthetic components follow the experimental data well.

As before, the functional groups were monitored with increasing energy density, Table 4-10 and Figure 4-22.

Energy Density (kJm^{-2})	Relative Concentration (%)						*G*
	C-C	C-OX	C_{epoxy}	C=O	X-O-C=O	CO_3	
0.0	100.0	0.0	0.0	0.0	0.0	0.0	
15.0	92.5	4.2	1.0	1.0	0.8	0.6	5.1
30.0	92.4	2.9	1.8	1.3	1.0	0.7	1.9
45.0	89.6	3.7	2.2	1.8	1.7	0.9	2.5
60.0	86.7	4.8	2.6	2.5	2.6	0.9	1.7
150.0	82.6	5.0	4.2	3.0	2.8	2.5	2.9

Table 4-10: Relative concentration of functional groups incorporated into polypropylene film by atmospheric pressure plasma treatment in helium/1% oxygen

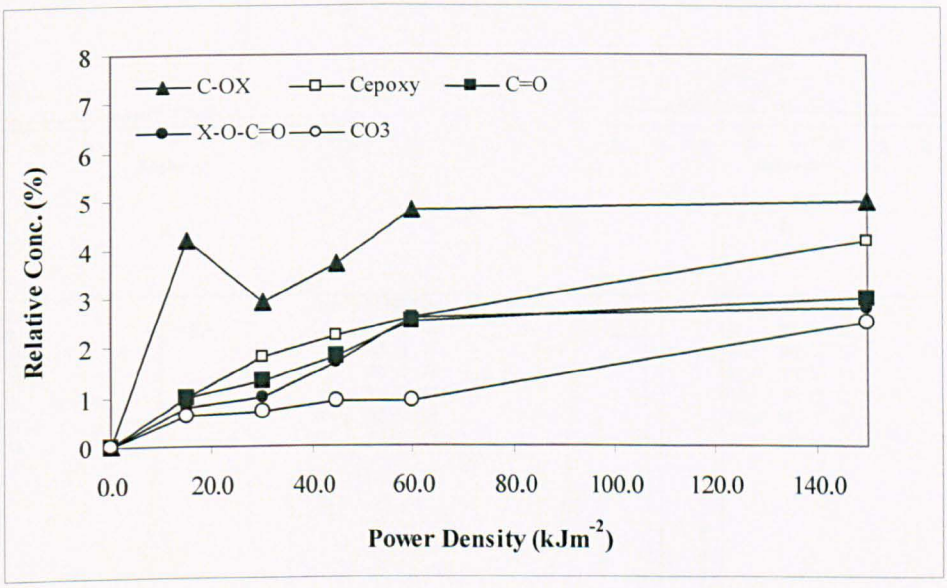

Figure 4-22: Relative concentration of functional groups incorporated into polypropylene film by atmospheric pressure plasma treatment in helium/1% oxygen

As for helium plasma treatment, a considerable difference was observed between the concentration of C-OX species, compared with the other functional groups when the lowest energy density was used. However, the intensity of the remaining groups, C-O-O·, C=O and CO_2X also increased with increasing energy density, in a similar fashion to

the trend observed following corona treatment. At the highest energy density, 150 kJm^{-2}, the concentration of all functional groups is similar.

d) Curve-fitting of the C 1s core level of helium/1% air plasma treated BOPP film

The curve-fits for the C 1s core level for helium/1% air APP treated polypropylene film are presented in Figure 4-23.

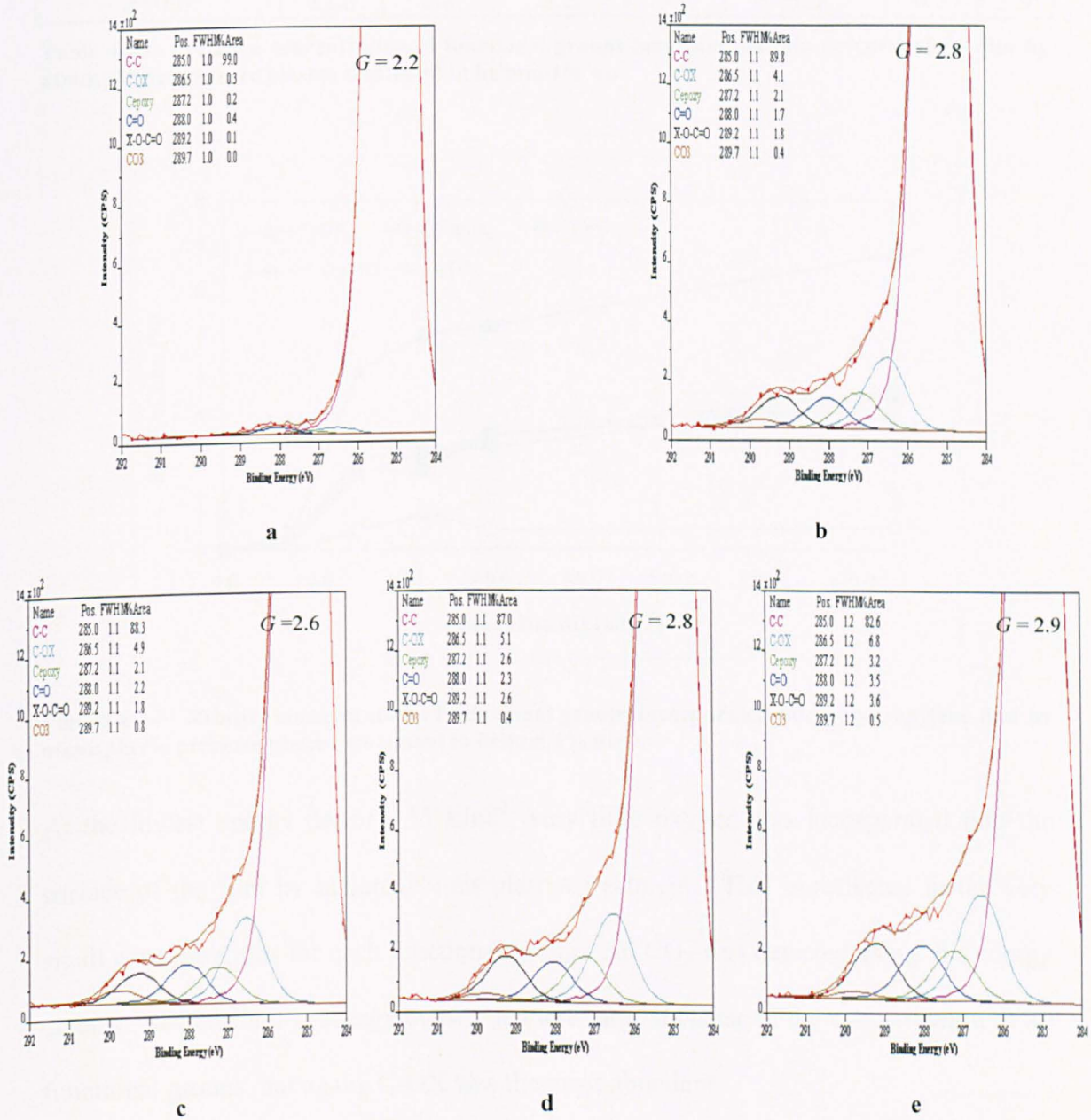

Figure 4-23: XPS curve fit for the carbon (C 1s) core level of polypropylene film activated using helium/1% air APP with energy density a) 15 kJm^{-2}, b) 30 kJm^{-2}, c) 45 kJm^{-2}, d) 60 kJm^{-2}, e) 150 kJm^{-2}

Table 4-11 and Figure 4-24 present the relative concentration of functional groups determined from the curve-fitting procedure.

Energy Density (kJm^{-2})	Relative Concentration (%)						*G*
	C-C	C-OX	C_{epoxy}	C=O	X-O-C=O	CO_3	
0.0	100.0	0.0	0.0	0.0	0.0	0.0	
15.0	99.0	0.3	0.2	0.4	0.1	0.0	2.2
30.0	89.8	4.1	2.1	1.7	1.8	0.4	2.8
45.0	88.3	4.9	2.1	2.2	1.8	0.8	2.6
60.0	87.0	5.1	2.6	2.3	2.6	0.4	2.8
150.0	82.6	6.8	3.2	3.5	3.6	0.5	2.9

Table 4-11: Relative concentration of functional groups incorporated into polypropylene film by atmospheric pressure plasma treatment in helium/1% air

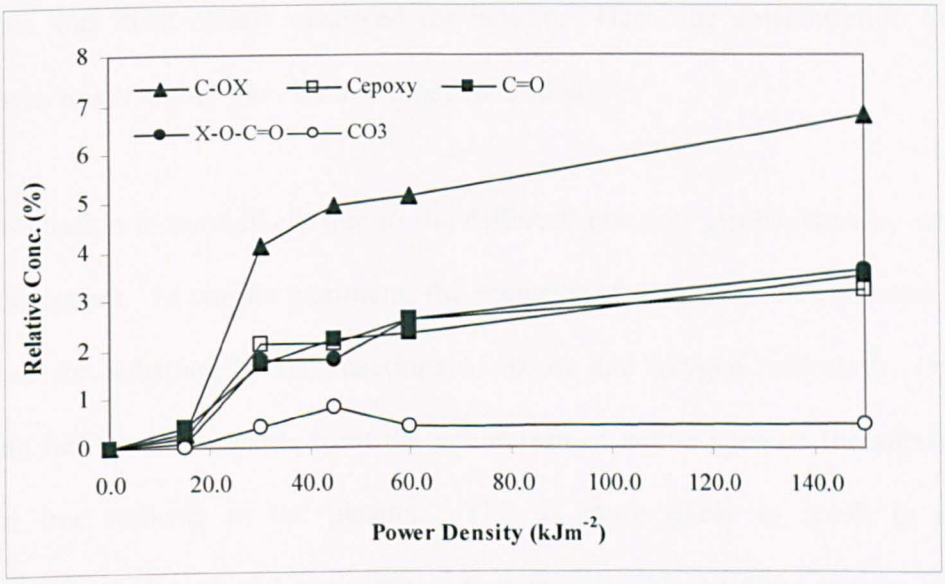

Figure 4-24: Relative concentration of functional groups incorporated into polypropylene film by atmospheric pressure plasma treatment in helium/1% air

At the lowest energy density, 15 kJm^{-2}, very little oxygen was incorporated into the surface of the film by helium/1% air plasma treatment. This is reflected in the very small concentrations for each functional group. No CO_3 was detected using this energy density. Increasing the energy density led to a large increase in the concentration of all functional groups, but again, C-OX was the most abundant.

e) Summary of effect of treatment method on surface chemistry

The functional groups incorporated into the surface of the polypropylene film following each of the treatment methods were found to be the same: C-OX (where X = H or C), C-O-O·, C=O and CO_2X (where X = H or C). However, their intensities varied between polypropylene films treated using corona discharge or atmospheric pressure plasma. For corona treated BOPP, all functional groups were introduced in similar concentrations under the conditions used. For helium, helium/oxygen or helium/air atmospheric pressure plasmas, a significant difference was always observed between C-OX and the other functionalities. For the atmospheric pressure plasma treatments, this difference was most clearly observed for helium. Here, the concentration of C-OX groups was much higher than for any other functionality.

This observation is most likely due to the different reaction mechanisms by which the oxidation occurs. In corona treatment, the majority of oxygen is incorporated into the surface of the substrate by the reactions of ozone and oxygen radicals[18]. Oxidation following helium APP results from the generation of active sites on the substrates by UV and free radicals in the plasma. This is more likely to result in a larger concentration of alcohol and ether groups than more highly oxidised species in helium APP treated polypropylene. For helium/oxygen and helium/air plasma the reaction of ozone and oxygen radicals becomes more apparent, with the additional functionalities increasing in concentration towards that of C-OX, although not to the same extent as observed following corona treatment.

4.3.8 Surface Stability: Effect of treatment method

As discussed in section 4.3.5, the generation of a water soluble layer at the surface of polypropylene film treated using corona discharge (commonly referred to as low-molecular-weight-oxidised-material - LMWOM) has been documented by several researchers[8,14,16]. The reduction in Δ(O/C) caused by immersion in water was noted previously for both corona and atmospheric pressure plasma treated BOPP. The following section discusses how the surface chemistry changes following immersion, and the effect of the treatment method on the stability of the modified surface

a) Surface chemistry of corona discharge treated BOPP film – immersed samples

The curve-fitting protocol described previously was also used to elucidate the chemistry of the corona discharge treated polypropylene film following immersion in water. Synthetic peaks representing the same functional groups were required to obtain a good fit to the experimental data, although their intensities varied following the immersion process, in agreement with the results of Gerenser *et al*[7] and previous work by O'Hare *et al*[14].

As noted in section 4.3.5, immersion of corona discharge treated polypropylene film resulted in a slight decrease in Δ(O/C) for samples treated using an energy density of 0 – 10 kJm^{-2}. At energy densities greater than this, a much larger decrease in Δ(O/C) was observed. This was reinforced by the curve-fitting data; at low energy densities, very little change in the concentration of the functional groups were observed, whereas at higher power densities, the decrease in the shoulder on the high binding energy side of the C 1s core level (and hence in the concentration of oxidised functionalities) was apparent. The concentrations of the functional groups following immersion are presented in Table 4-12, and Figure 4-25. By comparison with Table 4-8, for the samples prior to water immersion, it is noted that the functional groups that change least

are C-OX and C-O-O·, for low power density treatment. At power densities above 10 kJm^{-2}, the concentration of all functional groups decreased on washing, although C-OX remains most abundant.

Energy Density (kJm^{-2})	Relative Concentration (%)						*G*
	C-C	C-OX	C_{epoxy}	C=O	X-O-C=O	CO_3	
0.0	100.0	0.0	0.0	0.0	0.0	0.0	
15.0	97.2	1.7	0.3	0.4	0.2	0.1	1.3
30.0	94.9	3.0	0.3	1.0	0.7	0.1	3.6
45.0	95.4	2.3	0.9	0.8	0.5	0.1	4.3
60.0	96.2	1.9	0.8	0.6	0.4	0.1	2.5
150.0	95.5	2.0	0.9	0.9	0.6	0.1	2.0

Table 4-12: Relative concentration of functional groups incorporated into polypropylene film by corona discharge treatment in air. Samples immersed in water for 10 seconds prior to analysis

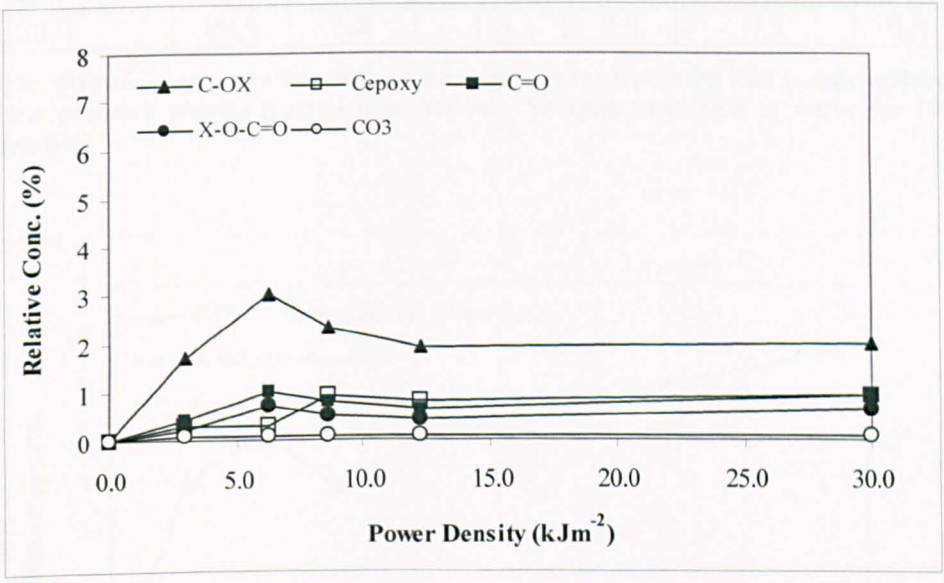

Figure 4-25: Relative concentration of functional groups incorporated into polypropylene film by corona discharge treatment in air. Samples immersed in water for 10 seconds prior to analysis

b) Surface chemistry of helium plasma treated BOPP film – immersed samples

There was little change in the concentration of functional groups following immersion, except at the highest energy density treatment, where the C-OX concentration increased somewhat. The data presented in Table 4-13 and Figure 4-26 indicate that the surface generated by helium atmospheric pressure plasma, whilst not being as highly oxidised as that generated by corona, is very stable to water immersion.

Energy Density (kJm^{-2})	Relative Concentration (%)						*G*
	C-C	C-OX	C_{epoxy}	C=O	X-O-C=O	CO_3	
0.0	100.0	0.0	0.0	0.0	0.0	0.0	
15.0	93.1	4.0	1.2	0.9	0.5	0.4	2.0
30.0	92.9	4.9	1.2	0.5	0.3	0.2	2.3
45.0	93.9	3.9	1.2	0.4	0.3	0.2	2.4
60.0	92.4	4.8	1.3	0.8	0.5	0.2	3.1
150.0	89.9	6.8	1.6	0.9	0.5	0.3	5.5

Table 4-13: Relative concentration of functional groups incorporated into polypropylene film by atmospheric pressure plasma treatment in helium. Samples immersed in water for 10 seconds prior to analysis

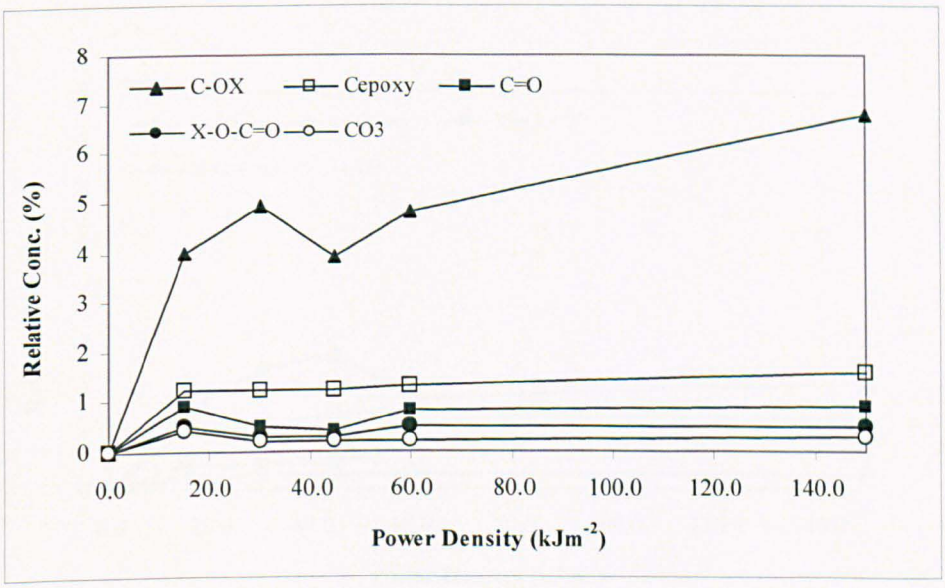

Figure 4-26: Relative concentration of functional groups incorporated into polypropylene film by atmospheric pressure plasma treatment in helium. Samples immersed in water for 10 seconds prior to analysis

c) Surface chemistry of helium/1% O_2 plasma treated BOPP film – immersed samples

A reduction in the concentration of oxidised carbon functional groups was observed following immersion in water. C-OX remained the most abundant species, although the relative concentration was not as high compared to the other functional groups, as was observed for corona treated, or helium APP treated polypropylene film. The data obtained from curve-fitting is presented in Table 4-14 and Figure 4-27.

Energy Density (kJm^{-2})	Relative Concentration (%)						*G*
	C-C	C-OX	C_{epoxy}	C=O	X-O-C=O	CO_3	
0.0	100.0	0.0	0.0	0.0	0.0	0.0	
15.0	96.2	1.6	1.2	0.5	0.3	0.2	2.0
30.0	95.1	2.4	1.2	0.5	0.5	0.3	2.4
45.0	94.3	2.7	1.5	0.7	0.5	0.3	1.8
60.0	94.7	1.8	1.5	0.8	0.9	0.3	4.3
150.0	94.0	2.1	1.4	1.1	1.1	0.3	2.8

Table 4-14: Relative concentration of functional groups incorporated into polypropylene film by atmospheric pressure plasma treatment in helium/1% oxygen. Samples immersed in water for 10 seconds prior to analysis

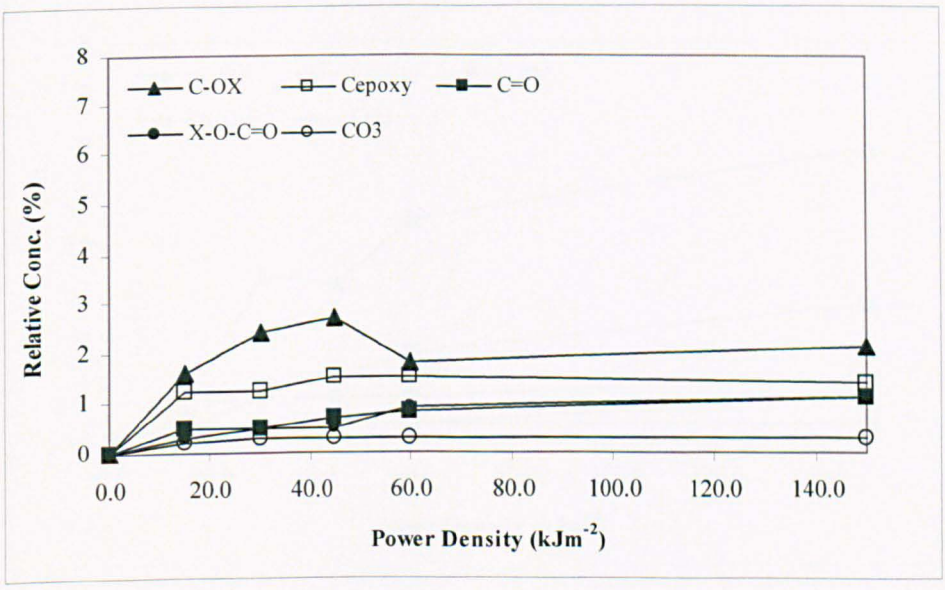

Figure 4-27: Relative concentration of functional groups incorporated into polypropylene film by atmospheric pressure plasma treatment in helium/1% oxygen. Samples immersed in water for 10 seconds prior to analysis

d) Surface chemistry of helium/1% air plasma treated BOPP film – immersed samples

The curve-fits for the helium/air plasma treated polypropylene following immersion follow the same trend as observed prior to immersion. The most abundant group is C-OX, with the other functionalities having similar concentrations. A decrease in concentration of all functional groups was observed following immersion, as presented in Table 4-15 and Figure 4-28.

Energy Density (kJm^{-2})	Relative Concentration (%)						*G*
	C-C	C-OX	C_{epoxy}	C=O	X-O-C=O	CO_3	
0.0	100.0	0.0	0.0	0.0	0.0	0.0	
15.0	98.5	0.7	0.1	0.5	0.3	0.0	3.2
30.0	94.6	3.3	0.2	1.0	0.8	0.0	2.2
45.0	94.7	3.1	0.2	1.2	0.8	0.3	1.9
60.0	92.5	4.4	0.3	1.7	0.8	0.3	3.0
150.0	89.3	5.8	0.8	2.7	1.2	0.3	2.0

Table 4-15: Relative concentration of functional groups incorporated into polypropylene film by atmospheric pressure plasma treatment in helium/1% air. Samples immersed in water for 10 seconds prior to analysis

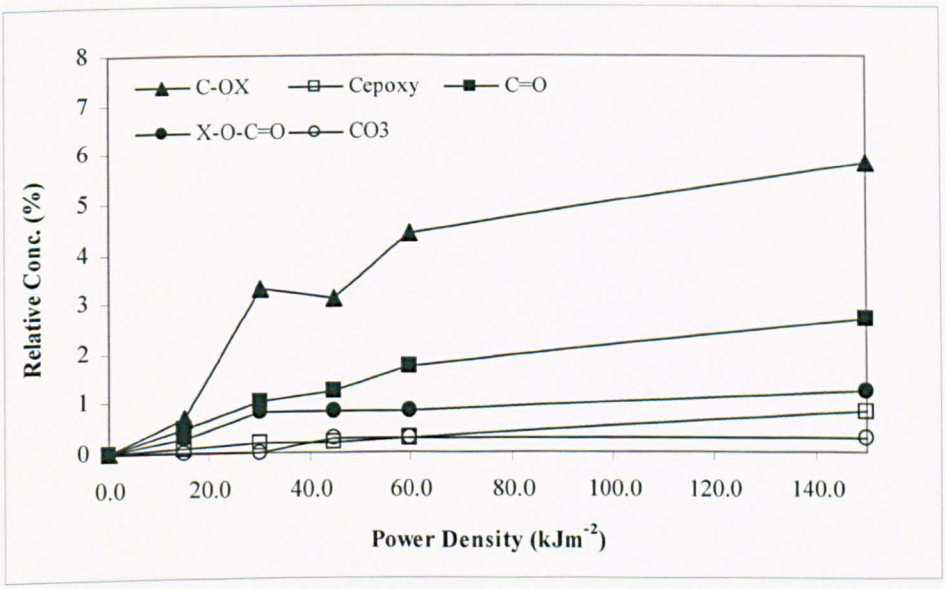

Figure 4-28: Relative concentration of functional groups incorporated into polypropylene film by atmospheric pressure plasma treatment in helium/1% air. Samples immersed in water for 10 seconds prior to analysis

e) Summary of the effect of treatment conditions on surface hydrolytic stability

The stability of the modified layer was easily evaluated by the changes in the surface chemistry following immersion in water. The most apparent change was noted for corona treated polypropylene film, which showed the greatest percentage reduction in both Δ(O/C) and in oxidised carbon functional groups. The amount of water-soluble materials was lowest for helium APP treated polypropylene films. Helium/oxygen and helium/air treated polypropylene films had intermediate amounts of water-soluble material present.

4.3.9 The effect of treatment method on surface morphology

The surface morphology of polypropylene film is well documented[39], and Figure 4-29 clearly shows the defined fibrillar structure often commented upon. In the enhanced contrast phase image, the biaxial orientation of the crystalline lamellae of the polypropylene film, as observed by Boyd *et al.*[3] is apparent.

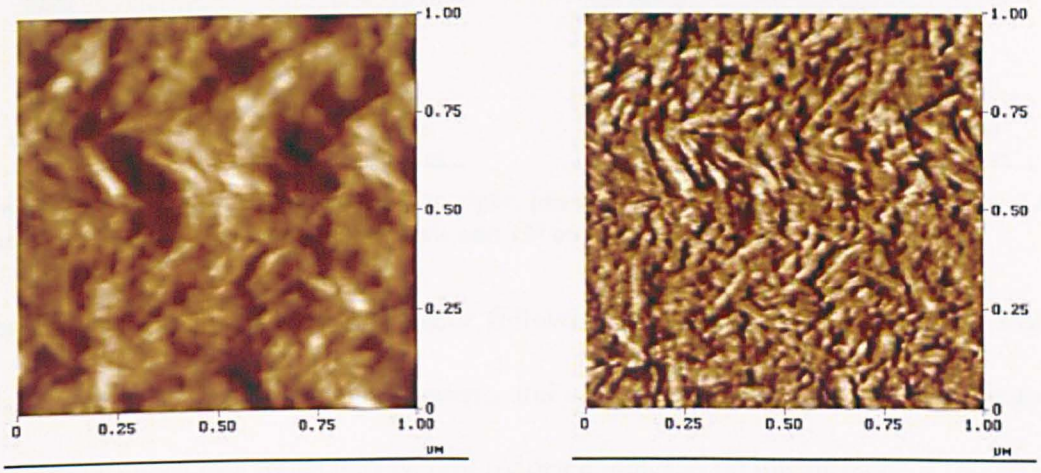

Figure 4-29: 1μm AFM images left: height, right: phase of 'as received' polypropylene film. Light to dark corresponds to 20nm on height scale and 15° on phase scale

No evidence of the spherulitic structure of crystalline BOPP[40,41] was observed, Figure 4-30, but the observation of spherulites is very dependent on the specific nature of the film, e.g. the degree of crystallinity, molecular weight, polydispersity and processing conditions. Furthermore, in cases where spherulites have been observed, the analyses have tended to be carried out on microtomed samples, whereas in this work, it was the surface of an untreated, unwashed film that was analysed.

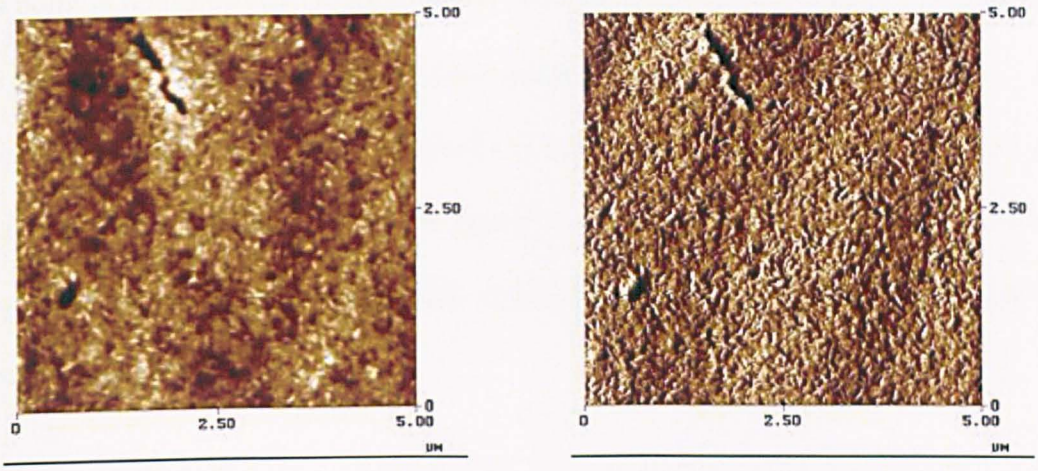

Figure 4-30: 5μm AFM images left: height, right: phase of 'as received' polypropylene film. Light to dark corresponds to 30nm on height scale and 15° on phase scale

Clear changes in the morphology occur following corona discharge treatment, Figure 4-31. Globular features became apparent, and are generally accepted as occurring due to the formation of low molecular weight oxidised material on the surface[3,8,14, 18].

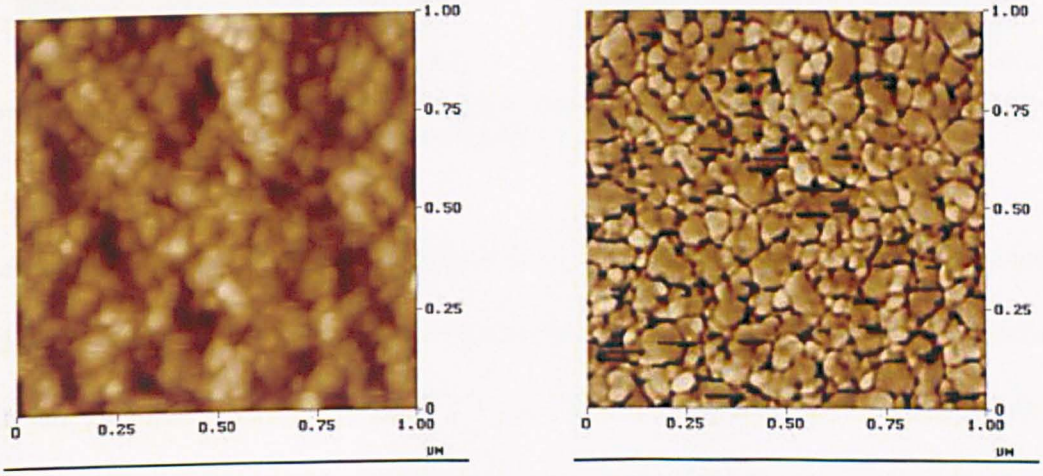

Figure 4-31: 1μm AFM images left: height, right: phase of polypropylene film corona discharge treated at 6 kJm^2. Light to dark corresponds to 20nm on height scale and 15° on phase scale CDT = 6 kJm^{-2}

When the corona energy density during treatment is increased further, a different morphology was observed. In this case, as presented in Figure 4-32, the height image (left) a fibrillar structure is observed. However, while the data scale for the height image was maintained at 30 nm, the area of the image is 5 x 5 μm. The hypothesis is

that ablation of the amorphous regions[39] of the film is occurring at high power density. This point is reinforced by the information from the phase image (right). The data scale here is only 3°, compared with previous images where the data scale was 15°. This indicates that there is very little chemical or viscoelastic heterogeneity on the film. Any variations seen here appear to relate purely to topographic features. The remaining structure relates to a film that has been uniformly modified, both from a chemical and physical point of view.

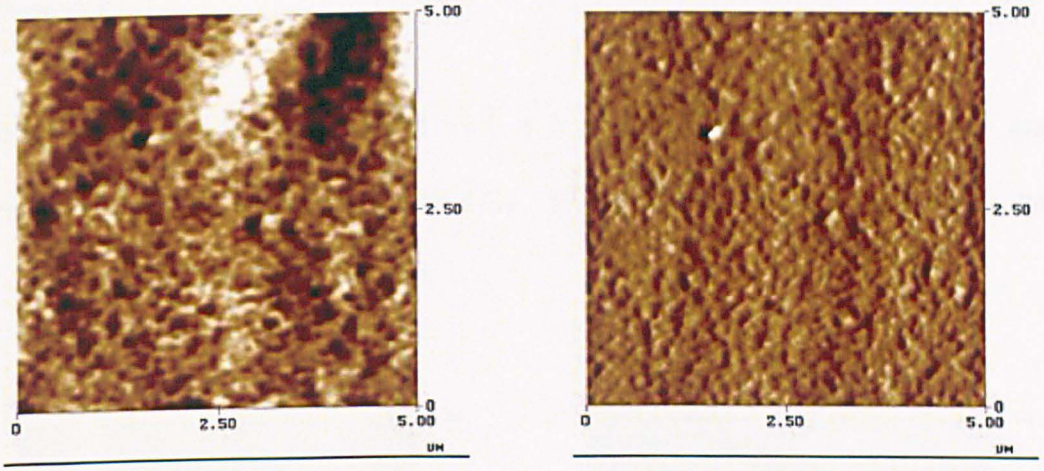

Figure 4-32: 5μm AFM images left: height, right: phase of polypropylene film corona treated at 15 kJm^{-2}. Light to dark corresponds to 30nm on height scale and 3° on phase scale

When the energy density was maintained at 15 kJm^{-2}, but the method of film treatment used was helium APP, the fibrillar structure occurring following corona discharge treatment was not observed. In the 5 x 5 μm images in Figure 4-33 both the height and phase images have a grainy appearance. The data scale for the phase image was returned to 15°, indicating a greater variation in chemistry following helium APP.

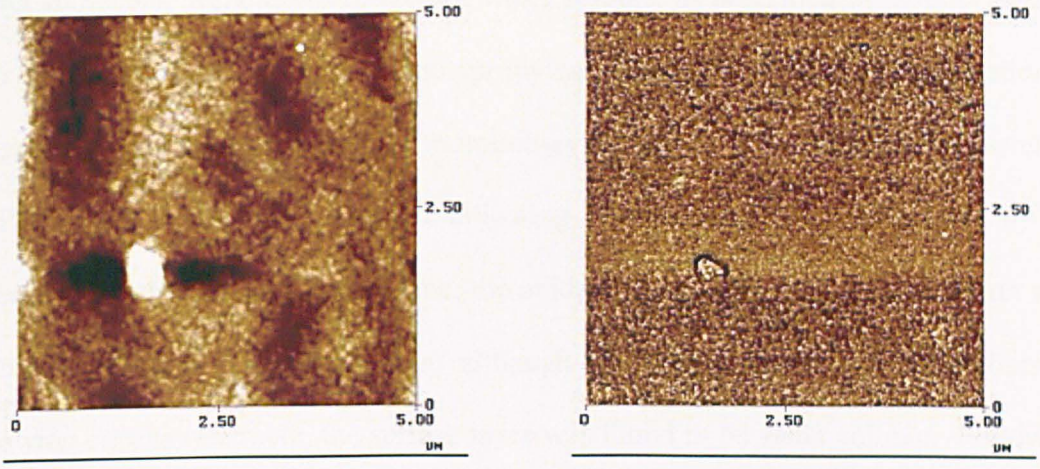

Figure 4-33: 5μm AFM images left: height, right: phase of polypropylene film treated at 15 kJm^{-2} in helium atmospheric pressure plasma. Light to dark corresponds to 30nm on height scale and 15° on phase scale

When the image size was reduced to 1 x 1 μm^{-2} scale, the reason for the grainy morphology becomes apparent, Figure 4-34. The globular features caused by oxidation and chain scission are clearly present.

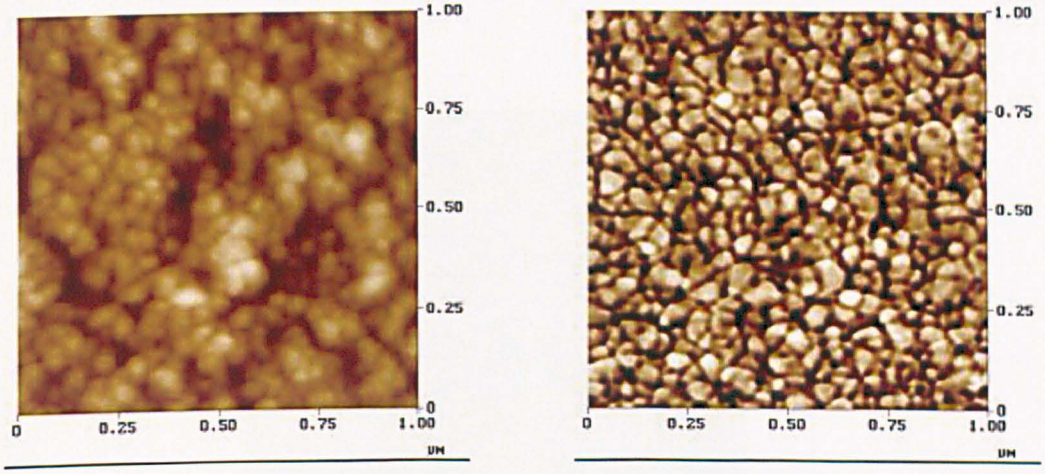

Figure 4-34: 1μm AFM images left: height, right: phase of polypropylene film treated at 15 kJm^{-2} in helium atmospheric pressure plasma. Light to dark corresponds to 20nm on height scale and 15° on phase scale

However, as discussed in Table 4-4, which presents the Δ(O/C) on helium APP treated polypropylene before and after immersion in water, no water soluble material is generated by helium plasma treatment. As such, it is proposed that the globular materials observed in Figure 4-34 are due to agglomeration of oxidised materials of

higher molecular weight, which are not water soluble, as described by Strobel *et al* in their paper on flame treatment of polypropylene film[18]. They noted no reduction in oxygen concentration or change in morphology following immersion of flame-treated BOPP. The limited chain scission following flame treatments is explained by the absence of atomic oxygen in the flame; the oxidation proceeds instead *via* reaction with hydroxyl radicals. By comparison, although a similar morphology was observed following corona treatment, the surface layer was found to be water soluble. Following immersion, although the structure did not appear identical to that of the untreated film, the globular features previously observed have been removed, Figure 4-35. This supports the observations made by XPS, whereby the oxygen content did not return to that of the untreated film following immersion, but reached a finite value. Also noted is the appearance of two crevices of ~ 200 nm in length. It is surmised that these are damaged areas caused by localised arcs in the corona. It is only following removal of the LMWOM that these features were visible.

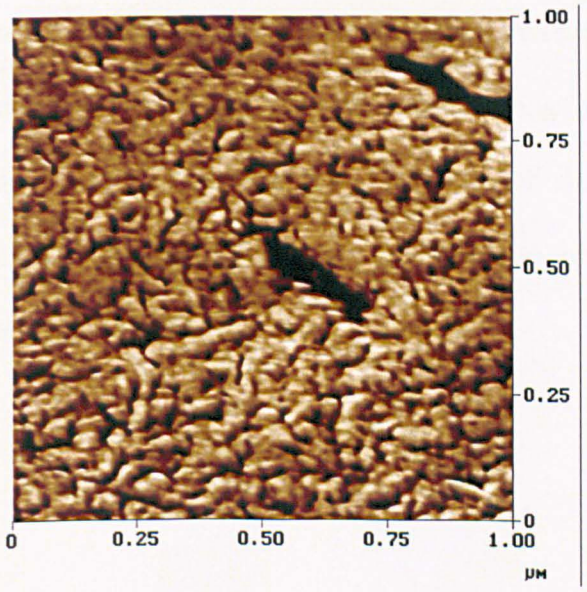

Figure 4-35: 1µm AFM phase image of polypropylene film corona discharge treated at 6 kJm^{-2} then immersed in water. Light to dark corresponds to 15° on phase scale

A very similar morphology is observed following treatment in helium atmospheric pressure plasma containing 1% oxygen, Figure 4-36. In this case, however, the globular features are slightly bigger than those formed in helium plasma. Examination of the 5 x 5 μm images, Figure 4-37, where the topographical features are more apparent than those for helium plasma treated polypropylene film.

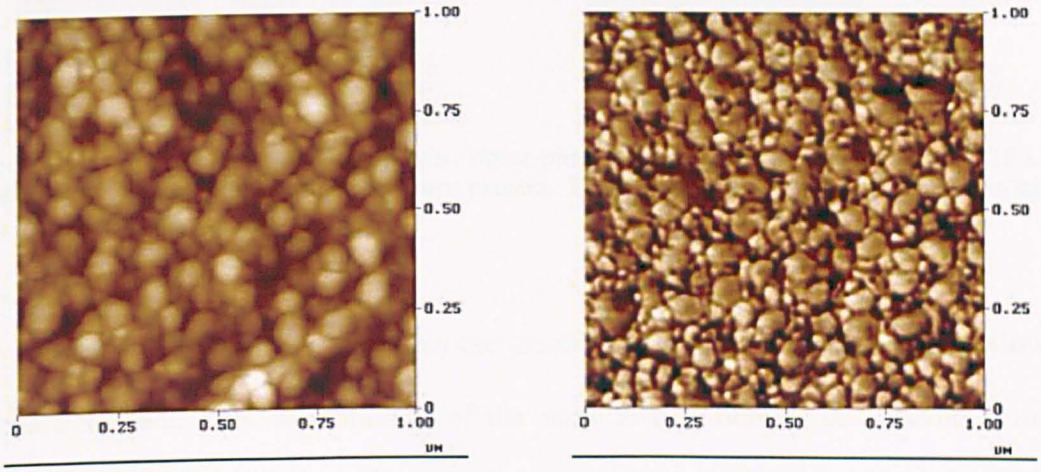

Figure 4-36: 1μm AFM images left: height, right: phase of polypropylene film treated at 15 kJm^{-2} in helium/ 1% oxygen atmospheric pressure plasma. Light to dark corresponds to 20nm on height scale and 15° on phase scale

A very small amount of LMWOM was generated using these treatment conditions, Table 4-5. By comparison, no LMWOM was created using helium plasma. The oxygen present in the plasma here led to the formation of shorter, oxidised chain fragments that were more mobile, and thus more easily able to agglomerate, leading to the larger globular features in the AFM images.

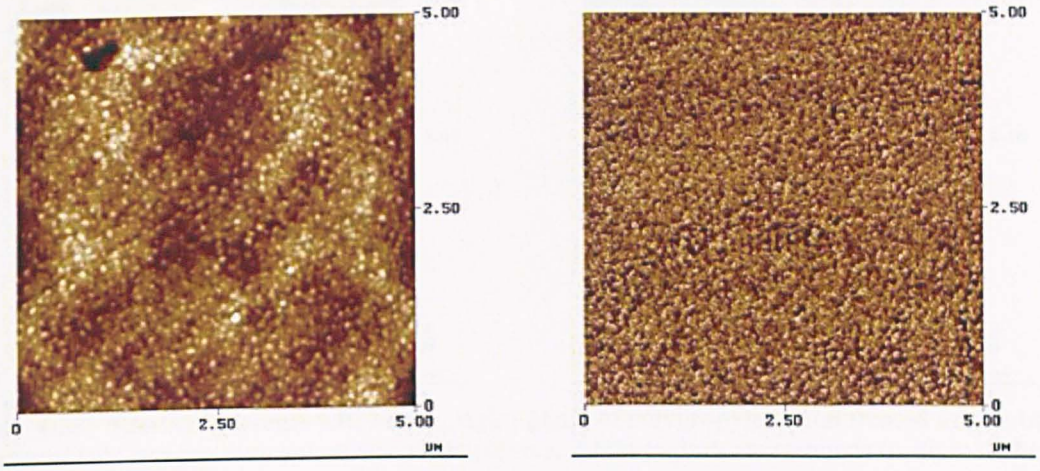

Figure 4-37: 1μm AFM images left: height, right: phase of polypropylene film treated at 15 kJm^{-2} in helium/ 1% oxygen atmospheric pressure plasma. Light to dark corresponds to 30nm on height scale and 15° on phase scale

The presence of oxygen also explains the greater damage caused to the film following corona treatment, even with the use of the same energy density of 15 kJm^{-2}. In the corona treated samples, there was 21% oxygen during treatment, compared with ~1% during APP. This also explains the greater level of oxidation achieved for similar energy densities using corona, Figure 4-10. Furthermore, a greater deal of localised damage to the film during corona treatment is caused by the filamentary nature of the discharge. These may be exemplified by creating a filamentary discharge in the atmospheric pressure plasma apparatus by increasing the oxygen concentration to 10% in the helium plasma. Figure 4-38 clearly indicates the damage to the film caused by aggressive treatment conditions. Large variations in the height image demonstrate the formation of 1μm sized crevices and mounds. However, as observed for the corona treated sample, the lack of variation in the phase image indicates a more homogeneous chemistry.

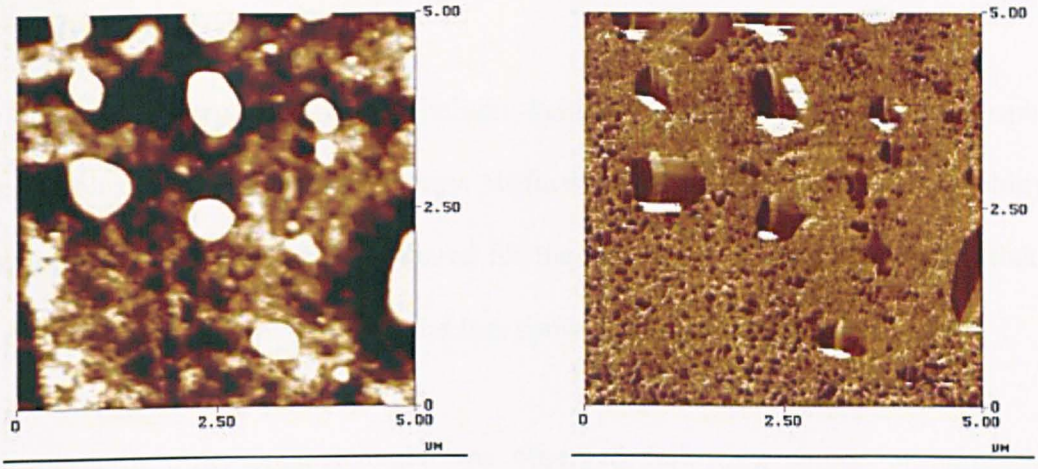

Figure 4-38: 5μm AFM images left: height, right: phase of polypropylene film treated at 15 kJm^{-2} in helium/ 10% oxygen atmospheric pressure plasma. Light to dark corresponds to 30nm on height scale and 15° on phase scale

4.4 CONCLUSIONS

The effect of corona discharge and helium, helium/oxygen and helium air atmospheric pressure plasma on the surface energy, surface chemistry and surface morphology of polypropylene film have been compared for the first time. It is our hypothesis that the use of APPs lead to more uniform, and less damaging treatment of the substrate.

A decrease in water contact angle was observed following corona or atmospheric pressure plasma treatment of the polypropylene surface. As expected, this was due to incorporation of oxygen at the surface of the film. The amount of oxygen incorporated was presented as Δ(O/C), to enable future comparison between other polymer substrates.

Δ(O/C) increased with energy density for all treatment methods. Corona treatment led to the largest increase in Δ(O/C), followed by helium/air and helium/oxygen. At power densities below 60 kJm^{-2}, all helium/oxygen and helium APP treatments resulted in similar oxygen uptakes. Helium APP resulted in a lower Δ(O/C) at higher energy densities. These trends were reflected by the water contact angle measurements.

Further information about the surface chemistry was obtained by carrying out curve-fitting of the carbon (C 1s) core level. A consistent curve-fitting protocol was developed, described, and applied to all high-resolution carbon spectra. The functional groups observed on the surface of polypropylene film following either treatment by corona discharge in air or helium, helium/1% oxygen or helium/ 1% air plasma treatment have been assigned as C-OX (where X = H or C), C_{epoxy}, C=O, CO_2X (where X = H, C or O-C=O) and CO_3.

All functional groups were present following each treatment, independent of energy density, with the exception being helium/air treatment at the lowest energy density. The relative intensity of each of the synthetic peaks associated with each functional group varies depending on both the method of treatment, and the energy density used.

The same functional groups were present following immersion in water, although their relative concentrations tended to vary. The modified surface generated by helium plasma treatment of polypropylene film was the most stable, whilst the corona discharge treated polypropylene surface was most water soluble. This has been explained by the higher oxygen gas concentration present during corona discharge treatment. The presence of atomic oxygen during this type of treatment leads to far higher rates of chain scission, and the generation of low molecular weight oxidised materials (LMWOM).

The existence of LMWOM has been confirmed using atomic force microscopy, where globular features are shown to represent the agglomeration of such materials. Removal of these features following immersion of the samples in water has been confirmed. The damage caused by the filamentary nature of the corona has also been demonstrated.

4.5 REFERENCES

[1] Briggs, D., *Surface Analysis and Pretreatment of Plastics and Metals*, Brewis, D.M. (ed), Applied Surface Science, London, 1982, 199

[2] Kinloch, A.J., *Adhesion and Adhesives, Science and Technology*, Chapman and Hall, London, 1990

[3] Boyd, R.D.; Kenwright, A.M.; Badyal, J.P.S.; Briggs, D., 'Atmospheric pressure plasma treatment of biaxially oriented polypropylene', *Macromolecules*, **30**, 1997, 5429 – 5436

[4] Briggs, D.; Kendall, C.R., ' Derivatisation of discharge-treated LDPE: and extension of XPS analsyis and a probe of specific interactions in adhesion', *Int. J. Adhes. Adhes.*, **2**, 1982, 13 -17

[5] Kim, C.Y.; Evans, J.; Goring, D.A.I., 'Corona-induced autohesion of polyethyelene', *J. Appl. Polym. Sci.*, **15**, 1971, 1365

[6] Owens, D.K., 'Mechanism of corona-induced self-adhesion of polyethylene film', *J. Appl. Polym. Sci.*, **19**, 1975, 265

[7] Gerenser, L.J.; Elman, J.F.; Mason, M.G.; Pochan, J.M., 'ESCA studies of corona discharge treated polyethylene surfaces by use of gas-phase derivatisation', *Polymer*, **26**, 1985, 1163 – 1166

[8] Strobel, M.; Dunatov, C.; Strobel, J.M.; Lyons, C.S.; Perron, S.J.; Morgen, M.C., 'Low-molecular-weight materials on corona-treated polypropylene', *J. Adhes. Sci. Technol.*, **3**, 1989, 321 – 335

[9] Strobel, M.; Lyons, C.S.; Strobel, J.M.; Kapaun, R.S., 'Analysis of air corona treated polypropylene and poly(ethylene terephthalate) films by contact angle measurements and X-ray photoelectron spectroscopy', *J. Adhes. Sci. Technol.*, **6**(4), 1992, 429 - 443

[10] Strobel, M.; Walzak, M.J.; Hill, J.M.; Lin, A.; Karbashewski, E.; Lyons, C.S., 'A comparison of gas-phase methods of modifying polymer surfaces', *J. Adhes. Sci. Technol.*, **9**, 1995, 365

[11] Foerch, R.; Izawa, J.; Spears, G.J., 'A comparative study of the effects of remote nitrogen plasma, emote oxygen plasma, and corona discharge', *J. Adhes. Sci. Technol.*, **5**, 1991, 549

[12] Foerch, R.; McIntyre, N.S.; Hunter, D.H., 'Oxidation of polyethylene surfaces by remote plasma discharge. A comparison study with alternative oxidation methods', *J. Polym. Sci. A: Chemistry*, **28**, 1990, 193 –204

[13] Zhang, D.; Sun, Q.; Wadsworth, L.C., *Polymer Eng. Sci.*, **38**, 1998, 965-970

[14] O'Hare, L.A.; Leadley, S.R.; Parbhoo, B. 'Surface physicochemistry of corona discharge treated polypropylene film', *Surface and Interface Analysis*, **33**, 2002, 335 - 342

[15] Massines, F.; Messaoudi, R.; Mayoux, C., 'Comparison between air filamentary and helium glow dielectric barrier discharges for the polypropylene surface treatment', *Plasmas and Polymers*, **3**(1), 1998, 43 - 59

[16] Guimond, S.; Radu, I.; Czermuszkin, G.; Carlosson, D.J.; Wertheimer, M.R., 'Biaxially oriented polypropylene (BOPP) surface modification by nitrogen atmospheric pressure glow discharge (APP) and by air corona', *Plasmas and Polymers*, 7(1), 2002

[17] van Roosmalen, A.J.; Baggerman, J.A.G.; Brader, S.J.H., 'The AC discharge', in *Dry Etching for VLSI*, Plenum Press, New York, 1991

[18] Strobel, M.; Jones, V.; Lyons, C.S.; Ulsh, M.; Kushner, M.J.; Dorai, R.; Branch, M.C., 'A comparison of corona-treated and flame-treated polypropylene films,' *Plasmas and Polymers*, **8**(1), 2003, 61 - 95

[19] Owens, D.K.; Wendt, R.C., 'Estimation of the surface free energy of polymers', *J. Appl. Polym. Sci.*, **13**, 1969, 1741

[20] Kaelble, D.H., 'Dispersion-polar surface tension properties of organic solids', *J. Adhesion*, **2**, 1970, 66

[21] Pabhoo, B.; O'Hare, L.A, 'Surface physico-chemistry of polyester films – Part 2: Surface energy measurements after corona discharge treatment', *Dow Corning Internal Report # 2000-I0000-49070*

[22] Rjeb, A.; Letarte, S.; Tajounte, I.; Chafike El Idrissi, M.; Adnot, A.; Roy, D.; Claire, Y.; Kaloustian, J., *J. Electron Spectrosc. Relat. Phenom.*, **107**, 2000, 221

[23] Sapieha, S.; Cerny, J.; Klenberg-Sapieha, J.E.; Martinu, L., 'Corona versus low pressure plasma treatment: Effect on surface properties and adhesion of polymers', *J.Adhesion*, **42**, 1993, 91-102

[24] Strobel, J.M.; Strobel, M.; Lyons, C.S.; Dunatov, C.; Perron, S., 'Aging of air-corona-treated polypropylene film', *J. Adhesion Sci. Technol.*, **5**(2), 1991, 119 – 130

[25] O'Hare, L.-A.; Leadley, S.R.; Parbhoo, B.P.; Francis, J.G., 'Adhesion of silicone coatings to plastic films', in *Organosilicon V: From Molecules to Materials*, Eds. Auner & Weis, Wiley-VCH, 2003

[26] Pochan, J.M.; Gerenser, L.J.; Elman, J.F., 'An esca study of the gas-phase derivatisation of poly(ethylene terephthalate) treated by dry-air and dry-nitrogen corona discharge', *Polymer*, **27**, 1985, 1058 – 1062

[27] Beamson, G.; Clark, D.T.; Kendrick, J.; Briggs, D., 'Observation of vibrational asymmetry in the high resolution monochromatized XPS of hydrocarbon polymers', *J. Electron Spectroscopy and Related Phenonomena*, **57**, 1991, 79 – 90

[28] Briggs, D. *Surface analysis of polymers by XPS and static SIMS*, Cambridge University Press, 1998

[29] Beamson, G.; Briggs, D. *High Resolution XPS of Organic Polymers: The Scienta ESCA300 Database*, John Wiley & Sons, Chichester, 1992

[30] Briggs, D., 'XPS studies of polymer surface modifications and adhesion mechanisms', *J. Adhesion*, **13**, 1982, 287 – 301

[31] Aouniti, M.; Bertrand, P.; Poncin-Epaillard, F., ''Characterisation of polypropylene surface treated in a CO_2 plasma', *Plasmas and Polymers*, **8**(4), 2003, 225 – 236

[32] Manjipudi, V.; Tirrell, M.; Pocius, A.V., 'Direct measurement of the surface energy of corona treated polyethylene using the surface forces apparatus', *Langmuir*, **11**, 1995, 19 – 23

[33] Alexander, M.R.; Duc, T.M,, 'The chemistry of deposits formed from acrylic acid plasmas', *J. Mat. Chem.*, **8**(4), 1998, 937 –943

[34] Leadley, S.R.; Watts, J.F., 'The use of XPS to examine the interaction of poly(acrylic acid) with oxidised metal substrates', *J. Electron Spectroscopy and Related Phenomena*, **85**, 1997, 101 - 121

[35] Beamson, G.; Clark, D.T.; Kendrick, J.; Briggs, D., 'Observation for vibrational asymmetry in the high resolution monochromatised XPS of hydrocarbon polymers', *J. Electron Spectrosc. Relat. Phenom.*, **57**, 1991, 79 - 90

[36] Briggs, D.; S*urface analysis of polymers by XPS and static SIMS*, Cambridge University Press, Cambridge, 1998

[37] Borcia, G.; Anderson, C.A.; Brown, N.M.D., 'The surface oxidation of selected polymers using an atmospheric pressure air dielectric barrier discharge. Part 1', *Appl. Surf. Sci.*, **221**, 2004, 203-214

[38] Watts, J.F.; Leadley, S.R.; Castle, J.; Blomfield, C.J., 'Adsorption of PMMA on oxidised Al and Si substrates: An investigation by high-resolution X-ray photoelectron spectroscopy', *Langmuir*, **16**(5), 2000, 2292 - 2300

[39] Vansco, G.J.; Allston, T.D.; Chun, I.; Johansson, I.S.; Liu, G.; Smith, P.S.' Surface morphology of polymer films imaged by atomic force microsopy', *Int. J. Polymer Analysis and Characterisation*, **3**, 1996, 89-105

[40] Daniels, C.A., *Polymers: Stucture & Properties*, Technomic Publishing: Lancaster, Basel, 1989

[41] Magonov, S.M.; Whangbo, M.H., 'AFM of polymer crystal surfaces', in *Surface Analysis with STM and AFM: experimental and theoretical aspects of image analysis*, VCH: Weinheim, New York, 1996

CHAPTER 5

DEVELOPMENT OF A METHODOLOGY FOR XPS CURVE-FITTING OF THE O 1S, C 1S AND SI 2P CORE LEVELS OF SILOXANE MATERIALS

5.1 INTRODUCTION

In a manner analogous to the chemical shift in NMR, an electron binding energy shift in XPS can be used to identify the atoms attached to an atom under investigation. (Of course, XPS has the added benefit of analysing only the surface of a material.) Identification of chemical environment can be relatively straightforward for carbon, since the C 1s core level often has clearly defined features. However, in the case of silicon, the range of siloxy chemical environments often make it difficult to resolve distinct features by curve fitting the Si 2p core level. In addition, the binding energy shift for the substitution of each methyl group with an oxygen atom (i.e. each new Si-O group) is estimated at 0.65 eV. By comparison, the effect of each additional C-O bond is to increase the binding energy shift by 1.5 eV. As such, it is difficult to obtain detailed information about the chemical environment of silicon atoms in a material of unknown composition. However, it is usually possible to distinguish silicon in 'organic'- silicone polymers from 'inorganic'- silicate, forms[1,2].

A procedure for obtaining reliable binding energies for the various chemical states of silicon has been described in the literature[3,4]. Curve-fitting of the Si 2p core level acquired from silicon oxides (siloxy units) typically fits the peak using four components, with an increase in binding energy for the replacement of each methyl group by an additional oxygen atom[5]. A useful notation and abbreviation of complex silicone structures takes advantage of the number of oxygen atoms around the silicon atom in a *siloxy* unit[6]. This notation uses the letters M (mono), D (di), T (tri) and Q (quaternary) to represent siloxy units where the silicon atom is linked to one $[(CH_3)_3SiO_{1/2}]$, two $[(CH_3)_2SiO_{2/2}]$, three $[(CH_3)SiO_{3/2}]$, or four $[SiO_{4/2}]$ oxygen atoms, respectively, Scheme 5-1. Fractions are used in this notation to take into account an equal share of an oxygen atom with adjacent siloxy monomeric units.

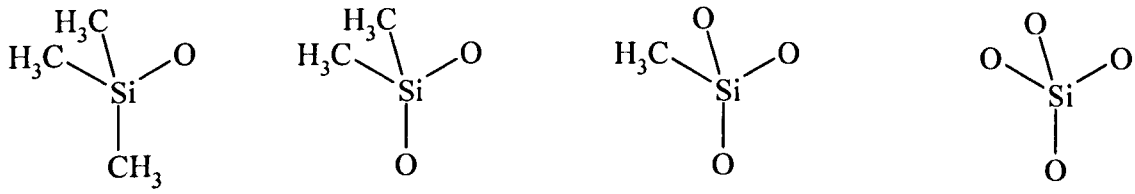

Scheme 5-1: Representations of the various siloxy units encountered in polysiloxanes

Alexander *et al*[4] have fitted one synthetic peak for each of the M, D, T and Q components of a film obtained by plasma deposition of hexamethyldisiloxane. In their work, the positions of D, (polydimethylsiloxane, PDMS) and Q (quartz) units were known. The positions of M and T were estimated to be shifted by one-half of the distance between D and Q, with full width at half maximum (FWHM) constrained to be equal. Similarly, Hillborg *et al*[7] resolved the Si 2p peak into D, T and Q components, although in this work the FWHM does not appear to have been constrained, nor is it possible to determine peak positions from the data provided in the publication. Roualdes *et al*[8] have used a fifth component (representing SiC_4) in curve-fitting the Si 2p core level of polysiloxane deposits formed using 'soft plasma polymerisation' of octamethyltrisiloxane, where a low energy per unit mass of monomer condition is employed.

Curve-fitting the Si 2p core level is further complicated by the presence of two signals for each chemical state, whereas carbon has only one. In Si 2p, these are associated with Si $2p^{3/2}$ and Si $2p^{1/2}$ electron spin states. Beamson and Briggs[3] have fitted a doublet (representing the Si $2p^{3/2}$ and Si $2p^{1/2}$ electronic states) to the Si 2p core level

obtained from analysis of PDMS and polymethylphenylsiloxane (PMPS) D siloxy units. However, no literature was found that described fitting both the Si $2p^{3/2}$ and Si $2p^{1/2}$ spins to a system containing all the M, D, T and Q components.

This chapter includes and expands upon work described in a short communication[9], and describes further development of previous work through the analysis of siloxane compounds, which model complex polysiloxane systems. The Si 2p curve-fits of data from such materials may then be used to determine the surface chemical composition of a high molecular weight homopolymer, and two methylated orthosilicate resins of different chemical compositions. Comparing the surface chemistry with the bulk composition, determined by ^{29}Si NMR spectroscopy, will be used to check the validity of the method. The binding energy positions determined by this method will then be applied to Si 2p curve-fits obtained for siloxanes prepared by atmospheric pressure plasma liquid deposition in *Chapter 6*.

5.2 EXPERIMENTAL

5.2.1 X-ray Photoelectron Spectroscopy

XPS was carried out on a Kratos Analytical Axis Ultra photoelectron spectrometer. The instrument is equipped with a spherical mirror analyser (165 mm mean radius HSA), an integral automatic charge neutraliser and a magnetic lens. A monochromated Al Kα X-ray source was used at a nominal power of 300 W to record spectra at normal emission. Survey spectra were captured using a pass energy of 160 eV, and core levels were captured at 20 eV. Typical acquisition time for the Si 2p core level was 3.6 minutes. All of the samples under consideration required charge compensation using the default settings for polymeric materials.

The use of χ^2 values, or RMS figure of merit may be used as a measure of goodness of fit of XPS data. However, these mathematical procedures do not take into account the operator's understanding of the chemistry of the system. For this reason, the quality of the curve-fit was determined by both examination of a plot of the residuals (a measure of the difference between the experimental envelope and the shape of the synthetic peaks), a goodness of fit parameter ***G*** (χ^2 / number of degrees of freedom), and the eye of the analyst[10].

5.2.2 Model Compounds

A high molecular weight polydimethylsiloxane (PDMS) linear homopolymer (Dow Corning SGM-36®) was used as the standard reference material for the D siloxy unit. This gum was analysed as received without purification or further treatment. Methylated orthosilicate resins of chemical structures $D_{0.14}$-$D^{OH}_{0.12}$-$T_{0.74}$ (DT Resin) and $M_{0.47}$-$T^{OH}_{0.15}$-$Q_{0.38}$, (MQ resin) as determined by ^{29}Si NMR, were also analysed. D^{OH}

and T^{OH} respectively, represent D and T units where a methyl group has been replaced by a hydroxyl group. The siloxane resin samples were prepared by spin coating from a xylene solution of each compound onto a silicon wafer (DT resin – 30 % w/w; MQ resin – 50 % w/w). Spin coating was carried out on a Model P6700 spin coater (Speciality Coating Systems, Indianapolis, USA), for 30 seconds at approximately 2000 rpm. This provided a resin coating of approximately 400 μm thickness, ensuring that the signal from the silicon wafer did not interfere with the XPS analysis of the siloxane resin.

5.2.3 Complex polysiloxane systems

Two commercial polysiloxane materials (approximately 25 μm thick) were spin-coated onto silicon wafer from mesitylene (trimethylbenzene) at 1500 rpm for 30 seconds. The coatings then underwent a soft bake at 110°C for 2 minutes, followed by a full cure at 250°C for 30 minutes to remove any residual solvent. Polysiloxane 'A' contained more polymeric (D) siloxy units and less inorganic (Q) units than polysiloxane 'B'. The bulk composition of these materials was determined from formulation data and ^{29}Si NMR spectroscopy of the starting materials. The NMR compositions for polysiloxane A and B are presented in the results section, in Table 5-8 and Table 5-9, respectively.

5.3 RESULTS AND DISCUSSION

In order to determine unambiguously the binding energy positions of components of the silicon 2p core level for the M, D, T, Q environments, denoted hereafter as Si $2p^M$, Si $2p^D$, Si $2p^T$, Si $2p^Q$, a selection of siloxane compounds available within Dow Corning were analysed by XPS. To ensure that all the environments could be identified, the materials used were a PDMS homopolynmer 'D gum' (Si $2p^D$), a DT resin (Si $2p^D$ and Si $2p^T$), and an MQ resin (Si $2p^M$ and Si $2p^Q$). The D gum is considered first since the binding energy of O 1s, C 1s and Si $2p^D$ has been described in the literature[3].

5.3.1 Curve-fitting of high molecular weight PDMS homopolymer

The procedure for curve-fitting the O 1s, C 1s and Si 2p core levels for the high molecular weight polydimethylsiloxane (PDMS) homopolymer is described here. Two synthetic peaks were applied to the Si 2p core level, to represent the Si $2p^{3/2}$ and Si $2p^{1/2}$ spin states. The FWHM was constrained to be equal in both components, and the area of the peak assigned to Si $2p^{1/2}$ was constrained to be half the area of the Si $2p^{3/2}$ [3]. A good fit to the data was determined, and the energy separation between the Si $2p^{3/2}$ and Si $2p^{1/2}$ doublet was found to be 0.65 eV, Figure 5-1. This is within 0.05 eV of the doublet separation determined by Beamson and Briggs (0.61 eV)[3].

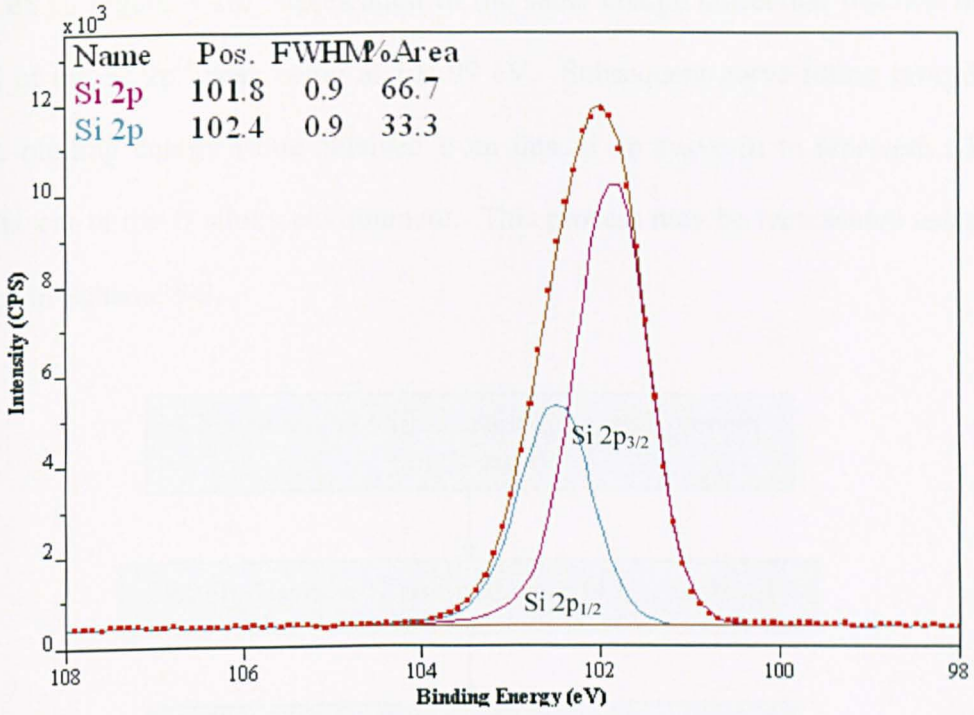

Figure 5-1: Curve-fitting of the Si 2p core level of high molecular weight linear PDMS homopolymer (D Gum) showing the use of two synthetic peaks to represent the Si $2p^{3/2}$ and Si $2p^{1/2}$ spin states of the D siloxy unit. Data presented has been charge corrected to position O 1s at 532.0 eV

A model line-shape that encompassed both these spin states was constructed from the synthetic envelope. This model line-shape was developed for ease of representation in curve-fits of Si 2p core levels with several oxidation states of silicon present. Application of this model line-shape to the high molecular weight siloxane homopolymer showed a good fit, Figure 5-2c.

A synthetic peak was applied to the O 1s core-level. Since there is only one oxidation state of silicon and no –OH groups present in D [-$(CH_3)_2SiO_{2/2}$-], only one synthetic curve was applied. A charge correction value was then applied to the binding energy scale to set this peak binding energy (BE) to 532.0 eV, as described by Beamson and Briggs for curve-fitting the O 1s core level of PDMS and poly(phenylmethylsiloxane) [PPMS][3], Figure 5-2a. A single synthetic peak was then applied to the C 1s core level found at 284.48 eV, which is within 0.1 eV of the value in the literature for PDMS

(284.38 eV)[3], Figure 5-2b. Application of the same charge correction resulted in the centroid of the Si $2p^D$ peak being at 101.99 eV. Subsequent curve-fitting procedures used the binding energy value obtained from this Si 2p curve-fit to represent silicon atoms present in the D siloxy environment. This process may be represented using the flowchart in Scheme 5-2.

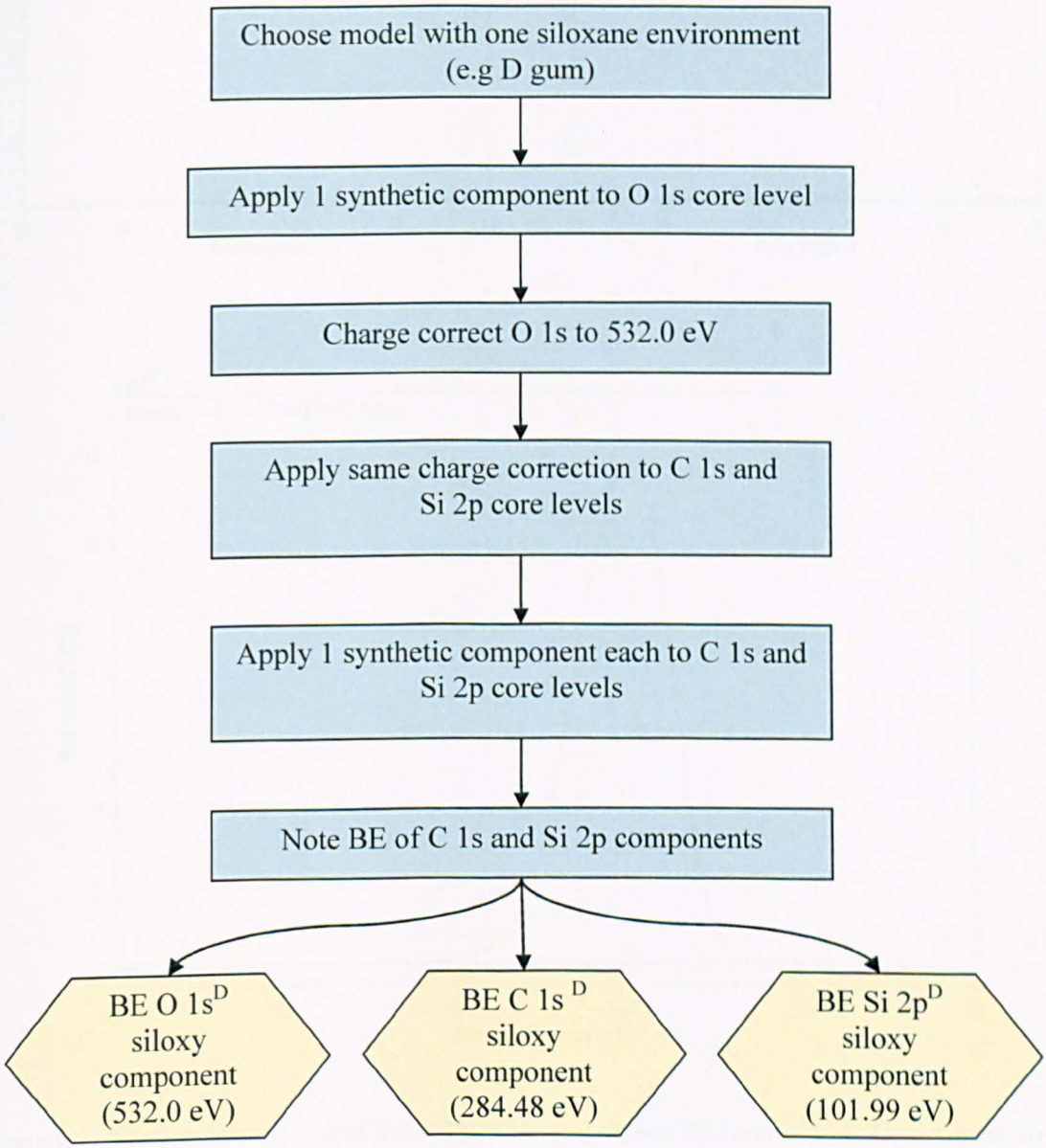

Scheme 5-2: Flowchart describing the procedure for curve-fitting polydimethylsiloxane to provide binding energy values for O $1s^D$, C $1s^D$ and Si $2p^D$ components

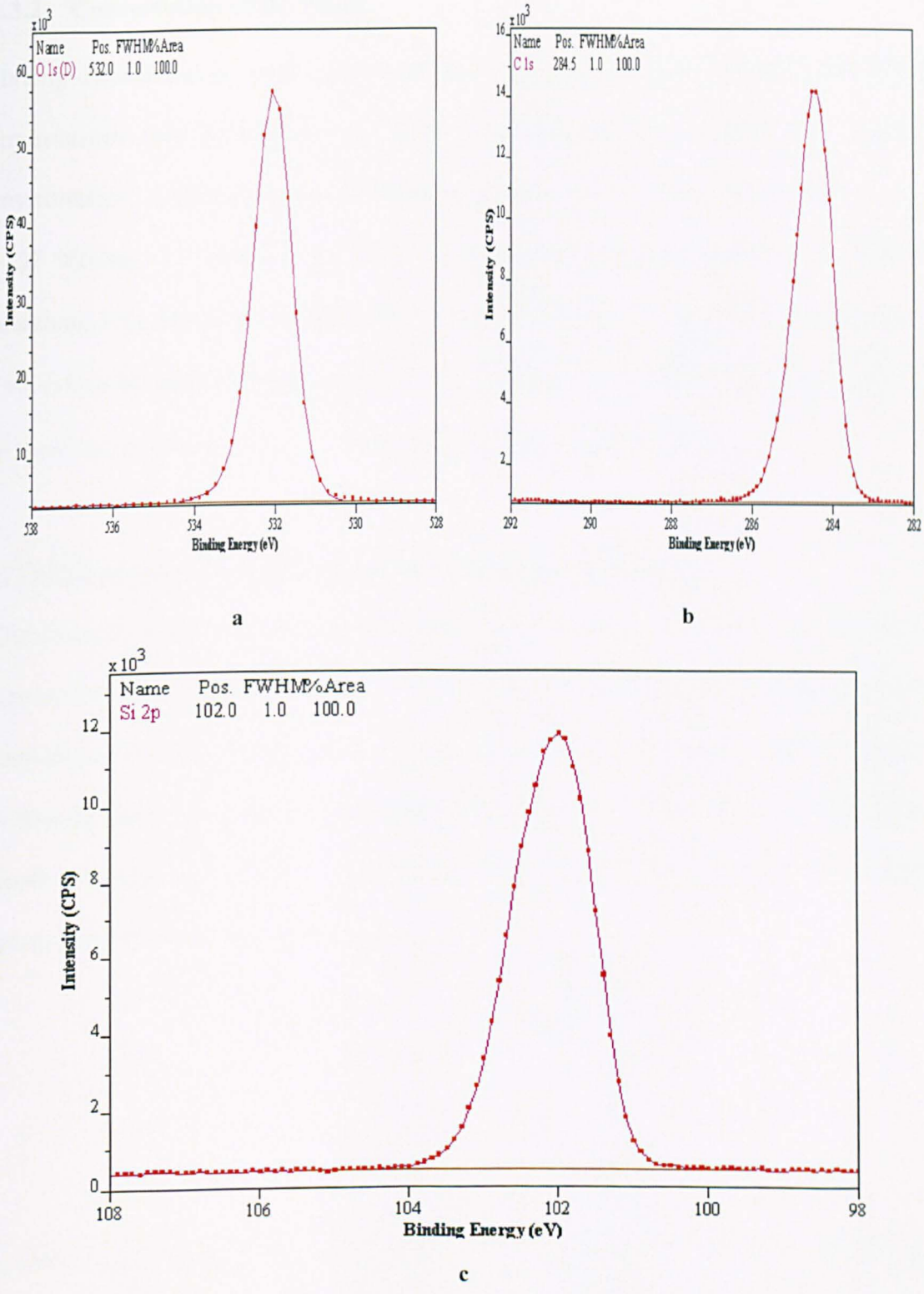

Figure 5-2: High molecular weight linear PDMS homopolymer (D Gum) - a) O 1s core level, b) C 1s core level, c) Si 2p core level using the model line shape. Data presented has been charge corrected to position the O 1s peak at 532.0 eV

5.3.2 Curve-fitting of DT Resin

Having determined the peak position of the Si 2p component for silicon in a D siloxy environment, this information was used to establish the BE of silicon in a T siloxy environment. A siloxane resin containing three silicon environments ($D_{0.14}$-$D^{OH}_{0.12}$-$T_{0.74}$ - DT Resin), was analysed by XPS. Two methods of curve-fitting were possible: assigning only one peak to represent C 1s in both D and T siloxy environments in the C 1s level; or by differentiating between C $1s^D$ [$(\underline{C}H_3)_2$-Si-$O_{2/2}$] and C $1s^T$ [$(\underline{C}H_3)$-Si-$O_{3/2}$] in the C 1s core level. Both of these approaches are explored below.

a) Using one synthetic component to curve-fit the C 1s core level

The core-levels were first charge corrected to position the C 1s core level at 284.48 eV, representative of the $(\underline{C}H_3)_2$-Si-$O_{2/2}$ environment. To curve-fit the Si 2p core level, the formulation was simplified to $D_{0.14}T_{0.86}$, assuming D^{OH} and T are equivalent by XPS. It is thought that the secondary effect of O-Si-O-$\underline{H}$ versus O-Si-O-$\underline{Si}$ will be relatively small compared with the binding energy shift caused by the replacement of a methyl group with an additional oxygen atom.

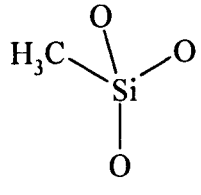

T

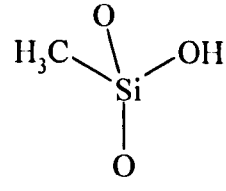

D^{OH}

A component with a binding energy of 101.98 ± 0.1 eV, representative of the D siloxy unit [-$(CH_3)_2SiO_{2/2}$-] and an additional peak representative of the T siloxy unit [-$CH_3SiO_{3/2}$-] were applied to the Si 2p core level. It was not possible to obtain a good curve-fit for the Si 2p core level when constraining the peak for the D siloxy unit to 14% of the total area as suggested by NMR data. Instead, the Si $2p^D$ peak area had to be increased to 22%, Figure 5-3 and Table 5-1.

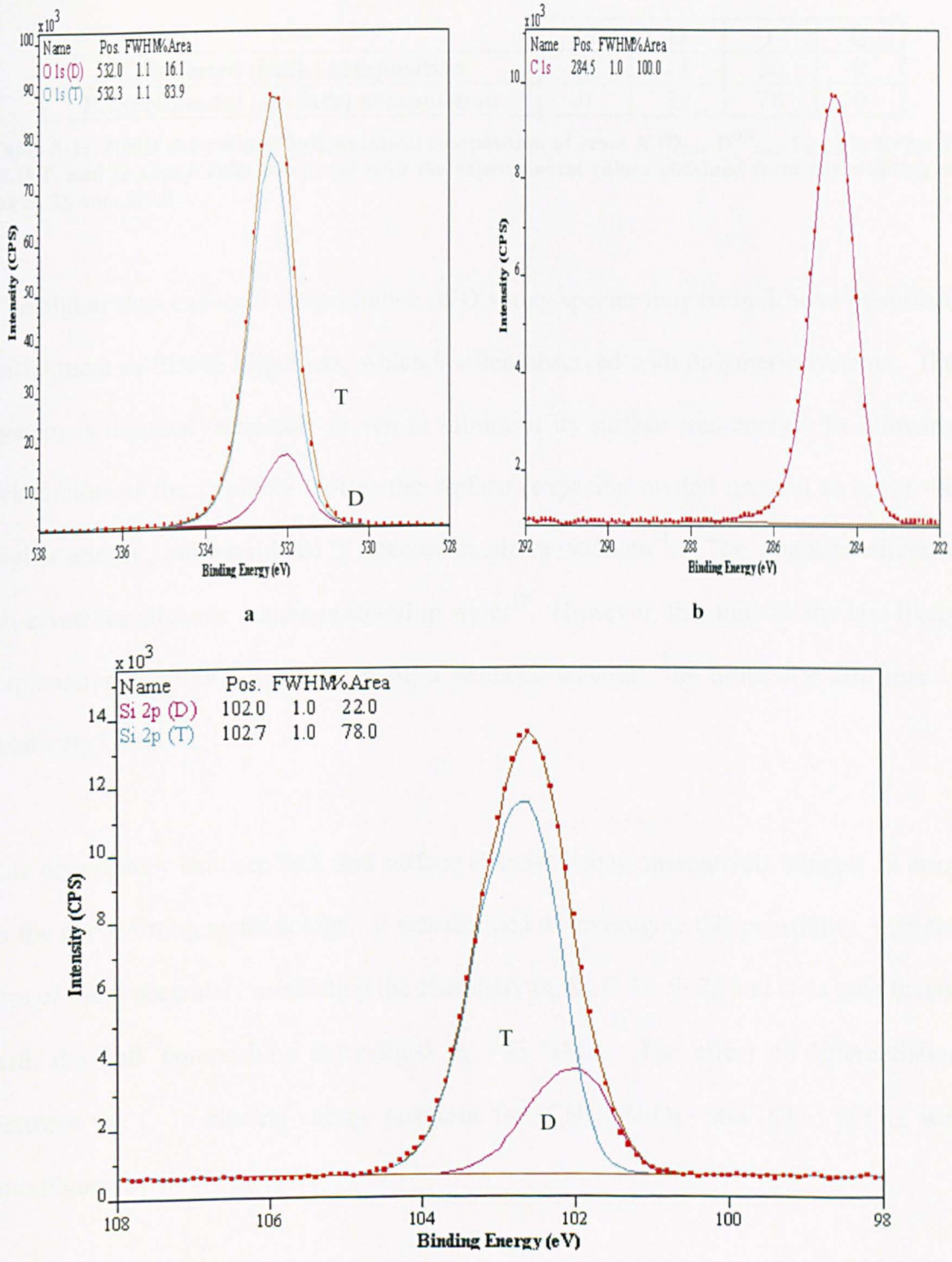

Figure 5-3: Curve-fits for DT resin [$D_{0.14}$-$D^{OH}_{0.12}$-$T_{0.74}$] a) O 1score level, b) C 1s core level, c) Si 2p core level. Spectra have been charge corrected to position C 1s at 284.48 eV

	M	D	T	Q
Calculated (bulk) composition	0	14	86	0
Experimental (surface) composition	0	22	78	0

Table 5-1: NMR determined bulk chemical composition of resin A ($D_{0.14}$-$D^{OH}_{0.12}$-$T_{0.74}$) in terms of M,D,T, and Q siloxy units compared with the experimental values obtained from curve-fitting of the Si 2p core level

The higher than expected concentration of D siloxy species may be indicative of surface enrichment of PDMS oligomers, which is often observed with polymeric systems. The system is thermodynamically driven to minimise its surface free energy, by allowing orientation of the D siloxy unit to the surface (exposing methyl groups) to cover the higher-energy, more-oxidised T species in air or vacuum[11]. The opposite effect is observed for siloxane materials stored in water[12]. However, this may be the less likely explanation for this system, as being a resinous material, the molecular structure is relatively fixed.

The discrepancy between bulk and surface chemistry may alternatively suggest an error in the curve-fitting methodology. It was decided to investigate this possibility, with the aim of more accurately correlating the chemistry of the C 1s, Si 2p and O 1s core levels, with the bulk composition determined by ^{29}Si NMR. The effect of differentiating between the C 1s binding energy positions for $(\underline{C}H_3)_2$-Si-$O_{2/2}$ and $(\underline{C}H_3)$-Si-$O_{3/2}$ was investigated.

b) Using two synthetic components to curve-fit the C 1s core level

The effect of replacing a C-C group with C-$SiO_{2/2}$ (D siloxy unit) on the binding energy of the C 1s core level is to decrease it from 285.0 eV to 284.48 eV, as described in the literature, and in section 5.3.1. The effect on the C 1s binding energy of replacement of

C-C with C-$SiO_{3/2}$ (T siloxy unit) or by C-$SiO_{1/2}$ (M siloxy unit) has not previously been determined.

As a first estimation, the effect of replacement of one methyl group from the C-$SiO_{2/2}$ species by an oxygen atom, was to shift the carbon binding energy up by one-half of the distance between the C-C group and C-$SiO_{2/2}$ environments. Conversely, the removal of an oxygen atom, with replacement by a methyl group to form a T siloxy unit (C-$SiO_{3/2}$), led to a decrease in binding energy by the same amount. This is illustrated in Table 5-2.

	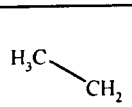	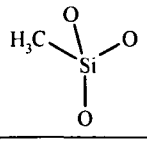	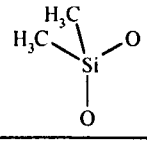	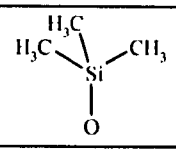
Binding Energy (eV)	**C-C**	**H_3C-$SiO_{3/2}$**	**H_3C-$Si(CH_3)O_{2/2}$**	**H_3C-$Si(CH_3)_2O_{1/2}$**
Measured	285.00	-	284.48	-
Estimated	-	284.74	-	284.22

Table 5-2: Measured and estimated binding energy and structures for carbon attached to various siloxy structures

For silicon in the 'M' siloxy environment, each silicon atom has three carbon atoms, and one-half an oxygen atom. For silicon in the 'D' siloxy environment, each silicon atom has two carbon and two-half oxygen atoms associated with it 'T' siloxy silicons have one carbon and three-half oxygen atoms, whereas silicon in the 'Q' siloxy environment is attached to four-half oxygen atoms. Each oxygen atom is represented as a fraction of two as it is shared between two silicon atoms. This information is summarized in Table 5-3.

Nomenclature	Molecular Structure	Number of atoms		
		Carbon	Silicon	Oxygen
M	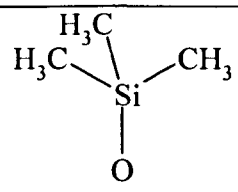	3	1	1/2
D	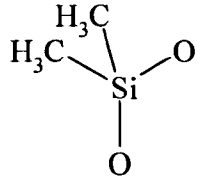	2	1	2/2
T	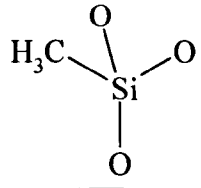	1	1	3/2
Q	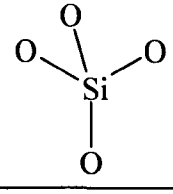	0	1	4/2

Table 5-3: Nomenclature and structure of various siloxy environments, indicating the number of carbon and oxygen atoms associated with each silicon atom

The concentration of carbon may be calculated by the summation of the concentration of carbon in an 'M' siloxy unit [C^M], plus the concentration of carbon in a 'D' siloxy environment [C^D], plus the concentration of carbon in a 'T' siloxy environment [C^T], equation [1]. Similarly for oxygen and silicon as presented in equations [2] and [3]:

$$[C] = 3[C^M] + 2[C^D] + [C^T] \quad [1]$$

$$[O] = 1/2[O^M] + 2/2[O^D] + 3/2[O^T] + 4/2[O^Q] \quad [2]$$

$$[Si] = [Si^M] + [Si^D] + [Si^T] + [Si^Q] \quad [3]$$

This method also allows the elemental composition to be determined. If the chemical environment of silicon is known from curve-fitting, then the associated number of carbon and oxygen atoms can be calculated.

For samples whose thickness is greater than the depth of analysis, this method provides a check on the curve-fitting process. The elemental composition determined from quantification should be similar to that calculated from the Si 2p curve-fit. The following example describes the calculation for a sample of DT resin of known molecular structure, Table 5-4.

Chemical Environment	Number of Atoms			
	Si	C	O	
M	0	0	0	
D	14	28	14	
T	86	86	129	
Q	0	0	0	total
	100	114	143	357 atoms

	Elemental Composition (%)	
	Calculated from Si 2p	Determined Experimentally
Si	26	28
C	35	32
O	39	40

Table 5-4: Total number of carbon, oxygen and silicon atoms for DT resin, with comparison between the elemental composition derived from Si 2p curve-fit, and experimentally from quantification information

Agreement in the elemental composition, within a few percent, was obtained by this method. In addition, equations [1 – 3] can be applied to determine the concentration of synthetic components within each core level. As discussed previously, DT resin, whose molecular structure is $D_{0.14}$-$T^{OH}_{0.12}$-$T_{0.74}$, has 14% of its silicon atoms in the 'D', or $(CH_3)_2SiO_{2/2}$ environment, and 86% of its silicon atoms are in the 'T', or $CH_3SiO_{3/2}$ form, therefore:

[C] = (2*0.14) + 0.86 = 1.14

$C^D = (0.28/1.14)*100 = 24.6\%$

$C^T = (0.86/1.14)*100 = 75.4\%$

[O] = (2/2*0.14) + (3/2*0.86) = 1.43

$O^D = (0.14/1.43)*100 = 9.8\%$

$O^T = (1.29/1.43)*100 = 90.2\%$

[Si] = 0.14 + 0.86 = 1.0

$Si^D = (0.14/1.0)*100 = 14.0\%$

$Si^T = (0.86/1.0)*100 = 86.0\%$

The C 1s core level was fitted with two synthetic components with the proportional concentrations calculated above. The C 1s core level was then charge corrected to set C $1s^D$ to 284.48 eV and C $1s^T$ to 284.74 eV. The BEs were allowed to vary ± 0.1 eV. The curve fit matched well with the experimental data, Figure 5-4b.

The same charge correction value was applied to both the O 1s and Si 2p core levels. One component was added to each, to represent O $1s^D$ and Si $2p^D$ using the known binding energy values. A second component (to represent O $1s^T$ and Si $2p^T$) was then added, and constrained in concentration according to the molecular structure. This provided binding energy values for O $1s^T$, Figure 5-4a and Si $2p^T$ Figure 5-4c. The binding energy value for Si $2p^T$ [$CH_3\underline{Si}O_{3/2}$] of 102.8 eV is in good agreement with previously published research[4].

This new method has demonstrated that differentiation between the binding energy of the C 1s for ($\underline{C}H_3$)$SiO_{2/2}$ and $\underline{C}H_3SiO_{3/2}$ provides consistent curve-fits whereby the relative concentration of the components can be matched to the molecular structure of

the material, and provide silicon BEs in agreement with the literature. The method is presented as a flowchart in Scheme 5-3.

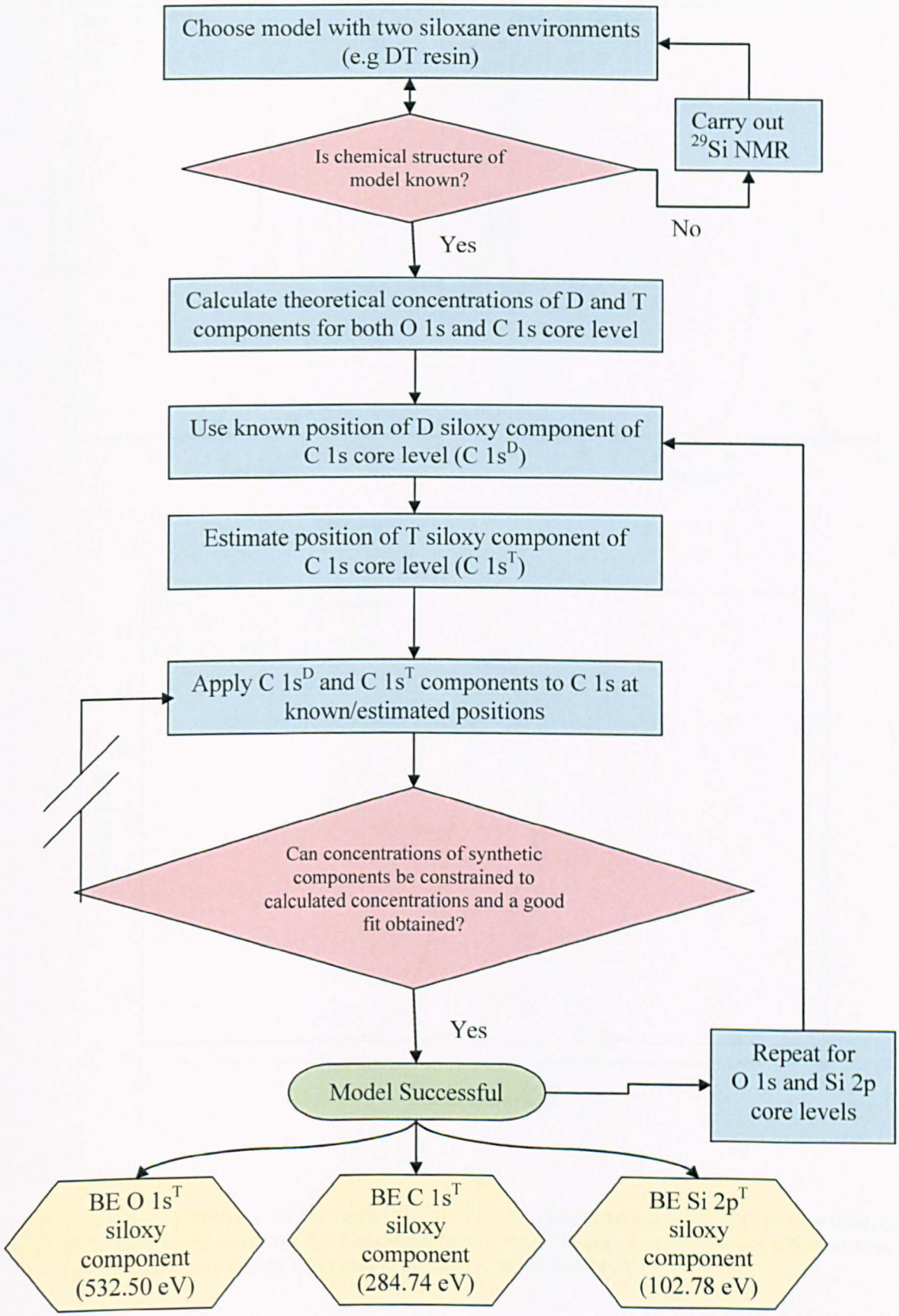

Scheme 5-3: Flowchart describing the procedure for curve-fitting DT resin to provide binding energy values for O 1s^{T}, C 1s^{T} and Si 2p^{T} components

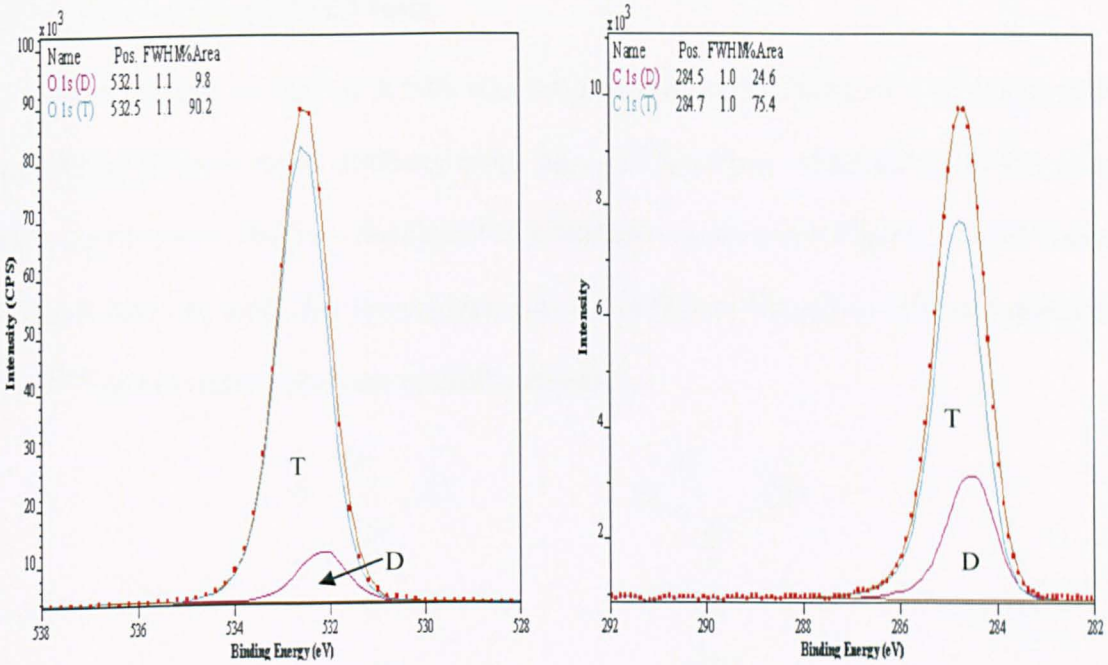

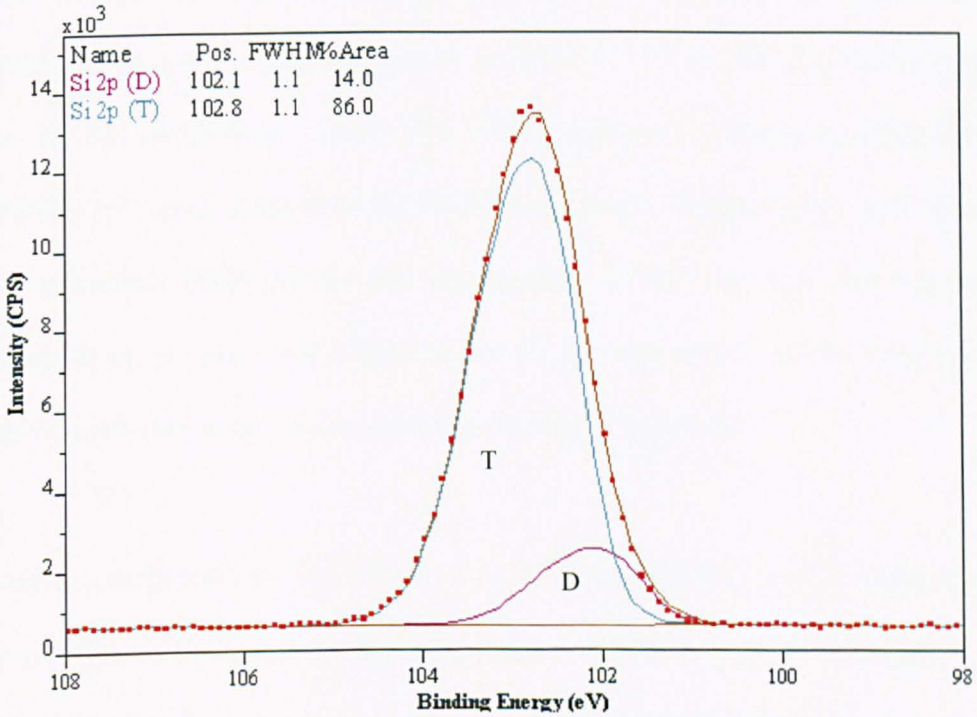

Figure 5-4: Curve-fits for DT resin [$D_{0.14}$-$D^{OH}_{0.12}$-$T_{0.74}$] a) O 1score level, b) C 1s core level, c) Si 2p core level, where the C-Si environments of the C 1s core level have been differentiated. Spectra have been charge corrected to position C $1s^{D}$ at 284.48 eV

5.3.3 Curve-fitting of MQ resin

A similar process to that in 5.3.2b was used in the curve fitting of a siloxane resin containing different ratios of siloxy units, $M_{0.47}$-$T^{OH}_{0.15}$-$Q_{0.38}$ – MQ resin. In this case, the Si 2p core level had two distinguishable features, as shown in Figure 5-5. To curve-fit the Si 2p core level, the formulation was simplified to $M_{0.47}Q_{0.53}$ as it was assumed that T^{OH} and Q siloxy forms are not differentiated.

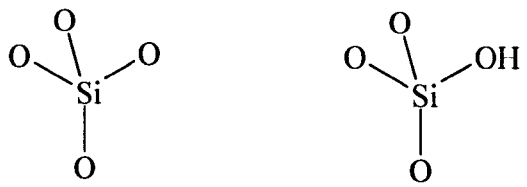

Q T^{OH}

A synthetic component representing carbon in a 'M' environment was fitted to the C 1s core level. This was charge corrected to position C $1s^M$ at 284.23 eV, the estimated position for this component, Figure 5-5b. Next, synthetic components representing Si $2p^M$ and Si $2p^Q$ were applied to the Si 2p core level. From Figure 5-5, where the furthest separated environments are represented, it is clear why the intermediate environments are so poorly resolved in the Si 2p core level. In the MQ resin, the separate components in the Si 2p core level are clearly resolved.

The synthetic peak representing silicon as an M siloxy unit fitted well, using a peak of similar FWHM as the other model compounds. However, it was necessary to use a broader peak to fit the Q component. The intensity ratio between the two synthetic peaks is presented in Table 5-5.

	M	D	T	Q
Calculated (bulk) composition	47	0	0	53
Experimental (surface) composition	39	0	0	61

Table 5-5: NMR determined bulk chemical composition of resin B ($M_{0.47}$-$T^{OH}_{0.15}$-$Q_{0.38}$) in terms of M,D,T, and Q siloxy units compared with the experimental values obtained from curve-fitting of the Si 2p core level

There are two possible hypotheses behind the need to broaden the Si 2p peak in Q siloxy units. The signal is resulting from a combination of T^{OH} and Q units, which would lead to an apparent broadening of the peaks within the experimental envelope, if these chemical environments did not result in the same chemical shift. A more detailed analysis will be needed to differentiate between Si $2p^{TOH}$ and Si $2p^{Q}$, but at this time, it has not been possible to examine a material containing only pure Si $2p^{TOH}$ siloxy units. However, in the analysis of the DT resin the peak position for Si $2p^{DOH}$ was in the same position as that for Si $2p^{T}$ units.

The second possibility is that the broadening of the Q signal is further due to a superposition of a multitude of Si 2p signals each arising from a Q unit in a slightly different molecular environment. In the core of the resin, various Q units are imbedded in cage-like structures of variable sizes and strains. This broadening effect is clearly seen in ^{29}Si NMR of methylated orthosilicate resins containing Q units[13].

Furthermore, the XPS curve-fit did not match the composition determined by quantitative ^{29}Si NMR. A higher concentration of [Q + T^{OH}] units was observed by XPS (61%), than in the NMR analyses (53%). Whilst it is not necessarily expected that the bulk and surface concentrations will be the same, any variations would normally be due to the enrichment of low energy (e.g. M or D siloxy groups) at the surface. It is not possible to explain explicitly the apparent enrichment of Q groups at present using this rationale, but one possible hypothesis is condensation occurring in the XPS vacuum.

Finally, O $1s^M$ and O $1s^Q$ components were then applied to the O 1s core level, with the binding energy allowed to vary, but with their relative intensities constrained to the values determined from Table 5-3. As for the DT resin, the elemental composition of the material can be estimated from the Si 2p curve-fits, Table 5-6.

Chemical Environment	Number of Atoms		
	Si	C	O
M	39	117	20
D	0	0	0
T	0	0	0
Q	61	0	122
	100	**117**	**142**

total 359 atoms

	Elemental Composition (%)	
	Calculated from Si 2p	Determined Experimentally
Si	28	26
C	33	35
O	40	40

Table 5-6: Total number of carbon, oxygen and silicon atoms for MQ resin, with comparison between the elemental composition derived from Si 2p curve-fit, and experimentally from quantification information

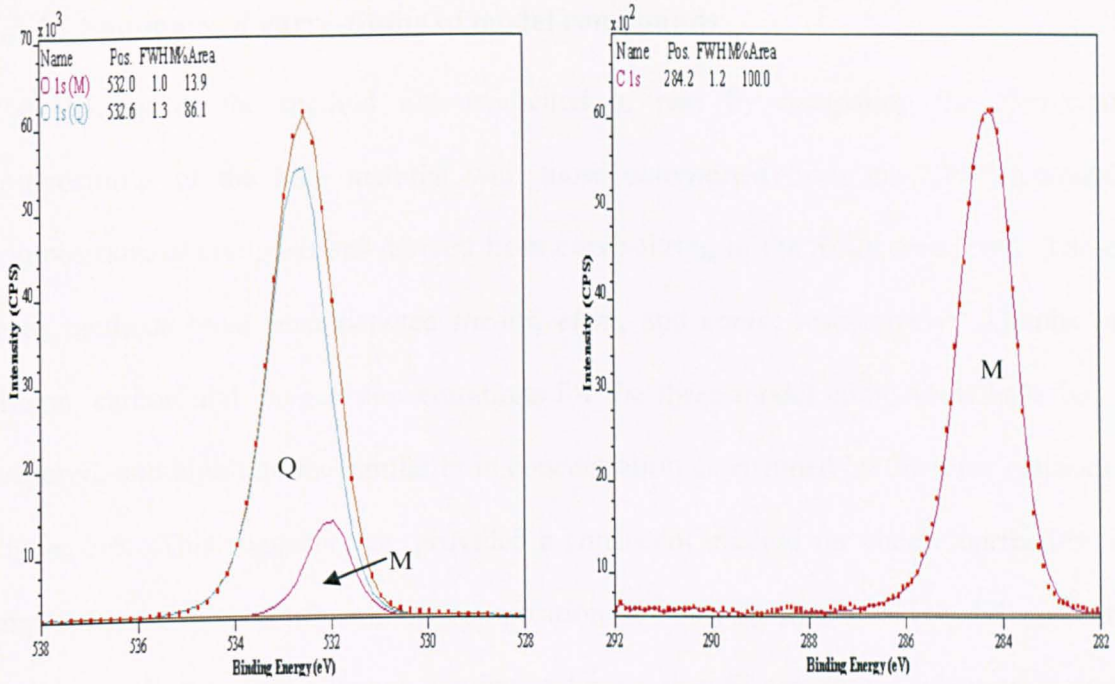

a b

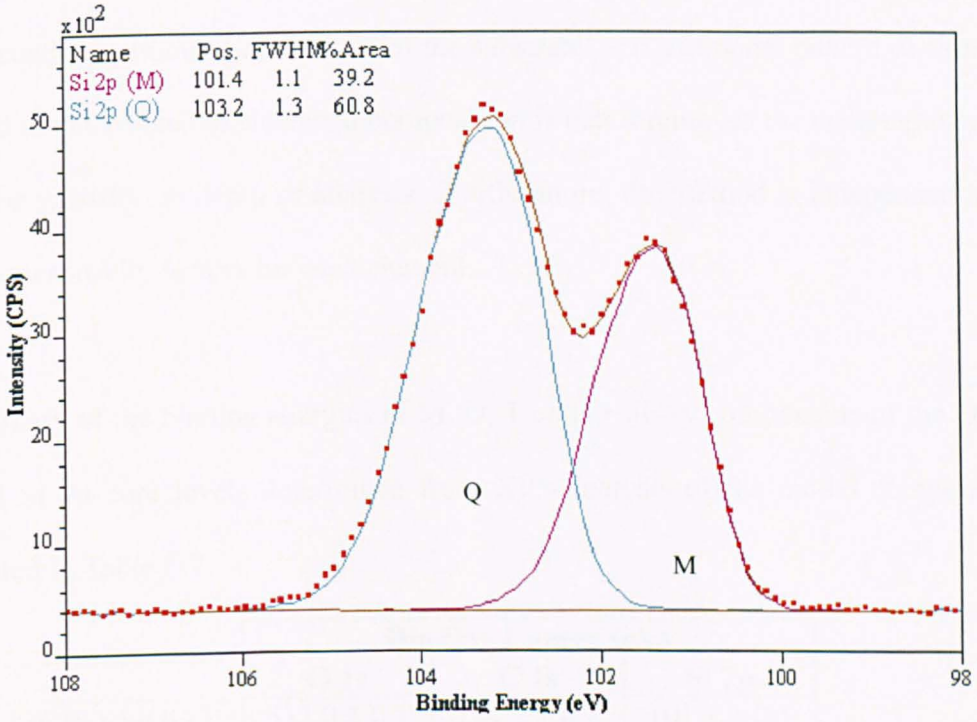

c

Figure 5-5: Curve-fits for MQ resin [$M_{0.47}$-$T^{OH}_{0.15}$-$Q_{0.38}$] a) O 1s core level, b) C 1s core level, c) Si 2p core level where the C-Si environments of the C 1s core level have been differentiated. Spectra have been charge corrected to position C $1s^{M}$ at 284.23

5.3.4 Summary of curve-fitting of model compounds

The validity of the method was evaluated in part by comparing the elemental compositions of the bulk material with those determined from the XPS elemental composition, or compositions derived from curve-fitting of the Si 2p core level. These three methods have been denoted *theory*, *elem*, and *comp*, respectively. Graphs of silicon, carbon and oxygen concentrations for the three model compounds have been prepared, and highlight the similarity in concentration determined by the three methods, Figure 5-6. This suggests that, provided a consistent method for charge correction is employed, the method of using the composition of the Si 2p core level is valid, and can thus be applied to thin siloxane coatings where a non Si-containing substrate is also being analysed, e.g polypropylene film. This will enable calculation of the composition of the coating, without the influence of the substrate. An additional benefit of using this method to determine the elemental composition is that it removes the uncertainty arising from the variation in depth of analysis. Furthermore, the method is independent of the relative sensitivity factors for each element.

A summary of the binding energies of M, D, T and Q siloxy components of the O 1s, C 1s and Si 2p core levels determined from XPS analysis of the model compounds is presented in Table 5-7.

	Binding Energy (eV)			
	O 1s	**C 1s**	**Si 2p**	
M [$(CH_3)_3SiO_{1/2}$]	532.0 ± 0.1	284.2 ± 0.1	101.4 ± 0.1	
D [$(CH_3)_2SiO_{2/2}$]	532.0 ± 0.1	284.5 ± 0.1	102.0 ± 0.1	**Δ M-D = 0.6**
T [$CH_3SiO_{3/2}$]	532.5 ± 0.1	284.7 ± 0.1	102.8 ± 0.1	**Δ D-T = 0.8**
Q [$SiO_{4/2}$]	532.6 ± 0.1	NA	103.2 ± 0.1	**Δ T-Q = 0.6**

Table 5-7: Binding energies for various siloxy units in the Si 2p core level

This work has confirmed experimentally, using model compounds of known composition, that the binding energy positions of Si $2p^M$, Si $2p^D$, Si $2p^T$ and Si $2p^Q$ are in good agreement with the estimated values presented in the literature. It has also

demonstrated that binding energy shifts for components of the O 1s, and particularly C 1s core levels, can be assigned for siloxanes containing a range of siloxy environments.

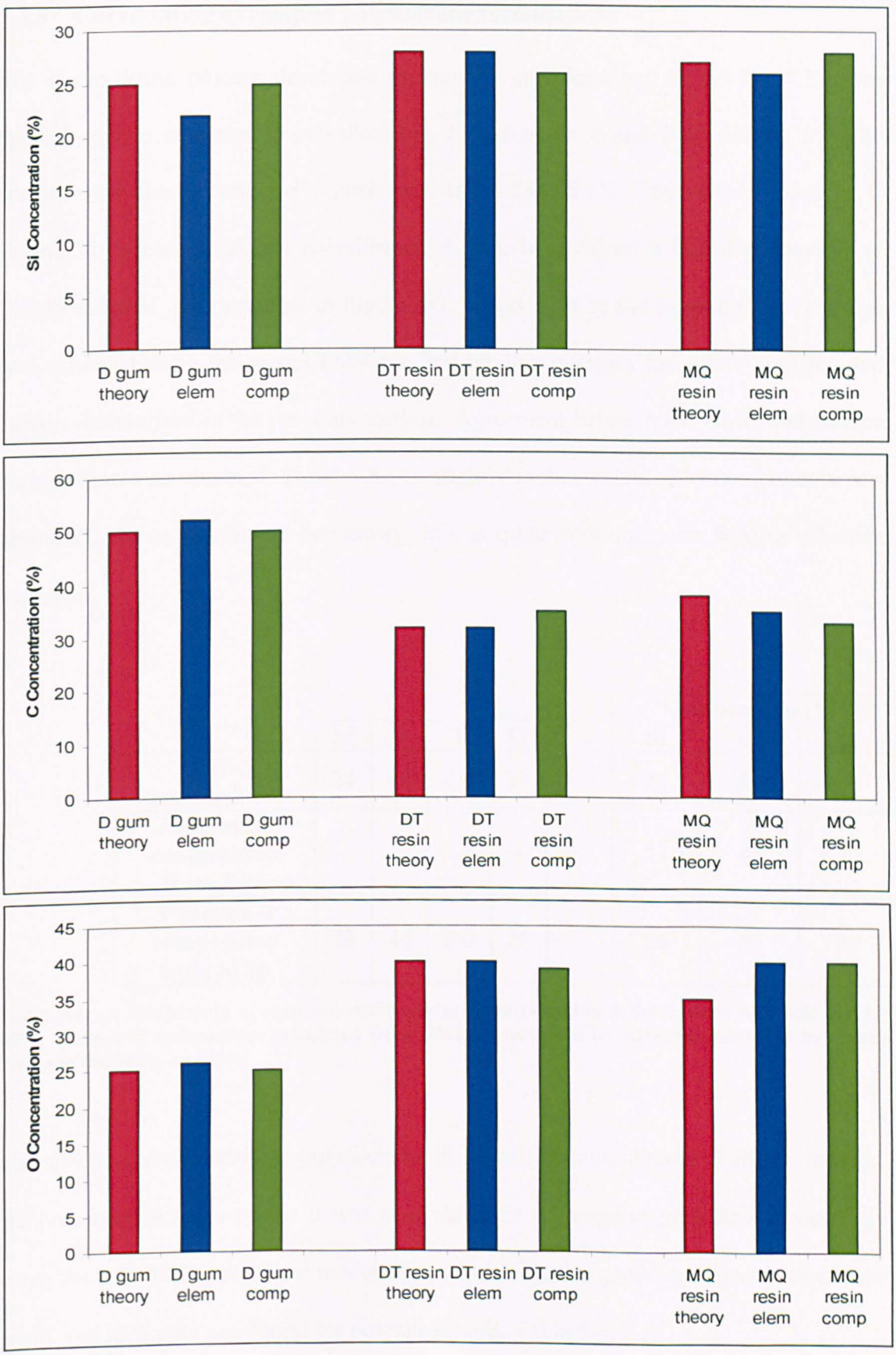

Figure 5-6: Silicon, carbon and oxygen concentrations for D gum, DT resin, and MQ resin determined from the bulk *(theory)*, by XPS elemental composition *(elem)*, or by curve-fitting of the Si 2p core level *(comp)*

5.3.5 Curve-fitting of complex polysiloxane formulations

The curve-fitting process developed previously, and described in 5.3.1 - 5.3.4 was applied to two commercial polysiloxanes, *Polysiloxane A* and *Polysiloxane B*. The spectra were charge corrected to position C $1s^D$ at 284.48 eV. The curve-fitted O 1s, C 1s and Si 2p core levels for polysiloxane A, which contained a higher percentage of PDMS material, are presented in Figure 5-7. A good fit to the experimental envelope was achieved using the model lineshape and binding energies for silicon, oxygen and carbon summarised in the previous section. Agreement between the NMR and surface composition was obtained, Table 5-8. A slightly higher value of M components was observed, but as mentioned previously, this is quite common with flexible siloxane materials.

	M	D	T	Q	Composition (%) Si	C	O
Bulk composition	24	45	0.4	31	26	43	31
Elemental composition from XPS	-	-	-	-	23	45	32
Functional composition from Si 2p	28	44	0.0	28	26	45	30

Table 5-8: A comparison of chemical environment of polysiloxane A determined by NMR and by XPS. Elemental composition calculated from NMR, determined by XPS, and obtained by curve-fitting of the Si 2p core level

The spectra corresponding to polysiloxane B, known to contain more Q siloxy material, are presented in Figure 5-8. It was possible to fit the experimental data successfully using the information from the model compounds. Again, good agreement between the NMR and XPS data was found for polysiloxane B, Table 5-9.

	M	D	T	Q	Composition (%) Si	C	O
Calculated (bulk) composition	32	26	0.5	41	27	40	33
Elemental composition from XPS	-	-	-	-	23	41	36
Functional compositional from Si 2p	35	28	0.5	36	26	43	31

Table 5-9: A comparison of chemical environment of polysiloxane B determined by NMR and by XPS. Elemental composition calculated from NMR, determined by XPS, and obtained by curve-fitting of the Si 2p core level.

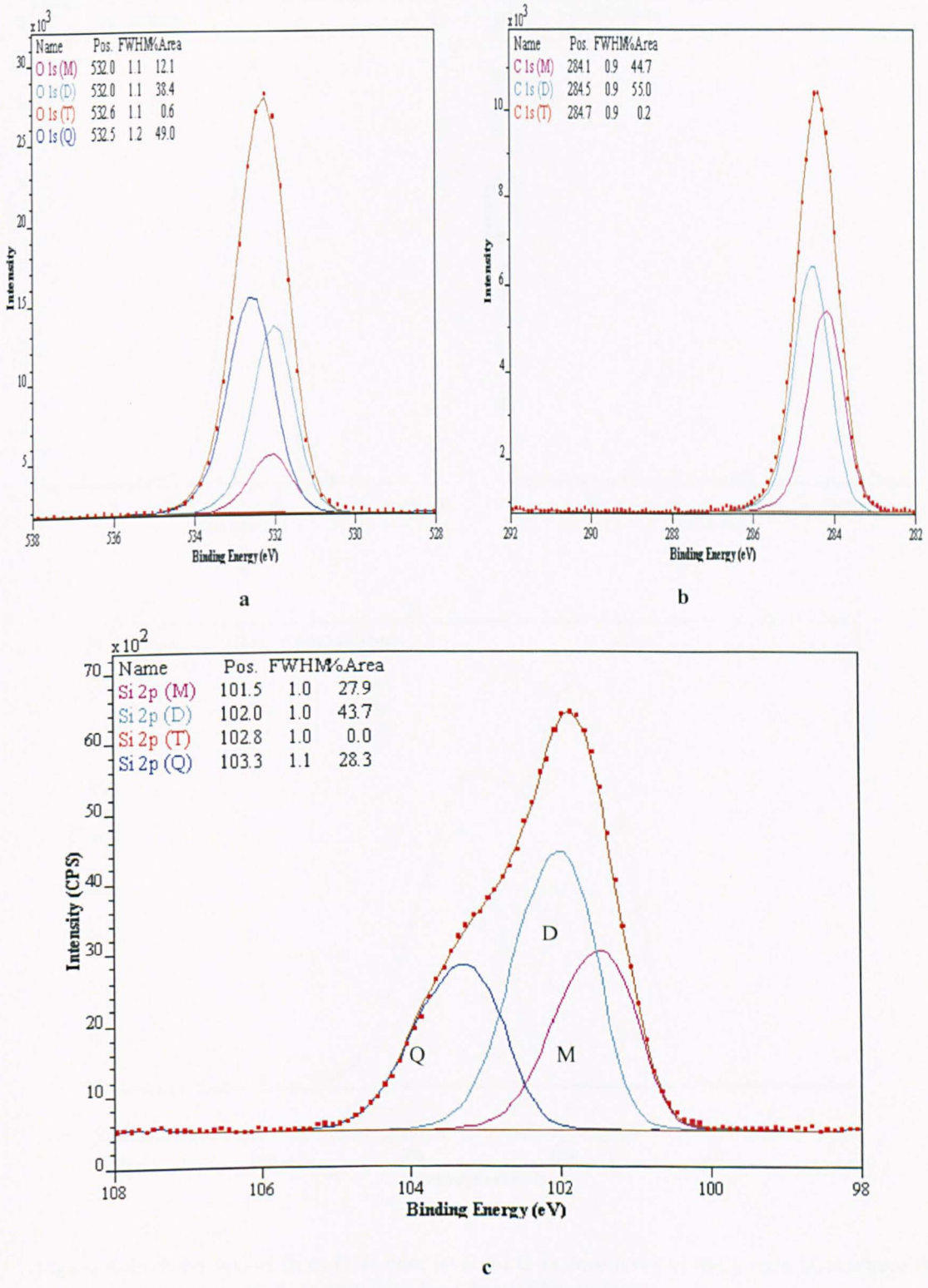

Figure 5-7: Polysiloxane A, a) O 1s core level, b) C 1s core level, c) Si 2p core level where the C-Si environments of the C 1s core level have been differentiated

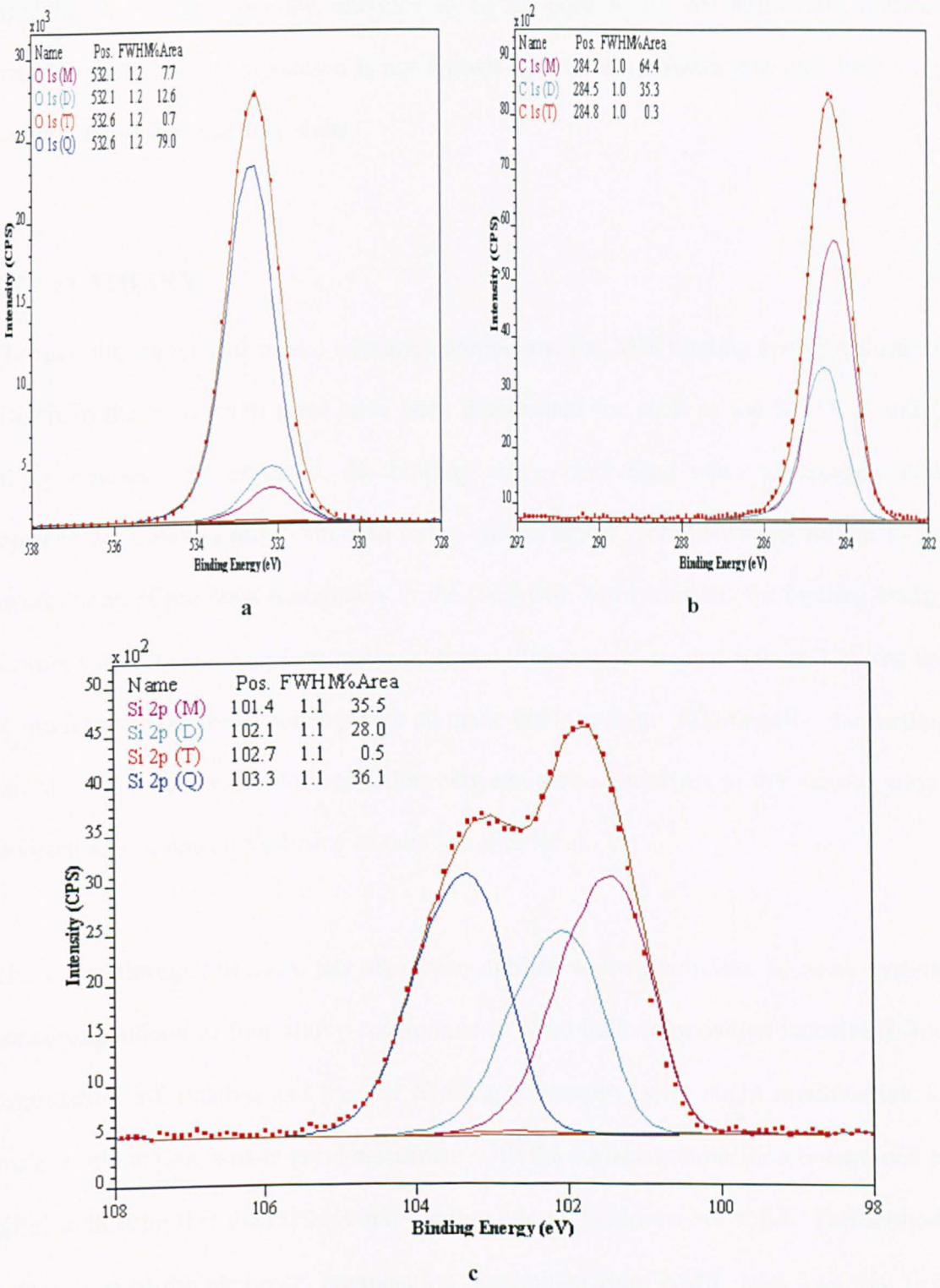

Figure 5-8: Polysiloxane B, a) O 1s core level, b) C 1s core level, c) Si 2p core level where the C-Si environments of the C 1s core level have been differentiated

Good agreement between the composition known from the formulation and by NMR, and the composition determined from curve-fitting of the Si 2p core-level indicates the validity of this method, with some variation assigned to surface enrichment.

Application of these binding energies to Si 2p core levels of industrially relevant materials where the composition is not known by any other means can now be carried out with confidence in the results.

5.4 SUMMARY

Through the analysis of model siloxane compounds, the XPS binding energy values for silicon in the Si 2p core level have been determined for each of the M, D, T and Q siloxy species. As expected, the binding energy increased when an oxygen atom replaces each methyl group attached to the silicon atom. The results are similar to the assumptions of previous researchers in the field who had estimated the binding energy positions of siloxane based on linear addition. The results are strengthened by the use of model compounds containing each siloxane environment. Additionally, the method has also allowed for the differentiation between carbon attached to the various siloxy environments using curve-fitting of the C 1s core level.

The curve-fitting procedure has also been applied to two complex siloxane systems containing silicon in four siloxy environments. The bulk composition calculated from formulation information and by ^{29}Si NMR spectroscopy, with slight modification for surface orientation, was in good agreement with the surface composition determined by XPS, indicating that the method and binding energy positions are valid. Furthermore, comparison of the elemental composition determined from NMR data, with that from XPS elemental quantification using the core level intensities, and from the composition determined only from fitting of the Si 2p core level has highlighted the similarities between the results. This validates the method and enables the calculation of the elemental composition of thin coatings where the substrate is also being analysed.

5.5 REFERENCES

[1] Morra, M.; Occhiello, E.; Marola, R.; Garbassi, F.; Humphrey, P.; Johnson, D., 'On the ageing of oxygen plasma-treated polydimethylsiloxane surfaces', *J. Coll. Int. Sci.*, 1990; **137**: 11

[2] Hillborg, H.; Gedde, U.W.; *'Hydrophobicity recovery of polydimethylsiloxane after exposure to corona discharges', Polymer*, 1998; **39**: 1991

[3] Beamson, G.; Briggs, D.; *High Resolution XPS of Organic Polymers: The Scienta ESCA300 Database*, John Wiley & Sons: Chichester, 1992

[4] Alexander, M.R.; Short, R.D.; Jones, F.R.; Michaeli, W.; Blomfield, C.J., 'A study of HMDSO/O_2 plasma deposits using a high-sensitivity and –energy resolutions XPS instrument: curve-fitting of the Si 2p core level', *Appl. Surf. Sci.* 1999; **137**: 179

[5] Ward, L.J.; Schofield, W.C.E.; Badyal, J.P.S.; Goodwin, A.J.; Merlin, P.J., 'Atmospheric pressure glow discharge deposition of polysiloxanes and SiO_x films', *Langmuir*, **19**, 2003, 2110-2114', *Langmuir*. 2003; **19**: 2114

[6] Noll, W., *Chemistry and Technology of Silicones*. Academic Press, New York, 1968

[7] Hillborg, H.; Ankner, J.F.; Gedde, U.W.; Smith, G.D.; Yasuda, H.K.; Wilkström, K., 'Crosslinked polydimethylsiloxane exposed to oxygen plasma studied by neutron reflectomertry and other surface specific techniques', *Polymer*, 2000; **41**: 6851

[8] Roualdes, S.; Berjoan, R.; Durand, J.; '^{29}Si NMR and Si 2p XPS correlation in polysiloxane membranes prepared by plasma enhanced chemical vapour deposition', *Separation and Purification Technology*. 2001; **25**: 391

[9] O'Hare, L.A.; Parbhoo, B.; Leadley, S.R. ' Development of a methodology for XPS curve-fitting of the Si 2p core level of siloxane materials', *Surf. Interface Anal.*, 2004, **36**, 1427

[10] Leadley, S.R.; Watts, J.F.; 'The use of XPS to examine the interaction of poly(acrylic acid) with oxidised metal substrates', *J Elec Spectroscopy*, 1997, **85**: 107

[11] Kim, J.; Chaudhury, M.K.; Owen, M.J.; 'Hydrophobicity loss and recovery of silicone HV insulation', *IEEE Trans Dielectrics and Electrical Insulation*, 1999; **6**: 695

[12] Hillborg, H.; Gedde, U.W.; 'Hydrophobicity changes in silicone rubbers', *IEEE Trans Dielectrics and Electrical Insulation*, 1999; **6**: 703

[13] Taylor, R.B.; Parbhoo, B.; Fillmore, D.M.,*NMR spectroscopy, The analytical chemistry of silicones*, Vol 112 pp 347 - 419 in Chemical Analysis, Lee Smith A, (Ed). J. Wiley & Sons: New York, 1991

CHAPTER 6

CHARACTERISATION OF SILOXANE COATINGS PREPARED USING ATMOSPHERIC PRESSURE PLASMA LIQUID DEPOSITION

6.1 INTRODUCTION

The aim of the work presented in this chapter was to determine the effect of certain processing parameters on the chemistry of coatings obtained by atmospheric pressure plasma liquid deposition (APPLD) of siloxane precursors. The effect of the precursor chemistry on the deposition rate and coating chemistry was also investigated using poly(dimethylsiloxane) and poly(hydrogenmethylsiloxane).

Preliminary analysis comparing deposition of siloxanes onto polypropylene and poly(ethylene terephthalate) films suggested that the siloxane coatings being deposited were thinner than the depth of analysis of X-ray photoelectron spectroscopy. As shown in Figure 6-1, the silicon concentration determined by XPS was between 5 and 13% for all samples. For a continuous siloxane coating of thickness greater than the XPS analysis depth, a silicon concentration of ~ 25% would be expected and it is therefore concluded that the PET and BOPP substrates contribute significantly to the XPS analysis.

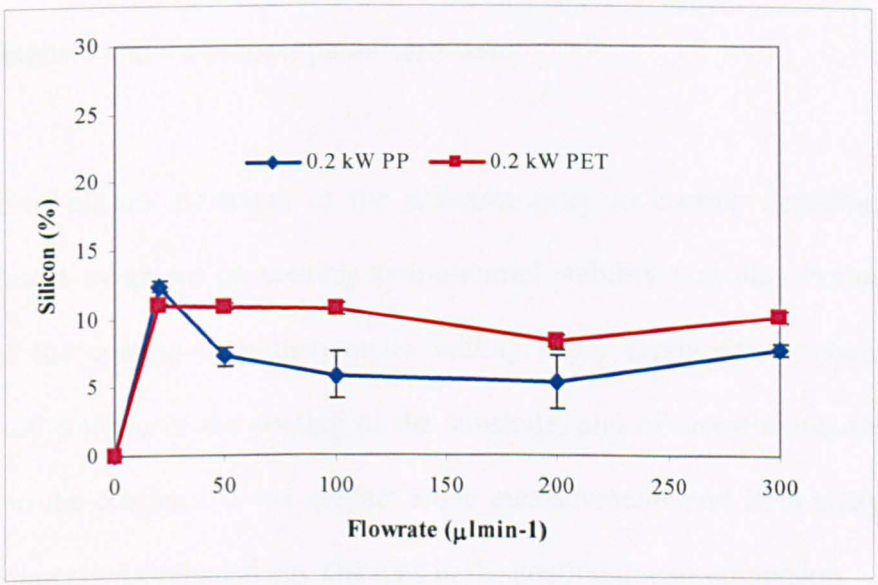

Figure 6-1: Silicon concentration versus precursor flowrate for siloxane coatings deposited using atmospheric pressure plasma liquid deposition.

A method was thus required to enable the elemental composition of the coating to be determined despite the contribution from the substrate to the analysis. We first consider deposition onto a poly(ethylene terephthalate) (PET) film as substrate since a clearly resolved component relating to the substrate, the ester functionality, was present in the C 1s core level when the coating was thinner than the depth of analysis of XPS. This enabled the substrate and the deposited coating to be distinguished and the composition of the latter to be estimated using the curve-fitting protocol based on that described for thick siloxane materials in *Chapter 5*. A model lineshape encompassing both Si $2p^{1/2}$ and Si $2p^{3/2}$ spin states was obtained by curve-fitting a high molecular weight poly(dimethylsiloxane) homopolymer. The binding energy and lineshape were then applied to model compounds containing each siloxane environment, to obtain unambiguous binding energies for Si $2p^{M}$, Si $2p^{D}$, Si $2p^{T}$ and Si $2p^{Q}$.

It was also possible, using a combination of angle-resolved XPS (AR-XPS) and a film thickness algorithm derived from the Beer Lambert expression, to determine the thickness of the siloxane coatings, and to relate this information to the chemistry of the coatings obtained and the process parameters used.

The effect of plasma treatment of the substrate prior to coating deposition, and of coating plasma treatment on coating hydrothermal stability was also evaluated. The stability of the coating to immersion in boiling water represents a measure of the efficiency of grafting of the coating to the substrate, and of crosslinking and network formation in the coating. Water contact angle measurements and XPS analysis before and after immersion evaluated any changes in the coating due to immersion.

6.2 EXPERIMENTAL

6.2.1 Atmospheric pressure plasma liquid deposition apparatus

Siloxane coatings were deposited onto poly(ethylene terephthalate) films using Dow Corning Plasma Solutions Mark I atmospheric pressure plasma liquid deposition (APPLD) apparatus. The apparatus is described in detail in *Chapter 3*.

The substrate was passed though the APPLD apparatus. In the first zone, the film is plasma treated prior to deposition, Scheme 6-1. This activation, or *pre-treatment* step may be considered to be analogous to corona discharge treatment, which is an essential step for the application of liquid siloxane materials to low surface energy substrates[1]. The resulting improved adhesion is a consequence of modification of the surface chemistry of the substrate by incorporation of oxygen-containing functional groups which allow the formation of chemical bonds between the substrate and the coating, and results in an increase in the surface energy of the substrate sufficiently to allow complete wetting and spreading of the siloxane, which is a crucial first stage in adhesion. In the second zone, the plasma contains the liquid precursor, and the coating is formed.

Due to the novelty of the APPLD process, the range of properties that can be obtained for coatings deposited are not well defined. It is essential in the development of the technology that the way in which the plasma parameters affect the properties of the coatings obtained are understood.

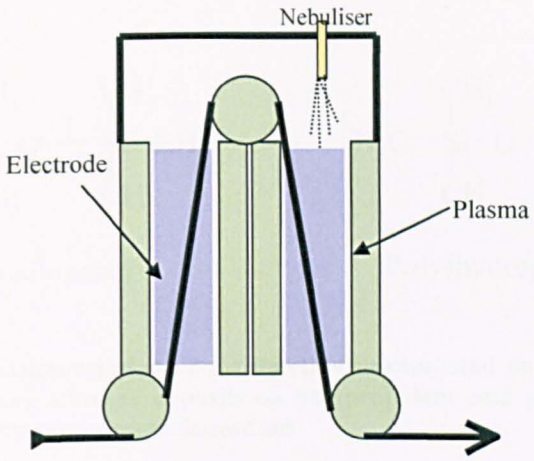

Scheme 6-1: Typical atmospheric pressure plasma liquid deposition process. Web is passed through an APP treatment zone prior to passing though the plasma zone where the precursor is deposited.

The substrate used in this work was poly(ethylene terephthalate), PET film. The PET film was 25 μm film, commercially available from Goodfellow, UK. Two polysiloxane liquids were evaluated as precursors for atmospheric pressure plasma liquid deposition (APPLD) on PET film. The first was a linear poly(dimethylsiloxane) - PDMS, and the other a linear poly(hydrogenmethylsiloxane) - PHMS, both of viscosity (10 cSt). The molecular weight of PDMS and PHMS were approximately 1300 and 3500, respectively. Both precursors were supplied by Dow Corning Corporation. The generalised molecular structures of the precursors are presented in Scheme 6-2. Further information on the substrate and precursors is presented in *Chapter 3*.

Deposition of the precursors was carried out at 4 $mmin^{-1}$, in a helium APP, using a gas flow of 15 $lmin^{-1}$ at standard temperature and pressure.

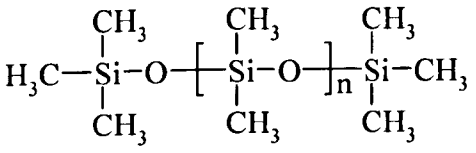

Poly(dimethylsiloxane)

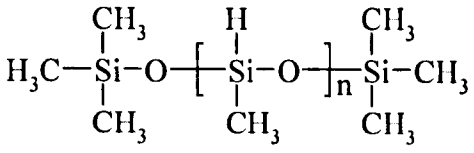

Poly(hydrogenmethylsiloxane)

Scheme 6-2: Chemical structures of the poly(dimethylsiloxane) and poly(hydrogenmethylsiloxane) precursors used to prepare siloxane deposits on polypropylene and poly(ethylene terephthalate) film using atmospheric pressure plasma deposition

XPS measurements were carried out with a take-off angle (TOA) of 90° with respect to the sample surface unless explicitly stated. Five positions within a 1 cm^2 area were analysed for each sample. The values for elemental concentrations are presented as the average from these five measurements. Error bars representing the standard deviation of the mean are also presented (SD/N^{-2}).

6.3 RESULTS AND DISCUSSION

6.3.1 XPS Curve-fitting of thin siloxane coatings

A protocol for the XPS curve-fitting of siloxane materials was developed and described in *Chapter 5*. Whilst this method is applicable to the curve-fitting of all siloxane materials, some slight modification is required when curve-fitting materials where the substrate is included in the analysis .

a) Poly(ethylene terephthalate) substrate

Curve-fitting of the C 1s core level was carried out on the 'as received' PET film, Figure 6-2. Synthetic components relating to the three functionalities present: C1 - C-C (aromatic); C2 – C-O-C=O; and C3 - C-O-C=O, were required, in accordance with the molecular structure of PET, and in good agreement with the curve-fit for PET by Beamson and Briggs[2].

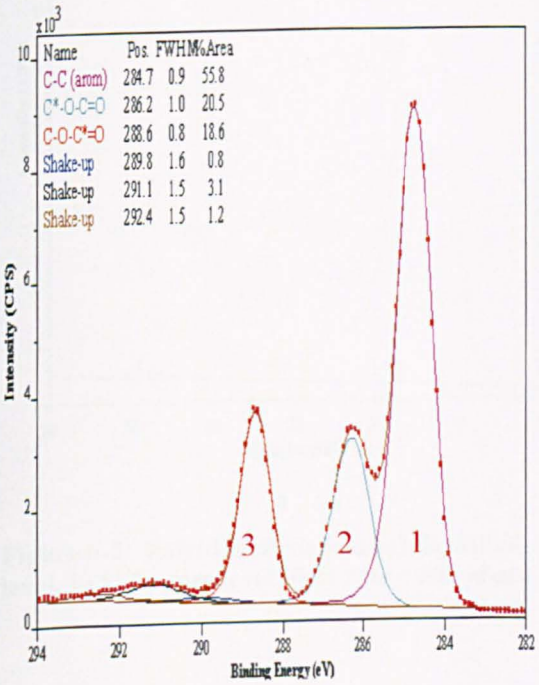

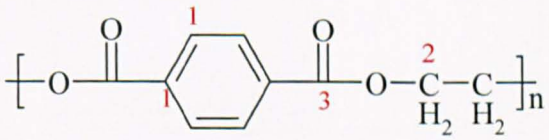

Figure 6-2: Molecular structure and curve-fit for the C 1s core level of 'as received' poly(ethylene terephthalate) film. Spectrum charge corrected to position synthetic component assigned to C-C(aromatic) at 284.7 eV. The * on the components annotation in the XPS spectrum denote which of the carbons in the ester groups is represented

b) Siloxane coated poly(ethylene terephthalate) film – charge correcting to substrate

An example of the C 1s and Si 2p core levels for a coating formed from PDMS is presented in Figure 6-3. The characteristic shape in the C 1s core level for PET is clearly visible, although the intensity of the components relating to the ester functionality are less intense than for the 'as received' substrate. Figure 6-2. The presence of silicon is a clear indicator of a siloxane coating being present. However, the presence of the substrate peaks in the C1s indicate either a thin or patchy coating. Angle-resolved XPS suggested that the film is continuous rather than patchy, described in *Section 6.3.2*: *Film Thickness*.

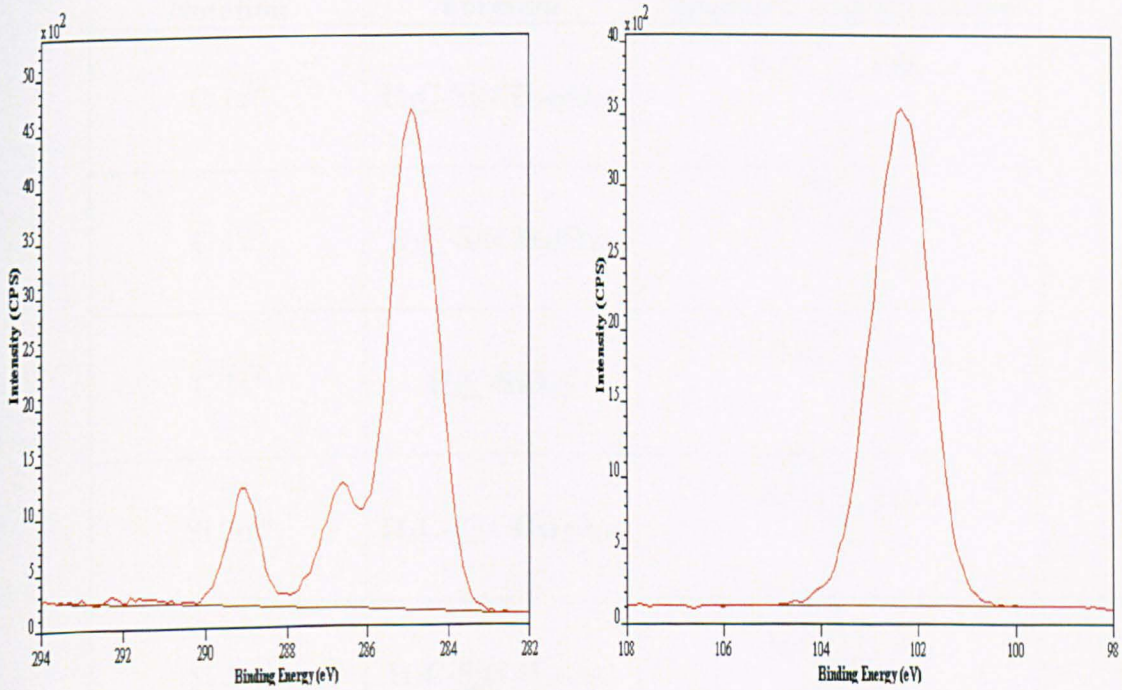

a b

Figure 6-3: Poly(dimethylsiloxane) deposited on poly(ethylene terephthalate) film a) C 1s core level, b) Si 2p core level (flow rate = 300 µlmin^{-})

To represent the substrate, peaks C1, C2 and C3 were applied to the experimental data from the siloxane coated PET film, shown in Figure 6-4a. The intensity of peaks C2 and C3 were constrained to be equal, with peak C1 = 3 x C3. The binding energy

positions for C1 and C3 were set using the shifts between the peaks on the 'as received' sample.

To account for the siloxane coating, three peaks relating to carbon attached to silicon, denoted C $1s^M$, C $1s^D$, and C $1s^T$ were applied to the curve-fit, at BEs of 281.2 eV, 281.4 eV and 284.7 eV respectively (prior to charge correction). These are shown with the peaks representing the PET in Figure 6-4b. The intensities of these peaks were guided by the experimental envelope. The position of C $1s^M$ was fixed at a value chosen to obtain a good fit to the low binging energy side of the C 1s core level. The positions of C $1s^D$ and C $1s^T$ were constrained to C $1s^M$ (+0.26 eV and +0.52 eV, repectively) A summary of the formula and structural representation is presented in Table 6-1.

Notation	Formula	Structural Representation
C $1s^M$	$H_3\underline{C}\text{-}Si(CH_3)_2O_{1/2}$	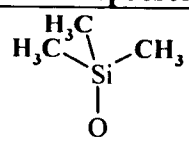
C $1s^D$	$H_3\underline{C}\text{-}Si(CH_3)O_{2/2}$	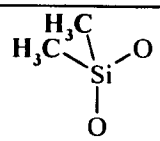
C $1s^T$	$H_3\underline{C}\text{-}SiO_{3/2}$	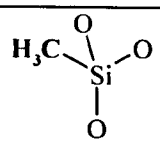
Si $2p^M$	$H_3C\text{-}\underline{Si}(CH_3)_2O_{1/2}$	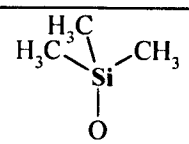
Si $2p^D$	$H_3C\text{-}\underline{Si}(CH_3)O_{2/2}$	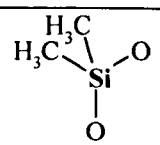
Si $2p^T$	$H_3C\text{-}\underline{Si}O_{3/2}$	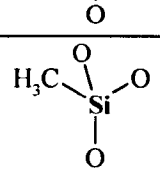
Si $2p^Q$	$\underline{Si}O_{4/2}$	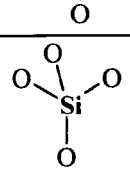

Table 6-1: Notation, formula, and structural representations of the components used to curve-fit the C 1s and Si 2p core levels of siloxane coatings

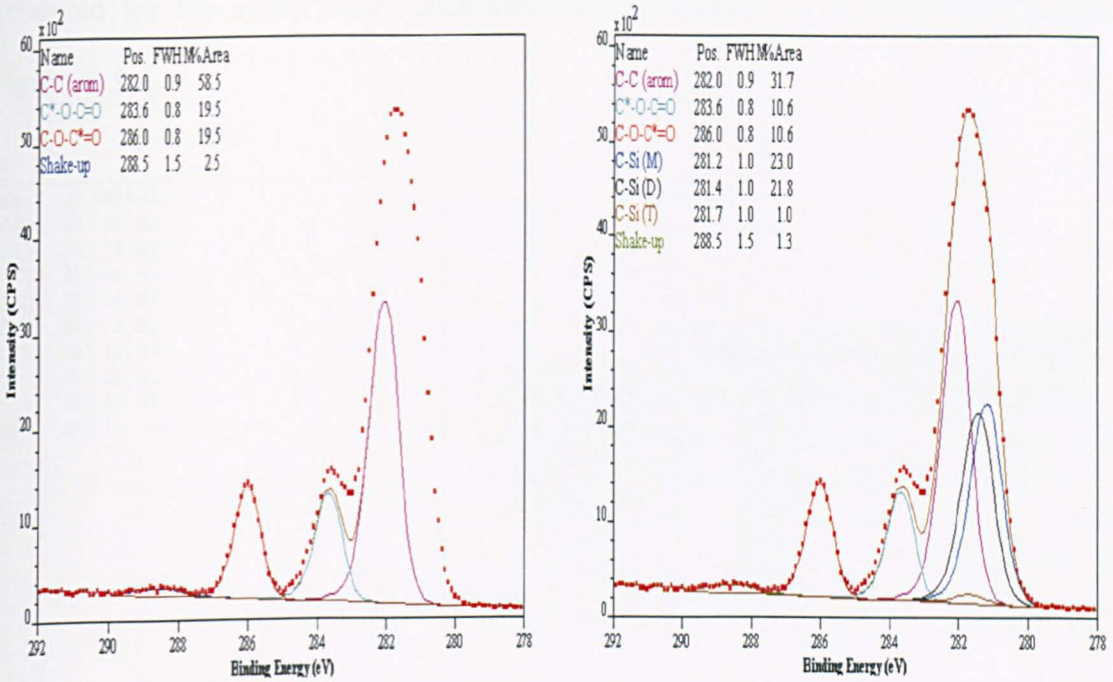

Figure 6-4: Curve-fits for the C 1s core level of siloxane deposited on poly(ethylene terephthalate) film a) Synthetic components assigned to the 'as received' PET substrate, b) Synthetic components assigned to the siloxane and the 'as received' PET substrate. No charge correction applied

Some deviation between the experimental data and the envelope generated from the synthetic components remained, as can be seen in Figure 6-4b. Two additional peaks were required to obtain a good fit. These have been assigned as C-OX (+0.9 eV shift from C-C arom) and C=O (+2.5 eV shift from C-C arom). Both these peaks have been previously been necessary in obtaining good fit to the experimental data during corona treatment of PET film[3]. The lower than expected BE shift is most likely due to the effect of Si-C. The spectrum was then charge corrected to position the carboxyl ester peak at 288.66 eV, as per Beamson and Briggs[2]. This component was chosen rather than the C-C (aromatic) component as the ester peak was clearly resolved, whereas there would be some uncertainty as to the accurate position of C-C (arom) due to the presence of C-Si components. This method resulted in the three peaks relating to the PET substrate having binding energy positions as expected, C-C (arom) at 284.7 eV; C-O-C=O at 286.3 eV and C-O-C=O at 288.7 eV. However, the binding energy positions of the three peaks relating to C-Si ($C\ 1s^M$, $C\ 1s^D$, $C\ 1s^T$) were much lower than

observed for the model compounds discussed in *Chapter 5*, or from the literature, Figure 6-5.

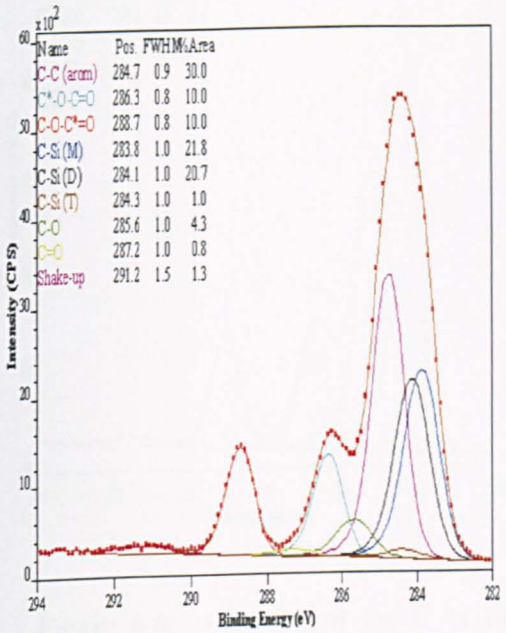

Assignment	Binding Energy Position (eV)	
	Literature	Experimental
C-C (arom)	284.7	284.7
C-O-C=O	286.2	286.3
C-O-C=O	288.7	288.7
C $1s^M$	284.2	283.8
C $1s^D$	284.5	284.1
C $1s^T$	284.7	284.3

Figure 6-5: Curve-fit of the C 1s core level and tabulated binding energy positions of the components for siloxane deposited on poly(ethylene terephthalate) film. The spectrum has been charge corrected to position the carboxyl ester component at 288.66 eV

c) Siloxane coated poly(ethyelene terephthalate) film – charge correcting to coating

An alternative charge correction to the data was applied to position C $1s^D$ at 284.48 eV, Figure 6-6. The new positions were consistent for siloxanes, C $1s^M$ at 284.2 eV; C $1s^D$ at 284.5 eV; and C $1s^T$ at 284.7 eV, but resulted in a binding energy shift of +0.5 eV for the components related to the substrate (C-C_{arom}. C-O-C=O and C-O-C=O)

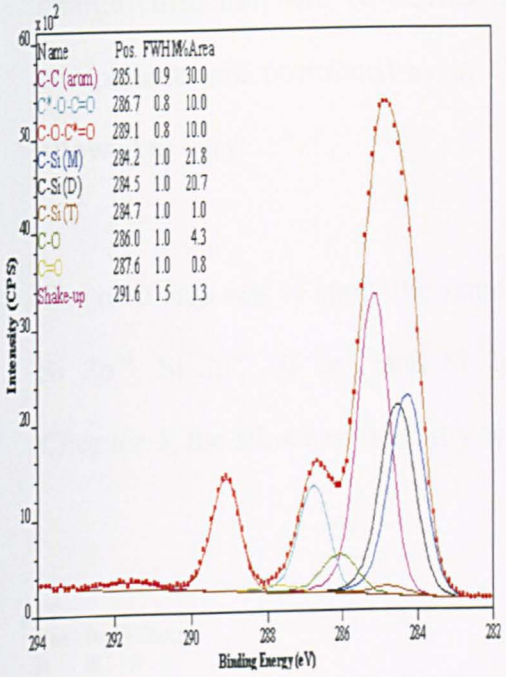

Assignment	Binding Energy Position (eV)	
	Literature	Experimental
C-C (arom)	284.7	285.1
C-O-C=O	286.2	286.7
C-O-C=O	288.7	289.1
C $1s^M$	284.2	284.2
C $1s^D$	284.5	284.5
C $1s^T$	284.7	284.7

Figure 6-6: Curve-fit of the C 1s core level and tabulated binding energy positions of the components for siloxane deposited on poly(ethylene terephthalate) film. The spectrum has been charge corrected to position C $1s^D$ at 284.48 eV

There are three hypotheses that may explain this shift in binding energy: vertical differential charging [4] between the siloxane coating and the PET film; chemical interactions occurring between the plasma treated PET and the siloxane coating shifting the components up in BE; or the binding energy position for aromatic carbons in the literature is incorrect. Since it has been previously determined that plasma treatments of PET film cause the formation of active species such as phenol and carboxylic acid groups[3], and plasma polymerisation and deposition of siloxanes occurs through the formation of free radicals and Si-OH species, it is highly likely that chemical interactions are occurring between these species. These would be easily observed by XPS in the situation we have here, where the deposited coatings are thinner than the depth of analysis by XPS. Chemical interaction between thin coatings and the substrate, reflected by increased binding energy shifts, have been noted by other researchers in XPS of thin poly(methyl methacrylate)[5,6,7] and poly(acrylic acid)[8] coatings Future

charge correction will be carried out using this method, ensuring C $1s^{M,D,T}$ components are positioned as in *Chapter 5*, and the C 1s substrate components are allowed to vary.

The next step was to apply the same charge correction to the Si 2p core level. Using the Si $2p^{M}$, Si $2p^{D}$, Si $2p^{T}$, and Si $2p^{Q}$ components and binding energies described in *Chapter 5*, the siloxane chemistry was elucidated.

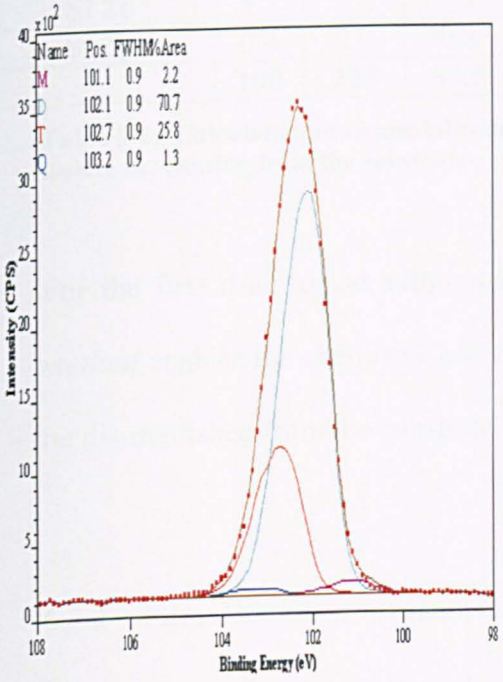

Assignment	Binding Energy Position (eV) Literature[2,9,10]	Experimental
Si $2p^{M}$	100.8- 101.5	101.2 ± 0.1
Si $2p^{D}$	101.8 – 102.1	102.0 ± 0.1
Si $2p^{T}$	102.8	102.8 ± 0.1
Si $2p^{Q}$	103.4 – 103.6	103.2 ± 0.1

Figure 6-7: Curve-fit of the Si 2p core level and tabulated binding energy positions of the components for siloxane deposited on poly(ethylene terephthalate) film. The spectrum has been charge corrected to position C $1s^{D}$ at 284.48 eV

The next step was to match the relative intensities of the C $1s^{M}$, C $1s^{D}$, and C $1s^{T}$ components in the C 1s core level to the silicon functional chemistry determined from fitting the Si 2p core level. The number of oxygen and carbon atoms associated with a silicon atom in each environment is known. From the relative concentrations of Si $2p^{M}$, Si $2p^{D}$, Si $2p^{T}$ and Si $2p^{Q}$, the number of oxygen and carbon atoms (and hence the total number of atoms) is calculated. The elemental composition is thus determined from the

ratio of each element to the total number of atoms, Table 6-2. The relative intensity of the C $1s^M$, C $1s^D$ and C $1s^T$ relative to each other are also calculated. These relative intensities are adjusted in the C 1s core level. If alteration of the charge correction is required to ensure a good fit, this new charge correction is also applied to the Si 2p core level. This process is iterated until both the C 1s and Si 2p chemistry are in agreement.

Chemical Environment	Number of Atoms		
	Si	C	O
Si $2p^M$	39.0	117.0	19.5
Si $2p^D$	55.4	110.8	55.4
Si $2p^T$	5.2	5.2	7.8
Si $2p^Q$	0.4	0.0	0.8
	100	**223**	**83.5**

total 416.5 atoms

	Elemental Composition (%) Calculated from Si 2p
Si	24.0
C	55.9
O	20.0

Table 6-2: Calculation of elemental composition of a siloxane coating, using the Si 2p core level to isolate the coating from the substrate

For the first time to the author's knowledge, the *iterative Si 2p – C 1s curve-fitting method* enables the chemistry and elemental composition of the thin siloxane coating to be distinguished from the substrate.

6.3.2 Film Thickness measurements using angle-resolved XPS

Following the development of the *iterative Si 2p – C 1s* curve-fitting protocol, it was then possible to apply the method to C 1s and Si 2p core levels of thin siloxane coatings, deposited in this work. Firstly, the thickness of a typical coating will be determined using a combination of ARXPS and the substrate-overlayer film thickness algorithm Next, the effect of varying the plasma parameters on the coating chemistry will be discussed. The plasma power during deposition, the precursor flowrate, the precursor chemistry, and the influence on coating stability of pre-treatment of the substrate or plasma treatment of the coating are the topics that will be investigated in this section.

Plasma polymerised poly(siloxane) – ppPSiOx, was deposited onto PET film using a precursor flowrate of 100 $\mu lmin^{-1}$. Initial investigations using XPS indicated that, as expected, the deposit comprised oxygen, carbon and silicon. Angle-resolved XPS was used to determine if a thin, continuous layer of ppPSiOx had been deposited, or if a thicker, patchy coating resulted. The TOA (w.r.t. sample surface) was varied from 90° to 30°. The elemental composition of the sample with decreasing TOA is presented in Table 6-3. The silicon concentration increased with decreasing sampling depth.

Take-Off Angle (°) w.r.t. sample surface	Elemental composition of sample (at. %)		
	Oxygen	Carbon	Silicon
90	25.1	63.5	11.4
60	23.3	62.6	14.2
45	22.4	60.7	16.9
30	20.0	60.0	20.0

Table 6-3: Elemental composition of the sample at varying take-off angle with respect to the sample surface

The *iterative Si 2p – C 1s curve-fitting method* was used to curve-fit the C 1s and Si 2p core levels of the siloxane coating at the various take-off angles, Figure 6-8. It is clear that as the TOA decreases, and the sampling depth is reduced, the intensity of the carboxyl peak associated with the substrate decreases.

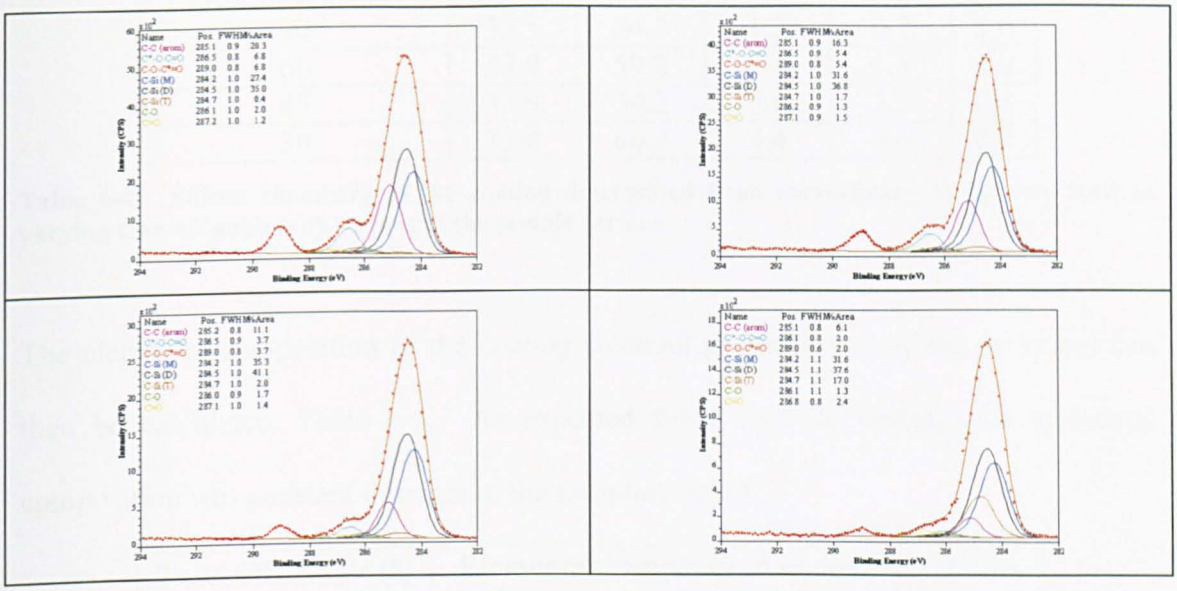

Figure 6-8: Curve-fits of carbon (C 1s) core levels for poly(dimethylsiloxane) deposited on poly(ethylene terephthalate) film. Spectra have been caprtured with decreasing take-off angle (wrt sample surface). Top row left to right TOA = 90°, 60°; bottom row left to right TOA = 45°, 30°. Spectra have been charge corrected to position C $1s^D$ at 284.48 eV

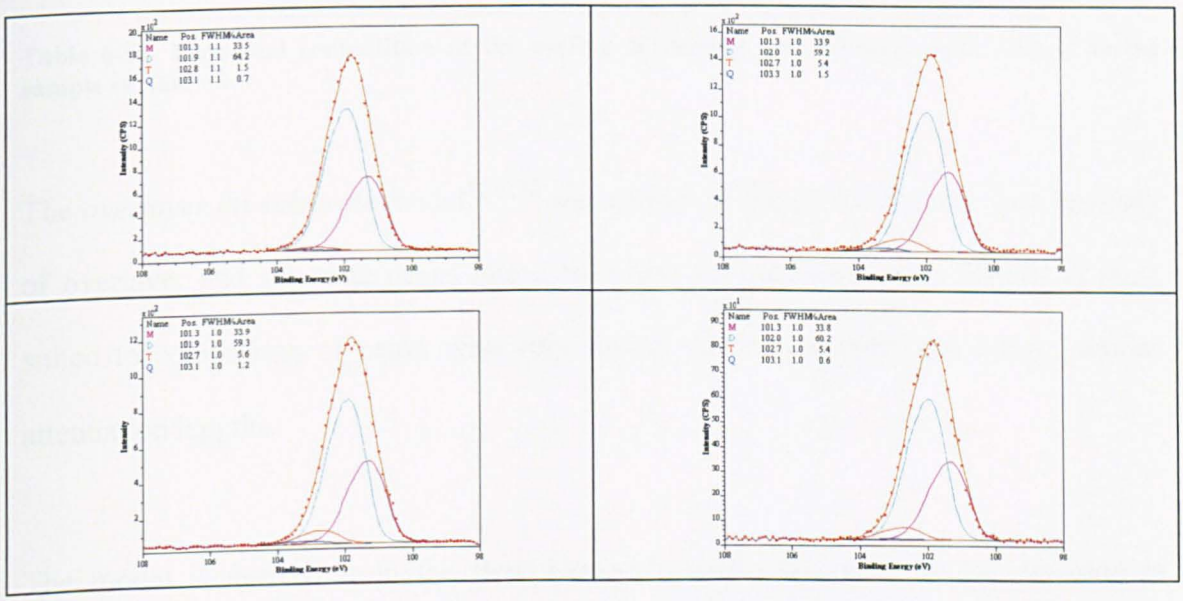

Figure 6-9: Curve-fits of silicon (Si 2p) core levels for poly(dimethylsiloxane) deposited on poly(ethylene terephthalate) film. Spectra have been caprtured with decreasing take-off angle (wrt sample surface). Top row left to right TOA = 90°, 60°; bottom row left to right TOA = 45°, 30°. Spectra have been charge corrected to position C $1s^D$ at 284.48 eV

A summary of the composition of the coating determined by curve-fitting is presented in Table 6-4. Also presented is ***G***, a measure of the goodness of fit (calculated by dividing χ^2 values by the number of degrees of freedom). The composition of the coating was very similar throughout the range of analysis depths.

Take-Off Angle (°) wrt sample surface	Relative Concentration (%) Si $2p^M$	Si $2p^D$	Si $2p^T$	Si $2p^Q$	*G*
90	33.5	64.2	1.2	0.7	0.6
60	33.9	59.2	5.4	1.5	1.0
45	33.9	59.2	5.6	1.2	0.4
30	33.8	60.2	5.4	0.6	0.7

Table 6-4: Silicon chemistry of the coating determined from curve-fitting Si 2p core level at varying take-off angle with respect to the sample surface

The elemental composition of the coating (without the influence of the substrate) can then be calculated, Table 6-5. As expected for a uniform coating, the elemental composition was constant throughout the sampling depth.

Take-Off Angle (°) wrt sample surface	Elemental composition of coating (at. %) Oxygen	Carbon	Silicon
90	20.3	55.6	24.1
60	21.1	54.6	24.2
45	21.1	54.7	24.2
60	20.9	54.9	24.2

Table 6-5: Elemental composition of the coating at varying take-off angle with respect to the sample surface

The *overlayer on substrate* model[11,12,13] was chosen as the method to translate intensity of overlayer and substrate peaks into a thickness measurement. This model is most suited to comparison of peaks with very similar kinetic energies, and hence, similar attenuation lengths.

The model is derived from the Beer Lambert expression, whereby the equation is integrated between 0 and d (d is the thickness of the overlayer, A). The signal from A is expressed as

$$I_A = I_A^{\infty}[1-\exp(-d/\lambda_{A,A}\cos\theta)]$$

The signal arriving from B at the B-A interface is I_B, and is given by

$$I_B = I_B^{\infty}[1-\exp(-d/\lambda_{B,A}\cos\theta)]$$

Taking the ratio ($R\infty = I_A\infty / I_B\infty$) of these signals, and assuming $\lambda_{A,A} = \lambda_{B,A} = \lambda_A$ (for a carbon-containing overlayer on a carbon-containing substrate)

$$R = R^{\infty}[\exp(d/\lambda_A\cos\theta) - 1]$$

Rearranging and taking the natural logarithm results in the following

$$\ln[R/R^{\infty}] = d/\lambda_A\cos\theta$$

A plot of sec(θ) against the natural log of 1 + the ratio of peak intensities should result in a straight line through the origin. The gradient of the line represents the thickness of the overlayer in units of effective attenuation length (EAL).

The overlayer thickness is calculated using the measured components (the intensity of the components relating to substrate and overlayer) and the known quantities (the TOAs -with respect to the sample normal for the calculation and the EAL) for the core level under investigation. In this work, the EAL for C 1s was obtained from the National Institute of Standards and Technology EAL database[14]. The peak intensities under investigation are both components of the C 1s core level: C̲OOX and C̲-Si. The C̲OOX component relates primarily to the substrate (although a small contribution from high level oxidation of the C̲-Si may be observed), and the C-Si appears only due to the coating.

Table 6-6 presents the intensities of C̲OOX versus C̲-Si against take-off angle. The siloxane coating thickness was determined to be 4.9 nm using the graph shown on the following page. The slope of the line equals the thickness in terms of EALs, therefore with $EAL_C = 2.3$ nm, thickness = 2.1493 * 2.3 = 4.9 nm

Take-off angle (°)	Intensity	
	C-Si	X-O-C=O
90	62.8	6.8
60	70.1	5.4
45	78.4	3.7
30	86.2	2.0

Table 6-6: Intensity of C-Si and COOX components of the C 1s core level of a siloxane coating deposited on poly(ethylene terephthalate) film prepared from APPLD of PDMS at 100 µlmin^{-1} at 0.2 kW in helium

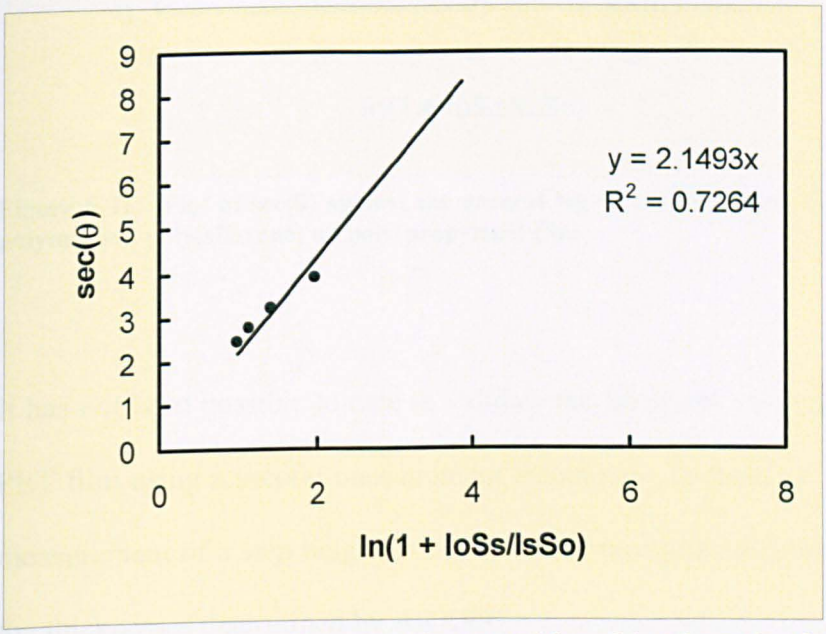

Figure 6-10: Plot of sec(θ) against the natural log of 1 + the ratio of peak intensities for plasma polymerised poly(siloxane) on poly(ethylene terephthalate) film

Interpretation of similar data for siloxane coating prepared on PP film did not result in a straight line through the origin. This film most likely was comprised of islands of coating.

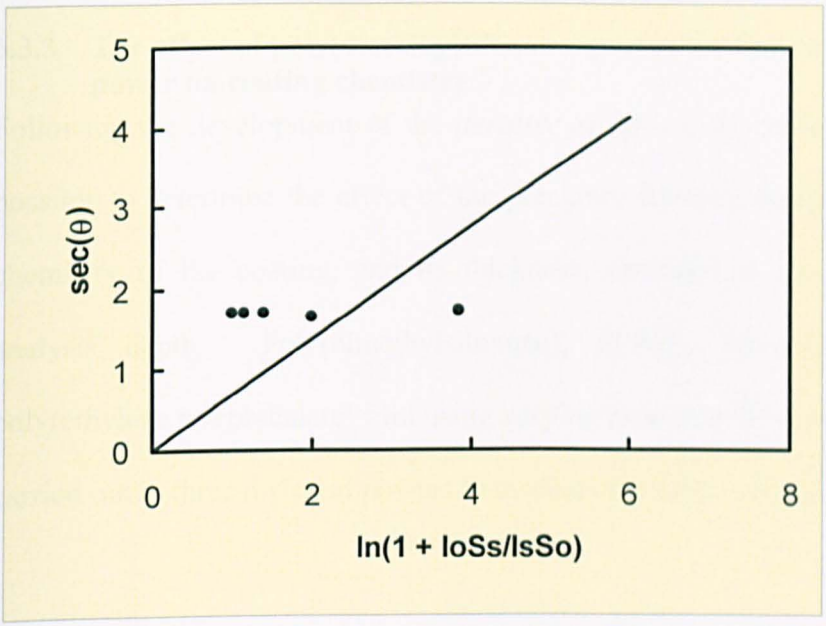

Figure 6-11: Plot of sec(θ) against the natural log of 1 + the ratio of peak intensities for plasma polymerised poly(siloxane) on poly(propylene) film

It has not been possible to date to validate the thickness value obtained for ppPSiOx on PET film using a second measurement technique. Techniques such as ellipsometry, or measurement of a step height using AFM are recommended for future work to validate the thicknesses determined by ARXPS.

6.3.3 The effect of poly(dimethylsiloxane) precursor flowrate and deposition power on coating chemistry

Following the development of the *iterative Si 2p – C 1s* curve-fitting protocol, it was possible to determine the effect of the precursor flowrate and deposition power on the chemistry of the coating, and its thickness, provided it was thinner than the XPS analysis depth. Poly(dimethylsiloxane), PDMS, precursor was deposited on poly(ethylene terephthalate) film using varying precursor flowrates. The deposition was carried out at three different powers to evaluate the effect of power on the deposition.

a) Coating Thickness

The thickness of the deposits was determined with increasing flowrate and varying deposition power, Figure 6-12.

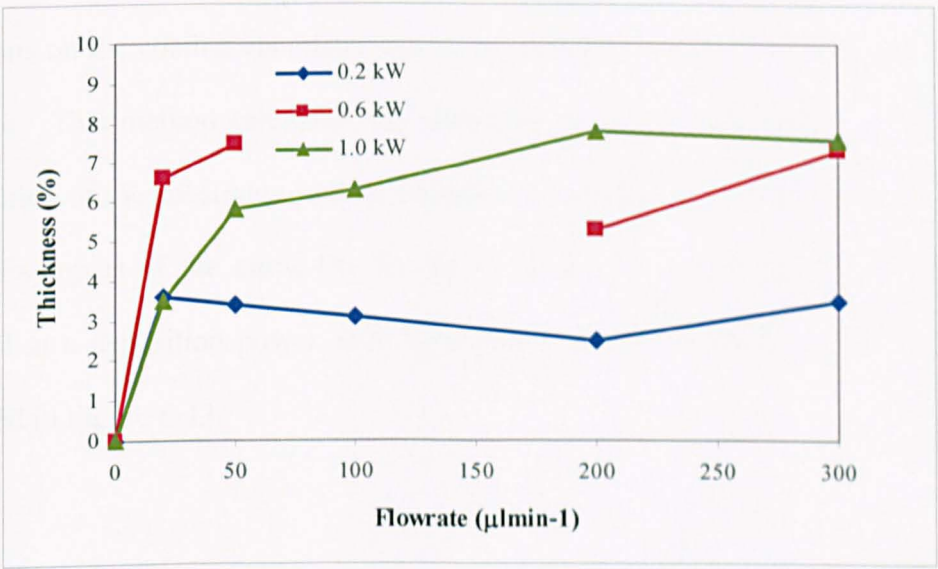

Figure 6-12: Thickness of siloxane coating deposited onto PET film with varying poly(dimethylsiloxane) precursor flowrate and deposition power Missing points correspond to samples where the COOX component of the substrate could not be seen in the spectra

The deposition power had a clear effect on the efficiency of the deposition process, if the thickness of the sample is taken as a measure of the deposition rate since the substrate residence time was equal for all samples. The low power, 0.2 kW, clearly resulted in the thinnest coatings, and the precursor flowrate had no effect on the

thickness of coating obtained. It is most likely that the low power density caused insufficient polymerisation of the precursor on the PET film.

Deposition with a power of 0.6 kW led to variable thickness; use of 100 $\mu lmin^{-1}$ led to a coating thicker greater than the depth of analysis of XPS – no carboxylic ester signal associated with the substrate was observed. However, at precursor flowrates higher than this, a decrease in thickness was noted. At the highest power, 1.0kW, a gradual increase in thickness with the precursor flowrate was observed.

b) Coating chemistry

The *iterative Si 2p – C 1s* curve-fitting protocol, allows the chemistry of coatings thinner than XPS analysis depth to be determined. Hence the effects of process conditions on the coating chemistry can be investigated without contributions from the substrate. This method calculates the chemistry of the overlayer only, removing the contribution of the substrate to allow comparison between all samples shown in Figure 6-10. Examples of the curve-fits for the C 1s and Si 2p core levels for a coating prepared at a deposition power of 0.2 kW and precursor flowrate of 100 $\mu lmin^{-1}$ are presented in Figure 6-13.

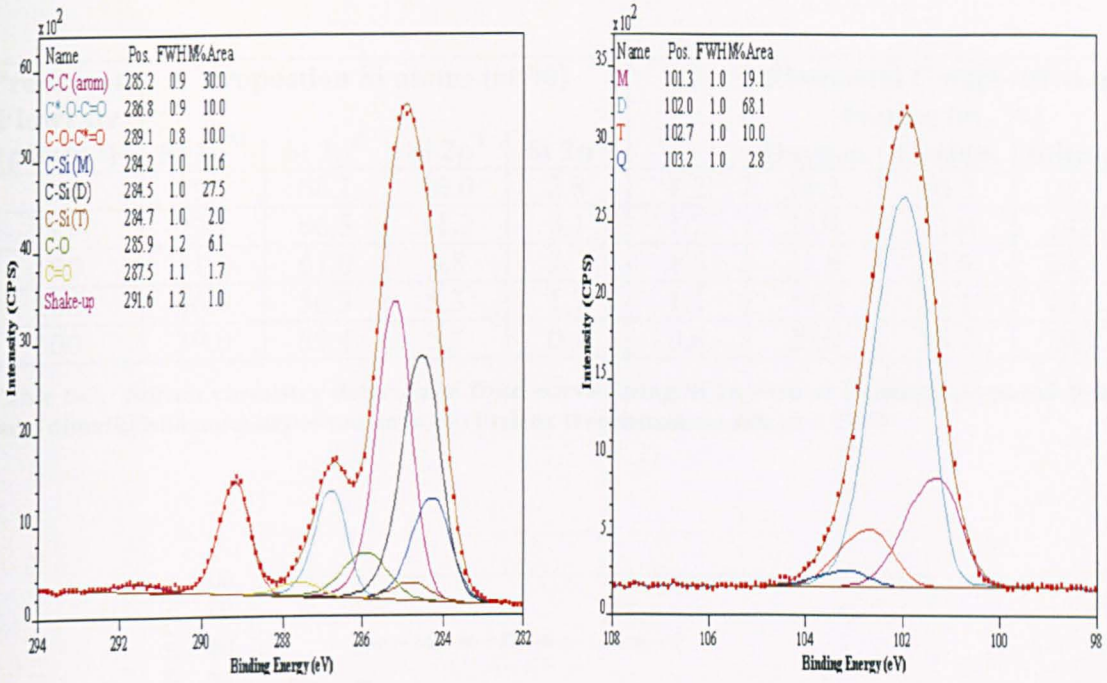

Figure 6-13: Curve-fits of C 1s and Si 2p core levels for poly(dimethylsiloxane) deposited on poly(ethylene terephthalate) film at 0.2 kW using a precursor flowrate of 20 µlmin^{-1}. Spectra have been charge corrected to position C 1s^{D} at 284.48 eV

The chemistry (in addition to ***G*** – goodness of fit) of the siloxane deposits prepared with varying flowrates at 0.2 kW on PET are presented in Table 6-7, and Figure 6-14. A clear effect of varying the precursor flowrate was observed on the relative proportion of silicon environments. As the precursor flowrate increased, the concentration of Si 2p^{M} siloxy units [$(CH)_3SiO_{1/2}$] increased. Although the concentration of Si 2p^{D} siloxy units decreased, the total concentration of 'polymeric' forms of silicon increased with increasing flowrate, whilst the inorganic – Si 2p^{T} and Si 2p^{Q} siloxy units, decreased. The decrease in cross linked T units is consistent with a decrease in power supplied to the precursor as the flowrate increases. For the same reason an increase in end M groups is consistent with this rationalisation of the observed flow rate dependence of chemistry.

Precursor Flowrate ($\mu lmin^{-1}$)	Propostion Si atoms (at %)				*G*	Elemental Composition of coating (at. %)		
	Si $2p^M$	Si $2p^D$	Si $2p^T$	Si $2p^Q$		Oxygen	Carbon	Silicon
20	19.1	68.1	10.0	2.8	1.2	24.5	50.7	24.9
50	22.1	66.5	11.3	0.1	1.2	23.4	52.0	24.7
100	31.5	61.0	4.8	2.7	1.5	21.8	53.9	24.4
200	36.9	56.3	5.3	1.7	1.1	20.8	55.1	24.2
300	39.0	55.4	5.2	0.4	0.6	20.0	55.9	24.0

Table 6-7: Silicon chemistry determined from curve-fitting Si 2p core of a coating prepared from poly(dimethylsiloxane) deposited on poly(ethylene terephthalate) film at 0.2 kW

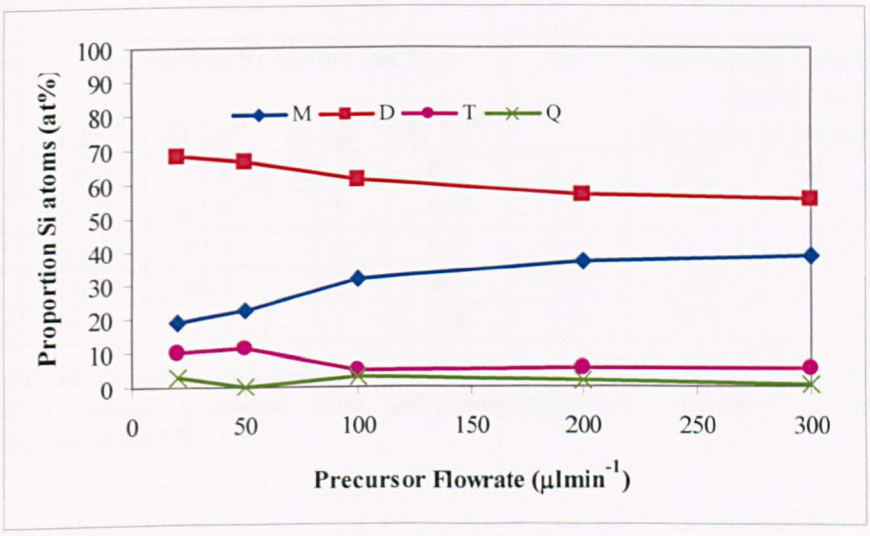

Figure 6-14: Silicon chemistry determined from curve-fitting Si 2p core of a coating prepared from poly(dimethylsiloxane) deposited on poly(ethylene terephthalate) film at 0.2 kW

An additional benefit of the *iterative Si 2p – C 1s* curve-fitting protocol is that the elemental composition of the coating may be determined, with the substrate effects being removed. As shown in Table 6-7, with increasing precursor flowrate, a decrease in oxygen concentration was observed, with a corresponding increase in carbon concentration.

For deposition at 0.6 kW, the silicon chemistry is presented for increasing precursor flowrate in Table 6-8 and Figure 6-15. Again, the same trend was observed: increasing precursor flowrate leads to an increase in polymeric silicon forms. Deviation from the

trend was noted for the sample prepared using the precursor flowrate of 200 $\mu lmin^{-1}$. Here a much larger (30%) T siloxy component was observed, with lower intensity M and D components than expected.

The thickness of the coating prepared under this condition was lower than for the rest of the samples prepared at 0.6 kW. It was noted that the power density per unit volume of precursor was higher for this case, and resulted in the formation of a more oxidised siloxane coating.

Precursor Flowrate ($\mu lmin^{-1}$)	Propostion Si atoms (at %)				*G*	Elemental Composition of coating (at. %)		
	Si $2p^M$	Si $2p^D$	Si $2p^T$	Si $2p^Q$		Oxygen	Carbon	Silicon
20	16.3	57.8	26.0	0.0	1.1	26.5	48.2	25.3
50	24.9	67.6	7.5	0.0	1.2	22.3	53.2	24.5
100	33.1	59.4	7.6	0.0	1.2	21.1	54.6	24.2
200	18.8	46.3	30.2	4.7	0.8	28.3	46.0	25.7
300	35.1	60.2	4.1	0.4	1.0	20.4	55.5	24.1

Table 6-8: Silicon chemistry and coating elemental composition determined from curve-fitting Si 2p core of a coating prepared from poly(dimethylsiloxane) deposited on poly(ethylene terephthalate) film at 0.6 kW

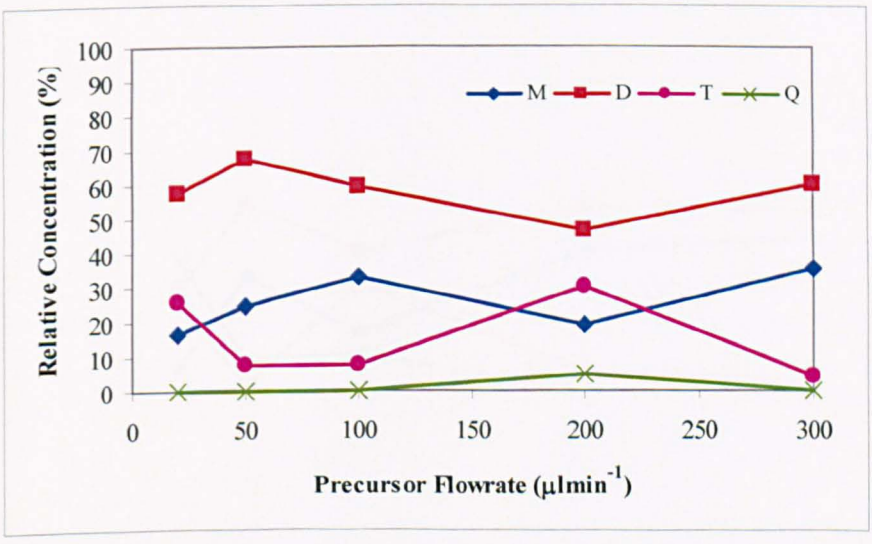

Figure 6-15: Silicon chemistry and coating elemental composition determined from curve-fitting Si 2p core of a coating prepared from poly(dimethylsiloxane) deposited on poly(ethylene terephthalate) film at 0.6 kW

The elemental composition of the coating as a function of precursor flowrate is presented in Table 6-8.

Finally, the siloxane chemistry of the coatings deposited at 1.0 kW are summarised in Table 6-9 and Figure 6-16. Here no trends in elemental or functional composition are apparent. For most of the samples prepared at at 1.0 kW, it would appear that the trend of increasing polymeric nature with increasing precursor flowrate observed at the other powers holds. The sample prepared at 100 $\mu lmin^{-1}$ deviates from this, however, with a much higher T siloxy component than would be expected. It is not possible to explain this observation currently.

Precursor Flowrate ($\mu lmin^{-1}$)	Propostion Si atoms (at %)				*G*	Elemental Composition of coating (at. %)		
	Si $2p^M$	Si $2p^D$	Si $2p^T$	Si $2p^Q$		Oxygen	Carbon	Silicon
20	7.4	30.0	24.6	38.0	1.7	41.5	30.2	28.3
50	33.6	54.6	2.3	9.5	1.0	23.1	52.3	24.6
100	17.1	40.8	31.1	11.0	1.0	30.9	42.9	26.2
200	40.4	53.5	6.0	0.2	0.9	19.9	56.1	24.0
300	45.0	52.8	2.1	0.1	1.2	18.7	57.6	23.7

Table 6-9: Silicon chemistry and coating elemental composition determined from curve-fitting Si 2p core of a coating prepared from poly(dimethylsiloxane) deposited on poly(ethylene terephthalate) film at 1.0 kW

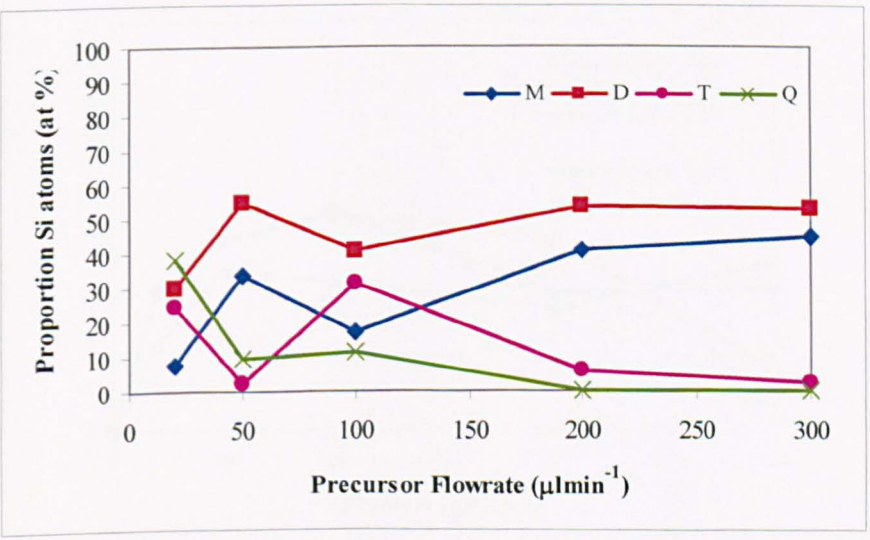

Figure 6-16: Silicon chemistry determined from curve-fitting Si 2p core of a coating prepared from poly(dimethylsiloxane) deposited on poly(ethylene terephthalate) film at 1.0 kW

The elemental composition of the coating is presented in Table 6-9

6.3.4 The effect of poly(hydrogenmethylsiloxane) (PHMS) precursor flowrate and deposition power on coating chemistry

In order to compare the effect of the precursor chemistry on the chemistry of the coating obtained, a second precursor – poly(hydrogenmethylsiloxane) was deposited. The same precursor flowrates and deposition powers were used as for the experiments with poly(hydrogenmethylsiloxane). It was expected that the presence of an Si-H group on each silicon, replacing one of the Si-Me groups, would result in the precursor being more reactive, leading to the formation of more oxidised coatings. In addition, the reactivity of the precursor may lead to a change in the deposition rate.

a) Coating Thickness

The calculated thickness of the coatings deposited using PHMS are shown in Figure 6-17. The values were less predictable than those deposited using PDMS. A maxima in thickness at intermediate flowrates was observed for deposition at 0.2 and 1.0 kW. Thick coatings were occasionally produced at 0.6 kW.

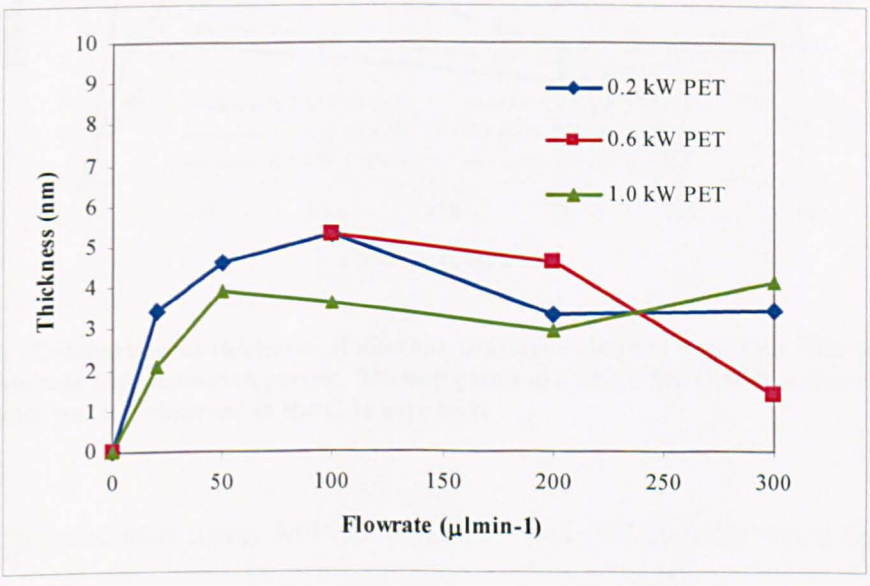

Figure 6-17: Thickness of siloxane coating deposited onto PET film with varying poly(hydrogenmethylsiloxane) precursor flowrate and deposition power

Deposition at 0.2 kW with low precursor flowrates led to an increase in thickness with flowrate. However, the use of flowrates greater than 100 μl min^{-1} led to a decrease in thickness. At 20 and 50 μl min^{-1}, deposition at 0.6 kW resulted in coatings whose thicknesses were greater than the depth of analysis of XPS. At the highest power, the thickness of the coating varied with no relation to flowrate.

With the exception of deposition in a power-deficient regime (0.2 kW), the thickness of coatings generated from PDMS rather than PHMS was greater for the same deposition conditions, Figure 6-18. This may be due to the reactivity of the PHMS molecule, resulting in crosslinking in the gas phase rather than polymerisation at the surface, which could result in deposition of a thinner coating

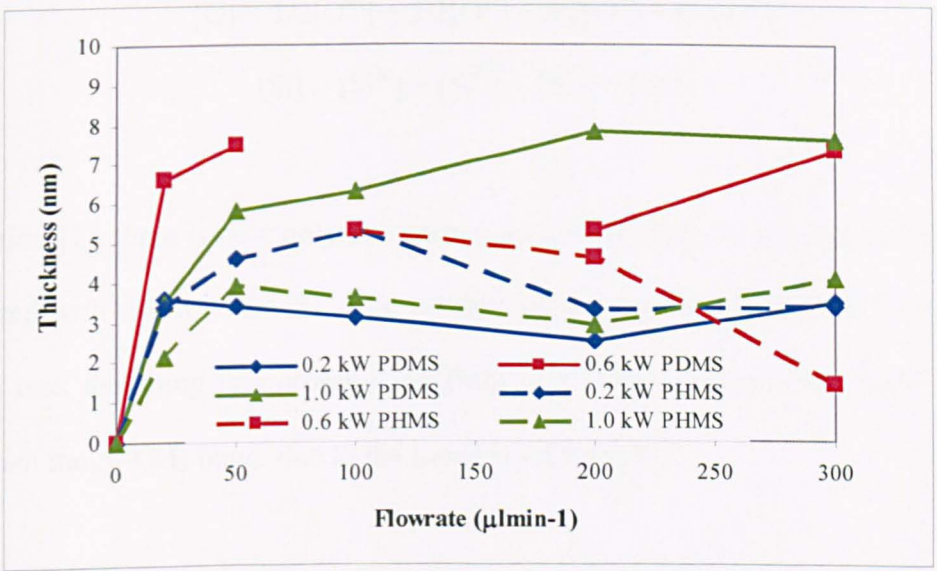

Figure 6-18: Comparison of thickness of siloxane coatings deposited onto PET film with varying precursor flowrate and deposition power. Missing points are where the COOX component relating to the substrate was not observed in the C 1s core level

The coatings generated using APPLD of PDMS and PHMS were much thinner than those deposited by Ward *et al*[15] using OMCTS and TMCTS at the same precursor flowrate. Thicknesses of ~ 3 – 8nm were typically generated from PDMS/PHMS versus ~280 nm for OMCTS/TMCTS. This difference has been accredited to PDMS/PHMS deposition being carried out on a reel-to-reel system at 4 $mmin^{-1}$. Deposition of

OMCTS/TMCTS was carried out with the substrate static, with deposition for 10 minutes. In some cases, the deposition rates were similar, at ~30 $nmmin^{-1}$.

b) Coating Chemistry

As the influence of the substrate has been removed using the curve-fitting process, the chemistry of the coatings was evaluated as a function of precursor flowrate for three deposition powers. In a similar manner to that used for $ppSiO_x$ deposited from PDMS, the elemental composition of $ppSiO_x$ coatings from PHMS can be determined. However, the calculation is slightly different:

$$[C] = 3[C^M] + [C^D] + [C^T] \quad [1]$$

$$[O] = 1/2[O^M] + 2/2[O^D] + 3/2[O^T] + 4/2[O^Q] \quad [2]$$

$$[Si] = [Si^M] + [Si^D] + [Si^T] + [Si^Q] \quad [3]$$

In equation [1], there is now only one carbon associated with the D siloxy environment (compared with two for PDMS). The number of carbons associated with T siloxy unit remains one, assuming that crosslinking from D to form T occurs via the Si-H bond rather than the $Si-CH_3$ bond, due to the lower bond energy[16].

Using a deposition power of 0.2 kW, the coating chemistry was found to be relatively constant, irrespective of precursor flowrate, as observed for deposition using PDMS under these conditions. However, as shown in Table 6-10 and Figure 6-19, whilst the coating primarily comprises D siloxy units, the concentration of T siloxy units is much larger (~20%) than for the corresponding experiment carried out using the poly(dimethylsiloxane) precursor (see Table 6-7 and Figure 6-14).

Precursor Flowrate ($\mu lmin^{-1}$)	Propostion Si atoms (at %)				*G*	Elemental Composition of coating (at. %)		
	Si $2p^M$	Si $2p^D$	Si $2p^T$	Si $2p^Q$		Oxygen	Carbon	Silicon
20	3.7	64.7	31.6	0.0	1.12	35.5	33.4	31.1
50	4.4	70.8	24.8	0.0	1.43	34.5	34.1	31.3
100	3.9	68.6	25.2	2.3	2.18	35.5	33.1	31.4
200	1.7	73.6	22.9	1.8	1.55	35.8	32.4	31.8
300	2.2	70.7	25.8	1.3	2.08	35.8	32.6	31.6

Table 6-10: Silicon chemistry and elemental composition of coating determined from curve-fitting Si 2p core of a coating prepared from poly(hydrogenmethylsiloxane) deposited on poly(ethylene terephthalate) film at 0.2 kW

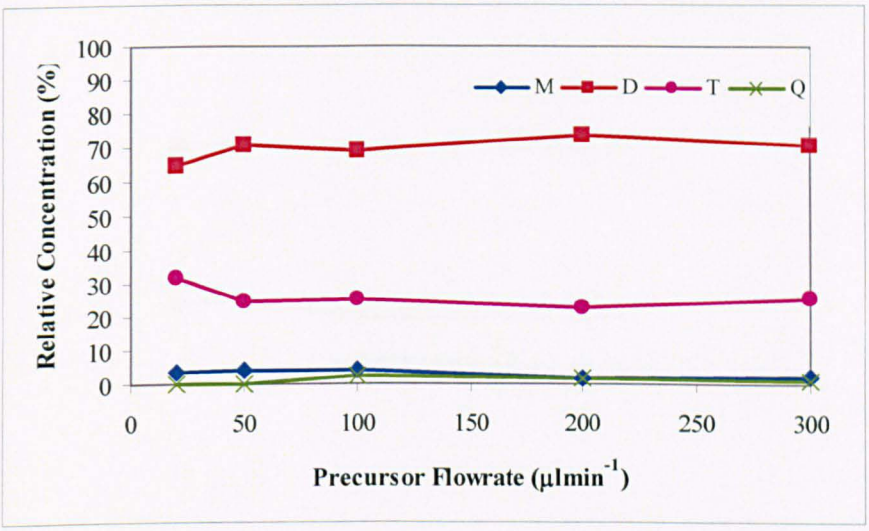

Figure 6-19: Silicon chemistry determined from curve-fitting Si 2p core of a coating prepared from poly(hydrogenmethylsiloxane) deposited on poly(ethylene terephthalate) film at 0.2 kW

An increase in concentration of T siloxy species in the coating deposited from PHMS, compared with PDMS, was reflected in the decreased carbon and increased oxygen concentration, Table 6-10.

The silicon chemistry of coatings deposited from PHMS at 0.6 kW was similar to the chemistry of those deposited at 0.2 kW, with D and T siloxy units being most abundant, Table 6-11 and Figure 6-19. However, a precursor flowrate of 300 $\mu lmin^{-1}$ had a lower D concentration, and a correspondingly higher T concentration than the other precursor flowrates.

Precursor Flowrate ($\mu l min^{-1}$)	Proportion Si atoms (at %)				*G*	Elemental Composition of coating (at. %)		
	Si $2p^M$	Si $2p^D$	Si $2p^T$	Si $2p^Q$		Oxygen	Carbon	Silicon
20	4.3	70.5	24.1	1.1	2.23	34.9	33.8	31.4
50	3.6	71.3	25.1	0.0	1.44	34.8	33.7	31.5
100	3.5	69.2	20.0	7.4	7.16	36.7	31.6	31.7
200	5.3	69.3	20.1	5.3	1.62	35.4	33.1	31.4
300	3.0	47.2	38.4	11.4	0.47	39.9	29.2	30.9

Table 6-11: Silicon chemistry and elemental composition determined from curve-fitting Si 2p core of a coating prepared from poly(hydrogenmethylsiloxane) deposited on poly(ethylene terephthalate) film at 0.6 kW

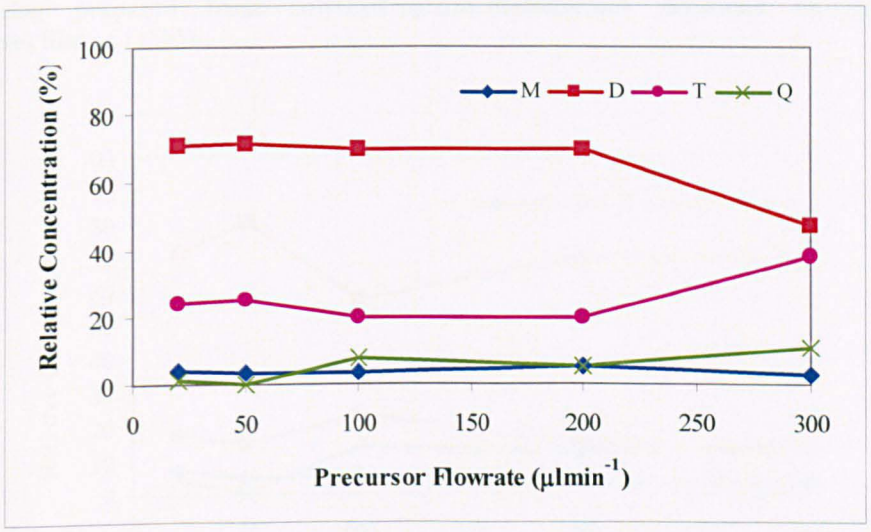

Figure 6-20: Silicon chemistry determined from curve-fitting Si 2p core of a coating prepared from poly(hydrogenmethylsiloxane) deposited on poly(ethylene terephthalate) film at 0.6 kW

The elemental composition of the coating is presented in Table 6-11. The elemental composition appeared independent of PHMS flowrate, with the exception of deposition at 300 $\mu l min^{-1}$, where the oxygen concentration was significantly higher. This datapoint represented the thinnest coating deposited at this power, again suggesting that deposition of thinner coatings at the same power results in the formation of more oxidised coatings.

An increase in the concentration of Q siloxy units (the most oxidised form of silicon) was observed for deposition using a 1.0 kW power, Table 6-12 and Figure 6-21. There

was no corresponding increase in the oxygen concentration, most likely due to the conversion of D and T units to Q.

Precursor Flowrate ($\mu lmin^{-1}$)	Propostion Si atoms (at %)				*G*	Elemental Composition of coating (at. %)		
	Si $2p^M$	Si $2p^D$	Si $2p^T$	Si $2p^Q$		Oxygen	Carbon	Silicon
20	6.9	71.6	17.0	4.4	1.07	34.3	34.3	31.4
50	4.5	80.6	14.7	0.2	0.92	33.5	34.6	31.8
100	5.1	57.6	23.3	14.0	0.64	38.6	30.1	31.3
200	3.7	70.4	14.2	11.7	1.47	37.4	30.6	32.0
300	2.9	69.5	12.4	15.2	0.91	38.6	29.2	32.2

Table 6-12: Silicon chemistry and elemental compostion determined from curve-fitting Si 2p core of a coating prepared from poly(hydrogenmethylsiloxane) deposited on poly(ethylene terephthalate) film at 1.0 kW

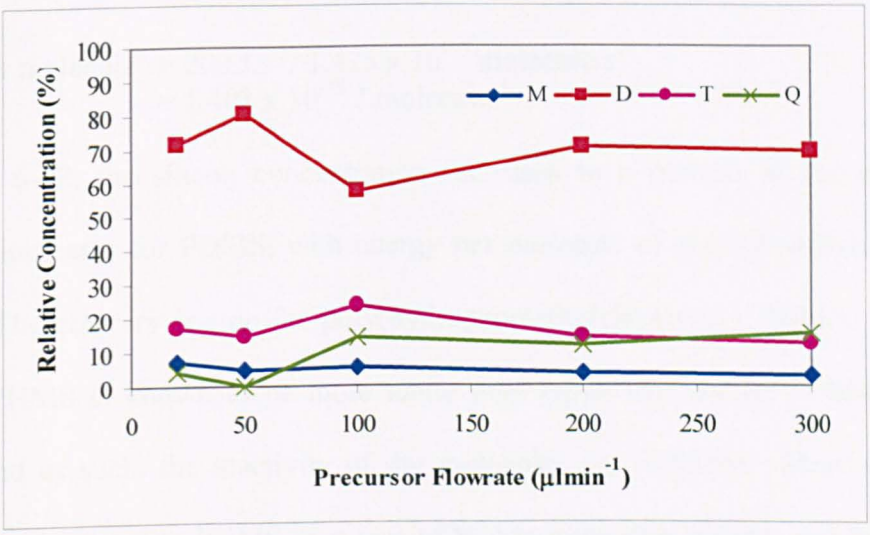

Figure 6-21: Silicon chemistry determined from curve-fitting Si 2p core of a coating prepared from poly(hydrogenmethylsiloxane) deposited on poly(ethylene terephthalate) film at 1.0 kW

The hypothesis that the use of a PHMS precursor would result in an enhanced deposition rate was not proven in this case. In fact, PDMS resulted in the formation of thicker coatings, except at the lowest power deposition. Since it was not possible to isolate the effects of power and precursor flowrate, Yasuda's 'composite parameter'[17] was used as measure of the plasma conditions - W/FM where W = power; F = precursor flowrate; and M = molar mass. Silicon concentration, rather than thickness was chosen as a measure of efficiency of deposition due to it being the average of five data points

rather than the value of one. An example of the energy per molecule calculation for a precursor flowrate of 20 $\mu l min^{-1}$, and power of 200W follows:

Precursor Flowrate, F = 20 $\mu l min^{-1}$
= 20 x 10^{-6} $l.min^{-1}$
= 20 x 10^{-6} x 0.903 $kg.min^{-1}$
= (20 x 10^{-6} x 0.903) / 60 $kg.s^{-1}$
= (20 x 10^{-6} x 0.903) / (60 x 1.272) $mol.s^{-1}$
= 2.367 x 10^{-7} $mol.s^{-1}$
= 2.367 x 10^{-7} * 6.022 x 10^{23} $molecule.s^{-1}$
= 1.425 x 10^{-17} $molecule.s^{-1}$

Power, W = 200 W
= 200 $J.s^{-1}$

Energy per molecule = 200 $J.s^{-1}$/ 1.425 x 10^{-17} $molecule.s^{-1}$
= 1.403 x 10^{-15} $J.molecule^{-1}$

In Figure 6-22, the silicon concentration increases to a plateau as the energy per molecule increases for PDMS, with energy per molecule of poly(dimethylsiloxane) – PDMS. The contrary is true for poly(hydrogenmethylsiloxane) – PHMS. The Si-H bond of PHMS is known to be more labile than either the $Si-CH_3$ or Si-O bond in PDMS, and as such, the reactivity of the molecules are different. More energy per molecule is delivered to PHMS as it was of higher molecular weight, and hence fewer molecules were nebulised. This could result in crosslinking in the gas phase rather than polymerisation at the surface.

This has been evidenced by the formation of silica powder during deposition of PHMS. Particles are often observed embedded in the coatings, and loose silica powder is found at the bottom of the deposition section of the deposition apparatus.

Deposition of thick coatings from PHMS resulted at low energy per molecule. A higher energy per molecule value was required for deposition of PDMS.

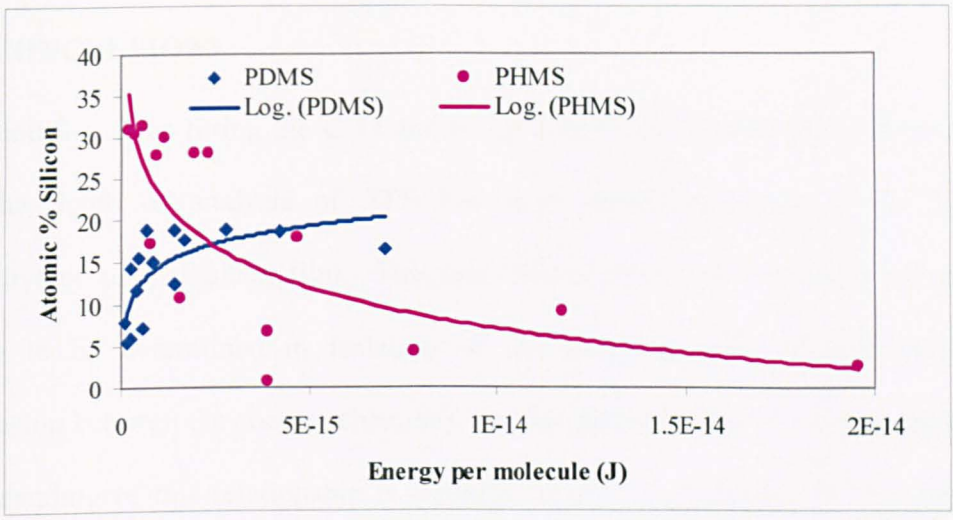

Figure 6-22: Silicon concentration as a function of energy per molecule of poly(dimethylsiloxane) precursor

6.4 CONCLUSIONS

A method for curve-fitting the C 1s and Si 2p core levels of siloxane coatings thinner than the depth of analysis of XPS has been developed when the substrate is poly(ethylene terephthalate) film. This has allowed the elemental composition of the coating to be determined in isolation of the substrate, and therefore allows the relationship between the coating chemistry and the plasma parameters to be determined. Understanding of this relationship is essential in the development of novel processes such as atmospheric pressure plasma liquid deposition, and leads to the deposition of coatings with controlled properties.

This curve-fitting protocol has been used in combination with an algorithm to determine the film thickness and confirmed the coating to be continuous, rather than patchy.

This work documents the first reported investigation of APPLD deposition power and precursor flowrate on coating thickness and coating chemistry for two precursors: poly(dimethylsiloxane) – PDMS, and poly(hydrogenmethylsiloxane – PHMS. Coatings generated from the PDMS precursor were thicker than those created from PHMS precursor, except for deposition in energy deficient regimes.

For PDMS, the coating chemistry was found to be dependent on both flowrate and deposition power. Using low power, a polymeric coating was generated, comprising mainly Si $2p^{D}$ siloxy species. An increase in Si $2p^{M}$ siloxy species was observed for increasing flowrate. Using higher deposition powers resulted in a more oxidised coating being formed from the PDMS precursor. A more oxidised coating resulted from the use of PHMS under comparative deposition conditions.

6.5 REFERENCES

[1] O'Hare, L.A.; Leadley, S.R.; Parbhoo, B.; Francis, J.G., 'Adhesion of silicone coatings to plastic films', in *Organosilicon Chemistry V: From molecules to materials*, Eds Auner, N.; Weiss, J., Wiley-VCH: Weiheim, 2003

[2] Beamson G, Briggs D, *High Resolution XPS of Organic Polymers: The Scienta ESCA300 Database*, John Wiley & Sons: Chichester, 1992

[3] O'Hare, L.A.; Smith, J.A.; Leadley, S.R; Parbhoo, B.; Goodwin, A.J.; Watts, J.F., 'Surface physico-chemistry of corona-discharge-treated poly(ethylene terephthalate) film', *Surface and Interface Analysis*, **33**(7), 2002, 617-625

[4] Beamson, G.; Bunn, A.; Briggs, D. 'High-resolution monochromated XPS of poly(methyl methacrylate) thin films on conducting substrate', *Surf. Interface Anal.* **17**(2), 1991, 105 - 115

[5] Beamson, G.; Bunn, A.; Briggs, D. 'High-resolutions monochromated XPS of poly(methyl methacrylate) thin films on a conducting substrate', *Surf. Interface Anal.*, **17**, 1991, 105 - 115

[6] Leadley, S.R.; Watts, J.F., 'The use of monochromated XPS to evaluate acid-base interactions at the PMMA/oxidised metal interface', *J. Adhesion*, **60**, 1997, 175 – 196

[7] Watts, J.F.; Leadley, S.R.; Castle, J.E.; Blomfield, C.J., 'Adsorption of PMMA on oxidised Al and Si substrates: An investigation by high-resolution X-ray photoelectron spectroscopy', *Langmuir*, **16**(5), 2000, 2292 - 2300

[8] Leadley, S.R.; Watts, J.F., 'The use of PXS to examine the interaction of poly(acrylic aicd) with oxidised metal substrates', *J. Elec. Spec.*, **85**, 1997, 107 - 121

[9] Roualdes, S.; Berjoan, R.; Durand, J. '^{29}Si NMR and Si 2p XPS correlation in polysiloxane membranes prepared by plasma enhanced chemical vapour deposition', *Separation and Purification Technology*, **25**, 2001, 391 397

[10] Alexander, M.R.; Short, R.D.; Jones, F.R.; Michaeli, W.; Blomfield, C.J., 'A study of HMDSO/O_2 plasma deposits using a high-sensitivity and –energy resolutions XPS instrument: curve-fitting of the Si 2p core level', *Applied Surface Science*, **137**, 1999, 179 - 183

[11] Fulghum, J.E.; 'Determination of overlayer thickness by angle-resolved XPS: a comparison of algorithms' *Surface and Interface Analysis*, **20**, 1993, 161 - 173

[12] Cumpson, P.J., 'Angle-resolved XPS and AES: depth-resolution limits and a general comparison of properties of depth-profile reconstruction methods', **73**, 1995, 25 - 52

[13] NPL ARCtick angle-resolved XPS spreadsheet, 13 –APR- 1999

[14] http://www.nist.gov/srd/nist82.htm

[15] Ward, L.J.; Schofield, W.C.E.; Badyal, J.P.S.; Goodwin, A.J.; Merlin, P.J., 'Atmospheric pressure glow discharge deposition of polysiloxanes and SiO_x films', *Langmuir*, **19**, 2003, 2110-2114

[16] *Handbook of Chemistry and Physics*, **76th Edition**, CRC Press Inc., Boca Raton, FL, 1995

[17] Yasuda, H.; Hirotsu, T., 'Critical evaluation of conditions of plasma polymerisation', *J. Polym. Sci. Poly. Chem.*, **16**, 1978, 743-759

CHAPTER 7

OPTIMISATION OF COATING PERFORMANCE

7.1 INTRODUCTION

It is expected that the hydrothermal stability of atmospheric pressure plasma liquid deposition (APPLD) coatings can be improved by either encouraging grafting of the coating to the substrate, or by increasing the cross-linking/network formation in the coating. Previous work has indicated that activation of the substrate prior to deposition, optimisation of plasma power, and plasma treatment of the coating can improve performance. This section describes the effects of these parameters on the surface chemistry and hydrothermal stability of deposits prepared using a linear poly(hydrogenmethylsiloxane) precursor.

7.2 EXPERIMENTAL

7.2.1 Atmospheric pressure plasma liquid deposition apparatus

Siloxane coatings were deposited onto poly(ethylene terephthalate) films using Dow Corning Plasma Solutions Mark I atmospheric pressure plasma liquid deposition (APPLD) apparatus. The apparatus is described in detail in *Chapter 3*.

Two experimental regimes were used during the deposition process in order to compare the effect of plasma treatment of the substrate prior to deposition, and plasma treatment of the coating following deposition. It was hypothesised that plasma treatment of the substrate prior to deposition may lead to enhanced hydrothermal stability through increased grafting. It was also believed that by plasma treatment of the coating following deposition, the crosslink density of the coating may be increased, again leading to improved hydrothermal stability.

The first experimental set-up relied on the film being passed through both activation zones prior to re-spooling the film. A further pass through the first activation zone was then carried out prior to deposition, shown schematically in Scheme 7-1.

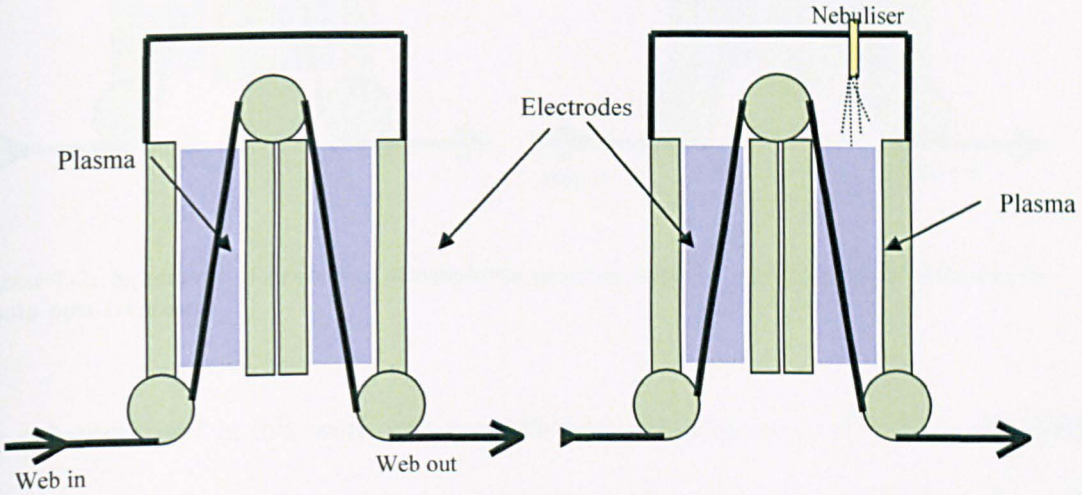

Scheme 7-1: Deposition process illustrating the film being APP treated in two activation zones prior to the typical atmospheric pressure plasma liquid deposition process

The second experimental set-up was used to investigate plasma treatment of a deposited coating to evaluate its effect on improving the stability of a coating. Here, a coating is prepared using the typical atmospheric pressure plasma liquid deposition configuration as described in **Chapter 6**. The coating was then exposed to APP by passing it through two activation zones with no precursor introduction, Scheme 7-2. It is expected that this plasma treatment step will increase crosslinking of the coating, leading to improved durability. The hydrothermal stability of the coating will be used as a measure of its durability.

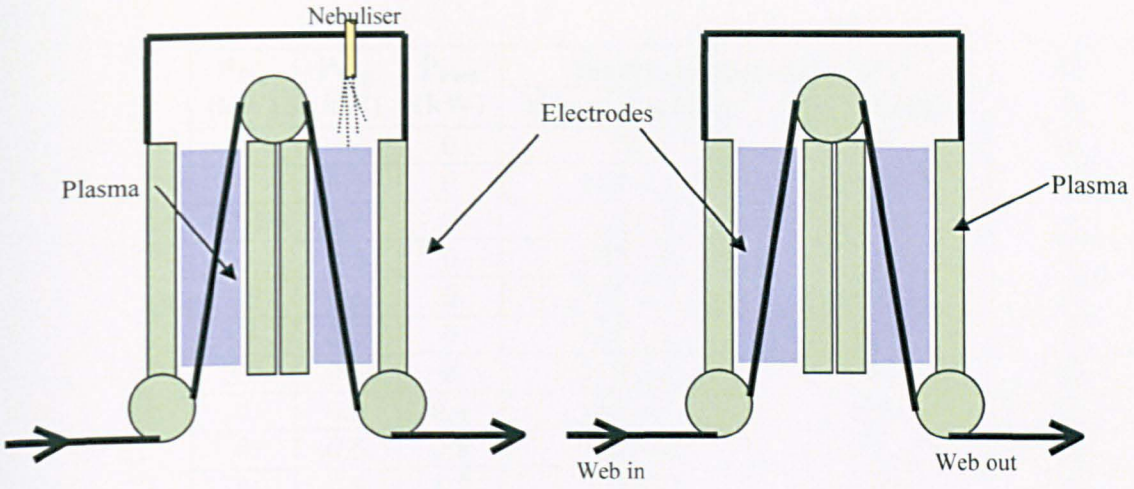

Scheme 7-2: Schematic of process of atmospheric pressure plasma liquid deposition followed by plasma post-treatment

The substrate used in this work was poly(ethylene terephthalate), PET film. The PET film was 25 μm film, commercially available from Goodfellow, UK. The precursor was linear poly(hydrogenmethylsiloxane) - PHMS, (10 cSt). Further information on the substrate and precursors is presented in *Chapter 3*. Deposition of the precursors was carried out at 4 $mmin^{-1}$, in a helium APP, using a gas flow of 15 slm.

The plasma power conditions were varied as described in Table 7-1. P_{Pre} refers to the plasma power used to treat the substrate prior to deposition. P_{Dep} represents the power used during the precursor deposition, whilst P_{Post} corresponds to the plasma power applied to the coating following deposition. The precursor was deposited onto poly(ethylene terephthalate) substrate through helium plasma at 1 $mmin^{-1}$, using a precursor flowrate of 200 $\mu Lmin^{-1}$. Contact angle results presented are the average of both angles for three drops.

P_{Pre} (kW)	P_{Dep} (kW)	P_{Post} (kW)	Water contact angle, θ (°)		Δθ (°)
			Before washing	After washing	
0	0	0	70	na	na
0	0.5	0	108 ± 2	106	-2
0.4	0.5	0	110 ± 2	104	-6
0.8	0.5	0	107 ± 3	103	-4
1.2	0.5	0	105 ± 3	103	-2
1.6	0.5	0	107 ± 1	105	-2
2.0	0.5	0	110 ± 1	104	-6
0	0.5	0.4	106 ± 2	106	0
0	0.5	0.8	105 ± 0	97	-8
0	0.5	1.2	106 ± 2	104	-2
0	0.5	1.6	108 ± 1	108	0
0	0.5	2.0	109 ± 2	109	0

Table 7-1: Activation conditions for poly(hydrogenmethylsiloxane) precursor deposited onto poly(ethylene terephthalate) film

Portions of the coated film were immersed in boiling water for 30 minutes. Both the unwashed and washed samples underwent water contact angle analysis and XPS.

7.3 RESULTS AND DISCUSSION

7.3.1 Water contact angle analysis

The 'as received' PET film had a water contact angle of 70°, which is as expected for a substrate containing significant amounts of oxygen in its molecular structure. High water contact angles (> 100°) were observed for all deposits, independent of the substrate plasma treatment, or plasma treatment of the coating, Table 7-1. These contact angles would suggest that a low surface energy coating was present at the surface of the PET film, consistent with siloxane deposition.

Whilst slight decreases in water contact angle occurred on some samples following immersion in water, there was no discernible relationship between these decreases, and the plasma processing parameters. The decreases in water contact angle indicate the

surface is becoming slightly more hydrophilic upon hydrothermal treatment. However, as the water contact angle remained far higher than for 'as received' PET film, we can conclude that the coating was not entirely removed. Partial coating removal, on a scale smaller than the probe liquid dimensions might account for slight reductions in the WCA or a change in siloxane coating chemistry to a more oxidised siloxy environment, which will be investigated using XPS.

7.3.2 The effect on coating chemistry of plasma treatment of the substrate prior to siloxane deposition

The appearance of silicon was noted for all conditions indicating that a siloxane coating had been deposited. The relative absence of substrate peaks in the C 1s core level indicated that contrary to the coatings discussed earlier in this chapter, these coatings are continuous, and thicker than the depth of analysis of XPS.

At low substrate plasma treatment power (P_{Pre} = 0.4, 0.8 1.2 kW), very little variation in the elemental composition of the coating was noted. With the use of higher powers, (P_{Pre} = 1.6, 2.0 kW) an increase in oxygen in the coating was observed, Table 7-2.

P_{Pre} (kW)	P_{Dep} (kW)	P_{Post} (kW)	Relative Concentration (at. %)			O/C	O/Si
			Oxygen	Carbon	Silicon		
0	0	0			0.0		NA
0	0.5	0	30.4	38.7	30.9	0.79	0.99
0.4	0.5	0	29.4	38.7	31.9	0.76	0.92
0.8	0.5	0	29.2	38.5	32.4	0.76	0.90
1.2	0.5	0	29.4	38.4	32.3	0.77	0.91
1.6	0.5	0	34.6	34.0	31.4	1.02	1.10
2.0	0.5	0	41.0	28.2	30.9	1.45	1.33

Table 7-2: Elemental composition of deposits prepared by APPLD of poly(hydrogenmethylsiloxane) precursor where the substrate was plasmas treated with increasing P_{Pre} prior to depostion

As the elements detected are only related to the coating, with no effect of the substrate, it is possible to compare the O/C and O/Si ratios of the sample. The increase in both these ratios at high P_{Pre} suggests that the silicon oxidation state is increasing when the substrate is plasma treated prior to deposition. In addition, the carbons of the methyl groups bonded to silicon may also be becoming oxidised during the deposition process. These hypotheses will be affirmed by elucidating the carbon and silicon chemistry using the curve-fitting method described in *Chapter 5* for the C 1s and Si 2p core levels.

The curve-fits for the C 1s and Si 2p core levels of a coating prepared from atmospheric pressure plasma liquid deposition at 0.5 kW, with no substrate plasma treatment (P_{Pre} = 0 kW) or plasma treatment of coating following deposition (P_{Post} = 0 kW) are presented in Figure 7-1. The majority of the siloxane coating is in the D and T environments.

The results may then be compared to the curve-fits for coatings prepared using the same deposition power, but where the substrate was plasma treated with increasing power, prior to deposition, Figure 7-2 for C 1s, and Figure 7-3 for Si 2p.

Examination of the C 1s core levels for each sample does not reveal the presence of the characteristic ester peak associated with the PET substrate. This confirms the hypothesis that under these conditions, a continuous coating, thicker than the depth of analysis of XPS, has been deposited.

The C 1s core level was curve-fitted using synthetic components assigned to C $1s^M$, C $1s^D$ and C $1s^T$. In addition, low intensity peaks assigned to C-O, C=O and COOX were also required to obtain a good fit in some cases. The intensity of these oxidised

carbon peaks increased with P_{Pre}. For the Si 2p core level, four components, representing Si $2p^M$, Si $2p^D$, Si $2p^T$and Si $2p^Q$ siloxy environments were fitted.

In agreement with the elemental composition, the chemistry of the coatings were similar for substrates treated at low powers. Where the substrate was plasma treated at P_{Pre} = 1.6, 2.0 kW prior to deposition, the chemistry was markedly different. The coatings had a far higher concentration of T and Q siloxy environments, with a corresponding decrease in the intensity of the D component. The data from the curve-fits are summarised for clarity in Table 7-3 and Table 7-4, for carbon and silicon, respectively.

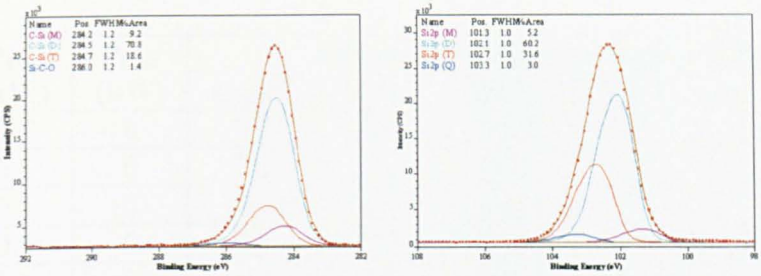

Figure 7-1: Curve-fits for the carbon (C 1s) and silicon (Si 2p) core level of poly(hydrogenmethylsiloxane) precursor deposited onto poly(ethylene terephthalate) film at a power of 0.5 kW

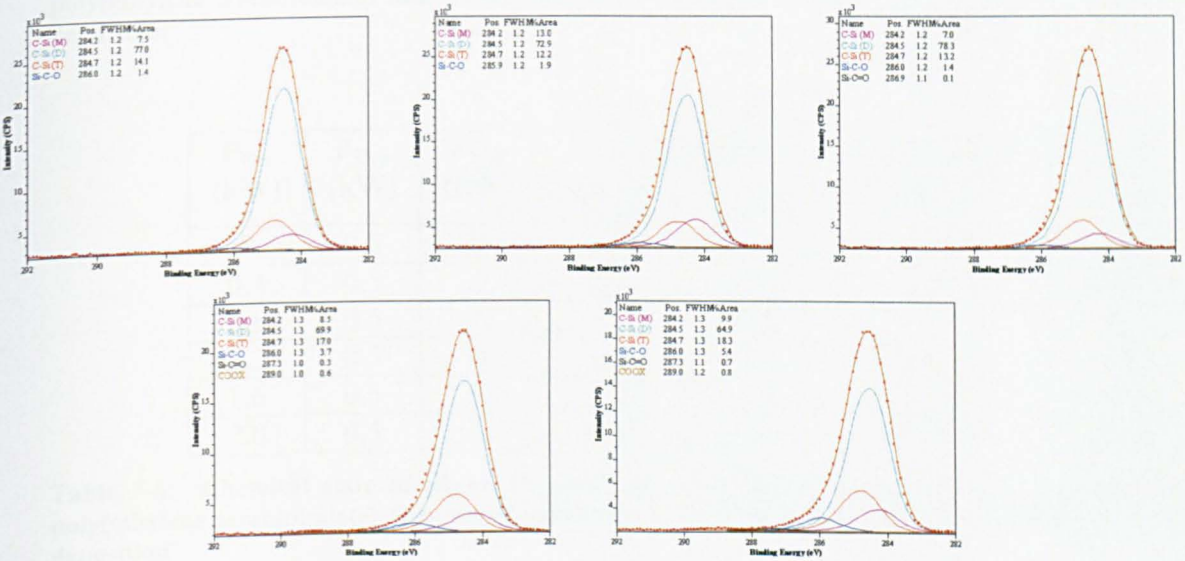

Figure 7-2: Curve-fits for the carbon (C 1s) core level of poly(hydrogenmethylsiloxane) precursor deposited onto poly(ethylene terephthalate) film at a power of 0.5 kW. Substrate was plasma treated prior to deposition with increasing power. Top row left to right: P_{Pre} = 0.4, 0.8, 1.2 kW; bottom row left to right P_{Pre} = 1.6 kW, 2.0 kW

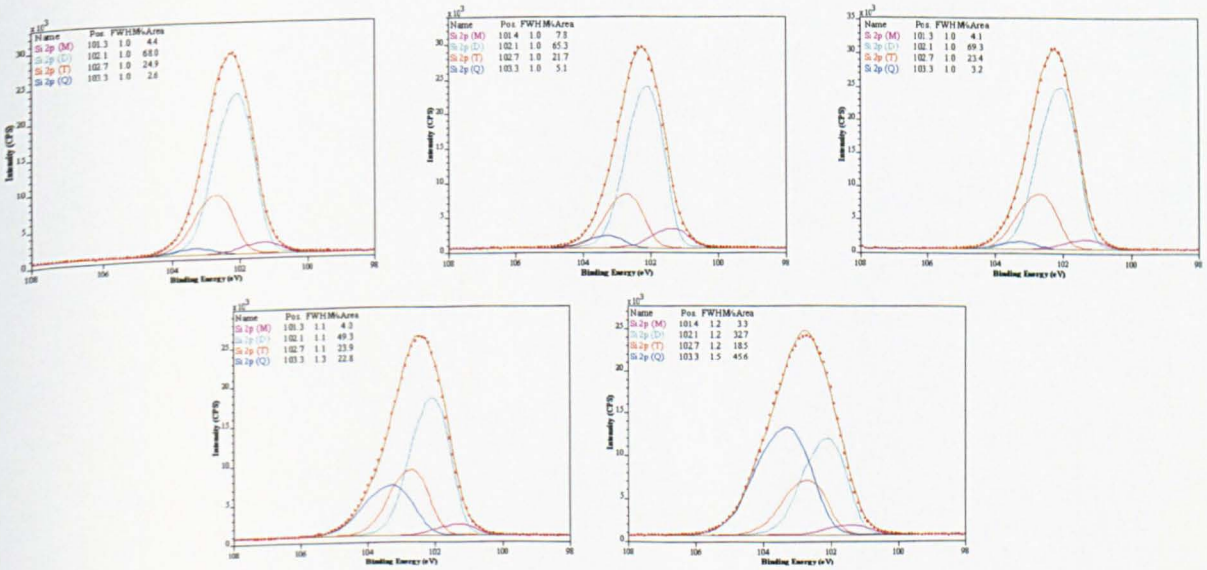

Figure 7-3: Curve-fits for the silicon (Si 2p) core level of poly(hydrogenmethylsiloxane) precursor deposited onto poly(ethylene terephthalate) film at a power of 0.5 kW. Substrate was plasma treated prior to deposition with increasing power. Top row left to right: P_{Pre} = 0.4, 0.8, 1.2 kW; bottom row left to right 1.6 kW, 2.0 kW

P_{Pre} (kW)	P_{Dep} (kW)	P_{Post} (kW)	Relative concentration from C 1s (%)					
			$C\text{-}Si^{M}$	$C\text{-}Si^{D}$	$C\text{-}Si^{T}$	C-O	C=O	COOX
0	0.5	0	9.2	70.8	18.6	1.4	0.0	0.0
0.4	0.5	0	7.5	77.0	14.1	1.4	0.0	0.0
0.8	0.5	0	13.0	72.9	12.2	1.9	0.0	0.0
1.2	0.5	0	7.0	78.3	13.2	1.4	0.1	0.0
1.6	0.5	0	8.5	69.9	17.0	3.7	0.3	0.6
2.0	0.5	0	9.9	64.9	18.3	5.4	0.7	0.8

Table 7-3: Chemical state of carbon for poly(hydrogenmethylsiloxane) precursor deposited on poly(ethylene terephthalate) film where substrate was plasma treated at various powers prior to deposition

P_{Pre} (kW)	P_{Dep} (kW)	P_{Post} (kW)	Relative concentration from Si 2p (%)			
			$Si\ 2p^{M}$	$Si\ 2p^{D}$	$Si\ 2p^{T}$	$Si\ 2p^{Q}$
0	0.5	0	5.2	60.2	31.6	3.0
0.4	0.5	0	4.4	68.0	24.9	2.6
0.8	0.5	0	7.8	65.3	21.7	5.1
1.2	0.5	0	4.1	69.3	23.4	3.2
1.6	0.5	0	4.0	49.3	23.9	22.8
2.0	0.5	0	3.3	32.7	18.5	45.6

Table 7-4: Chemical state of silicon for poly(hydrogenmethylsiloxane) precursor deposited on poly(ethylene terephthalate) film where substrate was plasma treated at various powers prior to deposition

7.3.3 The effect on coating chemistry of plasma treatment of the coating following siloxane deposition

Again, the presence of silicon following deposition is indicative of the presence of a siloxane coating. Increasing the plasma power applied to the coating following deposition (P_{Post}), led to an increase in the oxygen concentration, Table 7-5. A corresponding decrease in carbon concentration was also observed, whilst silicon remained relatively stable. An exception to this trend was noted for the sample where $P_{Post} = 2.0$ kW.

P_{Pre} (kW)	P_{Dep} (kW)	P_{Post} (kW)	Concentration (at %)			O/C	O/Si
			Oxygen	Carbon	Silicon		
0	0	0	73.8	26.2	0.0	0.36	NA
0	0.5	0	30.4	38.7	30.9	0.79	0.99
0	0.5	0.4	33.8	35.0	31.3	0.97	1.08
0	0.5	0.8	33.7	34.8	31.3	0.97	1.08
0	0.5	1.2	36.0	32.5	31.4	1.11	1.15
0	0.5	1.6	40.3	27.6	32.1	1.46	1.26
0	0.5	2.0	29.7	38.6	31.8	0.77	0.93

Table 7-5: Elemental composition for poly(hydrogenmethylsiloxane) precursor deposited on poly(ethylene terephthalate) film where the coating was plasma treated with increasing values of P_{Post}

As noted for the samples where the substrate was plasma treated at various powers, increases in the O/C and O/Si ratios suggest the silicon and carbon environments are becoming more oxidised when the coating is plasma treated with increasing P_{Post}. Again, this will be evaluated by curve-fitting the C 1s and Si 2p core levels, Figure 7-4 - Figure 7-6.

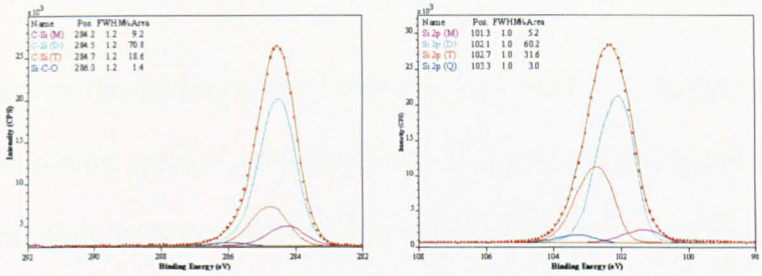

Figure 7-4: Curve-fits for the carbon (C 1s) and silicon (Si 2p) core level of poly(hydrogenmethylsiloxane) precursor deposited onto poly(ethylene terephthalate) film at a power of 0.5 kW

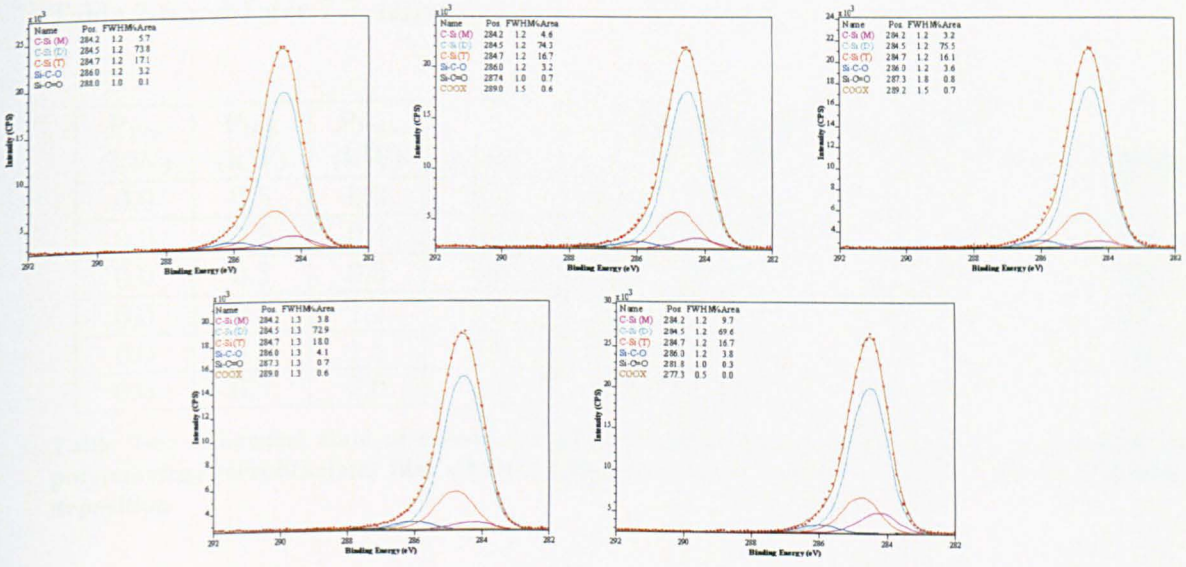

Figure 7-5: Curve-fits for the carbon (C 1s) core level of poly(hydrogenmethylsiloxane) precursor deposited onto poly(ethylene terephthalate) film at a power of 0.5 kW, followed by plasma treatment with increasing power. Top row left to right: P_{Post} = 0.4, 0.8, 1.2 kW; bottom row left to right P_{Post} = 1.6 kW, 2.0 kW

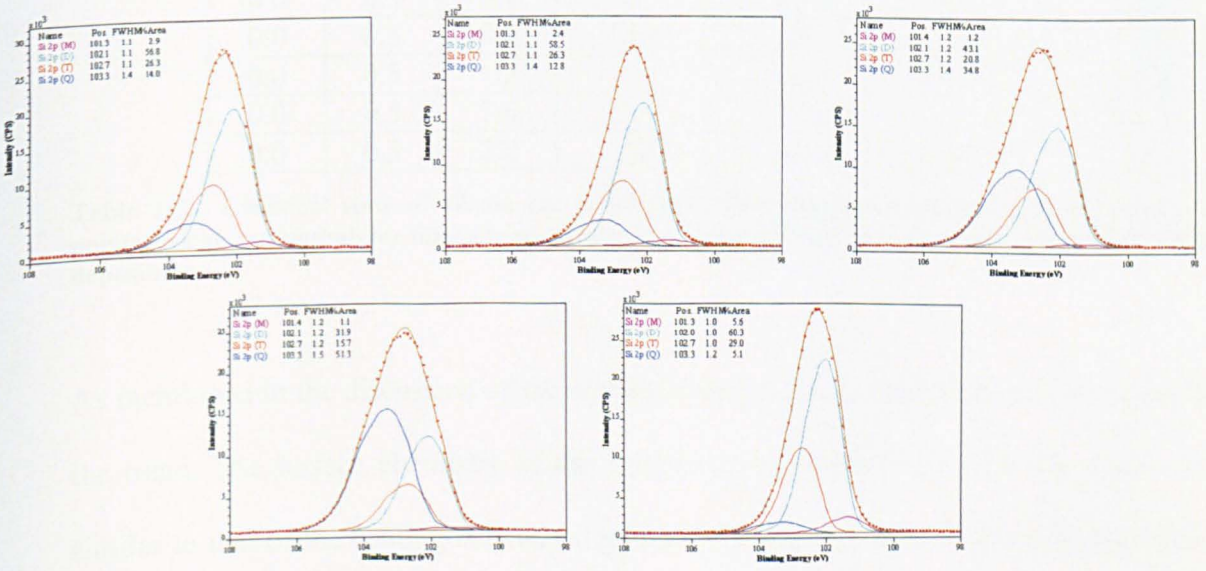

Figure 7-6: Curve-fits for the silicon (Si 2p) core level of poly(hydrogenmethylsiloxane) precursor deposited onto poly(ethylene terephthalate) film at a power of 0.5 kW, followed by plasma treatment with increasing power. Top row left to right: P_{Post} = 0.4, 0.8, 1.2 kW; bottom row left to right P_{Post} = 1.6 kW, 2.0 kW

Plasma treatment of the coating using increasing P_{Post} results in an increase in the more highly-oxidised silicon species[1], namely Q siloxy units, as reflected in the increase in oxygen concentration, with corresponding decrease in carbon. In addition, an increase in the concentration of oxidised carbon species was noted. The variations in chemical state information for carbon and silicon with increasing P_{Post} are summarised in Table 7-6 and Table 7-7, respectively.

P_{Pre} (kW)	P_{Dep} (kW)	P_{Post} (kW)	Relative concentration (%)					
			$C\text{-}Si^M$	$C\text{-}Si^D$	$C\text{-}Si^T$	C-O	C=O	COOX
0.0	0.5	0.0	9.2	70.8	18.6	1.4	0.0	0.0
0.0	0.5	0.4	5.7	73.8	17.1	3.2	0.1	0.0
0.0	0.5	0.8	4.6	74.3	16.7	3.2	0.7	0.6
0.0	0.5	1.2	3.2	75.5	16.1	3.6	0.8	0.7
0.0	0.5	1.6	3.8	72.9	18.0	4.1	0.7	0.6
0.0	0.5	2.0	9.7	69.6	16.7	3.8	0.3	0.0

Table 7-6: Chemical state of carbon for poly(hydrogenmethylsiloxane) precursor deposited on poly(ethylene terephthalate) film where coating was plasma treated at various powers following deposition

P_{Pre} (kW)	P_{Dep} (kW)	P_{Post} (kW)	Relative concentration (%)			
			$Si\ 2p^M$	$Si\ 2p^D$	$Si\ 2p^T$	$Si\ 2p^Q$
0.0	0.5	0.0	5.2	60.2	31.6	3.0
0.0	0.5	0.4	2.9	56.8	26.3	14.0
0.0	0.5	0.8	2.4	58.5	26.3	12.8
0.0	0.5	1.2	1.2	43.1	20.8	34.8
0.0	0.5	1.6	1.1	31.9	15.7	51.3
0.0	0.5	2.0	5.6	60.3	29.0	5.1

Table 7-7: Chemical state of silicon for poly(hydrogenmethylsiloxane) precursor deposited on poly(ethylene terephthalate) film where coating was plasma treated at various powers following deposition

As mentioned in the discussion of the elemental composition, there was an exception to the trend. The surface chemistry of the sample treated with P_{Post} = 2.0 kW was very similar to that of the coating that was deposited without any coating plasma treatment. Excessive plasma treatment of siloxane coatings is known to result in the formation of defects in the coating. These could then present a facile route for migration of short

siloxane oligomers from the bulk of the sample. This could result in a surface which appears similar to the sample with no P_{Post}.

It could be expected to see a relationship between the extent of oxidation at the surface, as determined by XPS, and the water contact angle[2]. The water contact angle would be expected to decrease with increasing abundance of oxygen, as the coating becomes more hydrophilic. However, this was not observed for these samples: despite an increase in oxygen under both deposition regimes, the observed water contact angles were all very similar, with an average value of 107° ± 3°.

This is most likely due to migration of low molecular weight siloxane oligomers to the surface in an attempt to lower the surface energy. This phenomenon is often observed in plasma treatment of siloxane materials[3,4,5]. The difference in the 'depth of analysis' of both techniques is quite different: XPS analyses up to ~8nm into the coating, whereas contact angles probe the outermost molecular layers of a surface <1 nm. Bain and Whiteside concluded that water droplets could probe to ~ 5Å beneath the surface[6]. The surface of the coatings may be represented as shown in Scheme 7-3, and as such, the water droplet is more sensitive to the surface.

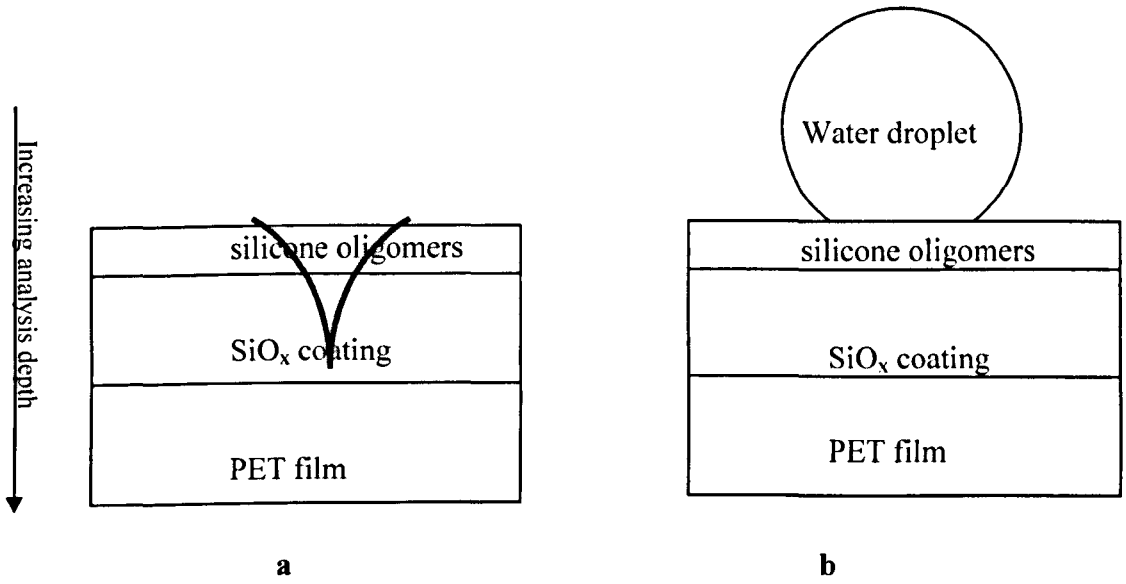

Scheme 7-3: Schematic of analysis of deposited poly(hydrogenmethylsiloxane) coating on poly(ethylene terephthalate) film using a) XPS at 90° take-off angle, b) water contact analysis

Similar results were presented by Ward *et al*[7] For an OMCTS deposit prepared in the presence of oxygen, the elemental composition as determined by XPS showed 25.5% carbon, 48.5% oxygen and 26.0 % silicon, and $SiO_{x>1}$ of 36%. The corresponding water contact angle was 56°, as would be expected for a highly oxidised silicon coating. However, samples prepared using TMCTS without oxygen, whilst exhibiting similar elemental composition (32.5 % carbon, 39.1 % oxygen and 28.4 % silicon, with $SiO_{x>1}$ of 65%) had water contact angles of 102°. This suggests that the surface that the water contact angle is probing is not the same as that analysed by XPS. One would expect that the coating with the higher concentration of $SiO_{x>1}$ species would be more hydrophilic. However, the authors did not comment on the disparity between results.

7.3.4 The effect of boiling water immersion on the chemistry of coatings where the substrate was plasma treated prior to deposition

In order to further evaluate the durability of the siloxane coatings, XPS was used to monitor the elemental composition and chemistry of some washed samples. This data is presented in Table 7-8, for samples where the substrate was plasma treated with increasing P_{Pre} prior to the deposition process.

P_{Pre} (kW)	P_{Dep} (kW)	P_{Post} (kW)	Concentration (at. %)			O/C	O/Si
			Oxygen	Carbon	Silicon		
0	0.5	0	29.9	35.4	31.4	0.84	0.95
0.4	0.5	0	29.6	38.6	31.8	0.77	0.93
0.8	0.5	0	29.3	38.7	32.1	0.76	0.91
1.2	0.5	0	29.5	40.4	30.1	0.73	0.98
1.6	0.5	0	31.6	38.5	29.9	0.82	1.06
2.0	0.5	0	29.7	39.2	31.1	0.76	0.95

Table 7-8: Elemental composition for poly(hydrogenmethylsiloxane) precursor deposited on poly(ethylene terephthalate) film where substrate was plasma treated at various powers prior to deposition. Samples immersed in boiling water for 30 minutes prior to analysis

The O/C and O/Si ratios of samples treated at low P_{Pre} (0.4. 0.8, 1.2 KW) did not vary significantly following immersion in boiling water. However, a large decrease was noted for both ratios for the samples prepared using P_{Pre} = 1.6 and 2.0 kW. This would suggest that the siloxane environment of the sample is becoming less oxidised. This will be affirmed by curve-fitting of the Si 2p core level spectra.

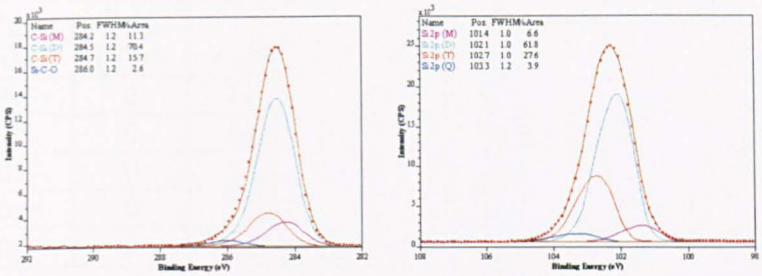

Figure 7-7: Curve-fits for the carbon (C 1s) and silicon (Si 2p) core level of poly(hydrogenmethylsiloxane) precursor deposited onto poly(ethylene terephthalate) film at a power of 0.5 kW. Samples immersed in boiling water for 30 minutes prior to analysis

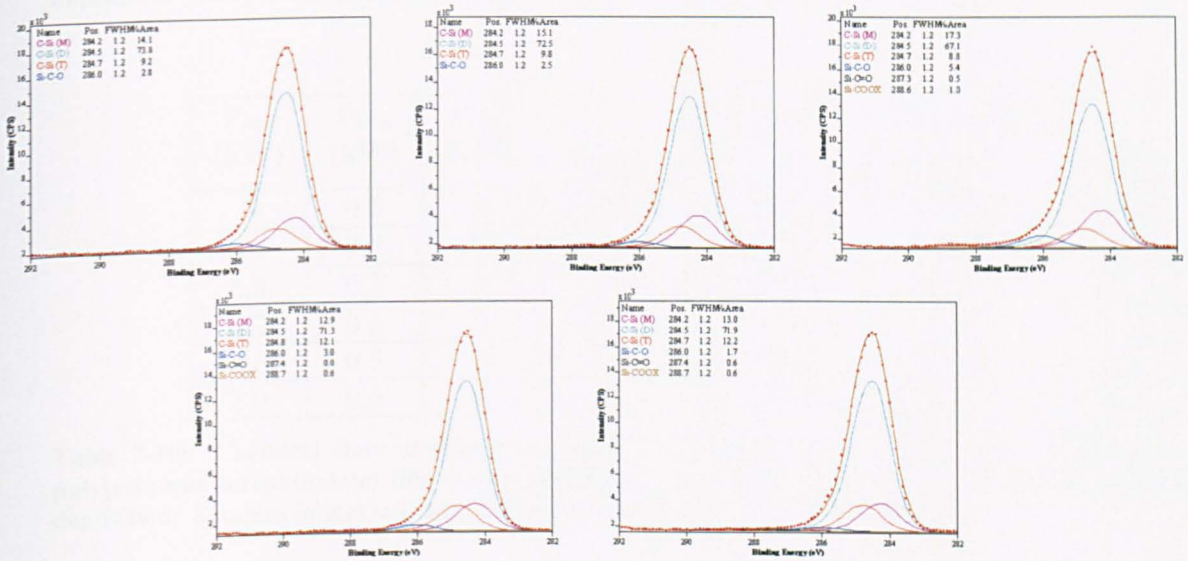

Figure 7-8: Curve-fits for the carbon (C 1s) core level of poly(hydrogenmethylsiloxane) precursor deposited onto poly(ethylene terephthalate) film at a power of 0.5 kW. Substrate was plasma treated prior to deposition with increasing power. Top row left to right: P_{Pre} = 0.4, 0.8, 1.2 kW; bottom row left to right P_{Pre} = 1.6 kW, 2.0 kW. Samples immersed in boiling water for 30 minutes prior to analysis

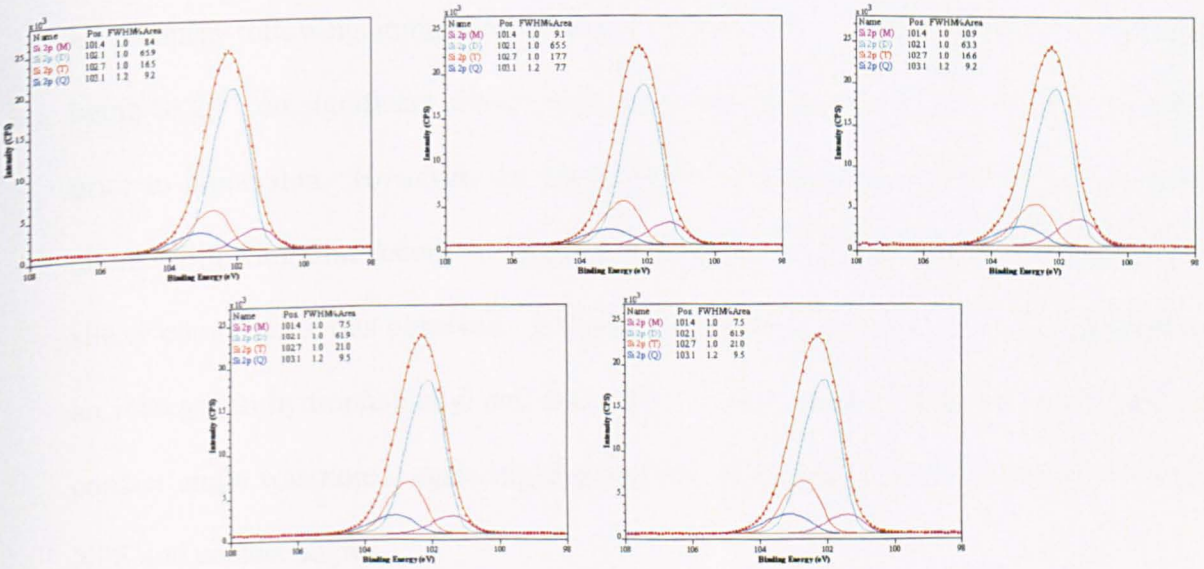

Figure 7-9: Curve-fits for the silicon (Si 2p) core level of poly(hydrogenmethylsiloxane) precursor deposited onto poly(ethylene terephthalate) film at a power of 0.5 kW. Substrate was plasma treated prior to deposition with increasing power. Top row left to right: P_{Pre} = 0.4, 0.8, 1.2 kW; bottom row left to right 1.6 kW, 2.0 kW. Samples immersed in boiling water for 30 minutes prior to analysis

P_{Pre} (kW)	P_{Dep} (kW)	P_{Post} (kW)	Relative concentration (%)					
			C-Si^M	C-Si^D	C-Si^T	C-O	C=O	COOX
0	0.5	0	11.3	70.4	15.7	2.6	0.0	0.0
0.4	0.5	0	14.1	73.8	9.2	2.8	0.0	0.0
0.8	0.5	0	15.1	72.4	9.8	2.5	0.0	0.2
1.2	0.5	0	17.3	67.1	8.8	5.4	0.5	1.0
1.6	0.5	0	12.9	71.3	12.1	0.0	0.0	0.6
2.0	0.5	0	13.0	71.9	12.2	1.7	0.6	0.6

Table 7-9: Chemical state of carbon for poly(hydrogenmethylsiloxane) precursor deposited on poly(ethylene terephthalate) film where substrate was plasma treated at various powers prior to deposition. Samples immersed in boiling water for 30 mins prior to analysis

P_{Pre} (kW)	P_{Dep} (kW)	P_{Post} (kW)	Relative concentration (%)			
			Si $2p^M$	Si $2p^D$	Si $2p^T$	Si $2p^Q$
0	0.5	0	6.6	61.8	27.6	3.9
0.4	0.5	0	8.4	65.9	16.5	9.2
0.8	0.5	0	9.1	65.5	17.7	7.7
1.2	0.5	0	10.9	63.3	16.6	9.2
1.6	0.5	0	7.5	61.9	21.0	9.5
2.0	0.5	0	7.5	61.9	21.0	9.5

Table 7-10: Chemical state of silicon for poly(hydrogenmethylsiloxane) precursor deposited on poly(ethylene terephthalate) film where substrate was plasma treated at various powers prior to deposition. Samples immersed in boiling water for 30 mins prior to analysis

Following immersion in boiling water for 30 minutes, the silicon chemistry of the coating was compared to the samples prior to immersion. The chemistry was similar for all samples following immersion in water, Table 7-10. With the major component being Si $2p^D$, no significant change was observed compared with the low P_{Pre} samples prior to immersion. However, the chemistry of the samples treated at high P_{Pre} were altered following immersion. A significant decrease in intensity of Si $2p^T$ and Si $2p^Q$ siloxy components was observed. It would be expected that this would be reflected in an increase in hydrophobicity, and thus water contact angle. However, a decrease in contact angle was noted, again highlighting the difference in analysis depths between XPS and contact angles.

7.3.5 The effect of boiling water immersion on the chemistry of coatings where the coating was plasma treated following deposition

The change in elemental composition for samples prepared with increasing values of P_{Post} were also investigated following immersion in water, Table 7-11.

P_{Pre} (kW)	P_{Dep} (kW)	P_{Post} (kW)	Relative Concentration (at. %)			O/C	O/Si
			Oxygen	Carbon	Silicon		
0.0	0.5	0.0	29.9	35.4	31.4	0.85	0.95
0.0	0.5	0.4	34.1	36.8	28.8	0.93	1.18
0.0	0.5	0.8	31.4	38.3	30.2	0.82	1.04
0.0	0.5	1.2	33.8	37.7	28.5	0.90	1.19
0.0	0.5	1.6	35.8	36.3	27.9	0.99	1.28
0.0	0.5	2.0	31.4	39.1	29.5	0.80	1.06

Table 7-11: Elemental composition for poly(hydrogenmethylsiloxane) precursor deposited on poly(ethylene terephthalate) film where coating was plasma treated at various powers following deposition. Sample immersed in boiling water for 30 mins prior to analysis

The trend observed for the unwashed samples was that O/C and O/Si increased with increasing P_{Post}, except at P_{Post} = 2.0 kW, where the elemental composition was similar to that for the sample where no plasma treatment of the coating was carried out. Following immersion, the O/C and O/Si ratios were found to have changed, but no trend was observed. It was noted that the O/C ratio for sample P_{Post} = 1.6 kW increased significantly. More details about the changes in chemistry will be obtained by examination of the curve-fitted C 1s and Si 2p core levels, Figure 7-11 and Figure 7-12 respectively.

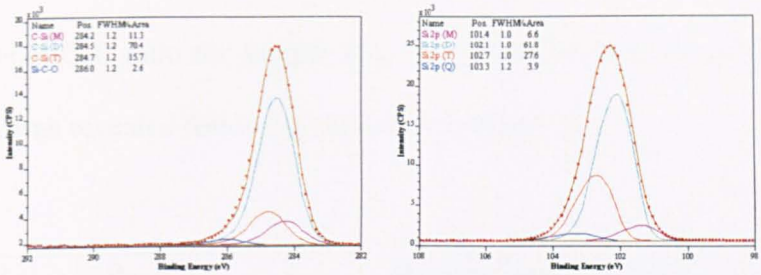

Figure 7-10: Curve-fits for the carbon (C 1s) and silicon (Si 2p) core level of poly(hydrogenmethylsiloxane) precursor deposited onto poly(ethylene terephthalate) film at a power of 0.5 kW. Sample immersed in boiling water for 30 mins prior to analysis

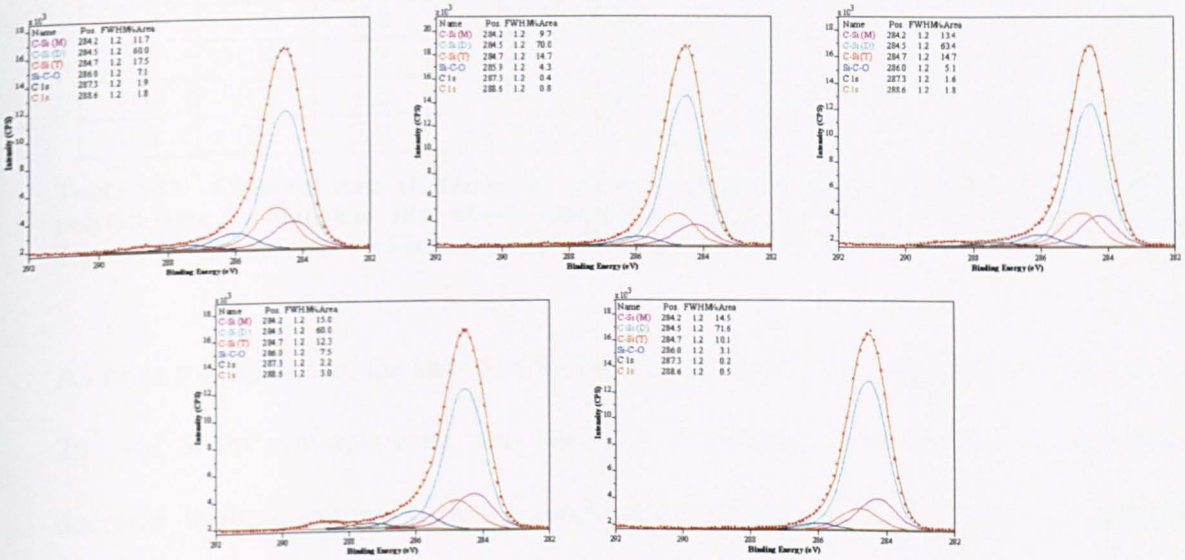

Figure 7-11: Curve-fits for the carbon (C 1s) core level of poly(hydrogenmethylsiloxane) precursor deposited onto poly(ethylene terephthalate) film at a power of 0.5 kW, followed by plasma treatment with increasing power. Top row left to right: P_{Post} = 0.4, 0.8, 1.2 kW; bottom row left to right P_{Post} = 1.6 kW, 2.0 kW. Sample immersed in boiling water for 30 mins prior to analysis

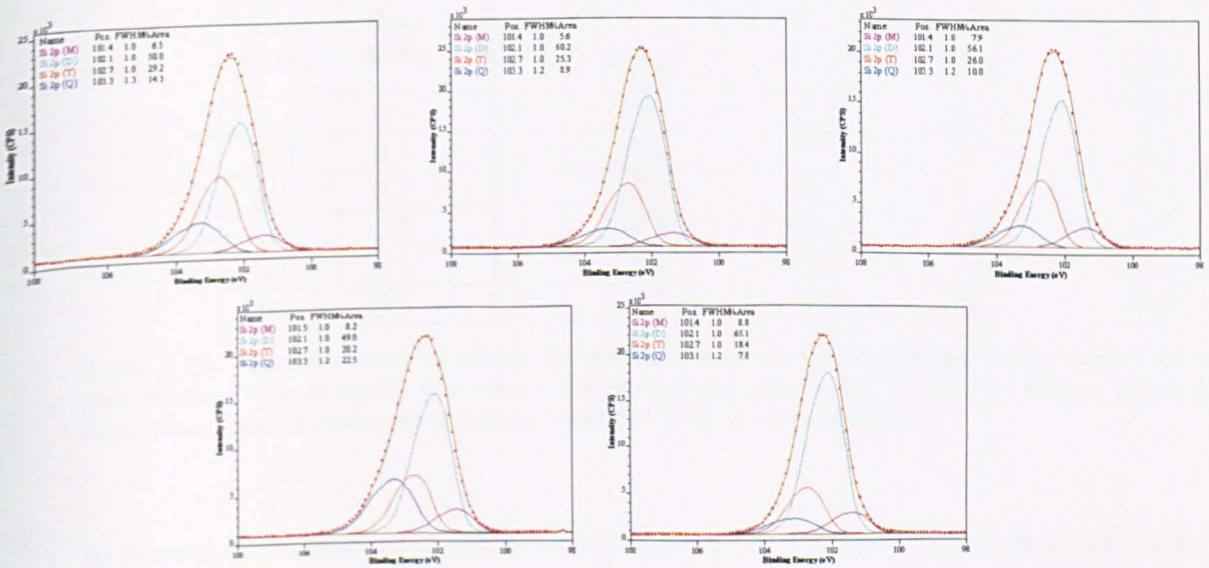

Figure 7-12: Curve-fits for the silicon (Si 2p) core level of poly(hydrogenmethylsiloxane) precursor deposited onto poly(ethylene terephthalate) film at a power of 0.5 kW, followed by plasma treatment with increasing power. Top row left to right: P_{Post} = 0.4, 0.8, 1.2 kW; bottom row left to right P_{Post} = 1.6 kW, 2.0 kW. Sample immersed in boiling water for 30 mins prior to analysis

The results of the curve-fitting are summarised in Table 7-12 and Table 7-13. As noted by the increase in O/C ratio for sample P_{Post} = 1.6 kW, an increase in oxidised carbon functionalities was revealed following the water immersion.

P_{Pre} (kW)	P_{Dep} (kW)	P_{Post} (kW)	Relative concentration (%)					
			C-Si^M	C-Si^D	C-Si^T	C-O	C=O	COOX
0.0	0.5	0.0	11.3	70.4	15.7	2.6	0.0	0.0
0.0	0.5	0.4	11.7	60.0	17.5	7.1	1.9	1.8
0.0	0.5	0.8	9.7	70.0	14.7	4.3	0.4	0.8
0.0	0.5	1.2	15.4	63.4	14.7	5.1	1.6	1.8
0.0	0.5	1.6	15.0	60.0	12.3	7.5	2.2	3.0
0.0	0.5	2.0	14.5	71.6	10.1	3.1	0.2	0.5

Table 7-12: Chemical state of carbon for poly(hydrogenmethylsiloxane) precursor deposited on poly(ethylene terephthalate) film where coating was plasma treated at various powers following deposition. Sample immersed in boiling water for 30 mins prior to analysis

As prior to immersion, the sample with the highest level of oxidised siloxy species: Si $2p^T$ and Si $2p^Q$ environments, was also P_{Post} = 1.6 kW. This sample did see some decrease in these groups, with a corresponding increase in Si $2p^D$ species. A large change in siloxane chemistry was also observed for the sample treated with P_{Post} = 1.2 kW.

P_{Pre} (kW)	P_{Dep} (kW)	P_{Post} (kW)	Relative concentration (%)			
			Si $2p^M$	Si $2p^D$	Si $2p^T$	Si $2p^Q$
0.0	0.5	0.0	6.6	61.8	27.6	3.9
0.0	0.5	0.4	6.5	50.0	29.2	14.3
0.0	0.5	0.8	5.6	60.2	25.3	8.9
0.0	0.5	1.2	7.9	56.1	26.0	10.0
0.0	0.5	1.6	8.2	49.0	20.2	22.5
0.0	0.5	2.0	8.8	65.1	18.4	7.8

Table 7-13: Chemical state of silicon for poly(hydrogenmethylsiloxane) precursor deposited on poly(ethylene terephthalate) film where coating was plasma treated at various powers following deposition. Sample immersed in boiling water for 30 mins prior to analysis

In general, in no case is the characteristic shape of C 1s for poly(ethylene terephthalate) visible. This indicates that the layer of siloxane material at the surface is greater than ~10 nm, even after the washing procedure.

7.4 CONCLUSIONS

Increasing the power of plasma treatment of the substrate, P_{Pre} led to similar coating chemistry for P_{Pre} = 0.4, 0.8, 1.2 kW. However, increasing P_{Pre} to 1.6 and 2.0 kW led to the formation of more oxidised coating chemistry. Increasing the power of plasma treatment of the coating, P_{Post} led to increasingly more oxidised coatings.

In all experiments, the siloxane coatings were able to withstand immersion in boiling water for 30 minutes. Some changes in the chemistry of the coatings were observed following immersion. Notably, at P_{Pre} = 1.6 and 2.0 kW, a reduction in oxidation of the coating was observed following immersion. A more highly oxidised siloxane overlayer wa removed by boiling in water, revealing the polymeric coating below.

It was not possible to directly relate the chemistry of the coatings determined by XPS and their observed water contact angle. Water contact angles of > 100° were observed irrespective of the coating chemistry. It is believed that this is due to differences in the 'depth of analysis' of the two techniques. Whilst XPS investigates around 8 nm of the coating, contact angles probe the outermost molecular layers (< 1 nm). It is proposed that the migration of hydrophobic siloxane oligomers from the bulk of the coating to the surface account for the apparent discrepancy between results from the two techniques.

7.5 REFERENCES

[1] Roualdes, S.; Berjoan, R.; Durand, J. '^{29}Si NMR and Si 2p XPS correlation in polysiloxane membranes prepared by plasma enhanced chemical vapour deposition', *Separation and Purification Technology*, **25**, 2001, 391 397

[2] O'Hare, L.A.; Leadley, S.R.; Parbhoo, B. 'Surface physicochemistry of corona discharge treated polypropylene film', *Surface and Interface Analysis*, **33**, 2002, 335 - 342

[3] Kim, J.; Chaudhury, M.K.; Owen, M.J., 'Hydrophobicity loss and recovery of silicone HV Insulation', *IEEE Transactions on Dielectrics and Electrical Insulation*, **6**(5), 1999

[4] Hillborg, H.; Gedde, U.W., 'Hydrophobicity recovery of polydimethylsiloxane after exposure to corona discharges', *Polymer*, **39**(10), 1998

[5] Hillborg, H.; Gedde, U.W., 'Hydrophobicity changes in silicone rubbers', *IEEE Transactions on Dielectrics and Electrical Insulation*, **6**(5), 1999

[6] Bain, C.D.; Whitesides, G.M., 'Depth sensitivity of wetting: monolayers of ω-mercapto ethers on gold', *J. Am. Chem. Soc.*, **110**, 1988, 5897 -5898

[7] Ward, L.J.; Schofield, W.C.E.; Badyal, J.P.S.; Goodwin, A.J.; Merlin, P.J., 'Atmospheric pressure glow discharge deposition of polysiloxanes and SiO_x films', *Langmuir*, **19**, 2003, 2110-2114

CHAPTER 8

DISCUSSION

8.1 INTRODUCTION

In the investigation of new technologies, such as atmospheric pressure plasma liquid deposition (APPLD), it is essential to understand the surface physicochemical properties of deposits that can be obtained. How these properties are affected by the parameters used during deposition, such as gas composition, plasma power and precursor flowrate are also of great interest. An understanding of the precursor chemistry, in addition to how the processing conditions can be varied to improve coating performance is also required.

In this thesis, a complementary suite of surface analytical techniques: contact angle analysis, X-ray photoelectron spectroscopy (XPS), and atomic force microscopy (AFM) were used and data interpretation methods developed to determine the effect of various plasma parameters on the chemistry of surfaces modified by APP, or of coatings deposited by APPLD.

8.2 A COMPARISON BETWEEN THE EFFECTS OF CORONA DISCHARGE AND ATMOSPHERIC PRESSURE PLASMA TREATMENTS ON POLYPROPYLENE FILM

In *Chapter 4*, a detailed comparison of the surface physicochemical properties affected by various atmospheric pressure plasma treatments was undertaken using contact angle analysis, XPS and AFM. Corona discharge treatment in air, and atmospheric pressure plasma treatments generated from helium, helium/1% air and helium/1% oxygen were compared. The effects of such parameters as gas composition and plasma energy density on the surface energy, surface chemistry and morphology and stability were evaluated.

A methodology for the curve-fitting of treated polypropylene film was developed. This involved a comprehensive review of the literature, and an understanding of the chemistry generated by the surface modification technique. The interaction of the functional groups generated, in addition to the hydrolytic stability of the modified layer were investigated. Through optimisation of the process parameters, particularly gas composition and plasma power, the formation of low molecular weight oxidised materials (LMWOM) was minimised. Although some previous research comparing the effect of corona and nitgoen or helium atmospheric pressure plasmas have been identified[1,2], the novelty of the current study lies in the use of APP in reel-to-reel conditions.

In the results reported by Massines *et al*[1] following treatment of polypropylene in helium plasma, a small concentration of nitrogen was observed in addition to the expected elements: carbon and oxygen. This was not observed in our work, except when air was added to the plasma gas. Corona discharge resulted in the incorporation of oxygen only, in agreement with the work of Guimond *et al*[2] and Strobel *et* al[3].

A decrease in water contact angle was observed following corona or atmospheric pressure plasma treatment of the polypropylene surface. As expected, this was due to incorporation of oxygen at the surface of the film. The amount of oxygen incorporated was presented as Δ(O/C), to enable future comparison between other polymer substrates. Δ(O/C) increased with energy density for all treatment methods. Corona treatment led to the largest increase in Δ(O/C), with up to Δ(O/C) = 0.18 at the highest energy density. APP in helium/air also reached this value, but required a higher energy density. By comparison, APP treatment in helium resulted in a Δ(O/C) value of only 0.07. Helium/oxygen plasma increased Δ(O/C) to 0.16.

Here, it was found that corona discharge treatment resulted in a more water-soluble surface. This is in agreement with previous observations that the filamentary nature of corona is more damaging than plasma treatment[1]. A measure of this was the change in Δ(O/C) following immersion in water. The largest change in Δ(O/C), a decrease to only 0.05. The surface generate by helium/air APP was much more stable, with Δ(O/C) only decreasing to 0.13. This is an important understanding as this water soluble layer to be detrimental to the adhesion of siloxane coatings, as it acts as a weak boundary layer.

8.3 DEVELOPMENT OF A METHODOLOGY FOR THE XPS CURVE-FITTING OF THE Si 2p CORE LEVEL OF SILOXANE MATERIALS

The requirement for a consistent method for curve-fitting of the Si 2p core level of siloxane materials was identified. In *Chapter 5*, the availability of proprietary materials characterised by ^{29}Si NMR aided development of a methodology to determine unambiguous binding energy positions for silicon in Si $2p^M$ $[(CH_3)_3SiO_{1/2}]$, Si $2p^D$ $[(CH_3)_2SiO_{2/2}]$, Si $2p^T$ $[(CH_3)SiO_{3/2}]$ and Si $2p^Q$ $[SiO_{4/2}]$ siloxy environments.

Analysis of a high molecular weight PDMS homopolymer gave the binding energy position of Si $2p^D$ to be 102.0 ± 0.1 eV. This was in good agreement with the value measured by Beamson and Briggs for PDMS oil[4], and used by Alexander *et al* in their curve-fitting of plasma deposits prepared from hexamethyldisiloxane[5] and by Roualdes *et al* for deposits prepared from octamethyltrisiloxane and hexamethylcyclotrisiloxane[6]. These values for the Si $2p^D$ siloxy environment are of significantly higher binding energy than that used by Massines *et al*[7], 101.5 eV, in their analysis of silane-based deposits. However, the rational for the component binding energies were not explained in this mancuscript. Again, good

agreement was found with the work of Alexander and Roualdes for the binding energy of Si $2p^T$ siloxy environments at 102.8 eV. However, the binding energy of Si $2p^M$ and Si $2p^Q$ determined in this thesis were different to those used by Roualdes, and those previously reported by O'Hare *et al*[8] in a short communication. The BE values for Si 2p reported here confirm the trend of the BE increasing uniformly with increasing substitution of a methyl group with an oxygen atom, as estimated by Alexander *et al.*

In addition, this work led to the novel observation that the C-Si component within the C 1s core level could also be differentiated for carbon in the C $1s^M$ [$H_3\underline{C}$-Si($\underline{C}H_3$)$_2O_{1/2}$], C $1s^D$ [$H_3\underline{C}$-Si($\underline{C}H_3$)$O_{2/2}$] and C $1s^T$ [$H_3\underline{C}$-$SiO_{3/2}$] environments due to variation in the binding energy of the C-Si bond, depending on the number of oxygen atoms attached to the silicon atom. The current literature places the C-Si component at 284.4 eV[4,5], as used in this work for C $1s^D$. With the exception of a -0.1 eV shift for replacement of a methyl group with a phenyl group[4], no further differentiation of the C-Si component of the C 1s core level could be found in the literature. The chemical structures and binding energy positions for C 1s and Si 2p components are summarised in **Table 5-7.** Application of the method to data from compounds containing multiple, overlapping oxidation states, giving agreement to compsotion from ^{29}Si NMR gives confidence in the validity of the method.

8.4 CHARACTERISATION OF THIN SILOXANE COATINGS PREPARED USING ATMOSPHERIC PRESSURE PLASMA LIQUID DEPOSITION

The *iterative Si 2p – C 1s* curve-fitting process has been used to elucidate the chemistry of thin siloxane coatings generated by APPLD, and to determine the elemental composition of such thin films without the influence of the substrate. Other potential uses for the method would be to providing understanding of the chemistry/property relationship for silicone release coatings[9], the chemistry of siloxane barrier coatings and water-repellent, anti-fouling, anti-stick or enhanced lubricity coatings.

The effect of deposition power, precursor flowrate, and precursor chemistry on the obtained coating chemistry were investigated. Two siloxane precursors: poly(dimethylsiloxane – PDMS, and poly(hydrogenmethylsiloxane) – PHMS were evaluated. It was also possible to gain understanding of how the thickness of the coatings varied with plasma parameters. The elemental composition and chemistry of each coating was determined, and related to the deposition parameters.

Use of the APPLD technique allows the preparation of plasma deposited coatings from liquid precursors . Previously, vacuum deposition using RF and microwave plasmas has been limited to gas- or vapour-phase monomer percursors such as hexamethyldisiloxane (HMDSO), tetraethoxysilane (TEOS), trimethylsilane, tetramethoxysilane (TMOS), tetramethyldisiloxane (TMDSO), and SiH_4. The work has tended to focus on deposition to achieve barrier properties. Further work using corona, or dielectric barrier discharges has also concentrated on these precursors. The use of octamethyltrisiloxane and hexamethylcyclotrisiloxane has been documented to obtain siloxane membranes using low

pressure plasma[6]. Recent developments using atmospheric pressure glow discharge utilised octamethylcyclotetrasiloxane (OMCTS) and tetramethylcyclotetrasiloxane (TMCTS) low molecular weight polymers to achieve siloxane coatings with tunable chemistries[10]. In this work, we report on the deposition of linear siloxane polymeric precursors, of MW > 1000, namely poly(dimethylsiloxane) - (PDMS) and poly(hydrogenmethylsiloxane) - (PHMS). This enables the formation of coatings retaining the precursor functionality, which can be tuned to provide a range of chemistries from polymeric through to inorganic.

8.4.1 Coating chemistry

Siloxane coatings discussed in the literature typically had highly oxidised silicon chemistry, with the majority of the coatings being $(CH_3)_1SiO_{3/2}$ and $SiO_{4/2}$[11,12,13], due to the addition of O_2 to the plasma, with the application being for barrier coatings. As reported here, it was possible to generate coatings from linear PDMS retaining up to 95% siloxane in the polymeric $[(CH_3)_3SiO_{1/2}]$ and $[(CH_3)_2SiO_{2/2}]$ forms. By closest comparison, deposition of cyclic PDMS retained up to 65% siloxane in a polymeric form[6,10].

It is believed that the increased chain length of the siloxane precursor used, and its lower reactivity due to it being linear rather than cyclic, is fundamental to the retention of the molecular structure of the precursor during deposition. Increasing the plasma power during deposition of linear PDMS resulted in coatings containing a lower concentration of polymeric siloxane forms. Enhanced ablation of the methyl groups, followed by crosslinking are the most likely explanation for this.

The use of a hydrogen-substituted polysiloxane as the precursor led to the formation of a more highly oxidised $ppPSiO_x$ coating at low and medium power, with $(CH_3)_1SiO_{3/2}$

concentrations of ~25% being obtained, compared with ~7% when PDMS was deposited under the same conditions. A similar observation was made by Ward *et al*[10]. This enhanced crosslinking is attributed to the more labile the Si-H bond compared with the Si-O and Si-C bonds.

8.4.2 Deposition rate

The deposition rate was dependent both on the precursor flowrate and the plasma deposition power, and ranged between 10 and 30 $nmmin^{-1}$, the higher of which was comparbable to the work by Ward *et al*[10]. This led to the investigation of the energy per molecule for each precursor, using Yasuda's 'composite parameter – W/FM[14], where W = power, F = precursor flowrate and M = molecular mass.

As was shown in **Figure 6-34**, two different trends were observed for the efficacy of deposition. For PDMS, an increase in deposition was observed with increasing W/FM, reaching a plateau. This has been previously observed for APP polymerisation, and has been proposed to be due to saturation of the precursor at the surface[15]. Increasing the partial pressure of the vapour did not result in enhanced deposition rate. This may be considered the equivalent to increasing the precursor flowrate at atmospheric pressure.

Under the same deposition conditions, a decrease in efficiency with increasing energy per molecule was observed for PHMS, indicating a change in reaction behaviour. As has been observed for siloxane coatings deposited under vacuum, it is suggested that gas-phase reactions causing crosslinking and the formation of particulates rather than conformal coatings is occurring[15]. This is most likely due to the enhanced reaction rate expected for PHMS due to the lability of the Si-H bond[16]. This leads to excess gas phase reaction,

which results in the formation of oxidized silica particles in the gas phase prior to deposition onto the substrate[12,15]. In vacuum deposition systems, the low molecular concentration in the gas phase prevents molecules from colliding, reacting and forming such particles. In atmospheric systems, molecular collisions are more common and powder formation is more likely to occur.

8.4.3 Coating thickness

The coatings generated using APPLD of PDMS and PHMS were much thinner than those deposited from OMCTS and TMCTS using the same precursor flowrate. Thicknesses between 3 - 8nm were determined by a combination of angle-resolved XPS and a film thickness algorithm.

8.5 IMPROVEMENT OF COATING PERFORMANCE

Plasma treatment of the substrate prior to deposition had no effect on coating chemistry except at highest powers. Increasing the power of plasma treatment of the coating, P_{Post} led to increasingly more oxidised coatings, as observed by Roualdes *et al*[6]. This is also in agreement with other groups where plasma treatment of siloxanes have resulted in increased oxidation[17,18,19]. However, the water contact angle of the surface remained constant at ~ 103°, independent of treatment conditions. The water contact angle did not reflect the change in surface chemistry by XPS, as would be expected.

Similar observations have been noted in the work by Ward *et al*[10]. For an OMCTS deposit prepared in the presence of oxygen, the elemental composition as determined by XPS showed 25.5% carbon, 48.5% oxygen and 26.0 % silicon, and $SiO_{x>1}$ of 36%. The corresponding water contact angle was 56°, as would be expected for a highly oxidised

silicon coating. However, samples prepared using TMCTS without oxygen, whilst exhibiting similar elemental composition (32.5 % carbon, 39.1 % oxygen and 28.4 % silicon, with $SiO_{x>1}$ of 65%) had water contact angles of 102°. This suggests that the surface that the water contact angle is probing is not the same as that analysed by XPS. One would expect that the coating with the higher concentration of $SiO_{x>1}$ species would be more hydrophilic. However, the authors did not comment on the disparity of the observation. The proposed mechanism of migration of oligomeric siloxanes to the surface of the coating, as shown in **Scheme 6-5**, may account for this observation[19,20,21,22].

8.6 FUTURE WORK

There is a clear need for continued investigation of how the parameters used in APPLD effect the deposition of siloxane coatings. Tailoring the surface properties occurring from deposition of these materials is desirable in the generation of new coating technologies. Other properties such as deposition rate, durability and the reaction mechanisms may be identified through careful application of the methodologies outlined in this thesis, and are recommended for future work. Additionally, of key importance, is developing understanding of how the plasma parameters can improve coating durability. In all experiments, the siloxane coatings were able to withstand immersion in boiling water for 30 minutes. This is believed to be the result of improved grafting and crosslinking of the coating have been identified as outcomes of varying plasma deposition parameters.

8.7 REFERENCES

[1] Massines, F.; Messaoudi, R.; Mayoux, C., 'Comparison between air filamentary and helium glow dielectric barrier discharges for the polypropylene surface treatment', *Plasmas and Polymers*, **3**(1), 1998, 43 - 59

[2] Guimond, S.; Radu, I.; Czermuszkin, G.; Carlosson, D.J.; Wertheimer, M.R., 'Biaxially oriented polypropylene (BOPP) surface modification by nitrogen atmospheric pressure glow discharge (APP) and by air corona', *Plasmas and Polymers*, 7(1), 2002

[3] Strobel, M.; Jones, V.; Lyons, C.S.; Ulsh, M.; Kushner, M.J.; Dorai, R.; Branch, M.C., 'A comparison of corona-treated and flame-treated polypropylene films,' *Plasmas and Polymers*, **8**(1), 2003, 61 - 95

[4] Beamson G, Briggs D, *High Resolution XPS of Organic Polymers: The Scienta ESCA300 Database*, John Wiley & Sons: Chichester, 1992

[5] Alexander, M.R.; Short, R.D.; Jones, F.R.; Michaeli, W.; Blomfield, C.J., 'A study of HMDSO/O_2 plasma deposits using a high-sensitivity and –energy resolutions XPS instrument: curve-fitting of the Si 2p core level', *Applied Surface Science*, **137**, 1999, 179 - 183

[6] Roualdes, S.; Berjoan, R.; Durand, J. '^{29}Si NMR and Si 2p XPS correlation in polysiloxane membranes prepared by plasma enhanced chemical vapour deposition', *Separation and Purification Technology*, **25**, 2001, 391 397

[7] Massines, F.; Gherardi, N.; Sommer, F., 'Silane based coatings on polypropylene, deposited by atmospheric pressure glow discharge plasmas', *Plasmas and Polymers*, **5**(3/4), 2000, 151-172

[8] O'Hare, L.A.; Parbhoo, B.; Leadley, S.R. ' Development of a methodology for XPS curve-fitting of the Si 2p core level of siloxane materials', *Surf. Interface Anal.*, 2004, **36**, 1427

[9] Gordon, G.V.; Perz, S.V.; Tabler, R.L.; Stasser, J.L.; Owen, M.J.; Tonge, J.S., 'Silicone release coatings: an examination of the release mechanism', *Adhesives Age*, Nov 1998

[10] Ward, L.J.; Schofield, W.C.E.; Badyal, J.P.S.; Goodwin, A.J.; Merlin, P.J., 'Atmospheric pressure glow discharge deposition of polysiloxanes and SiO_x films', *Langmuir*, **19**, 2003, 2110-2114

[11] Thyen, R.; Weber, A.; Klages, C.-P., 'Plasma-enhanced chemical-vapour-deposition of thin films by corona discharge at atmospheric pressure', *Surface and Coatings Technology*, **97**, 1997, 426 - 434

[12] Schmidt-Szalowski, K.; Rzanek-Boroch, Z.; Sentech, J.; Rymuza, Z.; Kusznierewicz, Z.; Misiak, M., 'Thin films deposition form hexamethyldisiloxane and hexamethyldisilazane under delectric-barrier discharge conditions', *Plasmas and Polymers*, **5**(3/4), 2000, 173 - 190

[13] Hegeman, D.; Vohrer, U.; Oehr, C.; Riedel, R. 'Deposition of SiO_x films from O_2/HMDSO plasmas', *Surface and Coatings Technology*, **116 -119**, 1999, 1033 - 1036

[14] Yasuda, H., *Plasma Polymerisastion*, New York:Academic, 1985

[15] Sawada, Y.; Ogawa, S.; Kogoma, M., 'Synthesis of plasma-polymerised tetraethoxysilxaxne and hexamethyldisiloxane films prepared by atmospheric pressure glow discharge', *J. Phys. D: Appl. Phys.*, **28**, 1995, 1661 – 1669

[16] *Handbook of Chemistry and Physics*, **76th Edition**, CRC Press Inc., Boca Raton, FL 1995.

[17] Frommer, J.; Sampson, D.; Campbell, R.; Miller, D.; Hawker, C.; Lee, V.; Miller, R.D., 'Curious morphology of silicon-containing polymer films on exposure to oxygen plasma'', *Chem, Mater.*, **10**, 1998, 3895 - 3901

[18] Rangel, E.C.; Gadioli, G. Z.; Cruz, N.C., 'Investigation on the stability of plasma modified silicone surfaces', *Plasmas and Polymers*, **9**(1), 2004, 35 - 48

[19] Owen, M.J., 'Plasma/Corona treatment of siloxanes', *Aust. J. Chem.*, **58**, 2005, 433 - 436

[20] Kim, J.; Chaudhury, M.K.; Owen, M.J., 'Hydrophobicity loss and recovery of silicone HV Insulation', *IEEE Transactions on Dielectrics and Electrical Insulation*, **6**(5), 1999

[21] Hillborg, H.; Gedde, U.W., 'Hydrophobicity recovery of polydimethylsiloxane after exposure to corona discharges', *Polymer*, **39**(10), 1998

[22] Hillborg, H.; Gedde, U.W., 'Hydrophobicity changes in silicone rubbers', *IEEE Transactions on Dielectrics and Electrical Insulation*, **6**(5), 1999

CHAPTER 9

CONCLUSIONS

- It has been shown that atmospheric pressure plasma (APP) can lead to the same level of oxidation as corona discharge. The APP has been shown to be less damaging to the substrate, and leads to a reduction in the formation of low molecular weight oxidised materials, despite the use of higher energy densities.

- A new methodology for curve-fitting of the XPS Si 2p and C 1s core levels of siloxane materials has been developed using siloxane standards. This method has been expanded to be used on siloxane coatings thinner than the depth of analysis of XPS. This enabled the chemistry of the coatings to be determined without the influence of the substrate.

- The chemistry of siloxane coatings deposited on poly(ethylene terephthalate) film have been related to the plasma parameters utilised during deposition. Up to 95% polymeric siloxane [$(CH_3)_3SiO_{1/2}$ and $(CH_3)_2SiO_{2/2}$] have been retained for deposition of poly(dimethylsiloxane) precursor. The use of a poly(hydrogenmethylsiloxane) precursor led to a more oxidised coating, with up to 25% siloxane in $(CH_3)SiO_{3/2}$ environment. The trends in deposition rate for PDMS and PHMS were also found to be different.

- Siloxane coatings durable to immersion in boiling water for 30 minutes have been achieved by plasma treatment of the substrate prior to deposition, and by plasma treatment of the coating following deposition. It is believed that improved grafting and enhanced crosslinking, respectively are the mechanisms behind this performance improvement.